Fall 1981

WATER QUALITY IMPACT OF NON-POINT SOURCE CONTAMINANTS IN SMALL TIDAL RIVERS

EDWARD JOHN SCHMIDT

INFORMATION TO USERS

This was produced from a copy of a document sent to us for microfilming. While the most advanced technological means to photograph and reproduce this document have been used, the quality is heavily dependent upon the quality of the material submitted.

The following explanation of techniques is provided to help you understand markings or notations which may appear on this reproduction.

1. The sign or "target" for pages apparently lacking from the document photographed is "Missing Page(s)". If it was possible to obtain the missing page(s) or section, they are spliced into the film along with adjacent pages. This may have necessitated cutting through an image and duplicating adjacent pages to assure you of complete continuity.

2. When an image on the film is obliterated with a round black mark it is an indication that the film inspector noticed either blurred copy because of movement during exposure, or duplicate copy. Unless we meant to delete copyrighted materials that should not have been filmed, you will find a good image of the page in the adjacent frame. If copyrighted materials were deleted you will find a target note listing the pages in the adjacent frame.

3. When a map, drawing or chart, etc., is part of the material being photographed the photographer has followed a definite method in "sectioning" the material. It is customary to begin filming at the upper left hand corner of a large sheet and to continue from left to right in equal sections with small overlaps. If necessary, sectioning is continued again--beginning below the first row and continuing on until complete.

4. For any illustrations that cannot be reproduced satisfactorily by xerography, photographic prints can be purchased at additional cost and tipped into your xerographic copy. Requests can be made to our Dissertations Customer Services Department.

5. Some pages in any document may have indistinct print. In all cases we have filmed the best available copy.

University
Microfilms
International

300 N. ZEEB RD., ANN ARBOR, MI 48106

Schmidt, Edward John

WATER QUALITY IMPACT OF NON-POINT SOURCE CONTAMINANTS IN SMALL TIDAL RIVERS

University of New Hampshire PH.D. 1981

PLEASE NOTE:

In all cases this material has been filmed in the best possible way from the available copy. Problems encountered with this document have been identified here with a check mark __√__.

1. Glossy photographs or pages _____
2. Colored illustrations, paper or print _____
3. Photographs with dark background _____
4. Illustrations are poor copy _____
5. Pages with black marks, not original copy _____
6. Print shows through as there is text on both sides of page _____
7. Indistinct, broken or small print on several pages ✓
8. Print exceeds margin requirements _____
9. Tightly bound copy with print lost in spine _____
10. Computer printout pages with indistinct print _____
11. Page(s) _____ lacking when material received, and not available from school or author.
12. Page(s) _____ seem to be missing in numbering only as text follows.
13. Two pages numbered _____. Text follows.
14. Curling and wrinkled pages _____
15. Other _____

University
Microfilms
International

WATER QUALITY IMPACT OF NON-POINT SOURCE CONTAMINANTS IN SMALL TIDAL RIVERS

BY

Edward J. Schmidt
B.S., Columbia University, 1961
M.S., Purdue University, 1963

DISSERTATION

Submitted to the University of New Hampshire
in Partial Fulfillment of
the Requirements for the Degree of

Doctor of Philosophy
in
Engineering

September, 1981

This dissertation has been examined and approved.

Dissertation director, Paul L. Bishop
Associate Professor of Civil Engineering

Barbaros Celikkol
Associate Professor of Mechanical Engineering

Yen-Hsi Chu
Assistant Professor of Civil Engineering

Robert W. Corell
Professor of Mechanical Engineering

Paul J. Ossenbruggen
Associate Professor of Civil Engineering

Aug. 21, 1981
Date

ACKNOWLEDGEMENTS

Completion of this research program and dissertation was made possible by the support and efforts of many individuals. While I will not endeavor to acknowledge each, I would like to express particular thanks to a few who were most instrumental. Paul Bishop has been involved throughout the effort, and was particularly helpful in defining the objectives, in ensuring a smooth progression through each phase of the Ph.D. program, and in performing an exhaustive review of the final document. The continued day-to-day involvement of Barbaros Celikkol in the technical details of the work, and his sincere interest in all aspects, is gratefully acknowledged.

I would also like to express thanks to my family for their patience and help throughout this seemingly endless program, and especially to Corey for her long hours of copying equations. The typing support of Diana Voyles is also appreciated, together with the timely completion of figures and graphics by Jane Lenharth. Finally, I would like to acknowledge the tireless efforts of Frank Smith who coordinated the production phases of the dissertation document, and without whom the final completion would have been virtually impossible.

TABLE OF CONTENTS

LIST OF TABLES

LIST OF FIGURES

ABSTRACT

WATER QUALITY IMPACT OF NON-POINT SOURCE CONTAMINANTS IN SMALL TIDAL RIVERS

by

EDWARD J. SCHMIDT
University of New Hampshire, September, 1981

An integrated numerical modeling methodology has been developed for analysis of non-point contaminant production and the resulting water quality impacts in estuarine receiving waters. The methodology was calibrated against both contaminant source observations and estuarine data on salinity and dye tracer distributions.

Contaminant source loading is based on a continuous analysis of overland runoff during one or more rainfall events which may be separated by dry periods. The runoff curve number technique is combined with a partial contributing area approach to represent spatial variability in the watershed. Sediment washoff is used as an indicator of contaminant quantities which are computed by application of potency factors representative of different land uses.

Hydrographs and contaminant load time series are introduced as a continuously varying source into a set of one-dimensional estuary models. Freshwater flow and tidal height are the primary forcing functions for dynamic computation of velocity and water surface profiles

throughout the estuary. The effect of longitudinal salinity distribution is included through a closed form solution of governing differential equations. This leads to a formulation of vertical velocity variation and a resulting density driven dispersion coefficient varying with tidal cycle averaged fresh water flow.

Sensitivity of the models to values of key parameters was investigated through a series of numerical experiments. Both runoff volume and contaminant weight were found to be greatest on impervious areas of the watershed. Hydrologic analysis could be calibrated by adjustment of a single parameter, the Antecedent Moisture Index. Contaminant load was affected by a number of parameters, but two sediment transport coefficients were most critical. Evaluation of hydrodynamic model results demonstrated that the key components of the dynamic force balance are the surface slope and acceleration of the water mass. Friction was found to be an important but significantly smaller component. The hierarchy of physical processes affecting contaminant dispersion was dominated by tidal velocity variations. Density driven circulation had a variable impact on contaminant dispersion, being most significant in deep sections with a large longitudinal density gradient.

Calibration runs and application to analysis of non-point source water quality impacts in the Oyster River, New Hampshire, were performed. Both storm hydrograph and contaminant loadings for a 2.6-inch rainfall were simulated

and compared favorably with field data for a one square mile sub-basin. Both salinity distribution for an average fresh water flow and dye distribution for two dye studies were adequately simulated with the model.

Investigation of receiving water impacts in the Oyster River Estuary revealed that following major storm events, BOD concentration and dissolved oxygen deficit can be dominated by the effect of non-point source contaminants. Although the impact is short-lived, concentrations exceed those due to discharge of secondary treated effluent by at least one order of magnitude.

CHAPTER 1

INTRODUCTION TO THE PROBLEM AND APPROACH

1.1 Non-point Source Impact on Receiving Waters

Concern for the quality of human lifestyle has become inseparably linked to improved understanding of our water resources. Availability of high quality water in sufficient quantity is important to such diverse activities as recreation, health and sanitation, industrial production, food supply, transportation and many others. A major role of the water resource engineer is application of mathematical tools to prediction of future conditions of this resource and to simulation of either past or present conditions when insufficient field observations are available.

Man's activities have great potential for impacting his environment, particularly aquatic systems. The difficulty of understanding and predicting impacts is compounded by the complexity of these systems. A virtually unlimited variety of physical, chemical and biological conditions may occur in surface and subsurface bodies of water. Among the most complex are those categorized as estuaries. These important water bodies occur at the interface between marine and fresh water environments. The transition may occur over a very small distance and large

gradients in water quality parameters may be observed. The importance of estuaries is twofold. Natural biological systems find estuaries to be favorable environments, and they are characteristically highly productive areas. Man has also found them favorable due to the variety and extent of water resource available for transportation, recreation and water supply. This dual importance can lead to conflicting priorities for use of estuaries.

Estuary water quality can be modified both by direct discharge of wastes or by-products of man's activities and by washoff of contaminants from the land surface (or subsurface) due to precipitation events. A major effort has been undertaken on a national scale to reduce or eliminate direct discharge of wastes. Controlling impacts from these sources has become primarily a matter of financial and scheduling priorities. Impacts of contaminants generated by precipitation have been more difficult to quantify and generally applicable abatement techniques are not yet available.

The importance of solving the precipitation-generated or non-point source contaminant problem is illustrated by the National Urban Runoff Project. This U.S. Environmental Protection Agency (EPA) program resulted from a congressional mandate that a better understanding of urban non-point source pollution be developed. The program is directed toward improving the data base relative to contaminant loads and developing cost effective methods for

their control. One of approximately 30 sites across the country being investigated through the National Urban Runoff Project is located in Durham, New Hampshire.

Durham is typical of many small coastal communities in southeastern New Hampshire and throughout New England which are undergoing a period of population growth and land development. These coastal communities are frequently located on sensitive estuaries such as the Oyster River in Durham. A problem of immediate national and regional concern is developing an improved understanding of the water resources implications of development in these areas. The most expedient and efficient way to address this question is through development of appropriate mathematical models.

The work to be described here has been directed toward modeling a specific aspect of the water resource problem, namely, the short term water quality effects of proposed land use changes on small tidal rivers typical of the New England coastline. It is assumed that direct waste discharges will be controlled at a satisfactory level through application of available technology. The major effort is involved with precipitation-generated contaminants. If necessary, residual direct discharges may be superimposed on the analysis. Such an analysis requires two major model categories: (1) upland rainfall-runoff-contaminant source modeling; and (2) estuary hydrodynamic-water quality modeling. The models

are intended to be sufficiently general that input of appropriate physical data and adjustment of a limited number of parameters would allow their application to any of a large number of similar locations.

1.2 Description of this Research

Development of any model must be preceded by an analysis of which system characteristics are to be included and the objectives to be addressed by the model results. Using the Oyster River system as an example, general characteristics important to the analysis can be defined. The perceived need and hence the objectives of the analysis are also described in terms of this system. It is apparent that similar conditions occur in other coastal areas of southeastern New Hampshire and throughout New England.

The Oyster River drainage basin is located primarily in the towns of Durham and Lee with headwaters in the towns of Barrington and Madbury. Each of these communities has undergone dynamic growth during the period 1960-1980, growth which is expected to continue in the coming few decades. Durham, for example, experienced a population increase of 61% from 1960 to 1980. Land use throughout the basin remains extremely diverse. In a recent planning study report, the Strafford Regional Planning Commission indicated that growth has been primarily in the eastern portion of the region and appears to be concentrated along

the major arterial highways. Generally, industrial development in central business areas has deteriorated, and expansion has occurred in fringe area industrial parks. Commercial development has been concentrated in shopping centers and along major highways. Residential development has occurred both within the towns and in the rural areas of the watershed. Interspersed among these developed areas, there continues to be large areas of undeveloped and agricultural land. This pattern of development creates a hydrologic environment uniquely different from major cities or their nearby surburban areas.

Under these conditions, hydrologic and non-point source analysis must be capable of distinguishing land areas as small as tens of acres from their surroundings. Conversely, the relatively small magnitude of each development requires that the analysis be both economical and rapid. Analysis of an entire watershed with a resolution of ten acres is prohibitive, so a method of aggregating areas must be employed without losing the capacity to isolate individual small parcels. A computerized grid data management and display system has been developed as part of this work to perform the required data aggregation.

The decentralization of development has other important implications for modeling hydrologic processes. Surface stormwater runoff is carried in a wide diversity of natural and man-made systems. In rural areas runoff occurs

as overland flow into small ditches and streams and then into larger surface water features. In developed areas surface runoff from rooftops and paved areas may be channeled through pipes, gutters and local sewer systems. However, even in the downtown commercial zones of small towns like Durham, no integrated storm sewer system exists. Modeling based on pipe flow is unlikely to adequately represent these conditions. Rather, the model must emphasize overland flow and natural channel processes with small localized pipe and gutter systems being handled as special extreme cases of natural channel systems.

The interface between fresh water streams and the tidal river is typically defined by a dam. Most of these small New England rivers were dammed during the 1800's to provide a source of power and hence a well defined boundary exists. Of the approximately 30 square-mile drainage area in the Oyster River basin, more than 75% drains over the tide head dam or directly into the upper reaches of the tidal river. The balance drains to small creeks and surface channels or directly overland to the lower reaches of the river. Virtually all of the area undergoing intense development is at the upper end of the tidal river. Futhermore, the only major point source, the Durham wastewater treatment plant, is located within one mile of the dam. Therefore, model development has been directed toward detailed evaluation of non-point sources in the upper reaches. Remaining flow into the estuary will be

handled as a uniformly distributed constant inflow during the period of the analysis.

The Oyster River and similar small tidal rivers present a significant modeling problem. In spite of their size, the hydrography results in wide temporal variations of flow and contaminant concentrations over a tidal cycle. Current velocity and contaminant concentration variation in the Oyster River is illustrated in Figure 1. Data reported by Loder and Glibert (1975) for a single station in the Oyster River showed a range of phosphorus (as PO_4) concentration from 1.79 to 3.56 mg/l and similar variations for other nutrients during a single tidal cycle. Geometrically these rivers exhibit a three-dimensional flow regime. In addition to longitudinal variations of velocity, tidal stage, and contaminant concentration, both vertical and lateral variations are significant. Laterally, large areas of the river bottom are exposed at low tide. These tidal flats generate lateral currents and lateral variation in both longitudinal currents and contaminant concentrations. In the third dimension, vertically, strong density stratification can produce large gradients in flow and water quality parameters. Salinity differences of ten parts per thousand between surface and river bottom can be observed in the Oyster River. These multi-dimensional effects must be reflected in the models.

Within the context of the systems described above many different models could be developed. Selection of the

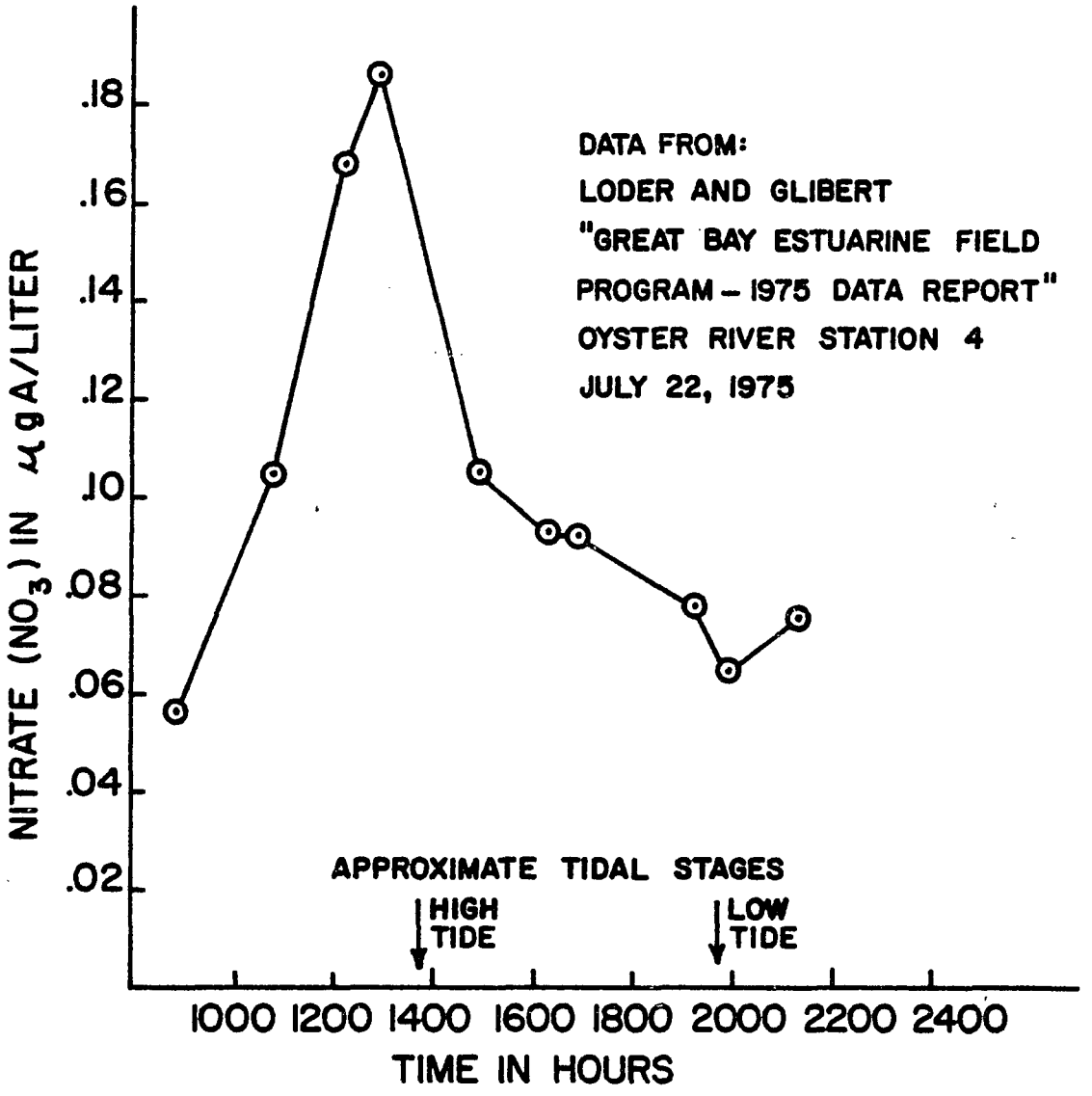

FIGURE 1

TEMPORAL VARIATION OF CONTAMINANT IN OYSTER RIVER

optimum approach requires definition of the results needed and their use. In this case the perceived need is for an efficient analytical tool for investigating potential impacts of alternative land management decisions. Modeling results would be used in preliminary evaluation of proposed developments, for selecting optimum non-structural control measures to minimize water quality impacts, for improving general understanding of conditions which may generate negative impacts, and for similar planning level activities. It is not intended that detailed or final analysis of a major project such as the 1973 proposal to build a refinery in Durham be undertaken with this model. Furthermore, the results are not expected to be compatible with microscale scientific investigation of conditions within the drainage basin or the estuary. On the other hand, the usefulness of the results depend on their ability to reflect important differences in water quality. It is unlikely that the yearly averaged concentration of an important parameter will be dramatically modified by land use decisions. However, short term peaks or localized "hot spots" could generate algal blooms, fish kills or other unacceptable water quality impacts. Therefore, the resolution of the results must be fine enough both temporally and spatially to provide useful information.

The research work described here encompasses three distinct activities. These are model development, calibration and validation of the models, and numerical

experiments to evaluate model sensitivity, data requirements and their ability to produce useful results. Taken in total, the most important objective is development of an efficient methodology for undertaking an investigation of potential water quality impacts. While results will be produced for the Oyster River Basin, the generality of analytical methods and their adaptability to other similar areas is considered important.

Model development focused primarily on optimum representation of physical and chemical processes and integration of upland and estuary analysis. Computer programming efforts have been minimized by using available models as a starting point. Characteristically, a major portion of computer models is devoted to input and output of data, setup of the data handling and manipulation techniques, and development of the overall flow and logic of the program. A much smaller component of most models is the representation of processes and computations. Use of existing models as a starting point allows recovery of most of the former program components. On the other hand, most of the scientifically important aspects of the model can often be significantly changed with minimal effort once a detailed understanding of the previous model is gained. This philosophy has been followed throughout this work with one significant exception. No readily applicable precedent was found for the management of data for the upland analysis. The importance of efficient manipulation of data

such as land use, slope and elevation, soil type, etc., in developing a readily applicable methodology justified departure from the general philosophy in this case.

Having developed a set of computational models, it is necessary to demonstrate their ability to give reasonable results and to adjust key parameters. This requires field observations which may be compared to the model results. Ideally, a research program includes sufficient funding and manpower to undertake both computational efforts and field investigations. Unfortunately, the broad scope of work encompassed by this problem required that priorities be established for use of available funds. Whenever possible, emphasis was placed on use of available data, interchange of both data and manpower with other programs, and minimal original field work. From the standpoint of future application of the methodology developed here, this approach is consistent with the constraints likely to be encountered in such studies. It is clearly better to develop models consistent with the needs and limits of potential users than to see a major effort go unused. Most data for the models are obtained from sources such as maps, publications of government agencies, university reports and the like. A field program to investigate mixing characteristics of the Oyster River was, however, undertaken due to the lack of adequate localized data. Furthermore, the simultaneous execution of the Durham Urban Runoff Project provided a local source of hydrologic and

contaminant data for a small but significant portion of the study area.

After validation and calibration of the models, their application was demonstrated through sensitivity studies and investigation of a specific question. Since large volumes of output data can be readily generated, it is necessary to carefully evaluate how such application runs will be made. Earlier calibration runs gave important information on the sensitivity of results to adjustable parameters of the model. These application runs were therefore oriented toward differences resulting when the models are used for different locations, for different rainfall sequences in a single basin and the relative impacts resulting from localized land use changes. The results of these application runs are described in Chapter 6 of this report.

CHAPTER 2

REVIEW OF HYDROLOGIC AND ESTUARINE PROCESSES

The impacts which stormwater-carried contaminants have on receiving water bodies such as lakes, streams and estuaries has received widespread attention during the past several years. Wanielista (1977) has indicated that downstream water quality is controlled by such non-point sources in approximately 80 percent of U.S. urban areas studied by the Federal Council on Environmental Quality. Field and Turkeltaub (1980) state that 40 to 80 percent of the total annual organic loading downstream of cities is caused by sources other than wastewater discharges. This proportion can be as high as 95 percent during a storm. Characteristics of non-point source flows summarized by Donigan and Crawford (1976) show that concentrations of solids, biochemical oxygen demand, chemical oxygen demand, and nutrients can approach or even exceed that of untreated municipal sewage. Considering the much larger volume of stormwater, the potential impact of non-point source discharges must be critically evaluated in any water quality analysis. The U.S. Environmental Protection Agency has been charged with responsibility for defining the national problem and developing required mitigation measures. Part of this is encompassed in the National Urban Runoff Project which seeks to evaluate the problem of

non-point source contamination in the vicintiy of towns and cities as distinct from rural, agricultural, forest, and other less developed areas.

2.1 Modelling Overland Flow

The occurrence and magnitude of non-point source contaminant flows are clearly related to surface water hydrology. It is essential that rainfall-runoff relationships be defined as part of the overall water quality evaluation. Hydrologic models employing both stochastic and deterministic techniques have been developed for this purpose. Since a wide range of objectives can be served by these models, the technique must be consistent with the problem to be solved. Hydrologic models can be developed for either single-event analysis or long-term water resource investigations. They may also consider all components of the hydrologic cycle or focus on a more limited set. Because of the random nature of stochastic models, they generally fall into the area of long-term water yield analysis and are employed for a limited number of variables. Deterministic models are employed for both long and short-term analysis and may consider virtually any number of parameters. Between these two extremes are so-called parametric models which seek to describe hydrologic processes through an integration of both basic physical principals and empirical data from field studies.

This type of approach has been followed here with emphasis placed on defining the controlling physical processes through mathematical expressions or models.

Parametric modeling of hydrologic processes has been highly refined as illustrated by the Stanford Watershed Model (Crawford and Linsley, 1966) and its later refinements, the Kentucky Watershed Model (James, 1970), and others. These models employ empirically derived expressions for all significant physical processes of the hydrologic cycle so as to provide a complete accounting of moisture due to observed rainfall. The primary advantage of these models is their completeness, but they are burdened by a very large number of adjustable parameters to be calibrated. They are also hampered by the fact that parameters are considered uniformly distributed with all portions of a watershed employing identical empirical expressions.

Field observations have shown that runoff generated by a storm event is seldom uniformly distributed but occurs on a more limited portion of the basin. Engman (1974) describes the evolution of a concept referred to as the Partial Area Theory. This concept seeks to describe the heterogeneous pattern of runoff generation and the spatial changes which occur during a storm. The Partial Area Theory was first proposed by the Tennessee Valley Authority (TVA) and the U.S. Forest Service to explain the existence of localized pockets of runoff contribution. Betson (1964)

indicated that these contributing areas were always located in the same geographic location, although the size of the area tended to grow during a continuous storm. Dunne and Black (1970) postulated that the partial area concept is primarily related to surface conditions and that subsurface flow is not an important factor. Freeze (1972), on the other hand, believes that the contributing areas grow in response to a locally rising water table during a storm. The application of these concepts to hydrologic modeling is suggested by these authors, but computational techniques were not defined.

During the 1960's, the U.S. Soil Conservation Service developed hydrologic analysis techniques which focus on surface conditions of land use and soil type. These are described in their National Engineering Handbook (SCS, 1966). The SCS method employs a simplified moisture accounting system wherein precipitation is broken down into losses and runoff. The magnitude of losses is related to surface conditions through a "Runoff Curve Number." The time series of downstream channel flow is then related to runoff by means of a dimensionless unit hydrograph developed from extensive observations throughout the country. A computer model using these methods is described in publication TR-20 (SCS, 1965), and a tabular technique for 24-hour storms only is discussed in publication TR-55 (SCS, 1975).

A number of integrated models of both hydrologic

processes and contaminant washoff from the land surface have also been developed. A comprehensive storm water analysis model was developed by Metcalf and Eddy et al. (1971) for the U.S. Environmental Protection Agency. The model emphasizes contaminants generated along urban streets and flow through integrated storm sewer systems. Initiation of overland flow and generation of contaminants are handled by simplified techniques. The model has the advantage of widespread application as a result of dissemination by the EPA. However, the model lacks the ability to evaluate overland flow over long distances (more than a few hundred feet), and contaminants are computed for curb length only and not land area.

A similar model for urban conditions was developed by the U.S. Army Corps of Engineers (1974) and is applied in their "STORM" model. The model is directed primarily toward individual storms and urban areas. A simplified hydrologic analysis produces runoff by application of a coefficient to incremental rainfall. Contaminants are computed as a function of curb length using data obtained in Chicago and other cities. A simple exponential decay function is used to calculate the contaminant washoff rate.

Statistical approaches have also been developed to evaluate the urban non-point source contaminant problem. In the EPA Simplified Stormwater Management Model (EPA, 1976a), regression analysis is used to relate observed runoff in a specific city to measured rainfall. Additional

regression expressions are developed for contaminant flow rate as a function of land use type, number of antecedent dry days, rainfall intensity, and other factors. The model was developed for a city where extensive field data had been taken over a period of years (Rochester, NY). The applicability of such techniques to other cities is limited by this large data requirement.

Work has also been done to define non-point contaminant generation from rural land uses. Most of this has been concentrated on agricultural areas, but the techniques could be extended to open land, forests, and other types of land use.

A model of agricultural chemical transport developed by Frere et al. (1975) illustrates such techniques. This model considers a relatively modest area (under 100 acres) typical of a small farm. However, the watershed is analyzed as a layered system so that infiltration and subsurface flow may be considered. A complete moisture accounting distributes rainfall to soil moisture, evapotranspiration, runoff, and ground water recharge. A modified "Universal Soil Loss Equation" is used to calculate sediment quantity transported to surface steams. The model also considers sediment detachment by raindrop impact, and both overland erosion and sediment deposition. A major component of the analysis relates to soil chemistry considering leaching, decay, plant uptake, method of chemical application, and other factors. The method is

both complete and sophisticated but is only applicable to a narrowly defined set of conditions.

A more general agricultural runoff model was developed for the EPA (EPA, 1976b). The "ARM" model is based on the moisture accounting analysis of the Stanford Watershed Model. Both nutrients and pesticides are evaluated using a broad range of hydrologic and chemical process models. Timesteps as short as five to fifteen minutes are used to determine water and contaminant flows from areas as large as two square miles. As with the previously described model, sediment washoff is considered the precursor for transport of contaminants. Detailed analysis of soil and sediment chemistry is included to account for both phosphorus and nitrogen nutrient cycles and losses and decay of pesticides.

A greatly simplified approach to agricultural chemical modeling was developed by Haith and Dougherty (1976). A large watershed (223 square miles) was analyzed for annual generation of agricultural contaminants. Hydrologic analysis techniques of the Soil Conservation Service described above were used to compute total runoff volume from rainfall data and the SCS Runoff Curve Numbers. Contaminant washoff was determined from regression expressions developed for both test plots and actual field observations. While directed toward annual contaminant generation only, the utility of the simplified moisture accounting of SCS hydrologic techniques for non-point

source analysis was demonstrated by this program.

The need for a model applicable to both rural and urban conditions was recognized by the U.S. Environmental Protection Agency. This led to development of the Non-Point Source (NPS) model by Hydrocomp, Inc. (EPA, 1976c). Hydrologic simulation is based on an improved version of the Stanford Watershed Model. The continuous contaminant simulation model is developed to simulate day-to-day accumulation, washoff, and transport of contaminants by rainfall events. Accumulation takes account of both wind-carried material and human activities, and allows for both decay and removal by street cleaning or other housekeeping operations.

All contaminant quantities are developed by applying "potency factors" to sediment washoff. Washoff is handled separately for pervious and impervious portions of the watershed. Sediment generation on pervious portions of the basin is based on the work of Meyer and Wischmeier (1969). Their work identified four key mechanisms whereby sediment is generated on the land surface. These include detachment and transport by direct rainfall forces, and detachment and transport by overland runoff. Only two--rainfall detachment and runoff transport--were found to contribute significantly to the non-point source analysis. To maintain the desired consistency between rural and urban conditions, the NPS model employs the latter process as the key mechanism for transport from impervious areas such as

paved areas and rooftops. The model has been developed with sufficient generality that different contaminant potencies can be applied to pervious and impervious portions of up to five different land use areas and up to five contaminant types.

Each of these models will produce runoff and contaminant volumes which are washed from the land surface. Temporally, they may consider a total annual production, a single storm contribution, or a continuous simulation of instantaneous runoff and contaminant flow rates over a period of months or a year. When these materials have been transported overland and through primary surface channels, the question of water quality of the receiving water body becomes problematic. It is therefore necessary to consider the hydraulic and chemical characteristics of these water bodies so that the impacts can be assessed.

2.2 Estuarine Modeling

When the receiving water body for non-point source contaminants is an estuary, water quality analysis is complex. A dynamic analysis of flow and water surface elevation must be included in the evaluation of contaminant transport and chemical interactions. The use of mathematical models for estuarine analysis is discussed in depth by Ward and Espey (1971) in the report by Tracor, Inc. A model is described as a formalism, or mathematical expression of the relevant physical processes. Employment of such a model is usually motivated by tractability and is justified by the ability of the model to reproduce observed results. In the present study, this motivation is basic, and the advantages of cost and time savings have allowed the evaluation of a complex problem to be reduced to the realm of feasibility. As indicated in that report, estuary models can be classified in terms of both spatial and temporal considerations.

Ideally, a model would encompass three dimensions and short time scale dynamic changes. Such total generality has not yet been attained and is probably not justified in terms of cost, time, and data requirements. However, a number of simplified approaches to this ideal have been developed. Yeh and Tsai (1976) developed a closed form analytical solution using Green's functions for the special case of constant depth and width, a uniform but time varying velocity throughout the estuary cross section, and

negligible vertical or lateral velocity. The model was applied to simulating dye concentrations observed in two field tests and predicting temperature distribution due to an artificial heat source. A similar three-dimensional analytical solution was developed by Kuo (1976) and applied to simulating dye concentrations in the Potomac River. Three-dimensional numerical models encompassing more general geometry and flow fields have been developed by Leendertse and Liu (1975), Hess (1976), and others. These models employ a layered, two-dimensional system with appropriate linking at the interfaces between layers. They do not, however, encompass the general case of non-conservative contaminants or systems of interacting components.

Where complete three-dimensionality is not required, two-dimensional models have been employed. The two dimensions may encompass two horizontal dimensions or one horizontal and one vertical dimension depending on the specific application. Generally, estuary models have been developed to consider complex shore geometry and, hence, fall into the first type. Leendertse (1967, 1970) developed one of the earliest and most useful two-dimensional estuary models. It employed an implicit time-stepping finite difference scheme to compute tidal height, flow, and contaminant concentrations for a grid of square regions. Connor and Wang (1973) employed an explicit finite element solution technique to solve the

two-dimensional equations of continuity and momentum for a grid of variable sized triangular elements. Due to the choice of triangular elements, irregular boundaries can be handled more readily with this model. The explicit time-stepping scheme has the disadvantage that short time increments must be used. A companion two-dimensional finite element dispersion model developed by Leimkuler et al. (1975) can be used to investigate concentrations of a single non-conservative contaminant.

The geometric advantages of the finite-element scheme have led to a number of refinements of the basic hydrodynamic and dispersion models. Superimposition of two layers allowed Christodoulou et al. (1976) to analyze hydrodynamics of a stratified estuary. A linked BOD-dissolved oxygen model for New Haven Harbor was developed by Schmidt (1979) using the basic single component dispersion model. A more advanced two-dimensional hydrodynamic and water quality model employing a semi-implicit time stepping scheme was developed by Niemeyer (1978a). An application of this model to Kaneohe Bay, Hawaii is described by Niemeyer (1978b).

Two-dimensional models are not always the optimum mode for estuary analysis. In particular, when the estuary is long and narrow, such as a tidal river, several problems may be encountered. Reichard and Celikkol (1978) applied the Connor and Wang finite element model to the Great Bay

estuary system of New Hampshire. In order to ensure computational stability of the model, the triangular elements were constrained to be approximately equilateral and to differ in area by less than 20% from element to element. The minimum number of elements across any channel section was three. These limitations required use of approximately 600 elements. Due to the explicit solution scheme, computational time-steps were held to less than one minute of real time. Resulting computations required computer time (CPU seconds) approaching real time in magnitude. A complete computation for a single tidal cycle required several hours of CPU time. Clearly, use of this model for multi-tidal cycle analysis is costly. The model gives reasonable results for tidal elevations, but its ability to simulate cross channel velocity variations is limited by the small number of elements across the width of the estuary. Data published by Swenson, Brown and Trask (1977) demonstrated that throughout much of the estuary, flow is concentrated in a high velocity core near the deepest part of the channel. The failure to adequately model these cross channel variations led to difficulty in simulating contaminant transport near mid-channel. A dye study and simulation by Schmidt (1980) using the finite element dispersion model and velocity data produced by Reichard's model demonstrated a 50% discrepancy between observed dye transport velocity and model results. Numerical dispersion due to averaging across the three

lateral elements was identified as a major contributor to this error.

For reasons of economy and as a control over extraneous lateral averaging of variables, one-dimensional models are often employed for modeling tidal rivers and other narrow estuaries. A one-dimensional hydrodynamic model developed by Harleman et al. (1969) employed an explicit finite difference technique to calculate tidal heights and velocities for channels having a variety of flow and bank storage configurations. A companion water quality model was developed by Lee (1970). This model employed an implicit finite difference scheme which allowed use of a much longer timestep and hence a more economical solution. Two disadvantages of these models were the lack of ability to handle branched channels and the omission of contaminant transport into the bank storage zones of the channel cross section. The hydrodynamic model was extended to handle a single side branch by Schmidt (1981) when required for an analysis of the North River, Massachusetts. The hydrodynamic and water quality models were linked together by Thatcher (1972) for the special case of salinity intrusion and an equation of state was used to incorporate the effect of longitudinal density profile.

A more general branched hydrodynamic model was developed by Muir (1975) for a channel cross section containing both a flow and a bank storage region. This one-dimensional model employed an efficient implicit finite

difference solution scheme with variable time weighting. It did not, however, include capability to handle contaminant transport. This weakness was corrected in part by Garrison (1979) who developed a contaminant model for a single unbranched channel using the Muir techniques.

A number of models employing branched systems of one-dimensional channels to approximate both one and two-dimensional water bodies have also been developed. While none is universally able to handle all conditions, various combinations of flow conditions, branching, transient analysis, dispersive transport and other alternatives are employed in these models. For example, the RECEIV module of the Storm Water Management Model by Metcalf and Eddy et al. (1971) accommodates up to 225 channel sections connected at up to 100 junctions. Either rivers or estuaries can be analyzed for both hydrodynamic and water quality parameters. Unfortunately, the model does not consider dispersive transport, and hence each timestep employs a plug flow approximation between junction points. Similar models were developed by Fisher (1972), the Texas Water Development Board (1970), Roesner et al. (1973), and others.

In selecting among this diversity of modeling techniques, it must be understood that each simplification of the complete three-dimensional dynamic system results in a loss of information. Where the simplification involves deletion of a process from the governing equations, the

impact is obvious. However, when the simplification involves reducing the dimensionality from three to two or one, and when it involves temporal averaging, the loss of information is more subtle. Referring to typical derivations of two-dimensional governing hydrodynamic and dispersion equations (for example, Connor and Wang (1973) and Leimkuler et al. (1975)), integration of the three-dimensional equation to two dimensions results in loss of information on fluctuations of variables about their means. The same is true when the dynamic equations are averaged in time.

Typically, advective transport of contaminants involves the product of two variables. Each variable can be represented by the sum of a mean and both spatial and temporal fluctuations about that mean. Averaging a product of two such terms leads to integrals of cross product terms containing two fluctuating components. These integrals have non-zero values which must be accounted for. Evaluating these terms is facilitated by applying an analogy to Fickian diffusion. This leads to terms such as

$$FLUX = \int U'C'dZ \equiv E_{XZ} \frac{dC}{dX} \qquad (2\text{-}1)$$

where terms U' and C' designate variations from mean velocity and concentration, respectively.

The parameter E_{XZ} is identified as a dispersion coefficient reflecting transport in the X direction due to fluctuations about the Z dimension, mean of velocity U, and concentration C. Similar expressions occur for a complete set of temporal and spatial fluctuations in each direction (e.g. E_{XZ}, E_{XY}, E_{XT}). During the past 30 years, an extensive effort has been made to develop analytical and empirical expressions to evaluate these dispersion coefficients.

The initial work was done by G. I. Taylor (1954) who studied longitudinal dispersion in uniform pipe flow. Using empirical data on the distribution of mean velocities across the pipe, he integrated the product of velocity and concentration variations to obtain the following expression for the longitudinal dispersion coefficient:

$$E = 10.1\ a\ u^* \qquad (2\text{-}2)$$

where a is the pipe radius and u* is the friction velocity (shear stress term).

The same type of analysis was done by Elder (1959) to assess the effect of vertical variation in velocity and concentration on longitudinal dispersion in a two-dimensional channel. He arrived at a similar expression,

$$E = 5.93\, h\, u^* \qquad (2\text{-}3)$$

where h is the depth of flow. He also verified his results using a laboratory flume.

Fisher (1968) extended these analyses by investigating the effect of cross channel variations of velocity and concentration. Using data for actual velocity distributions in a river, he demonstrated that these lateral variations are more significant than vertical variations for natural streams. He also introduced the concept of lateral mixing time as related to longitudinal dispersion. During an initial "convective period" after introduction of contaminant into a stream, cross channel mixing takes place before the predicted longitudinal dispersion coefficient is valid. Subsequent mass transport can then be described by the one-dimensional advective-dispersion equation using the derived value for dispersion coefficient.

To this point, all of the work described has dealt

with uniform flow conditions. In estuary flow, however, there are major oscillations in flow velocities due to tidal effects. Holley et al. (1970) investigated the effect of flow oscillation on longitudinal dispersion by integration of the velocity and concentration fluctuation terms over one tidal cycle. They found that the magnitude of the longitudinal dispersion coefficient could be related to the ratio of lateral mixing time to the period of oscillation, or to the ratio of vertical mixing time to the same period. This allowed development of a simple procedure for calculating the coefficient for either vertical mixing or lateral mixing dominated dispersion.

More recently, R. B. Taylor (1976) has investigated the effect of velocity phase variations across the estuary near the slack tide. He found that such phase differences will further increase the magnitude of longitudinal dispersion. He was also able to develop a graphical representation of the interplay of vertical and lateral mixing times so that a coefficient reflecting both effects simultaneously could be calculated.

It must be noted at this point that all of the work described above considers longitudinal dispersion only. Implicit in each analysis is the requirement that lateral and vertical mixing can be described analytically as a function of hydraulic parameters. It is commonly assumed that these processes can be described using a turbulent diffusion coefficient analogous to the eddy viscosity.

As a result of the work by G. I. Taylor and others, it has become standard practice to normalize dispersion coefficient models to the product of a length parameter, ℓ (usually depth or width of the channel), and the friction velocity. A large body of data exists which expresses dispersion coefficients as constants in the following expression:

$$E = K\ell u^* \qquad (2\text{-}4)$$

Depending on the conditions of the water body and the type of averaging encompassed by the dispersion coefficient, the value of constant K has been found to range over many orders of magnitude.

A more convenient form of the above equation for the dispersion coefficient is described by Harleman in the book edited by Ippen (1966). The length scale and friction term are replaced by the hydraulic radius of a one-dimensional channel, R, and an expression for friction in terms of mean velocity, U, and the Mannings roughness coefficient, n, commonly used in open channel flow computations. In this form the equation becomes

$$E = K' n U R^{5/6} \qquad (2\text{-}5)$$

where $K' = 3.182K$.

He also suggests that a coefficient $K = 0.067$ may be used to approximate eddy viscosity of estuarine flow using this expression.

More detailed work was done on the turbulent structure of estuarine flow by Reichard (1980). In developing several models of vertical velocity distributions, he related gross flow characteristics to observed fluctuations of velocities in Little Bay, New Hampshire. This led to alternative expressions to represent turbulent mixing in terms of an eddy viscosity coefficient, N_z . The most convenient of these expressions results from an assumption of constant eddy viscosity with depth:

$$N_z = \underline{K}\ell_0 u_t \qquad (2\text{-}6)$$

Here $\underline{K}$ is defined as von Karman's constant, approximately 0.4, and ℓ_0 and u_t are a length scale and turbulent velocity scale, respectively. The length scale is typically equal to a roughness dimension at the bottom, and the turbulent velocity scale is taken to be the friction velocity. Model calculations were related to field data for Little Bay, New Hampshire, and indicated that a depth scale of approximately 100 gave a reasonable approximation to both velocity and stress profiles in the water column. Using data from Reichard (1980), his constant viscosity model would be equivalent to a K value of approximately 0.0050, or roughly the same as the estimate given by Ippen.

In applying one-dimensional representations of estuary flow, it is also important to consider salt distribution. Hansen and Rattray (1965) point out that such models relate to integral properties of the flow, and they suppress the influence of density gradients on the velocity distribution. As a result, they indicate that such models can adequately portray conditions only in the innermost part of shallow estuaries where such influence is slight. To reflect these conditions, an analytical solution to the dynamic force balance equations for an idealized rectilinear, narrow estuary is developed by those authors. Different solutions are given for the central region of the estuary where vertical salinity stratification is relatively independent of longitudinal position, and for the inner region where salinity asymptotically approaches

the riverine value.

Empirical data from both field observations and laboratory flume tests describing vertical profiles of velocity and salinity is presented by Harleman and Ippen (1967). These data clearly demonstrate that inward circulation velocities at the bottom of a stratified flow field may exceed four times the average net fresh water velocity. Outward circulation velocities can exceed six times the fresh water velocity. Vertical salinity distributions show bottom salinities as high as 1.5 times the vertical average, and surface salinities as low as 0.3 times the average. The authors also relate both vertical and longitudinal distributions to dimensionless indices which may be used to describe the relative importance of inertial, gravitational, and other forces on the water mass.

A similar effort was undertaken by Officer (1977) which also encompassed the effect of longitudinal wind shear on the vertical distribution of velocity. The solution requires prior knowledge of longitudinal salinity distribution. For a simplified case of no wind shear, and ignoring the dynamic effect of fresh water flow, the vertical distribution of salinity was also defined. The author demonstrated that the combined effect of velocity and salinity variation is an upstream mixing or dispersion of salt which balances the net downstream advection due to fresh water flow. A technique for calculating an effective

circulation dispersion coefficient from these analytically defined distributions is presented.

As mentioned above, the effect of longitudinal density gradients on the net longitudinal force balance was investigated by Thatcher and Harleman (1972). Using empirical data to define the dispersion coefficient resulting from density driven circulation, they linked a one-dimensional salinity distribution model to a one-dimensional hydrodynamic model via an equation of state. Using a numerical solution technique, they were able to simultaneously determine the intratidal cycle variation of longitudinal salinity profile and its effect on water surface elevation and current velocities.

Throughout much of the work described above, the necessity for field observations to describe mixing processes in real estuaries has been recognized. For many years, dispersion phenomena have been investigated through the use of tracers injected into a flowing liquid. Early work, such as that of G. I. Taylor (1954), used salt as a tracer. Later, the use of fluorescent dyes and radioactive materials was found advantageous. Fluorescent dye has now become the most common tracer for such studies in natural water bodies and is discussed in detail by Wilson (1968).

Extensive work with dye release studies was done by the USGS during the 1960's and early 1970's. Yotsukura et al. (1970) undertook a large scale study of the Missouri River to determine transverse mixing coefficients. For

comparison and verification of the analysis, longitudinal dispersion was also measured through further dye testing. During these tests, slugs of dye were released, and concentrations were detected at distances up to 140 miles downstream of the release point. Estimates of longitudinal dispersion coefficients were made using a modified "Method of Moments" originally developed by Sayre and Chang (1968). This method is based on a correlation expression between dispersion and the standard deviation of dye concentration versus time at a sampling transect. Transverse coefficients were calculated by a Method of Moments approach and also through calibration of a mathematical model based on variation of concentration and velocity across the flow cross section.

Dye studies have also been utilized for determination of flushing time and equilibrium concentrations in estuaries. This technique was used in a study of the Piscataqua River by Webster and Martin, Inc. and Ebasco Services, Inc. (1969). Dye was released continuously at a low rate for an extended period so that equilibrium was obtained. After approximately six days concentrations at slack tide conditions stabilized. This allowed observation of equilibrium slack tide concentrations throughout the estuary due to the continuous release. Exchange of water between the open ocean and the release point was also estimated from these data.

Investigation of transient conditions in an estuary

requires a significantly more intensive sampling program, and few such studies have been undertaken. However, a program was undertaken by Fisher (1972) for a tidal lagoon in California as part of an effort to develop a mathematical pollutant dispersion model. A slug of dye was released at the mouth of the estuary just after a low slack tide. Concentrations were then measured for more than one tidal cycle. Data were applied for verification of a computer model of the basin. It should be noted that these data were used only for comparison with dispersion patterns predicted by a model. No effort was made to relate the data to a prediction of the dispersion coefficient.

More recently, a dye release study was conducted by Ward (1976) in the Fraser Estuary of British Columbia. A slug of dye was released approximately twelve miles above the mouth of the estuary, and transverse and longitudinal measurements were taken as the dye cloud was tracked. These data were used to calculate standard deviations of concentration versus distance. Dispersion coefficients were calculated from the time rate of change in these standard deviations. The obtained coefficients were correlated to theoretical formulations. Aerial photography was able to detect the dye cloud for over an hour. This study was performed within an estuary but is quite similar to prior studies of rivers because sampling was terminated before reversal of the flow.

Dye release studies continue to be a useful technique

for obtaining a variety of dispersion-related data. Programs are currently underway to obtain such data at several universities and in industry. At the University of New Hampshire, such studies were done for a site in the Piscataqua River in support of an estuary modeling program. Results are described by Schmidt (1980).

CHAPTER 3

NUMERICAL ANALYSIS OF RUNOFF AND NON-POINT CONTAMINANTS

The objective of this portion of the work was to model runoff hydrographs and key pollutographs that result from specific rainfall events. The spatial resolution of the analysis reflects land areas as small as tens of acres. Temporal resolution encompasses timesteps of a few minutes up to hours. It is intended that useful results be generated with a minimum of field data collection, and yet be sufficiently reliable that engineering decisions can be based on them.

The need to reflect small land areas within a larger drainage basin results in handling large amounts of data. Hydrologic and contaminant data must be developed for each area of interest. Specifically, the hydrologic and non-point analysis requires knowledge of soil types, land use, and topography. In turn, other data, such as proportion of impervious land surface, overland runoff travel time, and contaminant potency factors, etc., can be generated. A typical small basin may contain 1000 to 50,000 acres, or 100 to 5000 land areas of ten acres each. The resulting volume of data necessitates use of a computerized data management tool. While such tools are available in the literature and commercially, the specialized nature of this work did not fit such "canned"

techniques. For this reason, new analytical tools were developed which are described in Section 3.1 of this chapter.

Each significant storm will generate surface water discharges which modify the flow regime of the receiving estuary. Furthermore, this surface flow is the major mechanism whereby contaminants are transported from the land surface to the estuary. Hydrologic analysis is employed to produce real-time data on flow at any point of a river basin. Either stochastic or deterministic models could be employed for these analyses. However, to examine individual storms, a deterministic model based on a specified rainfall hyetograph has been employed. Many of the techniques used here were originally developed by the U.S. Soil Conservation Service (SCS) and have been extensively applied throughout the United States. Due to the critical relationship between runoff and contaminant washoff, the computational aspects of this model were carefully analyzed and are described in Section 3.2 of this chapter.

The most important aspect of the upland analysis is determination of the real-time variation of contaminant flow to the receiving estuary. While several models have been developed for such analysis, none adequately fit the requirements of this work. However, the contaminant generation and washoff algorithms of the EPA Non-Point Source Model (U.S. EPA, 1976c) are believed to be the best

Table 1

Hydrologic and Non-Point Contaminant Data

I. Hydrologic modeling

A. For each runoff area:
   1. hydrologic runoff curve number
   2. land area in acres
   3. time of runoff concentration

B. For each stream reach:
   1. length
   2. average velocity, or
   3. stage, discharge, velocity data

C. General
   1. rainfall hyetograph
   2. antecedent moisture condition

II. Non-Point Contaminant Analysis

A. For each runoff area:
   1. Proportion of area which is pervious
   2. Proportion of exposed soil surface
   3. Initial pervious and impervious area sediment load
   4. Pervious and impervious area potency factors for each contaminant

B. For each stream reach:
   1. length
   2. channel routing coefficient

C. General
   1. soil fines detachment parameters (2)
   2. soil fines transport parameters (2)
   3. imperviious area dust and dirt transport parameters (2)

representation of these processes available for the river basins of interest here. Integrating these algorithms with the hydrologic analysis of the Soil Conservation Service required extensive computer program modification and restructuring. The results of this model-building effort are described in this chapter.

3.1 Hydrologic and Contaminant Data Management

The data requirements of the hydrologic and contaminant analyses are listed in Table 1. Each item is described in detail in the appropriate section of this chapter. For purposes of discussing the data management system, only a brief description of the means for generating these data will be given here. The primary information is as follows: 1) land use type, 2) SCS soil classification, 3) drainage sub-basin designation, 4) surface elevation, and 5) river or stream type.

The data management system uses five data files, each containing a single data value for one of these five characteristics for each ten-acre land area. Assuming a thirty-square-mile basin, this results in 1920 data values in each file. All data values may be obtained from readily available map sources. At the present time, data are generally retrieved from the maps by overlaying a transparent grid and manually recording each value. However, in the future, as more use is made of digital

storage of map data by governmental agencies and other organizations, a more automated data retrieval system may be employed. For example, it is the goal of the U.S. Geological Survey (USGS) to complete digitization of most quadrangle maps over the next ten years. This would allow direct accessing of elevation data.

Land use types employed in this system are listed in Table 2. The first ten types are self-explanatory and are similar to classifications generally employed on county or state land use maps. Types 11 through 19 have been included to cover cases where most of a grid cell is one of the first nine types but a significant portion is more highly developed. "More highly developed" here means a greater proportion of impervious surface which will reduce the infiltration of precipitation into the ground. Typical examples of these land use types would be a forest area traversed by a major highway, or an open land area with a small commercial or residential development on one portion.

Soil Conservation Service classifications of soils are given on county soil maps readily available in libraries or SCS offices. Virtually all of the inhabited areas of the United States have been mapped. As many as 50 or more soil classes may be found in a single river basin, and no effort was made to generalize these classes for use here. However, the SCS has grouped these soil classifications into four types (plus transitional types falling between these four) for use in their hydrologic analysis. This

Table 2

Land Use Types

IDENTIFICATION	DESCRIPTION
1	SINGLE FAMILY RESIDENTIAL
2	MULTI-FAMILY RESIDENTIAL
3	COMMERCIAL
4	INDUSTRIAL
5	RECREATION
6	AGRICULTURE
7	OPEN LAND
8	FOREST
9	INSTITUTIONAL, SCHOOLS, ETC
10	OPEN WATER
11	SINGLE FAMILY+
12	MULTI-FAMILY+
13	COMMERCIAL+
14	INDUSTRIAL+
15	RECREATION+
16	AGRICULTURE+
17	OPEN LAND+
18	FOREST+
19	INSTITUTIONAL+

NOTE: SEE TEXT FOR EXPLANATION OF LAND USES WITH + SYMBOL.

reassignment of soil types is handled in the data management system.

Drainage sub-basin designations are assigned manually to control the pattern of drainage employed by the models. It is possible to make these assignments by manipulation of land surface elevation data. However, elevation data must be provided on a much finer grid than ten acres where terrain is irregular, as in much of the notheastern United States. When digitized elevation data is available it may be feasible to eliminate this primary data requirement. However, for the present, each ten-acre grid cell is assigned to a sub-basin by inspection of maps. Initially, sub-basins are selected for even the most minor surface water feature, but they are later regrouped into a more workable number of perhaps 10 to 25 sub-basins containing 100 to 1000 or more acres.

Surface elevations are assigned a single representative value for each grid cell. Since terrain may vary as much as 50 to 100 feet between elements or as little as a few feet, a precision of one foot has been selected for these data. Care must be exercised in assigning these values such that the elevation data is consistent with the sub-basin designations previously assigned. Each point within the sub-basin must drain to an adjacent lower point also within the sub-basin. Furthermore, when the grid cell contains a stream or other surface water feature, the assigned elevation must equal

that of the water surface to assure that adjacent areas drain to the stream. Where grid cells contain ponds or slow-moving streams, elevation differentials of a tenth of a foot or less may occur between adjacent ten-acre areas. In these places, elevation data must be specified to a precision of no more than 0.1 feet.

River or stream types are assigned by inspection of U.S. Geological Survey (USGS) quadrangle maps. However, field reconnaissance may be necessary to confirm stream conditions. For this data management system, surface water features have been divided into types on the basis of general channel characteristics that affect their flow velocity. These river types are listed in Table 3 together with the assigned hydraulic characteristics.

The five sets of data are manipulated by a computer program. The operations include regrouping, integrating two or more data values to determine a new data value, apportioning land area according to data values, and assigning new data values based on the relationship of a grid cell data point to those surrounding it. The algorithms employed to generate secondary data sets needed by the hydrologic and contaminant models are described below. In addition to these operations, the data management program may be used to produce any of several grid maps which can be used to evaluate the data visually or as a convenient tool for trouble-shooting.

The parameter that relates rainfall volume to runoff

Table 3

River Channel Characteristics

IDENTIFICATION	DESCRIPTION	HYDRAULIC RADIUS	MANNINGS "N"
1	UPLAND, <1 FT DEEP, MEANDERING, ROUGH	0.5	0.045
2	UPLAND, =1 FT DEEP MEANDERING, SMOOTH	1.0	0.040
3	UPLAND, >1 FT DEEP, MEANDERING, SMOOTH	1.5	0.040
4	SMALL STREAM, MODERATE ROUGHNESS, SHALLOW	1.0	0.030
5	SMALL STREAM, MODERATE ROUGHNESS, 1-2 FT DEEP	1.5	0.030
6	SMALL STREAM, MODERATE ROUGHNESS, >2 FT DEEP	2.0	0.030
7	MAIN RIVER, ROUGH BED, SHALLOW	1.0	0.030
8	MAIN RIVER, MODERATE ROUGHNESS, >2 FT DEEP	2.0	0.025
9	MAIN RIVER, WELL DEVELOPED CHANNEL, >3 FT DEEP	3.0	0.020
10	DEEP RIVERS, PONDS, RESERVOIRS	6.0	0.020

volume in the SCS hydrologic analysis model is called the "Runoff Curve Number." Data are available to relate land use type and soil type to a curve number. These data are found in SCS publication TR-55 (1975) and in Chapter 4 of their National Engineering Handbook (SCS, 1966). Curve numbers for the nineteen land use types and seven soil types have been abstracted from these sources and are given on Table 4. These are stored in the program and assigned to each ten-acre grid cell.

As described in a later section, the relationship between rainfall and runoff used in the SCS model is not linear. As a result, Runoff Curve Numbers cannot be simply averaged to compute a representative curve number for a larger area. As noted above, sub-basins made up of many grid cells are regrouped into larger sub-basins for analysis in the hydrologic model. These basins may contain hundreds of grid cells and representative curve numbers must be determined. The method employed here is to group the grid cells of a sub-basin according to curve number as follows. Five curve number groups were selected: 0-35, 35-71, 71-89, 89-97 and over 97. The ten acres of each grid cell is then linearly apportioned to the end points of a group. For example, a ten-acre grid cell with curve number of 53 would be apportioned five acres to CN-35 and five acres to CN-71. All curve numbers over 97 are apportioned 100% to CN-97. A CN-100 group would imply that 100% of the rainfall would become runoff -- a

Table 4

Runoff Curve Numbers

LAND USE	SOIL TYPE A	A/B	B	B/C	C	C/D	D
SINGLE FAM	54	62	70	75	80	82	85
MULTI-FAM	77	81	85	87	90	91	92
COMMERCIAL	89	90	92	93	94	94	95
INDUSTRIAL	81	84	88	89	91	92	93
RECREATIONAL	39	50	61	67	74	77	80
AGRICULTURAL	67	71	76	79	83	84	86
OPEN LAND	30	44	58	64	71	74	78
FOREST	35	47	60	66	73	76	80
INSTITUTIONAL	49	59	69	74	79	81	84
SINGLE FAM+	61	68	75	79	83	85	87
MULTI-FAM+	84	87	90	91	93	93	94
COMMERCIAL+	89	80	92	93	94	94	95
INDUSTRIAL+	81	84	88	89	91	92	93
RECREATIONAL+	49	59	69	74	79	81	84
AGRICULTURE+	72	76	81	84	88	89	91
OPEN LAND+	39	50	61	67	74	77	80
FOREST+	45	55	66	71	77	80	83
INSTITUTIONAL+	61	68	75	79	83	85	87

NOTE: CURVE NUMBERS FROM TABLE 2-2 SCS TR-55
SINGLE FAM - 1/2 ACRE SINGLE FAM+ - 1/4 ACRE
MULTI-FAM - 1/8 ACRE MULTI-FAM+ - 1/8 + INCREMENT
RECREATIONAL - OPEN SPACE GOOD CONDITION (+FAIR COND)
AGRICULTURAL - CULTIVATED LAND AVG WITH & W/O CONSERVATION (+ W/O CONS.)
OPEN LAND - MEADOW (+ OPEN SPACE - GOOD COND)
FOREST - AVG OF THIN STAND & GOOD COVER (+ THIN STAND)
INSTITUTIONAL - OPEN SPACE FAIR CONDITION (+ 1/4 ACRE RES.)

hydrologically unacceptable condition. The result of this apportioning is five area values for each sub-basin, one for each curve number end point. Since a curve number of 0 implies no runoff, the CN-0 area is ignored in subsequent computations.

In addition to curve number, a number of contaminant generation properties of each grid cell are apportioned. These include the proportion of the area which is impervious, the proportion of the soil exposed to direct raindrop impact, and the contaminant potency factors for pervious and impervious areas. Each of these is explained more fully later. It has been determined that land use is the most important factor influencing these characteristics. Therefore, the data management program makes use of data on these characteristics which is provided for each land use type. The data are summarized in Table 5. Averaging of these values is done in accordance with the apportionment of areas into curve number groups. For example, assume a ten-acre area which is apportioned five acres to CN-35 and five acres to CN-71 and which falls into a land use having an impervious proportion of 0.18. The resulting average impervious proportion for the CN-35 group will be based on a weighting of five acres at a value of 0.18. This is averaged with all other grid cell contributions to get the average impervious proportion for the CN-35 group of that sub-basin. Similar area-weighted averages are used for

Table 5

Contaminant Properties of Land Use Types

LAND USE TYPE	PROPORTION IMPERVIOUS	PROPORTION OF EXPOSED SOIL	CONTAMINANT POTENCY FACTORS	
			BOD	SUSPENDED SOLIDS
1	0.18	0.05	*	
2	0.30	0.05	*	
3	0.55	0.10	*	
4	0.75	0.10	*	
5	0.10	0.10	*	
6	0.05	0.20	*	
7	0.05	0.10	*	
8	0.02	0.10	*	
9	0.15	0.05	*	
10	0.00	1.00	*	
11	0.18	0.05	*	
12	0.30	0.05	*	
13	0.55	0.10	*	
14	0.75	0.10	*	
15	0.10	0.10	*	
16	0.05	0.20	*	
17	0.05	0.10	*	
18	0.02	0.10	*	
19	0.15	0.05	*	

* COMTAMINANT POTENCY FACTORS FOR EACH CONTAMINANT AND FOR BOTH PERVIOUS AND IMPERVIOUS AREAS ARE INPUT DATA AND ARE SUBJECT TO MODEL CALIBRATION. DEFAULT VALUES OF 0.71 FOR SUSPENDED SOLIDS AND 0.04 ARE USED IN THE DATA MANAGEMENT MODEL.

soil exposure and potency factors.

The previously described properties have all dealt with the quantity of material produced--either runoff water or contaminants. The hydrologic and contaminant models also require data on production rates and transport times. These include time of runoff concentration for each sub-basin and average velocity of travel through stream reaches. Both require knowledge of average surface slope and direction within each grid cell. These data are generated by the data management program using elevations and sub-basin assignments.

Slope and runoff directions are determined at each grid cell as follows. The elevation of each of the eight grid cells surrounding a cell is compared to its elevation. If the adjacent cell is lower and is located within the same basin, a slope is calculated. Slope is based on a 660-ft length (the side of a ten-acre square) for the four cardinal directions. For diagonally adjacent cells, the length used is given in equation (3-1).

$$L_D = L\sqrt{2} \qquad (3\text{-}1)$$

The steepest slope is selected as characteristic of that grid cell, and the direction of that slope is retained as the runoff direction. Having calculated a slope, it is possible to calculate a characteristic velocity and travel time across the grid cell. Where a river or stream is located in the grid cell (as identified in the primary data), flow velocity V is based on application of Manning's Equation:

$$V = 1.486 \sqrt{Slope} * R^{2/3}/n \qquad (3\text{-}2)$$

where R is the hydraulic radius and n is the Manning friction coefficient. Where no river or stream is present, an overland velocity is calculated from the following equation:

$$V = \exp(A_S + B_S * C_S) \qquad (3\text{-}3)$$

$$A_S = Ln(V_1) \qquad (3\text{-}4)$$

$$B_S = (LnV_{10} - LnV_1)/Ln\ 10 \qquad (3\text{-}5)$$

$$C_S = Ln(100 * Slope) \qquad (3\text{-}6)$$

This equation is developed From figure 3-1 of Soil Conservation Service Report TR 55 (1975) which illustrates a logarithmic relationship between overland velocity and slope. The values of V_1 and V_{10} are velocities for slopes of 1% and 10% taken from the figure for each land use type.

Using the travel time and flow direction across each grid cell, it is possible to track a particle of water from any point in a sub-basin to the low point of that sub-basin. Simultaneously, the travel time from the grid cell to the low point of the sub-basin is determined. The maximum travel time from any point in a sub-basin to the low point or discharge point is defined by SCS to be the time of concentration for the basin. Similarly, if a grid cell contains a river or stream, the computed travel time from that point is a channel travel time. Using this channel travel time and the summed length across grid cells, an average channel velocity is calculated. This velocity is later used to compute a channel routing coefficient as outlined in the description of the SCS hydrologic model.

3.2 Hydrologic Analysis

Hydrologic analysis here deals with the quantitative relationship between precipitation and surface water flow. A parameter of critical importance in developing a hydrologic model is the time scale over which the important processes operate. This may range from minutes for a single storm analysis to days or longer for an analysis of changes in annual water flow over several years. The analysis undertaken in this research program deals with individual storms. For that reason, many components of the hydrologic cycle may be ignored or assumed to remain constant during the analysis. This includes such processes as groundwater recharge and discharge, vegetative interception of precipitation, soil moisture changes, evaporation and transpiration of moisture, and others. On the other hand, the results of such a short time analysis are critically affected by the temporal characteristics of the river basin. Basin shape, slope, distribution of hydrologically important parameters such as soil type, velocity of overland and stream channel flow, and storage characteristics of surface water features must be considered in the analysis. Much of the hydrologic analysis is based on techniques developed by the U.S. Soil Conservation Service and reflected in their TR-20 Computer Program for Project Formulation. However, rather significant modifications have been made to accommodate the particular problem of interest here. For this reason a

complete review of the analysis techniques will be presented.

The approach taken here emphasizes the spatial variability of hydrologically important variables so that relatively small areas may be differentiated. This approach is closely related to the concept of partial area contributions which is receiving increased attention in hydrologic analysis (Engman, 1974). A simplified scheme of moisture accounting is employed whereby precipitation is divided into only two components: runoff and losses. The latter component encompasses all non-runoff hydrologic reservoirs, including vegetative interception, soil moisture storage, evapotranspiration, and ground water storage. The temporal variability of runoff is based both on the variation of rainfall intensity and on the effect of surface storage as reflected in a standardized unit hydrograph shape. Application of the hydrologic model includes: (1) discretization of the watershed, (2) development of unit hydrographs reflecting characteristics of each sub-basin, (3) calculation of incremental runoff volume for each timestep of a rainfall hyetograph, (4) development of a sub-basin hydrograph by step-wise convolution of the incremental runoff with the unit hydrograph, (5) routing of the sub-basin hydrograph through the basin, and (6) summing of the various sub-basin contributions. The following descriptions are not necessarily given in the order of their use in

applications, but rather in the manner the model was developed.

3.2.1 Computation of Sub-Basin Runoff

It is commmonly accepted that runoff from a watershed does not have a simple linear relationship to the quantity of precipitation falling on it. Small storms and the early stages of larger storms may produce essentially no immediate runoff. On the other hand, in the latter stages of a large storm, virtually all of the precipitation may enter the surface water system within a very short time. This condition is reflected in Figure 2 relating cumulative runoff to cumulative rainfall. Note that the curve is non-linear, has a non-zero intercept on the rainfall axis, and is assymptotic to a 45-degree slope. Both the intercept value and the rate at which this curve approaches the 45-degree slope are reflections of hydrologic conditions of the surface. The Soil Conservation Service method employed here represents this curve by the following empirical expression.

$$Q = \frac{(P-0.2S)^2}{P+0.8S} \qquad P > 0.2S$$

(3-7)

$$Q = 0 \qquad P \leq 0.2S$$

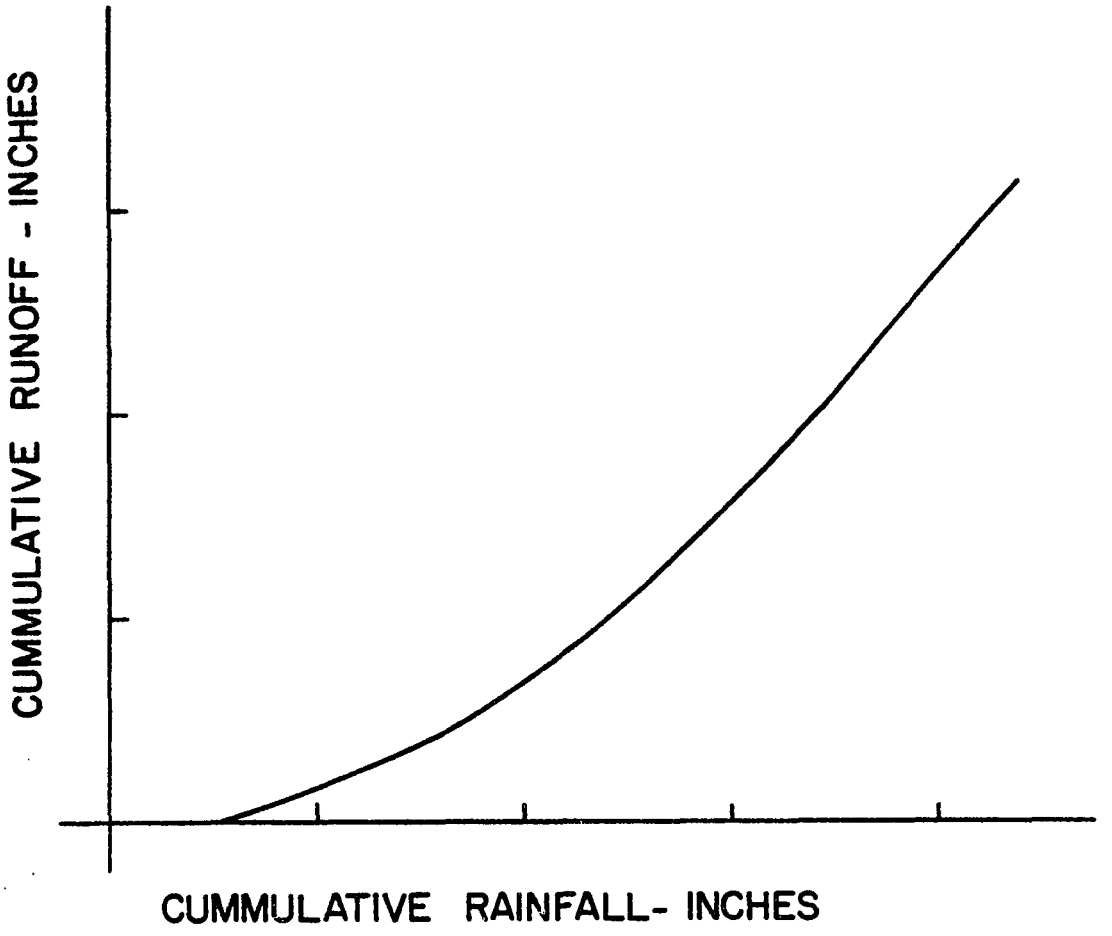

FIGURE 2

GENERALIZED NON-LINEAR RUNOFF / RAINFALL RELATIONSHIP

Where Q is the cumulative runoff in inches

P is the cumulative rainfall in inches

S is an index of surface condition related to soil type, land use and antecedent moisture levels.

They have further defined a Runoff Curve Number that is related to S as follows:

$$S = \frac{1000}{CN} - 10 \qquad 0 < CN < 100 \qquad (3\text{-}8)$$

where CN is the Runoff Curve Number.

Inspection of these equations shows that a limiting value of CN=100 would result in immediate initiation of runoff as rainfall begins and a cumulative runoff volume equal to the cumulative precipitation volume for the entire storm. On the other hand, a CN value approaching zero would prevent generation of any runoff. Intercept values for the onset of runoff, Po, for various runoff curve values are given below.

CN	Po - inches
100	0
80	0.5
60	1.33
40	3.00
20	8.00

In practice, the computation of sub-basin hydrographs requires that a runoff time series be generated from a rainfall time series using a time step consistent with an available unit hydrograph. Each increment of runoff is then multiplied by ordinates of the unit hydrograph to produce an incremental outflow hydrograph. Summation of these incremental hydrographs gives the complete sub-basin hydrograph.

The non-linearity of the runoff-rainfall curve is important to the overall hydrologic analysis. Hydrologic surface conditions, as reflected in parameter CN or S, vary dramatically within a small area. For example, runoff volume from an open pasture will be very different from that of an adjacent shopping center. Ideally, different hydrographs would be generated for each hydrologically different area. Pragmatically, such an approach is unreasonable for all but the smallest watershed. It is therefore necessary to aggregate small hydrologically diverse areas into larger sub-basins. An appropriate

method for computing representative properties of the sub-basin must therefore be developed.

The partial area theory of hydrology is based on the premise that at any time only a part of a watershed is contributing runoff to the surface water system. These partial areas are small at the beginning of a storm but continuously increase in size and intensity of runoff as rainfall continues. It is postulated here that these partial areas may be identified with the SCS Runoff Curve Number. Based on this premise, it matters little whether a CN of say 50 is generated by soil type X and land use M, or by soil type Y and land use N. The areas will produce identical runoff hydrographs when exposed to identical rainfall. The first level of aggregation within the sub-basin is therefore to combine areas of identical runoff curve number.

Unfortunately this still leaves a potential of 100 hydrologically different areas within a sub-basin if we consider integer values of CN from 1 to 100. It is therefore necessary to further aggregate areas within the sub-basin. This is done by selecting a number of discrete sets within the 100 integer values. Based on several trial distributions the sets finally selected for this work are as follows:

$$0<CN<35 \qquad (3\text{-}9a)$$

$$35<CN<71 \qquad (3\text{-}9b)$$

$$71<CN<89 \qquad (3\text{-}9c)$$

$$89<CN<97 \qquad (3\text{-}9d)$$

$$97<CN<100 \qquad (3\text{-}9e)$$

The range encompassed by each set is smaller at the higher curve numbers because of their greater significance in the total runoff quantity. It is assumed that areas having curve numbers within these sets may be linearly apportioned to the two end points. An area having a CN of 53, for example, would be divided half to CN-35 and half to CN-71. Due to the non-linearity of the runoff-rainfall relationship, this results in a small overestimate of runoff. This is illustrated in Table 6 which gives cumulative runoff for several CN values which are also computed using the proposed aggregation.

The overestimate is most significant for lower curve numbers and smaller rainfalls. It would be possible to adjust for this over-estimate. However, several trial runs of the SCS model produced inadequate runoff for small storms. For this reason, no adjustment was made in the modified model.

Application of this aggregation procedure results in six partial areas within each sub-basin, each with a uniform Runoff Curve Number. The CN-0 partial area can produce no runoff and is therefore ignored. In practice this is unlikely to account for more than one or two percent of the total area of a watershed. At the other end of the scale, the highest curve number expected for any combination of land use and soil type is 98, and generally

Table 6

Cumulative Runoff for Incremented Curve Numbers

CN	PRECIP	CALC. RUNOFF	AGGREGATED RUNOFF
50	1	0	0.003
50	2	0	0.111
50	3	0.263	0.317
75	1	0.030	0.069
75	2	0.38	0.435
75	3	0.96	1.013
90	1	0.32	0.337
90	2	1.09	1.107
90	3	1.98	1.992

only very large, elaborately sewered parking areas would produce this value. Therefore, the CN-100 area is also likely to be a small percentage of the basin of interest here. Only a small error results from lumping the CN-100 area into the CN-97 area, and this approach has been taken. The final apportionment of area is therefore reflected in partial areas with curve numbers 35, 71, 89 and 97. At each timestep of the analysis, cumulative runoff is calculated for each area by application of equation (3-7) to the cumulative rainfall.

3.2.2 Development of Unit Hydrographs

A sub-basin unit hydrograph describes the temporal variation of sub-basin outflow rate due to uniform application of a unit volume of runoff to the sub-basin. Extensive study of such hydrographs by hydrologists has led to commonly accepted relationships between their shape and characteristics of the sub-basin. Figure 3 illustrates several important parameters of a unit hydrograph.

The parameters illustrated here are defined as follows. Dimension D is the duration of the uniformly applied runoff volume which results from an incremental rainfall. Dimension Tc is the time from the end of runoff application to the inflection point of the falling limb of the hydrograph. A common way of estimating this value is to compute the time required for a particle of water to

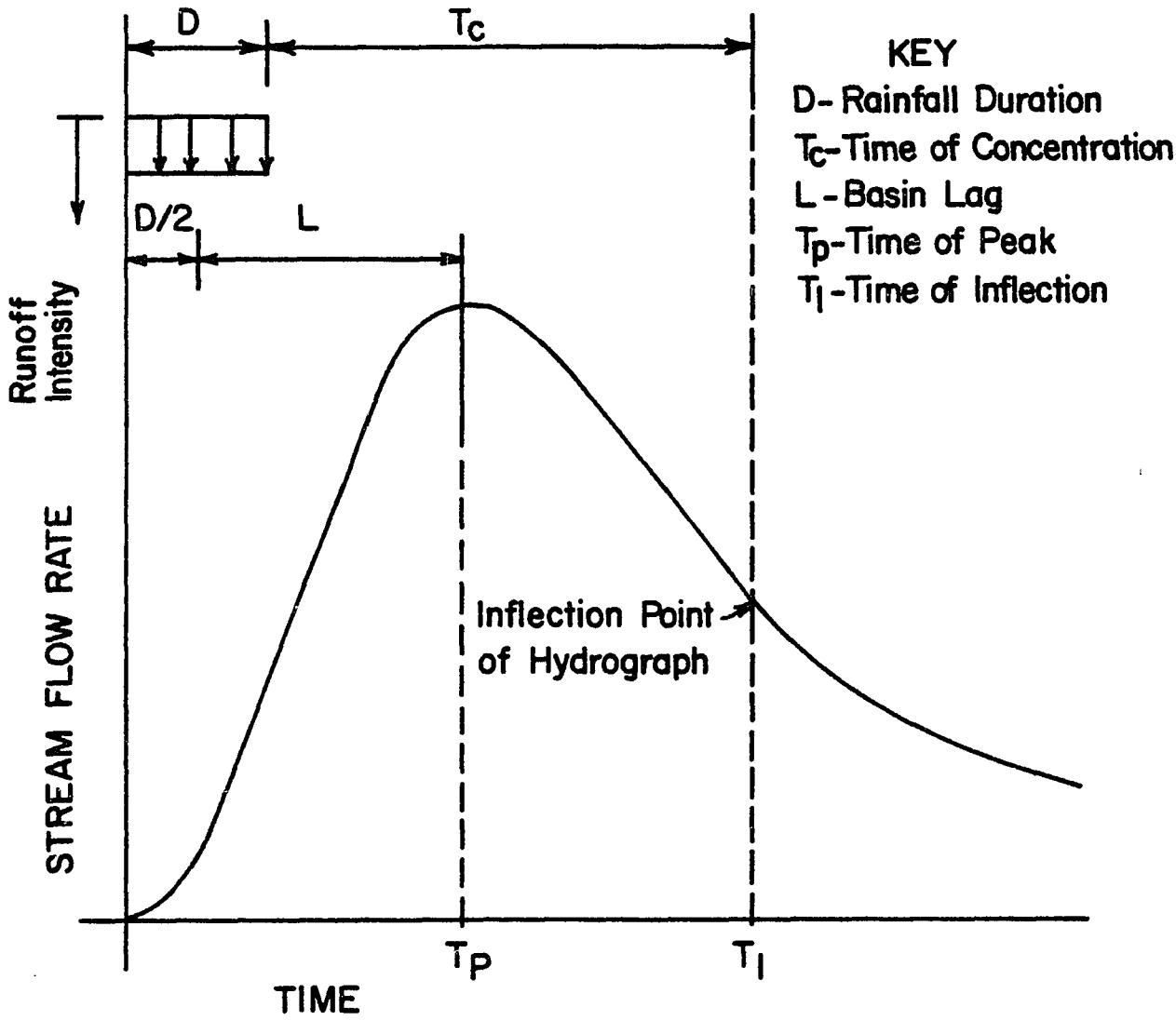

FIGURE 3

HYDROGRAPH RELATIONSHIPS

flow from the most remote point of the sub-basin to the discharge point. This dimension is therefore defined as the basin "time of concentration." Dimension L is the time from the mid-point of runoff application to the peak of the hydrograph. This dimension is referred to as the sub-basin "lag." A common way of estimating this dimension from sub-basin characteristics is to multiply the sub-basin time of concentration by 0.6. On the basis of these definitions we may state:

$$T_P = D/2 + L = D/2 + 0.6\ T_C \qquad (3\text{-}10)$$

$$T_I = D + T_C \qquad (3\text{-}11)$$

where D = rainfall duration

T_C = time of concentration

L = basin lag

T_P = time of peak

T_I = time of inflection

After review of many unit hydrographs, the SCS has developed a standardized hydrograph shape which has gained widespread acceptance. In the absence of very complete field observations of rainfall-outflow relationships, this standardized shape can be used to develop a sub-basin unit hydrograph. The SCS dimensionless unit hydrograph is shown on Figure 4. The important characteristics of this hydrograph are the following: (a) The inflection point is

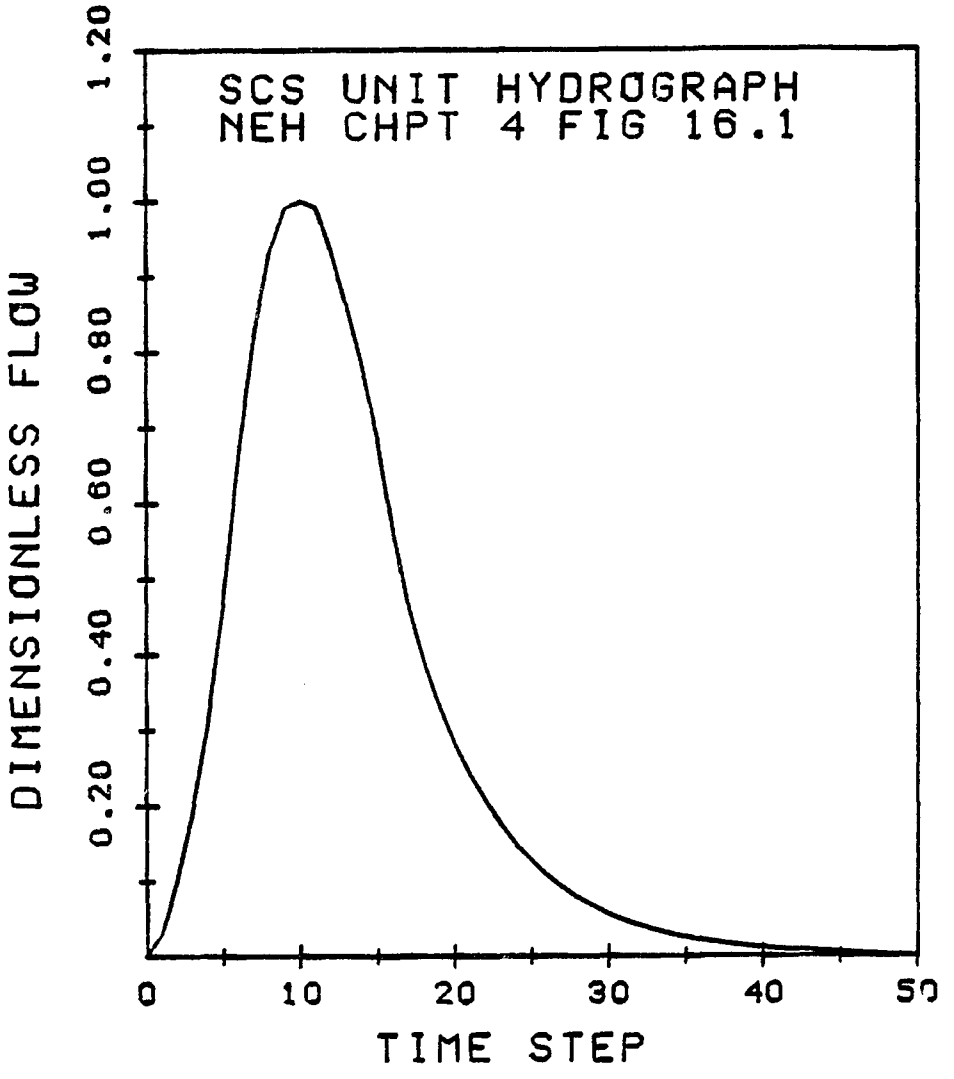

FIG 4 SCS UNIT HYDROGRPH

located at a point 1.7 times the time to peak of the hydrograph. (b) The duration of the outflow hydrograph is five times the time to its peak flow. c) The volume of water contained on the rising limb side of the hydrograph is 37.5% of the total outflow volume.

The peak flow is calculated from the following formula:

$$q_p = 484\,AQ\;T_p \qquad (3\text{-}12)$$

where q_p = peak flow in CFS

A = sub-basin area in square miles,

Q = total volume of runoff in inches over the entire sub-basin,

Tp = time to peak of the hydrograph in hours

From these equations and the characteristics of the dimensionless unit hydrograph it can be readily shown that:

D = o.1333 Tc

Tp = o.6667 Tc

For any given sub-basin, a unit hydrograph is completely defined by knowing its time of concentration, T_C . Application of the unit hydrograph requires that the runoff time increment be equal to D. In practice it is more convenient if D is equal to an exact fractional portion of the input rainfall timestep. Small deviations of D from the required value of 0.1333 T_C do not result in

any significant error.

A complete sub-basin outflow hydrograph is developed by convolution of the runoff time series with the sub-basin unit hydrograph. The convolution process is defined by the so-called convolution integral:

$$y(t) = \int_0^\infty h(\tau)x(t-\tau)d\tau \qquad (3\text{-}13)$$

where x is a function describing the input (runoff),
h is a weighting function describing the response of the system to a unit impulse applied at time τ before (unit hydrograph),
y is a function describing the response of the system to x (outflow).

It is often convenient to replace this integral formulation by the equivalent algebraic expression:

$$Y(f) = H(f) * X(f) \qquad (3\text{-}14)$$

where Y , H , and X are Fourier transforms of the corresponding terms of the convolution integral. Application of this simpler expression is dependent on existence of convenient forms of Fourier transforms H and X and an inverse transform of Y. It is, of course, possible to make use of finite Fourier transform techniques to carry out these operations.

Discrete data can also be processed numerically on a digital computer. This approach is used here for performing the required convolutions. In this form the convolution is represented by

$$HYD(T) = \sum_{n-1}^{N} UNIHYD(n)*RUNOFF(T-n\Delta t) \qquad (3\text{-}15)$$

where HYD(T) = outflow hydrograph value at time $T = m\Delta t$

UNIHYD(n) = the nth value of the unit hydrograph with timestep Δt

RUNOFF($T-n\Delta t$) = the runoff volume during a timestep at at time $t-n\Delta t$

Δt = the time increment applicable to the hydrograph

3.2.3 Contaminant Washoff and Pollutographs

The generation and washoff of contaminants is based on algorithms developed for the EPA Non-Point Source Model. These algorithms were intended to allow use of comparable techniques for computing washoff from both pervious and impervious land areas. The techniques are based on computation of sediment washoff as the key indicator of non-point source contaminants. All other materials are estimated by applying a "potency factor" to sediment. In the EPA model sediment washoff is calculated for a fifteen-minute timestep. Resulting contaminant washoff is then determined for a timestep equal to that of the pollutograph, and a complete time series or pollutograph is developed. Because these algorithms were developed for use with an updated version of the Stanford Watershed Model, they were not directly applicable to the hydrologic analysis of the Soil Conservation Service model. Significant modifications are contained in the version of these techniques used here and described below. Completely new computer coding was necessary to apply them to the SCS model results.

The computation of a contaminant time series is completely described by the following eight equations.

Soil Fines Detachment: RER (t) in tons/acre

$$RER(t) = (1\text{-}Cover)*KRER*PR(t)**JRER \qquad (3\text{-}16)$$

Soil Fines Overland Transport: SER (t) in tons/acre

$$SER(t) = KSER*OVFACT*OVQ(t)**JSER \quad SER(t) < SRER(t-1) \qquad (3\text{-}17)$$

Soil Fines Loss To Stream: ERSN (t)

$$ERSN(t) = SER(t)*FP*AP*4*DELTM \qquad (3\text{-}18)$$

Soil Fines Reservoir: SRER (t) in tons/acre

$$SRER(t) = SRER(t-1)*RER(t) - ERSN(t) \qquad (3\text{-}19)$$

Dust & Dirt Overland Transport: TSS (t) in tons/acre

$$TSS(t) = KEIM*OVQI(t)**JEIM \qquad (3\text{-}20)$$

Dust & Dirt Loss to Stream: EIM (t)

$$EIM(t) = TSS(t)*FI*AI*4.DELTM \quad (3\text{-}21)$$

Dust & Dirt Reservoir: TS (t) in tons/acre

$$TS(t) = TS(t\text{-}1) - EIM(t) \quad (3\text{-}22)$$

Contaminant Loss to Stream: POL (t)

$$POL(t) = PMP*ERSN(t)*PMI*EIM(t) \quad (3\text{-}23)$$

The terms of these equations are similar to but not identical with those in the EPA model. They are discussed further below.

Soil fines detachment refers to material dislodged from pervious areas by raindrop impact. It only occurs during rainfall and serves to increase the amount of material available for washoff. Detachment is calculated as an exponential function of PR(t), the amount of rain in inches occurring during a fifteen-minute timestep. The function is defined by constant KRER and exponent JRER. The term (1-Cover) takes account of the shielding effect of vegetation which allows raindrop impact on only part of the total area.

Soil fines overland transport is the total amount of

sediment being carried by OVQ(t), the overland flow in inches per fifteen-minute timestep across pervious areas. It is also described by an exponential function characterized by constant KSER and exponent JSER. It is important to note that not all material being transported will reach the stream or discharge point from the sub-basin during the fifteen-minute timestep. This is reflected in factor FP, the proportion reaching the stream. Soil fines loss to the stream is calculated using the total pervious area in acres, AP, and is adjusted for the length of pollutograph timestep, DELTM. At each timestep the reservoir of fines available for transport is increased by the amount of raindrop detachment and decreased by the amount of loss to streams.

Dust and dirt represents sediment on impervious areas, particularly paved portions of the sub-basin. Computations are similar to those for pervious areas except no additional material is generated during a storm. Dust and dirt accumulation takes place only between storms and is reflected in the pre-storm value of the dust and dirt reservoir.

The resulting pollutograph is given as contaminant loss to the stream, POL(t). This loss is calculated by multiplying soil fines loss, ERSN(t), and dust and dirt loss, EIM(t), by appropriate contaminant potency factors. Each contaminant of interest is represented by two values of these factors.

A most important aspect of the contaminant computation is the relationship to the hydrology of the basin. This is reflected in terms OVQ(t) and OVQI(t), the total overland flow on pervious and impervious areas, repectively, during a fifteen-minute timestep and factors FR and FI, the proportions of flow reaching the stream during a pollutograph timestep. The calculation of these key variables is described below. Average runoff rate in inches per hydrograph timestep is calculated using the SCS cumulative runoff formula as follows:

$$Q = \frac{(P2-0.2S)^2}{P2+0.8S} - \frac{(P1-0.2S)^2}{P1+0.8S} \qquad (3\text{-}24)$$

where Q = inches of runoff generated during the timestep

P1 = cumulative rainfall at start of timestep

P2 = cumulative rainfall at end of timestep

S = the SCS runoff characteristics for the area

Generally, the hydrograh timestep will not be equal to either the rainfall timestep or the fifteen-minute timestep of the contaminant washoff rate computation. For these calculations it is assumed that the rainfall rate, runoff rate and resultant contaminant washoff rate are all constant during the hydrograph timestep. Because of the exponential formulas used in several calculations, short term peak intensities may result in errors not readily compensated for.

The total volume of water in acre-inches on the surface available to transport contaminants is represented by the sum of this additional runoff, Q, and any water left after computation of discharge to the stream at the previous timestep. This storage includes both pervious and impervious area values and reflects the surcharging effect of water which must have a finite depth on the surface. The total surface flow is represented by:

$$TF = Q*(AI+AP)+STI+STP \qquad (3\text{-}25)$$

where TF = total flow

AI = impervious area (acres)

AP = pervious area (acres)

STI = impervious storage (acre-inches)

STP = pervious storage (acre-inches)

It is now assumed that essentially all of the storage and rainfall occuring on impervious areas is available for surface flow. Impervious area surface flow in acre-inches during the hydrograph timestep is therefore calculated as the lesser of

$$IF = (P2-P1)*AI+STI \tag{3-26}$$

$$IF = TF \tag{3-27}$$

By difference, the pervious area surface flow in acre-inches during the hydrograph timestep is

$$PF = TF - IF \tag{3-28}$$

The values of OVQ(t) and OVQI(t) in inches per fifteen minutes are calculated from these flows for each hydrograph timestep as follows:

$$OVQI(t) = IF/(AI*4*DELTM) \quad (3\text{-}29a)$$

$$OVQ(t) = PF/(AP*4*DELTM) \quad (3\text{-}29b)$$

Since not all of this flow reaches the stream during any timestep, discharge factors FI and FP must be calculated using the hydrograph value determined by the hydrologic model. The hydrologic model does not differentiate between water generated on the pervious and impervious portions of a sub-basin. Therefore, some method must be devised to allocate the hydrograph value between these two flows. It has been assumed that flow on pervious areas will move to surface streams more slowly than flow on impervious areas. This will reflect itself in a smaller value for the pervious area discharge factor. A ratio of 2 to 1 between impervious and pervious discharge factors was arbitrarily assigned. Therefore:

$$FP = 0.5*FI \quad (3\text{-}30)$$

Since the total hydrograph must be equal to the sum of appropriate fractions of the pervious and impervious total flow, this leads to

$$HYDSTO(t) = PF*FP+IF*FI \tag{3-31}$$

$$HYDSTO(t) = PF*0.5*FI+IF*FI \tag{3-32}$$

Therefore

$$FI = \frac{HYDSTO(t)}{0.5*PF+IF} \tag{3-33}$$

and

$$FP = 0.5*FI \tag{3-34}$$

where HYSTO(t) is the hydrograph flow in acre-inches during the hydrograph timestep.

At the end of each timestep the storage reservoirs STI and STP are recalculated to reflect the current remaining water as follows:

$$STI = IF*(1-FI) \quad (3\text{-}35)$$

$$STP = PF*(1-FP) \quad (3\text{-}36)$$

Using the computed values of overland flow on pervious and impervious portions of the area, corresponding values of soil fines transport and dust and dirt transport are determined for each fifteen-minute timestep. In the calculation of soil fines transport, a factor, OVFACT, appears (equation 3-17). This factor reflects the existence of both direct overland flow and interflow through the loose upper layer of soil. It is assumed that only the former is effective in transporting sediment, and hence the value of OVQ is multiplied by a factor whose value ranges between 0 and 1.0.

Computation of the contaminant flow time series employs "potency factors" which are multiplied times the computed soil fines loss and dust and dirt loss to the stream. Ideally, these factors will be determined by field investigations of representative land use areas. However, in the absence of such studies, data is available in the

literature for the relationship between contaminant flow and sediment flow (contaminant potency factor).

As noted previously, each storm is considered an isolated event, and the antecedent hydrologic and initial contaminant conditions of the basin must be specified. An Antecedent Moisture Index (AMI) is used to define the soil moisture conditions before a storm. A value of 1 indicates dry conditions which result in increased loss of moisture due to infiltration. A value of 3 indicates wet conditions which result in decreased infiltration and hence greater runoff. A value of 2 is considered a normal condition. Intermediate values can also be employed to approximate other conditions, but field data must be available to justify this greater precision. The moisture index is used in the model to adjust the specified runoff curve numbers upward or downward as necessary to reflect the change in runoff. A maximum adjustment of $\pm$ 20 occurs for curve numbers near 50. Extreme curve numbers of 0 or 100 are not changed at all with differing moisture indices. For each storm of interest, the appropriate antecedent moisture index must be selected based on knowledge about the recent rainfall history.

Initial contaminant conditions are specified for each runoff area. This is done by assignment of an initial value for the soil fines reservoir SRER and the dust and dirt reservoir EIM. If a sequence of storms is to be analyzed, it is desirable to give consideration to both the

final reservoir amounts after the preceding storm and the accumulation of contaminants which may occur between storms.

If accumulation of contaminant were considered a simple linear process employing a uniform rate, an unlimited increase would be possible. In reality losses also occur within the system due to wind transport, street cleaning and other housekeeping operations. These may be represented by a first order decay of contaminant load. The EPA model employs a daily computation of both accumulation and decay. For convenience, the discrete computation can be replaced by a continuous representation as follows:

let R_C = first order decay rate (1/day)

A_C = accumulation rate (wt/day)

C_C = contaminant load

Then

$$\frac{dC_C}{dt} = A_C - C_C R_C \qquad (3\text{-}37)$$

Solution of this differential equation leads to the following representation for initial condition at the second or subsequent storms.

$$SRER = SRER_0 * \exp(-R_{RER} * T) + A_{RER} * T \qquad (3\text{-}38)$$

where SRER & EIM = initial conditions for next storm

$SRER_0$ & EIM_0 = final condition for previous storm

R_{RER} & R_{EIM} = decay coefficients

A_{RER} & A_{EIM} = accumulation rates

T = length of time between storms

It can be readily shown that at steady state the reservoir values are

$$SRER_{(SS)} = A_{RER}/R_{RER} \tag{3-40}$$

$$EIM_{(SS)} = A_{EIM}/R_{EIM} \tag{3-41}$$

3.2.4 Routing of Hydrographs and Pollutographs

Having developed hydrographs and pollutographs for sub-basins, it is necessary to translate these time series downstream through the balance of the watershed. This process is called "routing." Distinction is often made between routing through rivers and streams, called channel routing, and through ponds or impoundments, called reservoir routing. The distinction is based on the relative importance of various dimensional and dynamic characteristics of the system.

Routing techniques can be developed from the basic hydraulic equations of continuity and conservation of energy. In the absence of lateral flow into the river reach or reservoir, these equations are

$$B\frac{\partial H}{\partial t} + BV\frac{\partial H}{\partial x} + A\frac{\partial V}{\partial x} = 0 \tag{3-42}$$

$$\frac{\partial H}{\partial x} + \frac{\beta}{g}\frac{\partial V}{\partial t} + \alpha\frac{V}{g}\frac{\partial V}{\partial x} = S_0 - S_f \tag{3-43}$$

where B = width

V = velocity

A = area

g = gravity

α, β = coefficients for flow distribution

S_0 = bottom slope

S_f = friction slope

H = water depth

Because of the complexity of a complete hydraulic analysis using these governing equations, empirical hydrologic routing techniques have also been developed. These methods are based on a simplified version of the continuity equation referred to as the storage equation:

$$\frac{dS}{dt} = I - O \qquad (3\text{-}44)$$

where ds/dt = rate of change of water volume within the reach

I = upstream inflow rate

O = downstream outflow rate

The energy conservation equation is replaced by an empirical expression relating water surface profile (and hence volume of water stored within the reach) to the inflow and outflow rates. One of the most universally applied hydrologic routing methods, the Muskingum method, is based on the following storage-flow relationship:

$$S = [XI+(1-X)O] \tag{3-45}$$

where S = total volume stored in the reach

K = a constant having units of time

X = a coefficient whose value lies between O and O.5

If it is assumed that storage volume, inflow and outflow all vary linearly during the routing timestep, equations (3-44) and (3-45) lead to:

$$\frac{S_2-S_1}{\Delta t} = \frac{I_1+I_2}{2} - \frac{O_1+O_2}{2} \tag{3-46}$$

$$S_2-S_1 = K[X(I_2-I_1)+(1-X)(O_2-O_1) \tag{3-47}$$

where subscripts 1 and 2 refer to conditions at the beginning and end of the timestep, respectively. These equations may be readily solved for the outflow at the end of the timestep, as a function of inflows at the beginning and end of the step, and outflow at the beginning.

$$O_2 = C_0I_2 + C_1I_1 + C_2O_1 \tag{3-48}$$

$$C_0 = \frac{-KX+.5\Delta T}{K-KX+.5\Delta T} \tag{3-49}$$

$$C_1 = \frac{KX+.5\Delta T}{K-KX+.5\Delta T} \tag{3-50}$$

$$C_2 = \frac{K-KX-.5\Delta T}{K-KX+.5\Delta T} \tag{3-51}$$

These equations form the basis of the Muskingum routing method. Application requires that equation (3-48) be employed in an explicit timestepping process to develop values for the outflow at each timestep. The storage time constant and coefficient X are determined from field data on inflow and outflow for the river reach. Timestep Δt must be small enough to adequately represent the shape of the hydrographs. Additionally, both physical and mathematical considerations require that the timestep be less than the travel time of water through the reach.

In practice, the value of coefficient X will usually lie between 0.2 and 0.3 for typical river cross sections. In the absence of other data, a value of 0.25 is a reasonable first approximation. The time constant K may also be estimated if field data is lacking. If we examine equation (3-45) for the case of uniform flow with inflow and outflow equal, it becomes

$$S = KQ \qquad (3\text{-}52)$$

where Q is the flow through the reach.

For a river reach with uniform flow, the storage volume is also represented by

$$S = AL \tag{3-53}$$

where A = cross sectional area

L = length of reach

Therefore,

$$K = AL/Q \tag{3-54}$$

However, since

$$A/Q = 1/V \tag{3-55}$$

and

$$\frac{1}{V} * L = \text{Travel time through the reach} \qquad (3\text{-}56)$$

the value of K for this condition is equal to the travel time of a particle of water through the river reach. In the absence of field data, it is common practice to estimate the value of K for other conditions by the travel time.

The hydrologic analyses employed here use the "Convex Routing Method" of the Soil Conservation Service. The development of the method is described in Chapter 4 of their National Engineering Handbook (SCS, 1966). However, it is also possible to develop the governing equations as a special case of the Muskingum method. In order to gain further insight into the convex method and allow its extension to routing of contaminants, its relationship to the Muskingum method is described below.

$$KX = 0.25 * T \qquad (3\text{-}57)$$

$$\Delta T = 0.5 * T \qquad (3\text{-}58)$$

where T = travel time through the reach. Therefore,

$$KX = 0.5\ \Delta T \tag{3-59}$$

Substituting this value for KX into equations (3-49) through (3-51), we get the following values for the Muskingum coefficients:

$$C_0 = 0$$

$$C_1 = 2X \tag{3-60}$$

$$C_2 = 1-2X$$

The Muskingum routing equation then becomes

$$O_2 = 2XI_1 + (1-2X)O_1 \tag{3-61}$$

If we now replace the term 2X by a coefficient C, the convex routing equation is obtained:

$$O_2 = (1-C)O_1 + CI_1 \qquad (3\text{-}62)$$

This routing formula has the advantage that outflow at the subsequent timestep is independent of inflow at that future time, thus simplifying calculations.

It now remains to select a value for the SCS routing coefficient, C. Selection of this value is based on further consideration of the physics of flood wave passage through a river reach. A wave disturbance at the upper end of a reach is propagated at a velocity which is independent of the translational velocity of an individual water particle and is often referred to as the celerity. If no change in storage volume is allowed between the ends of the reach during passage of the wave, and the flow is incompressible, the wave will pass through the reach unattenuated. The average velocity of water particles in this unattenuated wave must, therefore, be equal to the celerity of the wave. This condition is representative of surges in a pipe which is flowing full under pressure. For these conditions, consider a routing timestep equal to the travel time of the wave:

$$\Delta T = L/V_c \qquad (3\text{-}63)$$

where L = the length of reach, and V_C = celerity of the wave.

Under the conditions described above, where velocity equals celerity downstream, outflow at the end of the timestep will be equal to inflow at the beginning of the timestep.

If this case is applied to the routing equation, it requires that outflow O_2 be equal to inflow I, and therefore implies a value of 1.0 for C.

$$O_2 = (1.-1.0)O_1 + 1.*I_1 \qquad (3\text{-}64)$$

This defines an upper limit of C = 1.0 when the velocity of water particles, V, equals the wave celerity V_C.

Consider now a case where a very large storage volume is available within the reach. Virtually all of the inflow will be dissipated, and the outflow will be unaffected by an upstream flood wave. The average net velocity of water through the reach will be essentially zero. This condition is represented by a large reservoir fed by a small stream.

If this case is applied to the routing equation, it requires that outflow O_2 be unaffected by inflow and therefore implies a value of 0.0 for C.

$$O_2 = (1.-0)*O_1 + 0*I_1 \qquad (3\text{-}65)$$

This defines a lower limit of C = 0.0 when the velocity of water particles, V, equals zero. If a linear variation of C between these extreme cases is assumed, the SCS formula for C results:

$$C = \frac{V}{U_C} \tag{3-66}$$

This procedure requires that the wave celerity be calculated. Shallow water wave theory allows computation of a theoretical clerity

$$U_C = \sqrt{gh} \tag{3-67}$$

where g = acceleration of gravity

h = water depth

However, natural streams do not necessarily meet the assumptions of a shallow water wave. Empirical evidence is presented in Figure 17-13, Chapter 4, SCS National Engineering Handbook (SCS, 1966), which establishes the following relationship:

$$U_C = V + 1.7 \tag{3-68}$$

Application of this relationship gives the final form of the routing coefficient expression:

$$C = \frac{V}{V+1.7} \tag{3-69}$$

When applying the SCS routing method to contaminant pollutographs, it is necessary to re-evaluate the assumptions made in its development. In particular, the concepts of wave propagation and storage volume are not directly applicable to contaminant transport.

The concept of wave propagation which translates kinetic energy at a different velocity than water particle velocity permits downstream flow to incorporate different water particles than those contained in upstream flow. Contaminant propagation, however, requires that the actual particles of water be transported downstream. Furthermore, the storage concept employed in one-dimensional routing of

hydrographs requires that no significant cross channel elevation gradients exist and that stored water is uniformly distributed across the channel. Contaminant flow, on the other hand, is characterized by significant lateral gradients. Transport of contaminants may be confined to a high velocity stream near the center or deep section of the channel, with little flow or storage in other parts of the cross section. The routing coefficient must reflect these conditions.

If we first consider direct application of the convex routing method to contaminant routing, an error in effective translation velocity occurs. The convex method requires that the time lag between inflow and outflow of a reach be related to the wave celerity. Contaminant flow must be propagated at the velocity of water particles through the reach. Therefore, contaminant travel time is underestimated, and the pollutograph is moved through the reach too quickly. Alternatively, we may assume that the pollutograph is moved at the average velocity of water particles through the reach, previously defined by V. If the contaminant is transported in a higher velocity core (often called short circuiting), the latter method will overestimate the travel time. It is reasonable, therefore, that the correct velocity of transport is somewhere between the average velocity, V, and the celerity, V_C . Celerity has been previously indicated to be approximatly 1.7 times the velocity. Hence, contaminant velocity will lie in the

range:

$$1.0*V<V_C<1.7*V \qquad (3\text{-}70)$$

A reasonable first estimate of 1.35V has been employed in the non-point source model. Improvements in this estimate are possible through calibration against field data for average time of travel through a stream reach. The method employed here does not give consideration to any attenuation of the pollutograph due to the routing process. In effect, the routing of contaminants is handled as plug flow at a velocity roughly 1/3 larger than the average velocity of water in the reach.

3.3 Model Application

The hydrologic and non-point source models operate on a grid of runoff areas and stream channels which represent the topology of the system. Reasonable dimensioning of variables in the model limits a run to approximately 25 sub-basins. Since each sub-basin is represented by four runoff areas (curve numbers 35, 71, 81 and 97), up to 100 areas are considered. These are interconnected by stream reaches through which hydrographs and pollutographs are routed. The original SCS model also contains provisions

for routing through reservoirs with known storage-elevation-outflow relationships. As necessary, this capability can also be employed. The model can consider up to three contaminants. If a basin containing more than approximately 25 sub-basins is to be analyzed, additional runs may be performed using the outflow hydrograph and three pollutographs from the upper basin as inflow to the lower basin. Complete output data includes hydrographs and pollutographs for each individual runoff area and each downstream point of the basin for a single storm, or a sequence of up to seven storms separated by dry periods.

CHAPTER 4

NUMERICAL ANALYSIS OF HYDRODYNAMICS & ESTUARY WATER QUALITY

The objective of this portion of the work was to model temporal and spatial distributions of key water quality constituents in a small tidal river resulting from stormwater discharges. The models are designed to represent the general conditions listed below:

1) River length on the order of 2 to 10 miles.
2) River width/length ratio less than 0.1.
3) River depth on the order of 0 to 50 feet with provision for mudflat regions.
4) Significant tides resulting in a tidal prism of the same order of magnitude as the low tide volume.
5) A flow regime which causes density stratification over all or part of the length.
6) Flushing time related primarily to fresh water flow.

While three-dimensional dynamic modeling could produce the most complete results, the extensive data requirements, calibration effort, and analysis time are prohibitive. Rather, this program has been directed toward enhanced one-dimensional modeling which represents the three-dimensional characteristics by approximate analytical

expressions, but maintains the dynamic one-dimensional numerical solution necessary to describe the impact of individual storm discharges.

One-dimensional analysis of water quality in an estuary requires data on flow velocity and cross sectional area. For a tidal river such as described above, flow velocity may range from zero to plus or minus five feet per second or more over a tidal cycle. Cross sectional area may change by a factor of two to three over the tidal cycle. It is therefore necessary that data be available continuously, or at least for 25 to 50 points of the tidal cycle. The velocity data must also be representative of the entire flow area throughout the length of the river.

Three techniques may be employed to develop the required flow and area data: 1) field measurement, 2) an analytical solution, and 3) numerical modeling. Field measurement of representative velocities and cross sectional areas over a tidal cycle would require a major effort for even the smallest tidal river. For this reason, this approach was not considered. If the tidal river geometry can be approximated as an appropriate function of longitudinal position along the river, an analytical solution is the best choice. The accuracy of results is related to how well the function fits actual river hydrography. In most cases, however, a numerical model is required to produce the required data.

4.1 One-Dimensional Hydrodynamic Model

A basic one-dimensional hydrodynamic model was developed by Harleman et al. (1969). Applicaton of such a model to the conditions described previously requires that the effect of density gradients and mudflats be considered. Density gradients affect the simple one-dimensional hydrodynamic analysis in two ways. First, the longitudinal density gradient results in a net upstream force which must be balanced by an increased slope of the water surface. This effect was investigated by Thatcher and Harleman (1972) who used a one-dimensional dispersion model to compute a dynamically varying salinity/density gradient. The second effect of density gradients is to generate a net circulation characterized by inward currents at the bottom of the estuary and outward currents at the surface. This effect has been investigated analytically by Officer (1977).

The hydrodynamic model developed here incorporates much of the basic Harlemann-Lee model and integrates a circulation analysis based on portions of the work of Thatcher and Officer. The objective of the model development has been to provide adequate velocity and flow area data for the water quality model without undue effort to generate an elaborate hydrodynamic analysis. Therefore the following strategy was applied.

The basic Lee model was modified as suggested by Thatcher but was not directly linked to a one-dimensional

dispersion model. Rather, the longitudinal density gradient is determined by an analytical solution for the tidal cycle averaged conditions. The density-driven net circulation is also developed analytically for tidal cycle averaged conditions as suggested by Officer. The effect of this net circulation on the water quality model is reflected in a tidal cycle averaged circulation dispersion coefficient at each segment of the estuary. The model description given below reflects the integration of these concepts.

4.1.1 Solution of the Governing Equations

By considering the motion of a discrete mass of water moving through an estuary, Harlemann and Lee developed the following governing equations for the one-dimensional model.

Conservation of mass (continuity) equation:

$$b\frac{\partial H}{\partial t} + \frac{\partial Q}{\partial x} - q = 0 \qquad (4\text{-}1)$$

where b = total width of the estuary

$\partial H/\partial t$ = rate of change of surface elevation

$\partial Q/\partial X$ = flow rate change at the cross section

q = lateral inflow rate per unit of length

The three terms represent the change in volume at the cross section, the difference between upstream and downstream flow rate, and the source flow added to the estuary at this location.

Conservation of energy (momentum) equation:

$$\rho \frac{\partial Q}{\partial t} + \rho \frac{\partial}{\partial X}(uQ) + \rho g \frac{\partial h}{\partial x} A + \rho g \frac{Q|Q|}{AC^2R} = 0 \qquad (4\text{-}2)$$

where $\partial Q/\partial t$= rate of change of flow per unit of length

uQ = flow momentum (velocity times flow rate)

g = acceleration

$\partial H/\partial X$ = surface slope

A = cross sectional flow area

C = Chezy function coefficient =

R_h = hydraulic radius of the flow region

n = Mannings friction coefficient

ρ = density of water

The four terms represent the local acceleration, the advective acceleration, the longitudinal force due to surface slope, and the friction force. It is important to note that this development allows use of a total width greater than the width of the flow region. In the continuity equation, the total width is used to evaluate changes in the total water mass in the cross section of interest. In the momentum equation, however, the flow area may be based on a smaller width. This recognizes the possible occurrence of a core area of flowing water with adjacent shore zones where little or no longitudinal flow occurs.

If we now consider a longitudinal density gradient due to differences in salinity, an unbalanced force will exist. Referring to Figure 5, pressure on the downstream side is higher by an increment ΔP than that on the upstream side.

$$\Delta P = \frac{\partial P}{\partial x} dx \qquad (4\text{-}3)$$

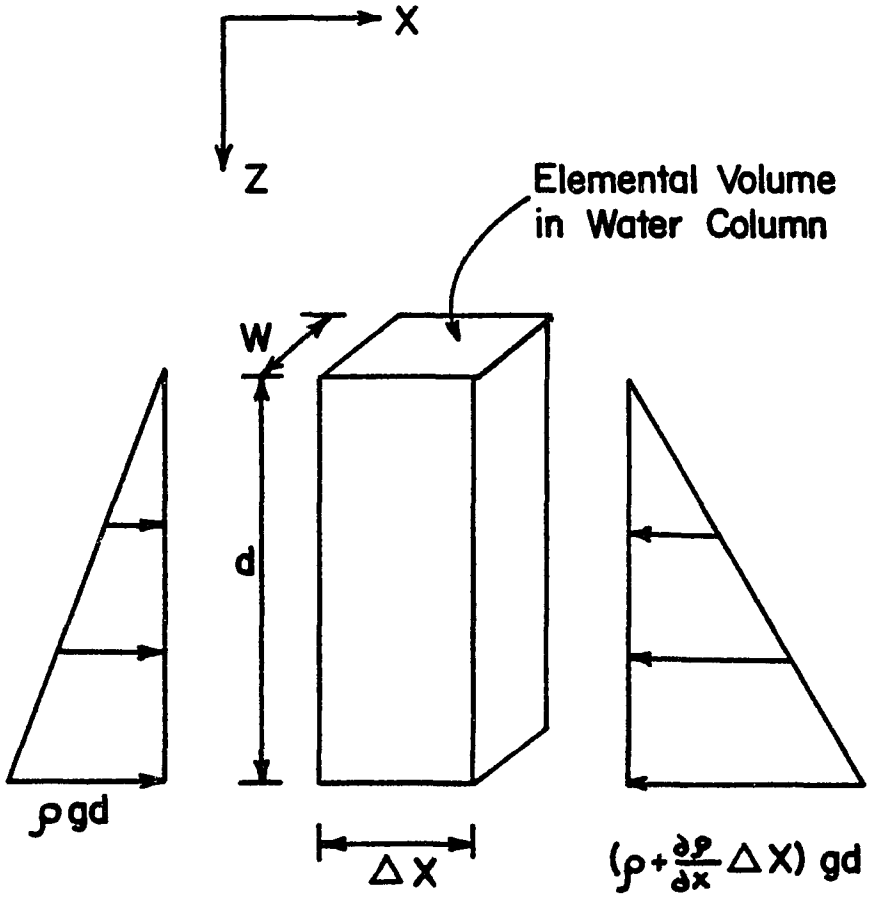

FIGURE 5

HYDROSTATIC FORCES DUE TO LONGITUDINAL DENSITY GRADIENT

This results in a net force, ΔF equal to

$$\Delta F = -\int_0^d \left(\frac{\partial P}{\partial x}\,\Delta x\right) g\, W\, z\, dz \qquad (4\text{-}4)$$

$$= \frac{\partial P}{\partial x}\,\Delta x g \int_0^d W\, z\, dz \qquad (4\text{-}5)$$

If the width, W, is constant over depth, this results in

$$\Delta F = -\frac{\partial P}{\partial x}\,\Delta x g\, W\, d\,\frac{d}{2} = -\frac{\partial P}{\partial x}\,\Delta x g\, A\,\frac{d}{2} \qquad (4\text{-}6)$$

or a rate of change of force per unit of length equal to

$$\frac{\Delta F}{\Delta x} = -\frac{\partial P}{\partial x}\, gA\,\frac{d}{2} \qquad (4\text{-}7)$$

Adding this term to the momentum equation and dividing by the density, ρ , yields

$$\frac{\partial Q}{\partial t} + \frac{\partial}{\partial x}(uQ) + g\frac{\partial h}{\partial x}A + g\frac{Q|Q|}{AC^2R} - g\frac{\partial P}{\partial x}\frac{Ad}{2\rho} = 0 \qquad (4\text{-}8)$$

Expansion of the nonlinear advective term (second term of this equation) leads to

$$\frac{\partial}{\partial x}(uQ) = u\frac{\partial Q}{\partial x} + Q\frac{\partial u}{\partial x} = \frac{Q}{A}\frac{\partial Q}{\partial x} + Q\frac{\partial}{\partial x}(Q/A) \qquad (4\text{-}9)$$

$$\frac{\partial}{\partial x}(uQ) = \frac{Q}{A}\frac{\partial Q}{\partial x} + Q\left[\frac{1}{A}\frac{\partial Q}{\partial x} + Q^2\frac{(1/A)}{\partial x}\right] \qquad (4\text{-}10)$$

$$\frac{\partial}{\partial x}(uQ) = \frac{2Q}{A}\frac{\partial Q}{\partial x} - \frac{Q^2}{A^2}\frac{\partial A}{\partial x} \qquad (4\text{-}11)$$

For a gradually varying cross sectional area, the second term of this expression is negligible. Computations performed for the Oyster River demonstrated that this term is at least two orders of magnitude smaller than other terms of the momentum equation. It has therefore been omitted from further consideration.

From the continuity equation, the term $\partial Q/\partial X$ can be replaced by

$$\frac{\partial Q}{\partial x} = q - b\frac{\partial H}{\partial t} \qquad (4\text{-}12)$$

which leads to

$$\frac{\partial}{\partial x}(uQ) = \frac{2Q}{A}\left(q - b\frac{\partial H}{\partial t}\right) \qquad (4\text{-}13)$$

The final form of the momentum equation is therefore:

$$\frac{\partial Q}{\partial t} + \frac{2Q}{A}\left(q - b\frac{\partial H}{\partial t}\right) + g\frac{\partial H}{\partial x}A + g\frac{Q|Q|}{AC^2R} - g\frac{\partial \rho}{\partial x}\frac{Ad}{2\rho} = 0 \qquad (4\text{-}14)$$

The model employs a straightforward explicit finite difference method for solution of these equations. The two unknowns are flow rate Q and surface elevation H. All other terms of the equations are related to these unknowns, the geometry of the estuary, and specified parameters. A staggered solution scheme is employed whereby Q and H are calculated at alternating timesteps and locations. The scheme is illustrated in Figure 6.

Variable J is an even valued index of segment location and n is an even valued index of timestep. Both Δx and Δt are uniform in the domain of the computations. Boundary conditions on H are specified at the ocean boundary J-1 = 1 for timesteps n-1 = 3, 5, 7 . . .. Boundary conditions on Q are specified at the river end following J = JMAX for timesteps n = 4, 6, 8 . . .. Initial conditions are generally specified as zero elevation and flow at all points, and the starting time is therefore midway between high and low water with n = 2.

At each odd-numbered timestep, the continuity equation is solved to determine each new value of H. The equation

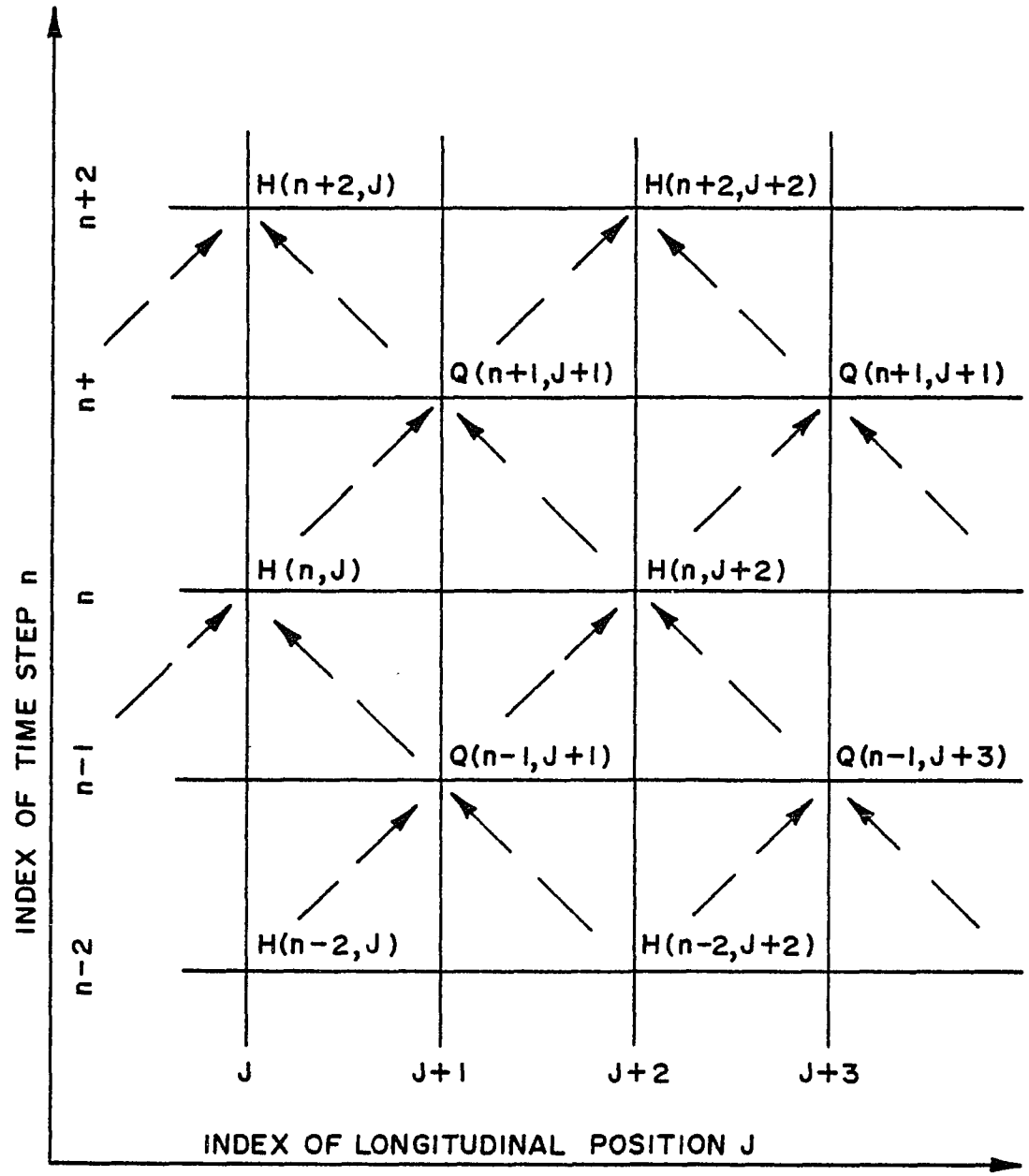

NOTE : ARROWS INDICATE DATA FLOW FOR EXPLICIT TIME-STEPPING

STAGGERED FINITE DIFFERENCE SCHEME

FIG 6 STAGGERED FINITE DIFFERENCE SCHEME

is represented in finite difference form as follows:

$$b\frac{H(n,j)-H(n-2,j)}{2\Delta t}+\frac{Q(n-1,j+1)-Q(n-1,j-1)}{2\Delta x}-q=0 \qquad (4\text{-}15)$$

Solving for the new value of H:

$$H(n,j)=H(n-2,j)-[Q(n-1,j+1)-Q(n-1,j-1)-2q\Delta x]\frac{\Delta t}{b\Delta x} \qquad (4\text{-}16)$$

Subsequently, at the next even numbered timestep, the momentum equation is solved for each new value of Q. In finite difference form this equation is:

$$\frac{Q(n,j)-Q(n-2,j)}{2\Delta t}+\frac{2Q(n-2,j)}{A}\left[q-b*\frac{1}{2}\left(\frac{H(n-1,j+1)-H(n-3,j+1)}{2\Delta t}+\frac{H(n-1,j-1)-H(n-3,j-1)}{2\Delta t}\right)\right]$$

$$+gA\left[\frac{H(n-1,j+1)-H(n-1,j-1)}{2\Delta x}\right]+g|Q(n-2,j)|*\frac{Q(n,j)+Q(n-2,j)}{2C^2AR}$$

$$-gA\frac{D}{2}\left(\frac{1}{\rho}\frac{\partial\rho}{\partial x}\right)=0 \qquad (4\text{-}17)$$

Several terms in this equation warrant further explanation. The area of the cross section, A, varies as a function of H. Hence, at each timestep, a value must be computed using the mean water depth at the location of interest and the H value at adjacent locations. As noted above, the area of interest for the momentum equation is the central flow area only. Hence a new term, b_s, is defined to represent width of this area. The resulting expression for area is:

$$A = b_s[D_j+.5(H(n-1,j-1)+H(n-1,j+1)\ ] \qquad (4\text{-}18)$$

Term C in equation (4-17) is the Chezy friction coefficient which can be related to the more convenient Manning's n as follows:

$$C = \frac{1.486}{n} R^{1/6} \qquad (4\text{-}19)$$

where R_h is the hydraulic radius defined as the flow cross-sectional area divided by wetted perimeter. For the flow area, the wetted perimeter is represented by width b_s plus twice the depth.

Term D/2 represents the depth to the centroid of a rectangular flow area and is used in computing the unbalanced longitudinal hydrostatic force due to the salinity gradient. Depth D is computed at each timestep from the local depth below mean water and the average surface displacement H of the adjacent x locations.

The term $\frac{1}{\rho}\,\partial P/\partial X$ is the normalized density gradient which is related to the salinity gradient. Its value is computed analytically for the average fresh water flow of the preceding tidal cycle and is held constant at each location for an entire tidal cycle. This computation is discussed further in a later section.

The finite difference equation can now be solved for the new value of Q as follows:

$$Q_{n,j} =$$

$$\{Q_{n-2,j}\left[\frac{1}{2\Delta t} - \frac{g|Q_{n-2,j}|}{2C^2AR} - \frac{2q}{A} + \frac{b}{A}\left(\frac{H_{n-1,j+1} - H_{n-3,j+1}}{2\Delta t} + \frac{H_{n-1,j-1} - H_{n-3,j-1}}{2\Delta t}\right)\right]\ldots \tag{4-20}$$

$$\ldots + gA\frac{H_{n-1,j+1}-H_{n-1,j-1}}{2\Delta x} - gA\frac{d}{2}\left(\frac{1}{\rho}\frac{\partial\rho}{\partial x}\right)\Big\}\Big/\frac{1}{2\Delta t} + \frac{g|Q_{n-2,j}|}{2C^2AR} \qquad (4\text{-}20)$$

Discretization of the estuary is illustrated in Figures 7 and 8. Longitudinally, the length is divided into an even number of segments, each identified with the cross section at the downstream end of the segment. Cross section 1 is the ocean boundary where tidal elevations are specified. Cross section JMAX is the last cross section before the end of the estuary where the upstream flow is specified. For a typical estuary bounded by a tidal head dam, the upstream tidal flow is equal to zero. Freshwater flow over the dam is incorporated into the lateral inflow in the last segment.

Laterally, the cross section of the estuary may be approximated in a number of ways as illustrated in Figure 8. Cases 1 and 4 utilize a rectangular cross section with no storage zones at the sides of the channel. For case 1, both depth and width of channel are specified at each section. For case 4, depth is specified, but width is calculated from an exponential function of X determined by constants BO and KB. Case 3 utilizes a trapezoidal cross section whose top width varies with water surface

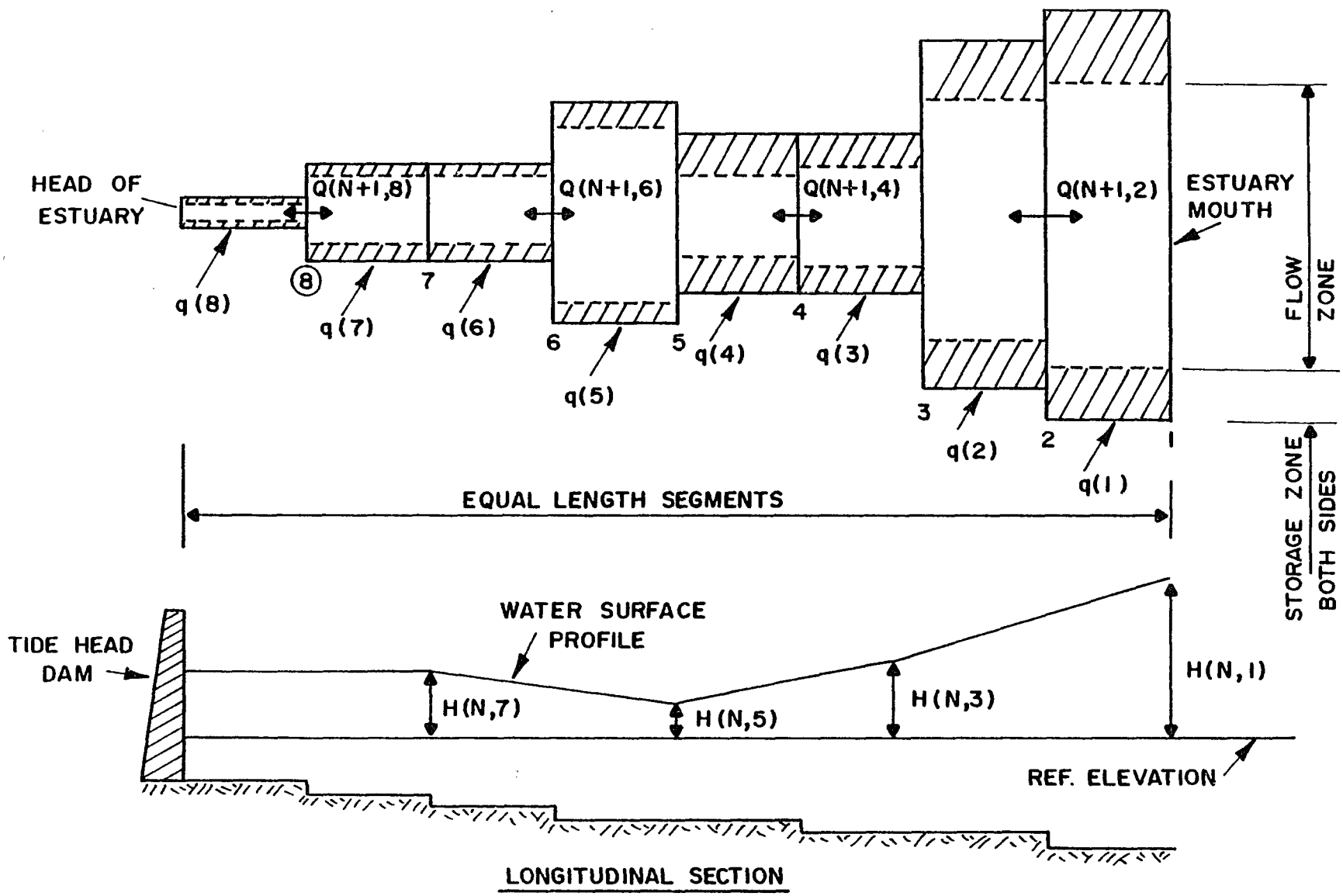

FIG 7 LONGITUDINAL SCHEMATIZATION OF AN ESTUARY

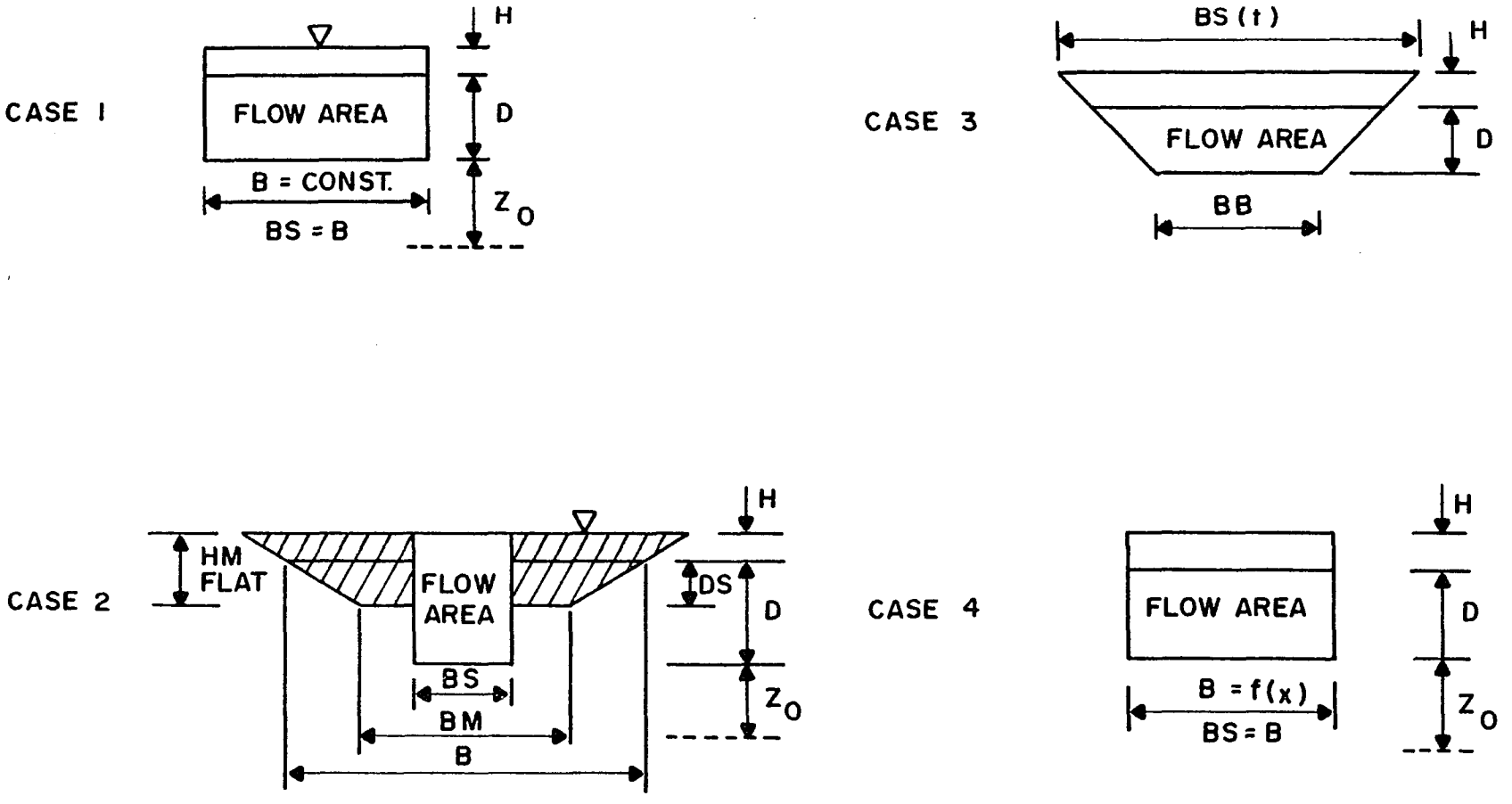

FIG 8 CHANNEL GEOMETRY

elevation. As with cases 1 and 4, the entire cross sectional area is considered flow area with no storage zones at the sides. Case 2 is the most general shape, and both flow and storage zones are considered. Furthermore, the width of the storage zone is allowed to vary as a function of water surface elevation. This shape allows consideration of natural channels having shallows or mudflats. It is possible for these areas to dry up completely at low water. To avoid negative area, the water height over these shallows is constrained, $H(t) \geq -ds$. As illustrated in the longitudinal section, mean water level is not necessarily horizontal. Flow may be dominated by the unidirectional fresh water flow, particularly in the upper reaches of tidal rivers. This can result in a significant superelevation of the mean water level.

4.1.2 Computational Stability of the Model

A significant factor affecting discretization of the estuary is stability of the numerical solution scheme. When partial derivative terms of the governing equations are replaced by finite difference approximations, error is introduced into the solution. These errors may be small, but their effects are significant long after their introduction into the dynamic solution process. Stability of explicit finite difference schemes for solution of the complete governing equations can not be investigated

analytically. However, it is possible to combine the two first order equations into a single second order hyperbolic equation which can be investigated further. When non-linear terms are ignored, this hyberbolic equation takes the form of the wave equation

$$\frac{\partial^2 u}{\partial t^2} = K \frac{\partial^2 u}{\partial x^2} \qquad (4\text{-}21)$$

Stability of explicit finite difference schemes for solution of the wave equation has been studied analytically by several investigators. This has led to the well known Courant condition for solution stability

$$\Delta t < \frac{\Delta x}{u_{MAX}\sqrt{gH}} \qquad (4\text{-}22)$$

Application of this criterion to numerical solution of the complete equations has generally indicated that this is an upper limit on Δt. More conservatively, Δt should be limited to approximately one-half of this value.

Evaluation of the stability criterion leads to the obvious conclusion that small timesteps must be used. For example, a typical segment size of 1/4 mile, a depth of 15 feet and estimated current velocity of 3 ft/sec leads to a Δt of less than one minute. Careful attention must be paid to discretization of the estuary to avoid excessive computational time. The segment length Δx must reflect the resolution needed in the final water quality investigation. Because of the staggered scheme for calculating Q and H, the Δx of the hydrodynamic analysis must be one-half the Δx of the water quality analysis. However, the longest possible segment should be employed to maximize the timestep. Since shorter segments result in both more computational points and more timesteps per total cycle, computational time increases as the inverse square of the segment length.

4.1.3 Modeling Density Driven Circulation

Returning now to the governing momentum equation, the final term requires data on the normalized density gradient throughout the estuary length. Computation of these values is based on an analytical solution for steady state salinity distribution. Clearly, the distribution will not, in fact, be at steady state during an analysis. Both intra-tidal cycle variations due to the periodic variation of height and current velocity, and longer time scale variations due to fresh water flow rate will occur. However, the importance of these variations is relatively small. The primary effect of the salinity gradient is to increase the slope of the estuary and hence raise surface elevations at the head end.

On a flooding tide the actual salinity profile will be compressed toward the head of the estuary, resulting in both a steeper gradient at the head and a lower gradient at the mouth than those predicted by the steady state assumption. However, it is virtually impossible to directly measure the slope of the water surface. Estimates of average slope are made by simultaneous observation of tidal stage at the mouth and head of the estuary. These would reflect the integrated effect of surface slope over the entire length and not a point value. Increased slope at the head end would be offset by decreased slope at the mouth, and the error would be virtually undetectable. Furthermore, in terms of the water quality computations,

the effect of these errors is even smaller. Surface slope due to the salinity gradient has little direct impact on water flux. The surface elevation may be raised at most a few inches, resulting in an error of under 5% in typical water depths. This small water volume will have even smaller error, and hence the effect on net flow is not expected to exceed 1%. For these reasons the tidal cycle averaged gradient is considered a satisfactory approximation.

Longer term variations due to fresh water flow rate can be more significant because of the extreme range of these flows. To account for these variations, the model can consider actual fresh water flows. The salinity gradient analysis is based on the average fresh water flow over the preceding tidal cycle which is provided as part of the input data.

The analytical solution is based on assumed exponentially varying velocity and dispersion coefficients as shown in Figures 9 and 10. Coefficients A and B in these figures represent the constant "decay" coefficients of the exponential variations. These figures are based on the assumption that the cross sectional area of typical small estuaries varies exponentially. Therefore, net velocity due to fresh water flow averaged over a tidal cycle will be greatest near the head and lowest near the mouth of the estuary. Conversely, tidal cycle averaged dispersion coefficients result primarily from intra-tidal

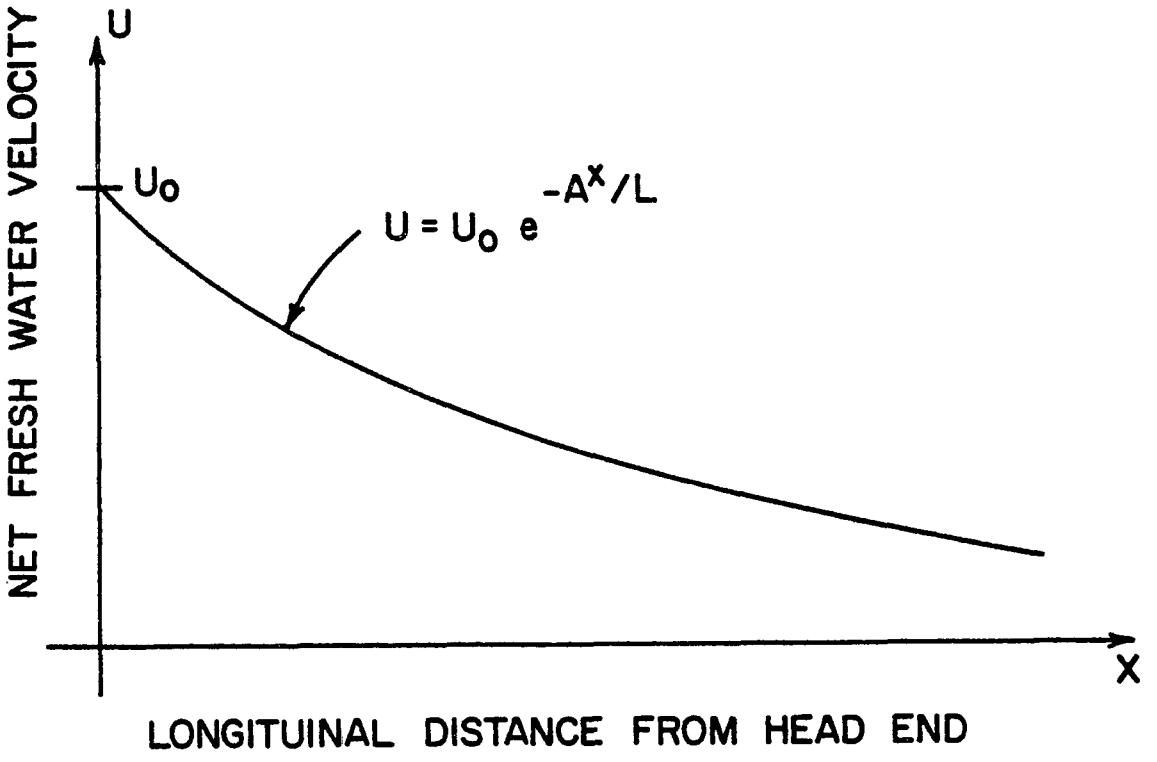

FIGURE 9

IDEALIZED LONGITUDINAL VELOCITY DISTRIBUTION

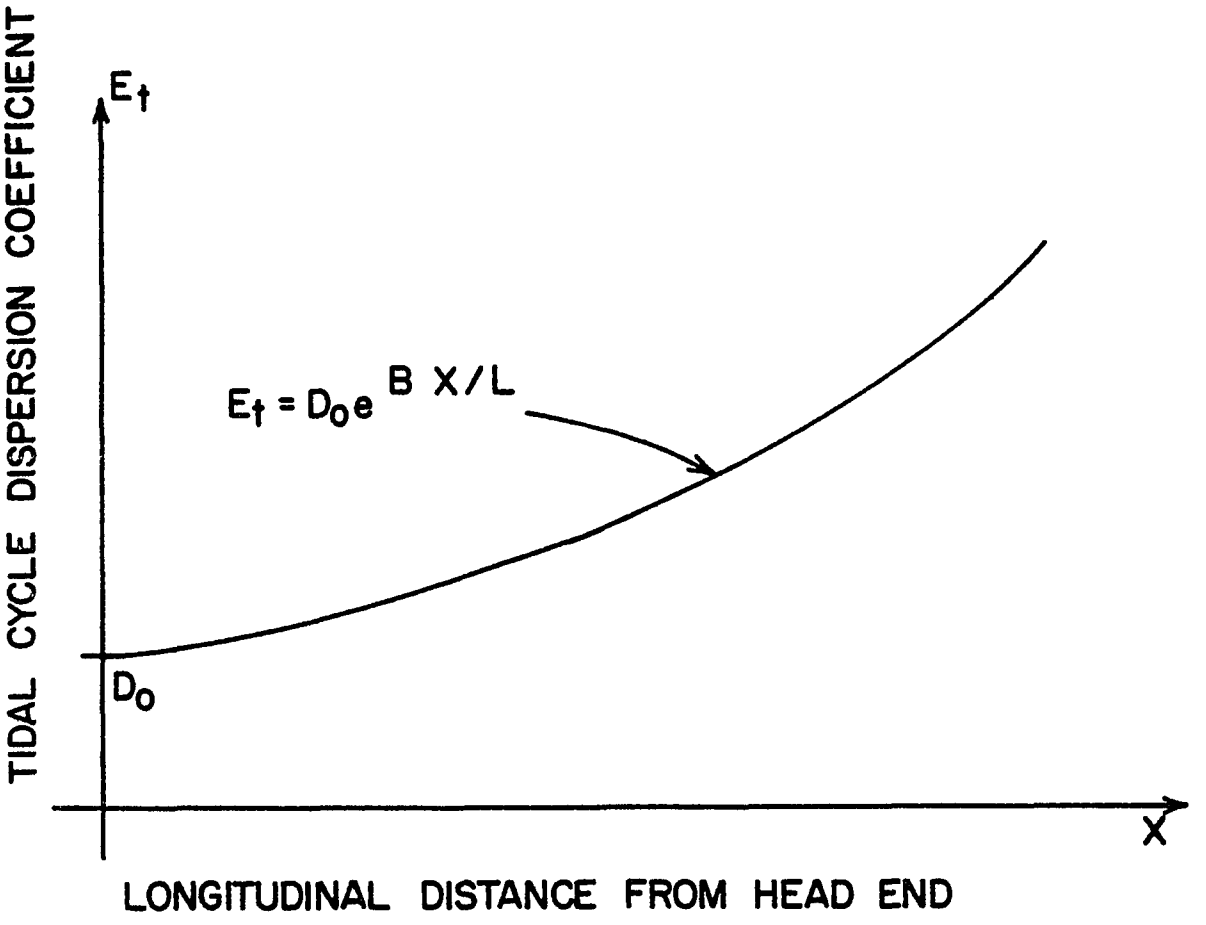

FIGURE 10

IDEALIZED LONGITUDINAL DISPERSION COEFFICIENT DISTRIBUTION

cycle velocity variation which is typically greatest at the mouth of the estuary.

At steady state, the tidally averaged advective salt flux due to net fresh water flow is balanced by upstream dispersive salt flux as given by

$$U\frac{dS}{dx} = \frac{d}{dx}\left(E\frac{dS}{dx}\right) \qquad (4\text{-}23)$$

where U = advective velocity.

Substituting the assumed functions for U and E

$$U_0 e^{-A^{x/\ell}}\frac{dS}{dx} = \frac{d}{dx}\left(D_0 e^{B^{x/\ell}}\frac{dS}{dx}\right) \qquad (4\text{-}24)$$

Expanding the right side of this equation, combining like terms, and dividing by $e^{Bx/\ell}$ results in

$$\left[\frac{U_0}{D_0}\left(e^{-(A+B)x/\ell}\right) - \frac{B}{\ell}\right]\frac{dS}{dx} = \frac{d^2S}{dx^2} \qquad (4\text{-}25)$$

defining

$$\frac{\partial S}{\partial x} = Z \qquad (4\text{-}26)$$

$$\left[\frac{U_0}{D_0}\, e^{-(A+B)x/\ell} - \frac{B}{\ell}\right] Z = \frac{dZ}{dx} \qquad (4\text{-}27)$$

which integrates to

$$\text{Ln } Z = \frac{U_0}{D_0}\,\frac{\ell}{A+B}\, e^{-(A+B)x/\ell} - \frac{Bx}{\ell} + C_1 \qquad (4\text{-}28)$$

Therefore

$$\frac{dS}{dx} = Ke\left[\frac{U_0 \ell}{D_0(A+B)} e^{-(A+B)x/\ell} - \frac{Bx}{\ell}\right] \qquad (4\text{-}29)$$

The constant K may be evaluated from the condition

$S_o = S_{MOUTH}$

$$\int_0^{\ell} \frac{dS}{dx}\, dx = \text{Salinity at mouth of estuary} \qquad (4\text{-}30)$$

$$S_0 = K\int_0^{\ell} e\left[\frac{U_0 \ell}{D_0(A+B)} e^{-(A+B)x/\ell} - B^{x/\ell}\right] \qquad (4\text{-}31)$$

$$K = \frac{S_0}{\int_0^{\ell} e\left[\frac{U_0 \ell}{D_0(A+B)} e^{-(A+B)x/\ell} - B^{x/\ell}\right]} \qquad (4\text{-}32)$$

For any set of constants, U_0, D_0, A and B, the integral can be evaluated by a numerical technique. The value of K is then used in Equation (4-29) to compute the salinity gradient at any point. Having the salinity gradient, salinity at any point can be computed by stepwise numerical integration beginning at either end of the estuary.

Application of this analytical solution for salinity gradient requires input of constants D_0, U_0, A and B and the average salinity at the mouth of the estuary. Evaluation of the constants and computations for the analytical solution are carried out within the hydrodynamic model as described below.

Constants U_0 and A describe the exponential variation of net fresh water velocity. An average fresh water flow rate over the preceding tidal cycle is employed. Average velocities at the head end and mouth of the estuary are computed using known dimensions at mean water level. Knowledge of average velocities at two points allows the two constants of the exponential equation to be evaluated directly.

Constants D_0 and B describe the exponential variation of tidal cycle averaged longitudinal dispersion coefficients along the channel. Computation of instantaneous values of dispersion coefficients is described in more detail in Section 4.2.4. These values include the effect of lateral and vertical variations of

velocity and contaminant concentration or salinity. However, in considering tidal cycle averaged dispersion, the effect of temporal variations must be superimposed. The work of R.B. Taylor (1976) and others has demonstrated that these temporal variations over a tidal cycle can amplify dispersion processes by more than one order of magnitude. To reflect this effect, an amplification parameter ETM has been defined. If we identify the "Taylor" dispersion coefficient discussed in Section 4.2.4 as E_t and employ a coefficient EFACT to account for lateral velocity variations in the natural channel, the amplified dispersion coefficient E_A is given by

$$E_A = ETM*EFACT*E_T \qquad (4\text{-}33)$$

To this must also be added the dispersion coefficient resulting from tidal cycle averaged density gradient, E_C. The final form of the equation for the tidal cycle averaged dispersion coefficient is therefore:

$$E = E_C + ETM*EFACT*E_T \qquad (4\text{-}34)$$

Parameter ETM is one of the calibration parameters which must be adjusted before application of the model.

Coefficient E_C reflects mixing due to the inward density driven current at the channel bottom and resultant outward currents at the surface. Computation of E_C is also discussed further in Section 4.2.4. For this tidal cycle averaged analysis, it is computed from the average longitudinal salinity gradient through the entire river length. Other required data are channel depths, fresh water flows and friction coefficients, all of which are readily available within the model data. Computation of the average salinity gradient is based on a calculated salinity at the mouth of the estuary. In turn, this salinity is based on the known average fresh water flow, QFRESH, using the following equations

$$S_0 = S_{MAX} + \exp(BCK*QFRESH) \qquad (4\text{-}35)$$

$$BCK = .001 * Ln\ (S1000/SMAX) \qquad (4\text{-}36)$$

where BCK is a constant selected by calibration against field data. Values of S_{1000} and S_{MAX}, representing salinity at the mouth for a high fresh water flow of 1000 cfs and a negliglible fresh water flow, are provided as data.

Having computed values of E at two locations, constants D_0 and B can be evaluated directly. All data is thus available for computation of salinity gradient and salinity at any point of the estuary, and the final term of the momentum equation can be evaluated.

4.1.4 Model Application and Linkage to Water Quality Analysis

The hydrodynamic model may be operated in either of two modes. If steady state conditions of fresh water flow prevail, the model can be used to determine a quasi-steady state condition in the estuary. Under these conditions, velocities and water surface elevations vary continuously over a tidal cycle but repeat identically for each successive cycle. An initial condition of zero velocity and zero displacement of the water surface is specified by the user, and the model iterates over successive tidal cycles until quasi-steady state is reached.

Alternatively, the model may be operated in a completely dynamic mode. Following the quasi-steady state solution, the model continues to calculate velocities and

elevations for additional tidal cycles with varying fresh water flow into the head end of the estuary. Fresh water flow is specified by a data file containing the hydrograph output from the upland hydrologic model. Since hydrodynamic computations are performed on a short timestep of a minute or less, the hydrograph may have a very short timestep. More realistically, a timestep of 30 minutes to an hour would be used for a single storm, or up to two or three hours for a succession of several storms.

Output from the hydrodynamic model can include detailed elevation and velocity data over each tidal cycle of the analysis. However, the important data for the analysis of water quality impact is written on a file which can be read directly by that model. This file contains channel flow velocity, channel cross sectional area, and storage zone (mudflat) cross sectional area for each timestep of the water quality analysis. As will be seen in the next section, the water quality model incorporates an implicit time- stepping scheme which allows much longer timesteps than those of the hydrodynamic model. Timesteps of 15 to 30 minutes are reasonable for the small tidal rivers considered here. Even longer steps may be used for larger estuaries. In addition to these hydrodynamic variables, the water quality model requires other related data for computation of dispersion coefficients. For each tidal cycle, the averaged density driven circulation is used to compute an equivalent dispersion coefficient as

described previously. The data file transferred to the water quality model includes this value at each river segment. Additionally, computation of an instantaneous "dispersion coefficient" reflecting cross sectional variation of velocity requires specification of the equivalent hydraulic radius of the flow area. This is also provided on the data file for each timestep at each river segment. The use of this data in computing dispersion coefficients is discussed further in Section 4.2.4.

4.2 One Dimensional Water Quality Model

Velocity and area data from the hydrodynamic analysis are integrated with contaminant source and sink data to analyze the distribution of water quality constituents. The major processes affecting these distributions are advective transport, dispersive transport, contaminant decay, internal generation of contaminant, and flushing at the mouth of the estuary. Each of these processes is represented in the water quality model. The model is written in general terms so that three broad classes of contaminants can be considered. These are:

1) a single conservative contaminant whose only source is at the mouth of the estuary and which results from a boundary concentration unaffected by conditions in the river (e.g., salinity);

2) a single non-conservative contaminant introduced

at one or more points along the estuary;

3) a contaminant system wherein up to ten interacting components may occur. At this time the system is limited to one where each component is affected by only one other component and in turn affects only one other component.

Schematically, such a system is shown on Figure 11. More complex systems require additional computer programming but no basic changes to the model.

4.2.1 Development of Governing Equations

The complete three-dimensional governing equation for advective/dispersive transport is

$$\frac{\partial C}{\partial t} + \frac{\partial}{\partial x}(uC) + \frac{\partial}{\partial y}(vC) + \frac{\partial}{\partial z}(wC) = \frac{\partial}{\partial x}(K_x \frac{\partial C}{\partial x}) + \frac{\partial}{\partial y}(K_y \frac{\partial C}{\partial y}) + \frac{\partial}{\partial z}(K_z \frac{\partial C}{\partial z}) - KC + \sum R \qquad (4\text{-}37)$$

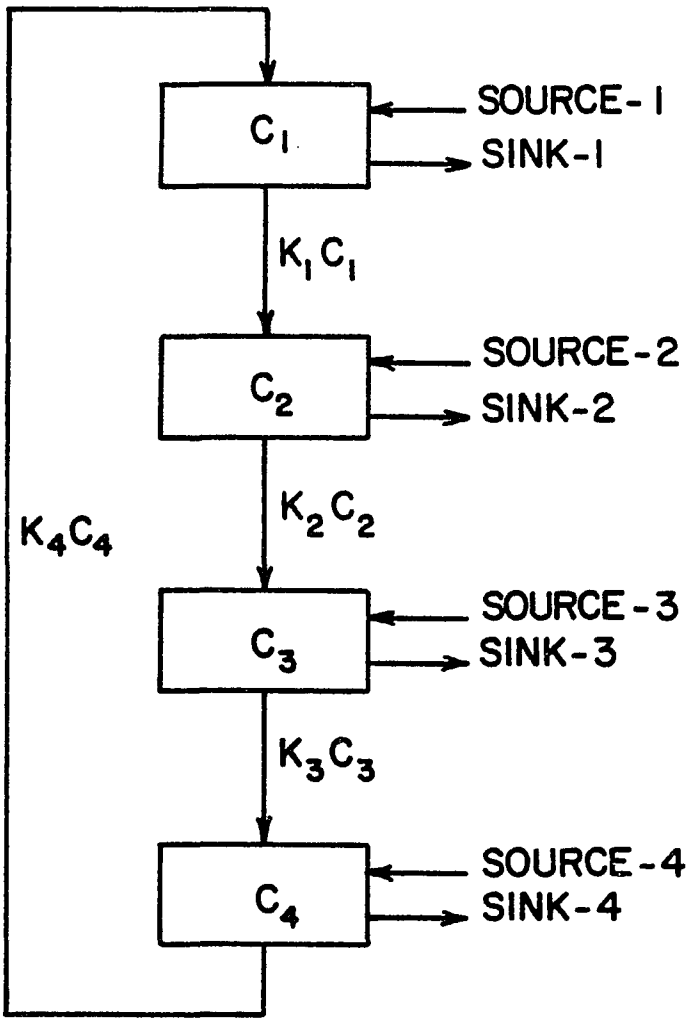

FIGURE 11

CYCLIC SYSTEM FOR WATER QUALITY ANALYSIS

where:

K_x, K_y, K_z = turbulent diffusion coefficients

K = first order decay coefficient

$\sum R$ = sum of all internal and external source and sink terms

Consider a channel whose width varies gradually with depth and longitudinal position. The three-dimensional equation can be integrated laterally (y-dimension) by assuming the following velocity and concentration functions:

$$C(x,y,z,t) = \overline{C}(x,z,t) + C'(y) \qquad (4\text{-}38a)$$

$$u(x,y,z,t) = \overline{u}(x,z,t) + u'(y) \qquad (4\text{-}38b)$$

$$v(x,y,z,t) = \overline{v}(x,z,t) + v'(y) \qquad (4\text{-}38c)$$

$$w(x,y,z,t) = \overline{w}(x,z,t) + w'(y) \qquad (4\text{-}38d)$$

where C = the contaminant concentration

$\overline{C}$ = the y averaged concentration

C' = the variation from the

u,v,w = the local velocities

$\overline{u},\overline{v},\overline{w}$ = the y averaged velocities

u',v',w' = the variations from $\overline{u}$, $\overline{v}$ and $\overline{w}$

Application of the Leibnitz rule for integration and no flux boundary conditions at the sides of the channel leads to

$$W\frac{\partial C}{\partial t} + W\frac{\partial}{\partial x}(\overline{u}\,\overline{C}) + W\frac{\partial}{\partial z}(\overline{w}\,\overline{C}) + \frac{\partial}{\partial x}\int_{-W/2}^{W/2} u'C'dy + \frac{\partial}{\partial z}\int_{-W/2}^{W/2} w'C'dy =$$

$$= W\frac{\partial}{\partial x}\left(N_x \frac{\partial \overline{C}}{\partial x} + W\frac{\partial}{\partial z}\left(N_z \frac{\partial \overline{C}}{\partial z}\right)\right) - WK\overline{C} + W\sum R \qquad (4\text{-}39)$$

where W = width of the channel.

Assuming an analogy between flux due to cross products of velocity and concentration and the "Fickian" diffusion process yields:

$$\int u'C'dy \equiv E_{xy}W\frac{\partial \overline{C}}{\partial x} \tag{4-40a}$$

$$\int w'C'dy \equiv E_{zy}W\frac{\partial \overline{C}}{\partial z} \tag{4-40b}$$

where E_{xy} and E_{zy} are longitudinal and vertical dispersion coefficients resulting from lateral variations in velocity and concentration. This results in the two-dimensional (longitudinal and vertical) governing equation:

$$\frac{\partial C}{\partial t} + \frac{\partial}{\partial x}(\overline{u}\,\overline{C}) + \frac{\partial}{\partial z}(\overline{w}\,\overline{C}) = \frac{\partial}{\partial x}\left[K_x+E_{xy}\right)\frac{\partial \overline{C}}{\partial x}\right]$$

$$+ \frac{\partial}{\partial z}\left[(K_z+E_{zy})\frac{\partial \overline{C}}{\partial z}\right] - KC + \sum R \tag{4-41}$$

In typical tidal channels, the magnitude of dispersion coefficient E_{xy} exceeds that of K_x by at least one order of magnitude. Therefore, it is common practice to neglect K_x. On the other hand, the vertical velocity encountered in these channels is small and its variation is correspondingly small. As a result, the value of K_z may equal or exceed that of E_{zy}. Frequently, the vertical dispersion coefficient E_{zy} is neglected in computations or incorporated into the vertical turbulent diffusion coefficient.

The two-dimensional equation may be further integrated in the vertical direction to arrive at a one-dimensional governing equation. The enhanced one-dimensional model employed here has been developed from these governing equations for a unit length control volume as shown in Figure 12.

This control volume approximates the three-dimensional configuration by a two-dimensional flow area with stepwise linearly varying depth and width and a one-dimensional shore area. Variables are defined as:

$C(x, z, t)$ = concentration in flow area

$C_S(x, t)$ = concentration in shore area

$u(x, z, t)$ = longitudinal velocity in flow area

$u_S = 0$ = longitudinal velocity in shore area

$v = 0$ = lateral velocity in flow area

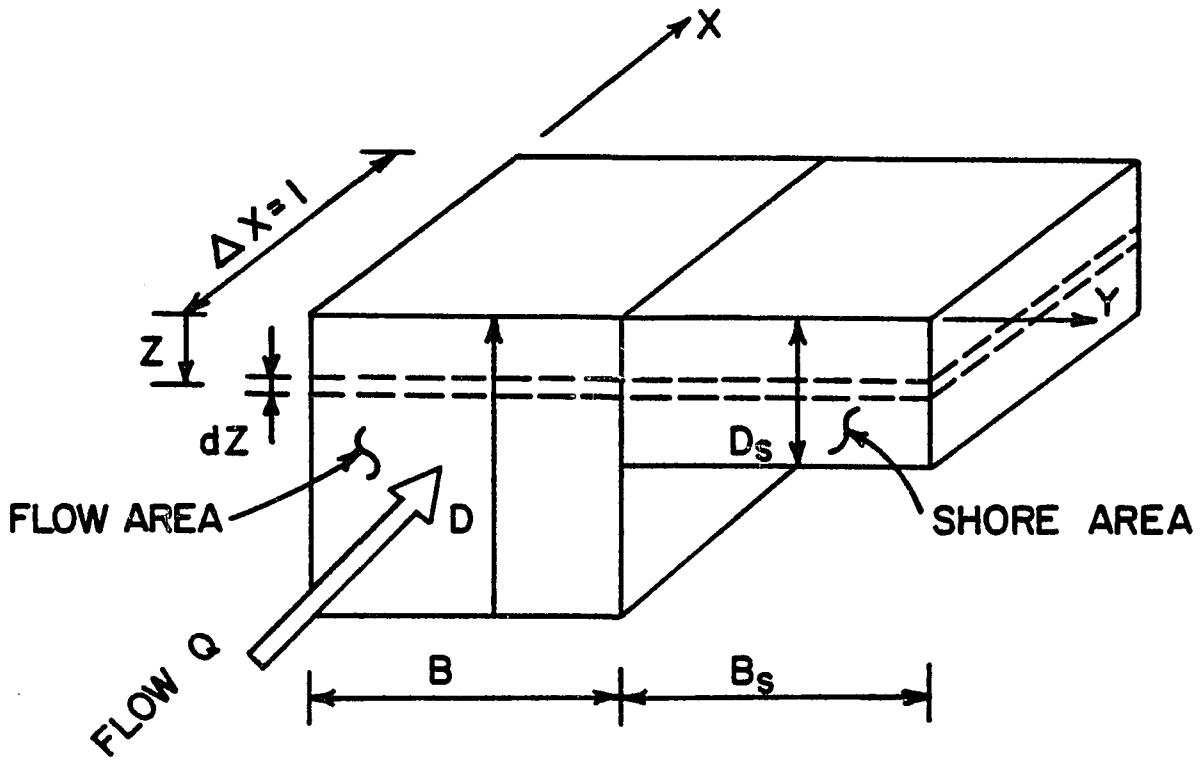

FIGURE 12

UNIT LENGTH CONTROL VOLUME FOR WATER QUALITY ANALYSIS

$v_S = 0$ = lateral velocity in shore area

$V(x, t)$ = lateral velocity at interface

$W(x, z, t)$ = vertical velocity in flow area

$W_S = 0$ = vertical velocity in shore area

$D(x, t)$ = depth of flow area

$D_S(x, t)$ = depth of shore area

$B(x)$ = width of flow area

$B_S(x)$ = width of shore area

γ = specific weight of water

E_{xy} = longitudinal dispersion coefficient due to transverse variation of velocity and concentration

r = source strength across side boundary of flow area in units of (wt/area-time)

Considering the mass balance for a horizontal "slice" of the flow area

$$\frac{\partial}{\partial t}(\gamma C dz B) + [\frac{\partial}{\partial x}(\gamma u dz B C)] - [\frac{\partial}{\partial x}(\gamma\{K_x+E_{xy}\}dz B\frac{\partial C}{\partial x})]$$

$$+ [\frac{\partial}{\partial z}(\gamma w B C)]dz - [\frac{\partial}{\partial z}(\gamma\{K_z+E_{xy}\}B\frac{\partial C}{\partial z})]dz$$

$$= \gamma dz - K\gamma BCdz - V\gamma C_V dz \qquad (4\text{-}42)$$

Replacing C and u by

$$C = \bar{C}(x,t) + C'(z) \qquad (4\text{-}43)$$

$$u = \bar{u}(x,t) + u'(z) \qquad (4\text{-}44)$$

and applying the Leibnitz rule with appropriate flux boundary conditions at the surface and bottom allows vertical integration to:

$$\frac{\partial}{\partial t}(\gamma\overline{C}DB) + [\frac{\partial}{\partial x}(\gamma\overline{u}DB\overline{C})] + [\frac{\partial}{\partial x}\gamma B\int_0^D u'C'dz]$$

$$- [\frac{\partial}{\partial x}\gamma\{K_x+E_{xy}\}DB\frac{\partial\overline{C}}{\partial x}] = \gamma D - K\gamma B\overline{C}D - V\gamma\overline{C}D \qquad (4\text{-}45)$$

Now define the total weight of contaminant per unit of length within the flow area control volume to be

$$W_T = \gamma\overline{C}_a D_a B_a = \gamma\overline{C}_a A_a \qquad A_a = D_a B_a \qquad (4\text{-}46)$$

where the subscripts "a" imply appropriate average values within the length Δx. This leads to:

$$\frac{\partial}{\partial t}(W_T) + \frac{\partial}{\partial x}(\overline{u}\,W_T) + [\frac{\partial}{\partial x}\gamma\frac{A_a}{D_a}\int_0^D u'C'dz]$$

$$- [\frac{\partial}{\partial x}\gamma\{K_x+E_{xy}\}A_a\frac{\partial\overline{C}}{\partial x}] = [\gamma\frac{A_a}{B_a} - KW_T - T] \qquad (4\text{-}47)$$

where

$$\int_0^D V\gamma C_V dz \tag{4-48}$$

T is defined as the contaminant flux per unit of length across the interface.

Now assume a "Fickian" analogy for contaminant flux due to the cross product term $c'(z)\, u'(z)$ such that

$$\int_0^D u'C'dz \equiv -DE_{xz} \frac{\partial \overline{C}}{\partial x} \tag{4-49}$$

where E_{xz} is defined as the longitudinal dispersion coefficient due to vertical velocity and concentration variation. This leads to:

$$\frac{\partial W_T}{\partial t} + \frac{\partial}{\partial x}(\bar{u} W_T) - \frac{\partial}{\partial x}[\gamma A_a \{K_x + E_{xy} + E_{xz}\} \frac{\partial \bar{C}}{\partial x}] = \gamma \frac{A_a}{B_a} - K W_T - T \qquad (4\text{-}50)$$

$$\bar{C} = \frac{W_T}{\gamma A} \qquad E = K_x + E_{xy} + E_{xz} \qquad (4\text{-}51)$$

$$\frac{\partial W_T}{\partial t} + \frac{\partial}{\partial x}(\bar{u} W_T) - \frac{\partial}{\partial x}\left[\gamma A_a E \frac{1}{\gamma} \frac{\partial}{\partial x}^{(W_T/A)}\right] = \gamma \frac{A_a}{B_a} - K W_T - T \qquad (4\text{-}52)$$

$$\frac{\partial W_T}{\partial t} + \frac{\partial}{\partial x}(\bar{u} W_T) - \frac{\partial}{\partial x}\left[A_a E \frac{\partial^{(W_T/A)}}{\partial x}\right] = \gamma \frac{A_a}{B_a} - K W_T - T \qquad (4\text{-}53)$$

Returning now to the contaminant flux across the interface between flow and shore areas, we have

$$T = \int_0^D V\gamma C_V dz \qquad (4\text{-}54)$$

where C_V = the contaminant concentration in the interface flow

We can define the flow rate per unit of length across the interface by

$$Q = \int_0^D V dz \qquad (4\text{-}55)$$

This rate is also equal to the rate of change of volume in the shore area:

$$Q = B_S \frac{d}{dt}(D_S) = \frac{d}{dt}(A_S) \qquad (4\text{-}56)$$

Therefore:

$$\int_0^D V dz = \frac{d}{dt}(A_S) \tag{4-57}$$

Hence, for a properly defined concentration C_V:

$$T = \gamma C_V \frac{d}{dt}(A_S) \tag{4-58}$$

If we consider C_V, the concentration in the interface flux, to vary slowly in comparison to other flux components, it can be approximated by:

$$C_V = \begin{cases} Cf \quad \text{for} \quad \frac{d}{dt}(A_S) > 0 \\ \\ C_S \quad \text{for} \quad \frac{d}{dt}(A_S) < 0 \end{cases} \tag{4-59}$$

This implies that the interface flux concentration is equal to the flow concentration, C_f, when the shore volume is increasing (flood tide in the estuary), and is equal to the shore concentration, C_S, when the shore volume is decreasing (ebb tide).

Consider now the shore area. The one-dimensional mass balance is:

$$\frac{\partial}{\partial t}(\gamma C_S D_S B_S) = -K\gamma B_S D_S C_S + V\gamma D_S C_V \qquad (4\text{-}60)$$

where all advective and dispersive terms are zero because velocities have been defined to equal zero.

Substituting for the total weight of contaminant per unit of length in the shore area control volume, we obtain the following:

$$W_S = \gamma \bar{C}_s D_{sa} B_{sa} = \gamma \bar{C}_S A_{Sa} \qquad (4\text{-}61)$$

$$A_{Sa} = D_{Sa} B_{Sa} \qquad (4\text{-}62)$$

We then get:

$$\frac{\partial}{\partial t}(W_S) = -KW_S + T \qquad (4\text{-}63)$$

The final governing equations are therefore:

Flow Area:

$$\frac{\partial W_T}{\partial t} + \frac{\partial}{\partial x}(\bar{u}\, W_T) - \frac{\partial}{\partial x}\left[\gamma A_a E \frac{\partial}{\partial x}(W_T/A)\right] = \frac{R}{B_a} - KW_T - T \qquad (4\text{-}64)$$

Shore Area:

$$\frac{\partial W_S}{\partial t} = -KW_S + T \qquad (4\text{-}65)$$

4.2.2 Numerical Solution Technique, Accuracy and Stability

Exact solutions of the partial differential equation for mass balance in estuary flow are available for only very limited geometric, source and boundary conditions. It is therefore necessary to resort to numerical solution techniques to obtain results for a more general class of conditions. These techniques make use of a discrete approximation to the true geometry of the estuary. For the one-dimensional model used here, this approximation takes the form of equal length longitudinal segments each characterized by a single time varying cross sectional flow area, a single time varying velocity, and a single time varying storage area which takes account of non-advective shore zones of the real estuary cross section. Data on these three independent variables are provided from output of the hydrodynamic model, or may be taken from actual field observations. The weight (or concentration) of contaminant in each longitudinal segment is calculated at each timestep using an implicit finite difference scheme for solution of linear parabolic differential equation (4-64). Equation (4-65) is a first order constant coefficient differential equation which is solved explicitly at each timestep.

Finite difference techniques employ discrete values of the dependent variables at different positions in time and space to approximate the terms of a differential equation. The difference operators which represent first and second

order derivations may be viewed as truncated Taylor series representations of these terms. Those terms which are dropped from the series represent the so-called truncation error. If the magnitude of these errors approaches zero as the increments in time and space are reduced, the finite difference operator is called "consistent." For a real finite difference solution, truncation errors will necessarily exist, and as time stepping proceeds, these truncation errors will accumulate. This accumulated truncation error is called the discretization error. If the discretization error approaches zero as the increments of time and space are made smaller, the finite difference operator is called convergent. Additional error enters the numerical computations because each successive value must be rounded off each time it is stored or manipulated, whether manually or with a digital computer. If the numerical solution scheme allows these roundoff errors to increase in successive timesteps, the scheme is considered unstable. A final consideration in developing a finite difference technique is that it conserve the quantity represented by the dependent variable, in this case a water quality component. The finite difference operator must be so defined that the sum of material quantity exchanged across internal and external interfaces equals the net source or sink. An ideal finite difference scheme would meet all of these requirements: consistency, convergency, stability, and conservativeness.

Fortunately, these four requirements may be reduced to three by application of the Lax Equivalence Theorem (Greenburg, 1978). This theorem states that if a properly posed linear initial value problem has a consistent finite difference approximation, stability is both a necessary and sufficient condition for convergence. Since the truncation error of a finite difference approximation derived from a Taylor expansion clearly goes to zero as the time and space increments go to zero, these operators are "consistent." Selection of a finite difference operator therefore becomes a problem of ensuring stability and conservation of mass at interfaces in the most efficient manner.

The problem of stability has been considered at length by several authors. Generally, it is pointed out that universally applicable analytical procedures for evaluating stability of finite difference techniques are not available. However, procedures have been developed for simplified versions of the governing equations. These methods are used to estimate the stability characteristics of the complete equations, but final assessment usually requires numerical experiments with the model. The most commonly used method for stability analysis is the Fourier method attributed to von Newman.

Consider the simplified linearized differential equation

$$\frac{\partial f}{\partial t} + V \frac{\partial f}{\partial x} - E \frac{\partial^2 f}{\partial x^2} = 0 \qquad (4\text{-}66)$$

where f is any dependent variable. It can be shown by back substitution that an exact solution of the equation is a Fourier series:

$$f(x,f) = \sum_{\omega=1}^{\infty} B_{\omega} e^{-\omega^2\pi^2 Dt} \sin \omega\pi(x-vt) \qquad (4\text{-}67)$$

If we now consider a finite difference approximation of the differential equation, limited only in that two time levels, t^n and t^{n+1} ,are employed, it can be shown that the exact solution of the difference equation is of the form

$$F_j^n = \sum_{\omega=1}^{j-1} A_{\omega} \rho^n \sin \omega \pi(j\Delta x - \phi n\Delta t V) \qquad (4\text{-}68)$$

where J-1 is the number of internal points in the solution domain.

The solutions to the continuous discrete equations are similar except for two differences. The propagation of disturbances in the continuous equation solution occurs at velocity V, whereas in the discrete solution the velocity is multiplied by a factor ϕ . Additionally, the decay term $e^{-\omega^2\pi^2 Dt}$ of the continuous solution is replaced by a term ρ^n . The terms ϕ and ρ are functions of $\omega\pi\Delta x$, $v\Delta t/\Delta x$, $E\Delta t/\Delta x^2$ and the particular finite difference

operators employed. The latter two represent the effective error of the advective and dispersive portions of the finite difference solution.

The Fourier technique for stability analyses is based on evaluation of these errors. The propagation of error is analyzed by investigating a single error at the first timestep of computation. It is assumed that no further errors occur as the time-stepping progresses.

For simplicity sake, the linearized differential equation will be considered in two steps--first evaluating stability related to the dispersion term $E\partial^2F/\partial x^2$, and then stability related to the advective term $V\partial F/\partial x$. Ignoring the advective term in the linearized differential equation yields

$$\frac{\partial F}{\partial t} - E\frac{\partial^2 F}{\partial x^2} = 0 \qquad (4\text{-}69)$$

which is immediately recognized as the classical heat transfer or diffusion equation. A family of finite difference analogies of the heat equation involving two levels of time and three levels of position are given by:

$$\frac{F_j^{n+1}-F_j^n}{\Delta t} - \frac{E}{\Delta x^2}\left[R(F_{j+1}^{n+1}-2F_j^{n+1}+F_{j-1}^{n+1})+(1-R)(F_{j+1}^{n}-2F_j^{n}+F_{j-1}^{n})\right] = 0 \qquad (4\text{-}70)$$

Here a subscript j indicates the level of position $(x=j\Delta x)$, and n indicates the level of time $(T=n\Delta t)$. Parameter R is a weighting factor whose value is given by

$$0 \leq R \leq 1 \qquad (4\text{-}71)$$

When the value zero is chosen, the equation represents the so-called explicit solution involving only one point at the future timestep and three at the present step. All other values of R result in implicit solutions involving three points at both timesteps. The solution of these equations is of the form

$$F_j^n = \sum_{\omega=1}^{j-1} A_\omega \rho^n \sin \omega \pi j \Delta x \qquad (4\text{-}72)$$

Considering the following two terms of the difference equation and substituting one term of the solution yields

$$F_{j+1}^n + F_{j-1}^n = A\omega\rho^n (\sin \omega \pi (j+1)\Delta x + \sin \omega \pi (j-1)\Delta x) \qquad (4\text{-}73)$$

Algebraic manipulation of these terms leads to

$$F_{j+1}^n + F_{j-1}^n = A\omega\rho^n \sin \omega \pi j \Delta x (2 \cos \omega \pi \Delta x)$$

$$= F_j^n (2 \cos \omega \pi \Delta x) \qquad (4\text{-}74)$$

This results in the following forms of the finite difference equation

$$F_j^{n+1} - F_j^n = \frac{E\Delta t}{\Delta x^2} [R(2 \cos \omega \pi \Delta x - 2) F_j^{n+1} + (1-R) (2 \cos \omega \pi x - 2) F_j^n] \quad (4\text{-}75)$$

and

$$\frac{F_j^{n+1}}{F_j} = \frac{1 + \frac{E\Delta t}{\Delta x^2} (1-R)(2 \cos \omega \pi \Delta x - 2)}{1 - \frac{E\Delta t}{\Delta x^2} R(2 \cos \omega \pi \Delta x - 2)} \quad (4\text{-}76)$$

Replacing the cosine term by

$$2 \cos \omega \pi \Delta x - 2 = -4 \sin^2 \omega \pi \Delta x \quad (4\text{-}77)$$

leads to

$$\frac{F_j^{n+1}}{F_j} = \frac{1 - \frac{4E\Delta t}{\Delta x^2}(1-R)\sin^2 \omega \pi \Delta x}{1 + \frac{4E\Delta t}{\Delta x^2} R \sin^2 \omega \pi \Delta x} \qquad (4\text{-}78)$$

Stability of the finite difference scheme is insured if this ratio has an absolute value less than one. That is, the effect of error at the present timestep is damped out at subsequent timesteps and does not grow without bounds.

Consider first an R value of 0. Stability of the resulting explicit finite difference expression requires that the absolute value of the following ratio be less than 1:

$$\frac{F_j^{n+1}}{F_j} = \frac{1 - \frac{4E\Delta t}{\Delta x^2}\sin^2 \omega \pi \Delta x}{1} \qquad (4\text{-}79)$$

Since the value of $\sin^2$ is always positive and no larger than 1, stability depends on the value of $4E\Delta t/\Delta x^2$.

$$0 \leq \frac{4E\Delta t}{\Delta x^2} \leq 1 \qquad \text{Stable solution decaying with positive sign} \qquad (4\text{-}80)$$

$$1 \leq \frac{4E\Delta t}{x^2} \leq 2 \qquad \text{Stable solution with oscillating decay} \qquad (4\text{-}81)$$

$$2 < \frac{4E\Delta t}{\Delta x^2} \qquad \text{Unstable solution (absolute value of ratio is larger than 1)} \qquad (4\text{-}82)$$

Consider now the case of R=1/2. Stability of this implicit scheme requires that the absolute value of the following ratio be less than 1.

$$\frac{F_j^{n+1}}{F_j} = \frac{1 - \frac{2E\Delta t}{\Delta x^2} \sin^2 \omega \pi \Delta x}{1 + \frac{2E\Delta t}{\Delta x^2} \sin^2 \omega \pi \Delta x} \qquad (4\text{-}83)$$

Stability properties of this scheme are:

$$0 \leq \frac{2E\Delta t}{\Delta x^2} \leq 1 \qquad \text{Stable, decays with positive sign} \qquad (4\text{-}84)$$

$$1 \leq \frac{2E\Delta t}{\Delta x^2} < \infty \qquad \text{Stable, oscillating decay} \qquad (4\text{-}85)$$

Thus, this scheme is unconditionally stable, but the rate of error decay will depend on the value of $E\Delta t/\Delta x^2$.

Finally, consider the case of R=1. Stability requires that the absolute value of the following ratio be less than 1:

$$\frac{F_j^{n+1}}{F_j^n} = \frac{1}{1 + \frac{4E\Delta t}{\Delta x^2} \sin^2 \omega \pi \Delta x} \qquad (4\text{-}86)$$

This scheme is unconditionally stable and decays with positive sign for all values of $E\,\Delta t/\Delta x^2$.

Conservation of mass for the system defined here can be evaluated by considering the truncation errors of the difference expressions. In general, the family of solutions considered here has a truncation error which is first order in time and second order in distance X. This is represented mathematically by

$$T = \mathbf{O}(\Delta t) + \mathbf{O}(\Delta x^2) \tag{4-87}$$

However, for the special case of R=1/2, the first order errors for the two time levels are equal and have opposite sign. The result is that the error in time is reduced to second order. That is,

$$\text{For } R = 1/2 \qquad T = \mathbf{O}(\Delta t^2) + \mathbf{O}(\Delta x^2) \tag{4-88}$$

A distinct advantage in accuracy therefore accrues to a choice of R=1/2. This value has been selected for use here with the result that the finite difference operator for the dispersion term is:

$$E\frac{\partial^2 F}{\partial x^2} \equiv \frac{E}{2\Delta x^2}\left[(F_{j+1}^{n+1}-F_j)-(F_j^{n+1}-F_{j-1}^{n+1})+(F_{j+1}^{n}-F_j^{n})-(F_j^{n}-F_{j-1}^{n})\right] \qquad (4\text{-}89)$$

This representation of the second derivative is referred to as a Crank-Nicholsen approximation, after the mathematicians of the same names.

Having established the form of the dipersion term approximation through arguments of stability and accuracy, we may now return to the complete linearized version of the governing parabolic equation and investigate the optimum finite difference formulation for the remaining terms. The approach followed here is based on the work of Stone and Brian (1963) to optimize numerical solution of convective transport problems.

Using the same six points employed in the Crank-Nicholsen approximation (two levels of time and three of space), Stone and Brian investigated an arbitrary weighting system for the advective term and time derivative approximations. These terms are defined as follows:

$$V\frac{\partial F}{\partial x} \equiv \frac{V}{\Delta x}\left[a(F^n_{j+1}-F^n_j)+\frac{\varepsilon}{2}(F^n_j-F^n_{j-1})+C(F^{n+1}_{j+1}-F_j)+d(F^{n-1}_j-F^{n+1}_{j-1})\right] \qquad (4\text{-}90)$$

$$\frac{\partial F}{\partial t} \equiv \frac{1}{\Delta t}\left[g(F^{n+1}_j-F^n_j)+\frac{\theta}{2}(F^{n+1}_{j-1}-F^n_{j-1})+m(F^{n+1}_{j+1}-F^n_{j+1})\right] \qquad (4\text{-}91)$$

where a, $\varepsilon/2$, c, d, g, $\theta/2$, m are arbitrary weighting coefficients subject to the following constraints of consistency:

$$a + \frac{\varepsilon}{2} + c + d = 1 \qquad (4\text{-}92)$$

$$g + \frac{\theta}{2} + m = 1 \qquad (4\text{-}93)$$

Referring to the exact solution of the linearized differential equation and the finite difference approximation given in equations (4-67) and (4-68), the objective of Stone and Brian's work was to select values of the weighting factors for which:

1) Disturbances are propagated in the finite difference solution at approximately the same velocity that they are propagated in the exact solution. That is, the value of ϕ approaches 1.0.

2) The time rate of decay of error in the finite difference solution and the exact solution are approximately the same.

The resulting finite difference operators will represent the optimized technique which most closely simulates the exact solution to the governing differential equation.

It is well known that problems of solution stability and convergence due to finite difference approximations of advective transport terms can be minimized by selection of an arbitrarily large value of the dispersion coefficient. In effect, instabilities are "smeared out" by the large dispersive component. Stone and Brian have therefore placed emphasis on this case when the dispersion coefficient is small. They show that when E approaches zero, the decay rate can be made to approach its correct

value if the following conditions are met:

$$c = \frac{\varepsilon}{2} \tag{4-94}$$

$$a = d \tag{4-95}$$

$$m = \frac{\theta}{2} \tag{4-96}$$

These conditions impart a symmetry to the finite difference operators. The remaining two conditions were then defined in terms of an optimum value for coefficients ε and ϕ. Selection of numerical values for these allows all other coefficients to be evaluated using the above sets of conditions, (4-92) through (4-96).

The characteristics of solutions based on various values of ε and θ were evaluated by Stone and Brian in terms of the disturbance propagation factor ϕ and the decay factor ρ. In all cases these factors varied as a function of ε and θ, but also as a function of ratios $V\Delta t/\Delta x$ and $E\Delta t/\Delta x^2$ and the value of the harmonic frequency being considered. From the standpoint of velocity of propagation a θ value of 1/3 gave the best results. That is, the propagation of disturbances most closely approximated the velocity in the exact solution. An ε of 2/3 gave slightly better propagation characteristics than a value of 1/2, but the decay term had erratic characteristics as the ratio

$V\Delta t/\Delta x$ was varied. In conclusion, values of $\theta = 1/3$ and $\varepsilon = 1/2$ were selected as the best choices.

On the basis of the foregoing discussion, the optimum finite difference approximation for the terms of the linearized differential equation are identified as

$$\frac{\partial F}{\partial t} = \frac{1}{\Delta t}\left[\frac{2}{3}(F_j^{n+1}-F_j^n) + \frac{1}{6}(F_{j-1}^{n+1}-F_{j-1}^n) + \frac{1}{6}(F_{j+1}^{n+1}-F_{j+1}^n)\right] \qquad (4\text{-}97)$$

$$V\frac{\partial F}{\partial x} = \frac{V}{\Delta x}\left[\frac{1}{4}(F_{j+1}^n-F_j^n) + \frac{1}{4}(F_j^n-F_{j-1}^n) + \frac{1}{4}(F_{j+1}^{n+1}-F_j^{n+1}) + \frac{1}{4}(F_j^{n+1}-F_{j-1}^{n+1})\right] \qquad (4\text{-}98)$$

$$E\frac{\partial^2 F}{\partial x^2} = \frac{E}{2\Delta x}\left[\{(F_{j+1}^{n+1}-F_j^{n+1})-(F_j^{n+1}-F_{j-1}^{n+1})\}+\{(F_{j+1}^n-F_j^n) - (F_j^n-F_{j-1}^n)\}\right] \qquad (4\text{-}99)$$

Returning now to the complete, non-linear differential equation, appropriate finite difference operators are determined by analogy to the above expressions. The general dependent variable F is now replaced by variable W representing the weight of contaminant contained in a discrete segment of the river. The time derivative term is unchanged from the linearized equation, and therefore:

$$\frac{\partial W_T}{\partial t} = \frac{1}{\Delta t}\left[\frac{2}{3}(W_j^{n+1}-W_j^n)+\frac{1}{6}(W_{j-1}^{n+1}-W_{j-1}^n)+\frac{1}{6}(W_{j+1}^{n+1}-W_{j+1}^n)\right] \qquad (4\text{-}100)$$

The non-linear advective term incorporates a variable velocity u . Therefore, each value of the dependent variable W must be multiplied by the corresponding velocity to define the finite difference expression for advection. This results in:

$$\frac{\partial(\bar{u}\,W)}{\partial x} = \frac{1}{4\Delta x}\left[(u_{j+1}^n W_{j+1}^n - u_j^n W_j^n)+(u_j^n W_j^n - u_{j-1}^n W_{j-1}^n)\right.$$

$$\left. + (u_{j+1}^{n+1} W_{j+1}^{n+1} - u_j^{n+1} W_j^{n+1})+(u_j^{n+1} W_j^{n+1} - u_{j-1}^{n+1} W_{j-1}^{n+1})\right] \qquad (4\text{-}101)$$

The dispersion term is more complex because both the dispersion coefficient and the cross sectional area vary with both time and location. Furthermore, these variables are found imbedded inside the first and second order derivatives. The resulting finite difference expression is as follows:

$$\frac{\partial}{\partial x}\left[AE\,\frac{\partial}{\partial x}(W/n)\right] = \frac{-1}{2\Delta x^2}\left\{\left[\left(\frac{E_{j+1}^{n+1}+E_j^{n+1}}{2}\right)\left(\frac{A_{j+1}^{n+1}+A_j^{n+1}}{2}\right)\left(\frac{W_{j+1}^{n+1}}{A_{j+1}^{n+1}}-\frac{W_j^{n+1}}{A_j^{n+1}}\right)\right.\right.$$

$$\left.-\left(\frac{E_j^{n+1}+E_{j-1}^{n+1}}{2}\right)\left(\frac{A_j^{n+1}+A_{j-1}^{n+1}}{2}\right)\left(\frac{W_j^{n+1}}{A_j^{n+1}}-\frac{W_{j-1}^{n+1}}{A_{j-1}^{n+1}}\right)\right]$$

$$+\left[\left(\frac{E_{j+1}^{n}+E_j^{n}}{2}\right)\left(\frac{A_{j+1}^{n}+A_j^{n}}{2}\right)\left(\frac{W_{j+1}^{n}}{A_{j+1}^{n}}-\frac{W_j^{n}}{A_j^{n}}\right)\right.$$

$$\left.\left.-\left(\frac{E_j^{n}+E_{j-1}^{n}}{2}\right)\left(\frac{A_j^{n}+A_{j-1}^{n}}{2}\right)\left(\frac{W_j^{n}}{A_j^{n}}-\frac{W_{j-1}^{n}}{A_{j-1}^{n}}\right)\right]\right\} \qquad (4\text{-}102)$$

These three terms completely specify the homogeneous, non-linear finite difference equation at internal points of the solution domain. To extend the homogeneous equation to the complete equation it is necessary to represent source terms on the right side of equation (4-64) in finite difference terms. The governing differential equation has been developed for a unit length of estuary. However, in practice, application of the finite difference equation is to a finite increment of length or segment. The weight of contaminant W may, therefore, be considered total weight within the segment, and source terms must be defined appropriately. Employing this approach, the source term representing total gain (or loss) of contaminant per unit time is

$$\frac{R}{B_a} - KWT = CQ_j^n - \frac{K}{2}\left(W_j^n + W_j^{n+1}\right) - T_j^n \qquad (4\text{-}103)$$

where CQ_j^n is defined as the average contaminant inflow and generation rate to segment j during the timestep beginning at $n\Delta t$.

We have yet to define the final term T_j^n representing average mass flux rate across the interface between the storage zone and the flow zone. For this, we now consider equation (4-65) for mass balance in the shore zone.

$$\frac{\partial W_S}{\partial t} = -KW_S + T \qquad (4\text{-}104)$$

Term T can be defined in terms of the water flow rate into the storage zone $\partial S/\partial t$as follows

$$T = \gamma C \frac{\partial S}{\partial t} \qquad (4\text{-}105)$$

where concentration, C, is time varying and dependent on whether flow is into or out of the storage zone. When flow is into storage (flood tide), C is defined by the concentration in the flow zone. When flow is out of storage, C is defined by concentration in the storage zone. If we employ a trapezoidal finite difference approximation for $\partial S/\partial t$, average flow rate across the interface can be extracted from the output of the hydrodynamic model:

$$\frac{\partial S}{\partial t} = \frac{S_{n+1}-S_n}{\Delta t} = \frac{\Delta x}{\Delta t}\left(AS_j^{n+1}-AS_j^n\right) \qquad (4\text{-}106)$$

where AS is the cross sectional area of the storage zone computed in the hydrodynamic analysis.

Concentration during flood tide can be represented by the average concentration during the timestep:

$$C_{Flood} = \left(\frac{W_j^{n+1}}{A_j^{n+1}} + \frac{W_j^n}{A_j^n}\right) \frac{1}{2\gamma\Delta x} \qquad (4\text{-}107)$$

Concentration during an ebb tide can also be represented by an average concentration:

$$C_{Ebb} = \left(\frac{WS_j^{n+1}}{A_j^{n+1}} + \frac{WS_j^n}{A_j^n}\right) \frac{1}{2\gamma\Delta x} \qquad (4\text{-}108)$$

This expression can be simplified by neglecting concentration changes in the storage zone during the timestep. This is reasonable because no longitudinal advection occurs, and during these ebb tide timesteps no higher or lower concentration water is introduced into the storage zone. Concentration changes occur only as a result of contaminant decay.

For a decay rate of 1.0/day and a timestep of 30 minutes, the error introduced by this approximation is only 2%. A simplified expression is therefore:

$$C_{Ebb} = \frac{WS_j^n}{A_j^n} \frac{1}{\gamma \Delta x} \tag{4-109}$$

The advantage of this simplification is that storage zone contaminant concentration is now handled explicitly in the flow zone computations. That is, the change in storage zone concentration does not have to be considered when calculating new flow zone concentrations. Decay of contaminant in the storage zone can still be correctly evaluated when new storage zone concentrations are subsequently computed.

The resulting expression for T_j^n is therefore

$$T_j^n = \begin{cases} \dfrac{AS_j^{n+1} - A_j^n}{2\Delta t} \left(\dfrac{W_j^{n+1}}{A_j^{n+1}} + \dfrac{W_j^n}{A_j^n} \right) & \text{For } AS_j^{n+1} > AS_j^n \text{ (Flood Tide)} \\ \dfrac{AS_j^{n+1} - AS_j^n}{\Delta t} \left(\dfrac{WS_j^n}{AS_j^n} \right) & \text{For } AS_j^{n+1} > AS_j^n \text{ (Ebb Tide)} \end{cases} \tag{4-110}$$

Before returning to the flow zone computation, the storage zone computation is completed as follows:

$$\frac{\partial W_S}{\partial t} = \frac{WS_j^{n+1} - WS_j^n}{\Delta t} \tag{4-111}$$

$$KW_S = K \left(\frac{WS_j^{n+1} + WS_j^n}{2}\right) \tag{4-112}$$

Therefore, the governing equation for the storage zone concentration can be approximated by:

$$\frac{WS_j^{n+1} - WS_j^n}{\Delta t} = -K \left(\frac{WS_j^{n+1} + WS_j^n}{2}\right) + N \left\{\left(\frac{AS_j^{n+1} - AS_j^n}{2\Delta t}\right)\left(\frac{W_j^{n+1}}{A_j^{n+1}} + \frac{W_j^n}{A_j^n}\right)\right\}$$

$$+ M \left\{\left(\frac{AS_j^{n+1} - AS_j^n}{\Delta t}\right)\left(\frac{WS_j^n}{AS_j^n}\right)\right\} \tag{4-113}$$

where

$$\text{Where } N = \begin{cases} 1 \text{ For } AS_j^{n+1} > AS_j^n \\ 0 \text{ Otherwise} \end{cases} \tag{4-114}$$

$$M = \begin{cases} 1 \text{ For } AS_j^{n+1} < AS_j^n \\ 0 \text{ Otherwise} \end{cases} \tag{4-115}$$

Solving for WS_j^{n+1} leads to

$$WS_j^{n+1} = WS_j^n \left\{ \frac{1 + M\left(\frac{AS_j^{n+1} - AS_j^n}{AS_j^n}\right) - \frac{K\Delta t}{2}}{1 + \frac{K\Delta t}{2}} \right\}$$

$$+ N \left\{ \frac{\left(\frac{AS_j^{n+1} - AS_j^n}{2\Delta_j^{n+1}}\right)(W_j^{n+1}) + \left(\frac{AS_j^{n+1} - AS_j^n}{2\Delta_j^n}\right)(W_j^n)}{1 + \frac{K\Delta t}{2}} \right\} \tag{4-116}$$

At each timestep of the computation, this equation can be solved explicitly using data from the hydrodynamic analysis. The values of W_j^n and WS_j^n are known from the previous timestep. The remaining variable, W_j^{n+1}, is provided by implicit solution of the flow zone governing equation which is solved before storage zone concentrations are updated.

Returning now to the flow zone computation and including the interface flux term T_j^n, we have

$$\frac{R}{B_a} - KW - T = CQ_j^n - \frac{K}{2}\left(W_j^n + W_j^{n+1}\right) - N\left\{\left(\frac{AS_j^{n+1} - AS_j^n}{2\Delta t}\right)\left(\frac{W_j^{n+1}}{A_j^{n+1}} + \frac{W_j^n}{A_j^n}\right)\right\} - M\left\{\left(\frac{AS_j^{n+1} - AS_j^n}{\Delta t}\right)\left(\frac{WS_j^n}{AS_j^n}\right)\right\} \qquad (4\text{-}117)$$

The complete governing finite difference equation at interior points is obtained by combining the expressions for the time derivative, advective transport, dispersive transport and sources (equations (4-100), (4-101) and (4-102)). By isolating similar terms, these expressions yield an equation with three unknown contaminant weights

$$\alpha_j^n W_{j-1}^{n+1} + \beta_j W_j^{n+1} + \gamma_j^n W_{j+1}^{n+1} = \delta_j^n \qquad (4\text{-}118)$$

where:

$$\alpha_j^n = \frac{u_{j-1}^{n+1}}{4\Delta x} - \frac{1}{2\Delta x^2}\left[\left(\frac{E_j^{n+1}+E_{j-1}^{n+1}}{2}\right)\left(\frac{A_j^{n+1}+A_{j-1}^{n+1}}{2}\right)\frac{1}{A_{j-1}^{n+1}}\right] + \frac{1}{6\Delta t} \qquad (4\text{-}119)$$

$$\beta_j^n = \frac{1}{2\Delta x^2}\left[\left(\frac{E_{j+1}^{n+1}+E_j^{n+1}}{2}\right)\left(\frac{A_{j+1}^{n+1}+A_j^{n+1}}{2}\right)\frac{1}{A_j^{n+1}} + \left(\frac{E_j^{n+1}+E_{j-1}^{n+1}}{2}\right)\left(\frac{A_j^{n+1}+A_{j-1}^{n+1}}{2}\right)\frac{1}{A_j^{n+1}}\right] + \frac{2}{3\Delta t} + \frac{K}{2} + N\left\{\left(\frac{j^{n+1}-AS_j^n}{2\Delta t}\right)\frac{1}{A_j^{n+1}}\right\} \qquad (4\text{-}120)$$

$$\gamma_j^n = \frac{u_{j+1}^{n+1}}{4\Delta x} - \frac{1}{2\Delta x^2}\left[\left(\frac{E_{j+1}^{n+1}+E_j^{n+1}}{2}\right)\left(\frac{A_{j+1}^{n+1}+A_j^{n+1}}{2}\right)\frac{1}{A_{j+1}^{n+1}}\right] + \frac{1}{6\Delta t} \qquad (4\text{-}121)$$

$$\delta_j^n = \left\{\frac{2}{3\Delta t} - \left(\frac{E_{j+1}^n+E_j^n}{4\Delta x^2}\right)\left(\frac{A_{j+1}^n+A_j^n}{2}\right)\frac{1}{A_j^n} - \left(\frac{E_j^n+E_{j-1}^n}{4\Delta x^2}\right)\left(\frac{A_j^n+A_{j-1}^n}{2}\right)\frac{1}{A_j^n} - \frac{K}{2} - N\left(\frac{AS_j^{n+1}-AS_j^n}{2\Delta t A_j^n}\right)\right\} * W_j^n + \left\{\frac{1}{6\Delta t} + \frac{u_{j-1}^n}{4\Delta x} + \left(\frac{E_{j+1}^n+E_{j-1}^n}{4\Delta x^2}\right)\left(\frac{A_j^n+A_{j-1}^n}{2}\right)\frac{1}{A_{j-1}^n}\right\} * W_{j-1}^n + \left\{\frac{1}{6\Delta t} - \frac{u_{j+1}^n}{4\Delta x} + \left(\frac{E_{j+1}^n+E_j^n}{4\Delta x^2}\right)\left(\frac{A_{j+1}^n+A_j^n}{2}\right)\frac{1}{A_{j+1}^n}\right\} * W_{j+1}^n + CQ_j^n - M\left\{\left(\frac{AS_j^{n+1}-AS_j^n}{\Delta t}\right)\frac{1}{AS_j^n}\right\} * WS_j^n \qquad (4\text{-}122)$$

Considering all points simultaneously, a tri-banded matrix equation can be written at each timestep:

$$\begin{vmatrix} — & — & — & & & \\ & & & & & \\ \alpha_{j-1}^n & \beta_{j-1}^n & \gamma_{j-1}^n & & & \\ & \alpha_j^n & \beta_j^n & \gamma_j^n & & \\ & & \alpha_{j+1}^n & \beta_{j+1}^n & \gamma_{j+1}^n & \\ & & & — & — & — \end{vmatrix} \begin{vmatrix} \\ W_{j-1}^{n+1} \\ W_j^{n+1} \\ W_{j+1}^{n+1} \\ \end{vmatrix} = \begin{vmatrix} \\ \delta_{j-1}^n \\ \delta_j^n \\ \delta_{j+1}^n \\ \end{vmatrix}$$

(4-123)

4.2.3. Boundary Conditions

Evaluation of the coefficients in the first and last rows requires application of the boundary conditions. This is discussed further below. Since the coefficients contain only known information, numerical values can be calculated. Using these coefficients, the value of W at the end of the timestep can be calculated for all points simultaneously. The numerical model employs the compact Thomas algorithm originally coded into the computer program by Lee. The method is straightforward wherein the coefficient matrix is triangularized and then solved by a two-step, row-by-row procedure. No further discussion will be made here, but more detail is provided by Lee (1970).

Returning now to the boundary conditions, evaluation of coefficients in the first row of the matrix requires that the river end condition be specified.

The evaluation of boundary conditions will be simplified if the advective and dispersive flux terms of the general finite difference expressions are broken down into flux components at the upstream end of the segment and the downstream end. The governing equation is therefore expanded to six terms

$$\frac{1}{\Delta t}\left[\frac{1}{6}\left(W_{j-1}^{n+1}-W_{j-1}^{n}\right)+\frac{2}{3}\left(W_{j}^{n+1}-W_{j}^{n}\right)+\frac{1}{6}\left(W_{j+1}^{n+1}-W_{j+1}^{n}\right)\right] \qquad (4\text{-}124)$$

$$\frac{1}{4\Delta x}\left[u_j^{n+1}W_j^{n+1}+u_j^{n}W_j^{n}+u_{j+1}^{n+1}W_{j+1}^{n+1}+u_{j+1}^{n}W_{j+1}^{n}\right] \tag{4-125}$$

$$\frac{1}{-4\Delta x}\left[u_{j-1}^{n+1}W_{j-1}^{n+1}+u_{j-1}^{n}W_{j-1}^{n}+u_j^{n+1}W_j^{n+1}+u_j^{n}W_j^{n}\right] \tag{4-126}$$

$$\frac{1}{-2\Delta x^2}\left[\left(\frac{E_{j+1}^{n+1}+E_j^{n+1}}{2}\right)\left(\frac{A_{j+1}^{n+1}+A_j^{n+1}}{2}\right)\left(\frac{W_{j+1}^{n+1}}{A_{j+1}^{n+1}}-\frac{W_j^{n+1}}{A_j^{n+1}}\right)+\left(\frac{E_{j+1}^{n}+E_j^{n}}{2}\right)\left(\frac{A_{j+1}^{n}+A_j^{n}}{2}\right)\left(\frac{W_{j+1}^{n}}{A_{j+1}^{n}}-\frac{W_j^{n}}{A_j^{n}}\right)\right] \tag{4-127}$$

$$\begin{aligned}\frac{1}{+2\Delta x^2}&\left[\left(\frac{E_j^{n+1}+E_{j-1}^{n+1}}{2}\right)\left(\frac{A_j^{n+1}+A_{j-1}^{n+1}}{2}\right)\left(\frac{W_j^{n+1}}{A_j^{n+1}}-\frac{W_{j-1}^{n+1}}{A_{j-1}^{n+1}}\right)\right.\\&\left.+\left(\frac{E_j^{n}+E_{j-1}^{n}}{2}\right)\left(\frac{A_j^{n}+A_{j-1}^{n}}{2}\right)\left(\frac{W_j^{n}}{A_j^{n}}-\frac{W_{j-1}^{n}}{A_{j-1}^{n}}\right)\right]\end{aligned} \tag{4-128}$$

$$\begin{aligned}= CQ_j^n-\frac{K}{2}\left(W_j^n+W_j^{n+1}\right)&-N\left\{\left(\frac{AS_j^{n+1}-AS_j^n}{2\ t}\right)\left(\frac{W_j^{n+1}}{A_j^{n+1}}+\frac{W_j^n}{A_j^n}\right)\right\}\\&-M\left\{\left(\frac{AS_j^{n+1}-AS_j^n}{t}\right)\frac{WS_j^n}{AS_j^n}\right\}\end{aligned} \tag{4-129}$$

The river end boundary has been described as a point of no flux into or out of the system. Contaminant entering the estuary is handled as a lateral boundary source and does not affect this description of the end boundary. Under these conditions the advective flux term for the first segment reduces to

$$\frac{\partial(\bar{u}\ W)}{\partial x} = \frac{1}{4\Delta x}\left[u_{j+1}^{n} W_{j+1}^{n} + u_{j}^{n} W_{j}^{n} + u_{j+1}^{n+1} W_{j+1}^{n+1} + u_{j}^{n+1} W_{j}^{n+1}\right] \qquad (4\text{-}130)$$

Similarly, the dispersive flux term reduces to

$$-\frac{\partial}{\partial x}\left[AE\frac{\partial^{(W/A)}}{\partial x}\right] = -\frac{1}{2\Delta x^{2}}\left\{\left(\frac{E_{j+1}^{n+1}+E_{j}^{n+1}}{2}\right)\left(\frac{A_{j+1}^{n+1}+A_{j}^{n+1}}{2}\right)\left(\frac{W_{j+1}^{n+1}}{A_{j+1}^{n+1}} - \frac{W_{j}^{n+1}}{A_{j}^{n+1}}\right)\right.$$

$$\left. + \left(\frac{E_{j+1}^{n}+E_{j}^{n}}{2}\right)\left(\frac{A_{j+1}^{n}+A_{j}^{n}}{2}\right)\left(\frac{W_{j+1}^{n}}{A_{j+1}^{n}} - \frac{W_{j}^{n}}{A_{j}^{n}}\right)\right\} \qquad (4\text{-}131)$$

Because the computation for this first segment does not include an adjacent segment J-1, it is also necessary to reconsider the Stone and Brian representation of the time derivative term $\partial W/\partial t$ To ensure conservation of mass, the sum of the weighting factors (1/6, 2/3, 1/6) must equal 1.0. The 1/6 weight previously committed to the J-1 segment must therefore be reallocated to the first segment, resulting in a new set of weighting factors (0, 5/6, 1/6). The time derivative term therefore becomes:

$$\frac{\partial W}{\partial t} = \frac{1}{\Delta t}\left[\frac{5}{6}(W_j^{n+1}-W_j^n)+\frac{1}{6}(W_{j+1}^{n+1}-W_{j+1}^n)\right] \tag{4-132}$$

Finally, the matrix coefficients for the first row of the matrix are:

$$\alpha_1^n = 0 \tag{4-133}$$

$$\beta_1^n = \frac{1}{2\Delta x^2}\left[\left(\frac{E_{j+1}^{n+1}+E_j^{n+1}}{2}\right)\left(\frac{A_{j+1}^{n+1}+A_j^{n+1}}{2}\right)\right]\frac{1}{A_j^{n+1}} + \frac{5}{6\Delta t} + \frac{K}{2} + \frac{u_j^{n+1}}{4\Delta x} + N\left\{\left(\frac{AS_j^{n+1}-AS_j^n}{2\Delta t}\right)\frac{1}{A_j^{n+1}}\right\} \tag{4-134}$$

$$\gamma_1^n = \frac{u_{j+1}^{n+1}}{4\Delta x} - \frac{1}{2\Delta x^2}\left[\left(\frac{E_{j+1}^{n+1}+E_j^{n+1}}{2}\right)\left(\frac{A_{j+1}^{n+1}+A_j^{n+1}}{2}\right)\frac{1}{A_{j+1}^{n+1}}\right] + \frac{1}{6\Delta t} \tag{4-135}$$

$$\delta_1^n = \left\{ \left(\frac{5}{6\,t} - \frac{1}{2\,x^2} \left(\frac{E_{j+1}^n + E_j^n}{2} \right) \left(\frac{A_{j+1}^n + A_j^n}{2} \right) \frac{1}{A_j^n} - \frac{K}{2} - \frac{u_j^n}{4\,x} - N \left(\frac{AS_j^{n+1} - AS_j^n}{2\Delta t A_j^n} \right) \right\} * W_j^n \right.$$

$$+ \left\{ \frac{1}{6\Delta x} - \frac{u_{j+1}^n}{4\Delta x} + \left(\frac{E_{j+1}^n + E_j^n}{2} \right) \left(\frac{1}{2\Delta x^2} \right) \left(\frac{A_{j+1}^n + A_j^n}{2} \right) \frac{1}{A_{j+1}^n} \right\} * W_{j+1}^n + CQ_j^n$$

$$\left. - M \left\{ \left(\frac{AS_j^{n+1} - AS_j^n}{t} \right) \frac{1}{AS_j^n} \right\} * WS_j^n \right. \qquad (4\text{-}136)$$

The ocean end of the estuary may be described in a number of different ways depending on the specific problem to be analyzed. However, all of these fall into one of two categories which specify either a concentration at the boundary or a flux across the boundary. These in turn may be constant or may vary during the tidal cycle and from one cycle to the next.

Consider first the concentration type boundary conditions where contaminant concentrations beyond the mouth of the estuary are known. This type of condition requires that the effect of contaminants discharged from the estuary is small in the adjacent ocean or other water body. This could result from either a large current across the mouth of the estuary or a rapid mixing of contaminants into a large volume of water. Under these conditions, all concentration terms for the J segment are known and provided as input data. These terms may therefore be moved to the right side of the matrix equation. When this type of boundary condition is used, the actual mouth of the estuary is upstream of the last segment, so velocity,

area and dispersion data can be determined for the J segment. The matrix equation is reduced by one row, and the coefficients of the last row (J-1) are:

$$\alpha^n_{j-1} = -\frac{u^{n+1}_{j-2}}{4\Delta x} - \frac{1}{2\Delta x^2}\left[\left(\frac{E^{n+1}_{j-1}+E^{n+1}_{j-2}}{2}\right)\left(\frac{A^{n+1}_{j-1}+A^{n+1}_{j-2}}{2}\right)\frac{1}{A^{n+1}_{j-2}}\right] + \frac{1}{6\Delta t} \qquad (4\text{-}137)$$

$$\beta^n_{j-1} = \frac{1}{2\Delta x^2}\left[\left(\frac{E^{n+1}_{j}+E^{n+1}_{j-1}}{2}\right)\left(\frac{A^{n+1}_{j}+A^{n+1}_{j-1}}{2}\right)\frac{1}{A^{n+1}_{j-1}} + \left(\frac{E^{n+1}_{j-1}+E^{n+1}_{j-2}}{2}\right)\left(\frac{A^{n+1}_{j-1}+A^{n+1}_{j-2}}{2}\right)\frac{1}{A^{n+1}_{j-1}}\right]$$
$$+ \frac{2}{3\Delta t} + \frac{K}{2} + N\left(\frac{AS^{n+1}_{j-1}-AS^{n}_{j-1}}{2\Delta t}\right)\frac{1}{A^{n+1}_{j-1}} \qquad (4\text{-}138)$$

$$\gamma^n_{j-1} = 0 \qquad (4\text{-}139)$$

$$\delta^n_{j-1} = -C^{n+1}_{BC} * A^{n+1}_{j}\left\{\frac{u^{n+1}_{j}}{4\Delta x} - \frac{1}{2\Delta x^2}\left(\frac{E^{n+1}_{j}+E^{n+1}_{j-1}}{2}\right)\left(\frac{A^{n+1}_{j}+A^{n+1}_{j-1}}{2}\right)\frac{1}{A^{n+1}_{j}} + \frac{1}{6\Delta t}\right\}$$
$$+\left\{\frac{2}{3\Delta t} - \left(\frac{E^{n}_{j}+E^{n}_{j-1}}{4\Delta x^2}\right)\left(\frac{A^{n}_{j}+A^{n}_{j-1}}{2}\right)\frac{1}{A^{n}_{j-1}} - \left(\frac{E^{n}_{j-1}+E^{n}_{j-2}}{4\Delta x^2}\right)\left(\frac{A^{n}_{j-1}+A^{n}_{j-2}}{2}\right)\frac{1}{A^{n}_{j-1}} - \frac{K}{2}\right.$$
$$\left. - N\left(\frac{AS^{n+1}_{j-1}+AS^{n}_{j-1}}{2\Delta t A^{n}_{j-1}}\right)\right\} * W^n_{j-1} + \left\{\frac{1}{6\Delta t} + \frac{u^n_{j-2}}{4\Delta x} + \left(\frac{E^{n}_{j-1}+E^{n}_{j-2}}{4\Delta x^2}\right)\left(\frac{A^{n}_{j-1}+A^{n}_{j-2}}{2}\right)\frac{1}{A^{n}_{j-2}}\right\}$$
$$* W^n_{j-2} + \left\{\frac{1}{6\Delta t} - \frac{u^n_{j}}{4\Delta x} + \left(\frac{E^{n}_{j}+E^{n}_{j-1}}{4\Delta x^2}\right)\left(\frac{A^{n}_{j}+A^{n}_{j-1}}{2}\right)\frac{1}{A^{n}_{j}}\right\} * C^n_{BC} * A^n_j + CQ^n_{j-1}$$
$$- M\left\{\left(\frac{AS^{n+1}_{j-1}+AS^{n}_{j-1}}{t}\right)\frac{1}{AS^{n}_{j-1}}\right\} * WS^n_{j-1} \qquad (4\text{-}140)$$

where C_{BC}^{n+1} and C_{BC}^{n} are the boundary concentrations at the next timestep and the present one, respectively, and capital J represents the last river segment.

Now consider the flux type boundary conditions where constraints are placed on the transport of contaminant across the mouth of the estuary. These boundary conditions are more difficult to relate to measurable or readily specified quantities. Furthermore, flux boundary conditions necessarily link the estuary and ocean concentrations (i.e., are dependent on both). This is different from the concentration boundary condition which was identified only with ocean concentrations.

Advective boundary flux at the downstream end of internal segments is based on the average flux in segment J and J+1 over timesteps n and n+1. When this segment is an ocean boundary segment, flux in the J+1 segment is meaningless. Therefore, a different way must be found to specify advective flux. If the current is flowing out of the estuary, it is reasonable to represent the boundary flux in terms of conditions in the last segment only. That is, the downstream advective flux from the last segment can be represented by:

$$\frac{1}{2\Delta x}\left[u_j^{n+1}W_j^{n+1}+u_j^{n}W_j^{n}\right] = F_A \qquad (4\text{-}141)$$

Equivalently, we may state that the flux through the nearby ocean region is equal to the average flux in the boundary segment at all times. This leads to the same expression for this term.

On the returning tide with current flowing into the estuary, we must consider the ocean concentration more thoroughly. If it is assumed that all contaminant discharged from the mouth of the estuary is carried away, then the flood tide advective transport will be equal to zero. On the other hand, if it is assumed that the flood tide flux is simply a mirror image of the ebb tide flux (that is, essentially all of the contaminant returns) then the boundary flux is defined in the same way as above. This leads to the possibility of intermediate conditions which can be defined by a return rate, RETRT, where:

$$0 \leq \text{RETRT} \leq 1.0 \qquad (4\text{-}142)$$

Under these conditions the advective boundary flux on a flood tide may be defined by:

$$RETRT * \frac{1}{2\Delta x} [u_j^{n+1} W_j^{n+1} + u_j^n W_j^n] = F_{AA} \qquad (4\text{-}143)$$

Now consider the dispersive flux; at the downstream end of an intermediate segment, this term is defined by average dispersion coefficients and areas for segments J and J+1, and a concentration gradient between these two segments. For a boundary segment, variables at segment J+1 are undefined. Therefore, approximations for these values are required. When the contaminant source is far removed from the ocean boundary (as in the cases of interest here), it is reasonable to state that the concentration gradient is not changing dramatically between segments. The boundary concentration gradient can therefore be approximated by the gradient occurring between the next to last segment and the boundary segment. That is,

$$\left(\frac{W_{j+1}^n}{A_{j+1}^n} - \frac{W_j^n}{A_j^n}\right) \equiv \left(\frac{W_j^n}{A_j^n} - \frac{W_{j-1}^n}{A_{j-1}^n}\right) \qquad (4\text{-}144)$$

Insofar as area and dispersion coefficients are concerned, the most reasonable values for computation of boundary flux are the values computed for the last segment. Combining these dispersive flux approximations with the advective flux terms leads to the following matrix coefficients for the ocean boundary segment for ebb tide:

$$\alpha_j^n = -\frac{u_{j-1}^{n+1}}{4\Delta x} - \frac{1}{2\Delta x^2}\left[\frac{-E_j^{n+1}A_j^{n+1}}{A_{j-1}^{n+1}} + \left(\frac{E_j^{n+1}+E_{j-1}^{n+1}}{2}\right)\left(\frac{A_j^{n+1}+A_{j-1}^{n+1}}{2}\right)\frac{1}{A_{j-1}^{n+1}}\right] + \frac{1}{6\Delta t} \tag{4-145}$$

$$\beta_j^n = \frac{u_j^{n+1}}{4\Delta x} - \frac{1}{2\Delta x^2}\left[\frac{E_j^{n+1}A_j^{n+1}}{A_{j-1}^{n+1}} - \left(\frac{E_j^{n+1}+E_{j-1}^{n+1}}{2}\right)\left(\frac{A_j^{n+1}+A_{j-1}^{n+1}}{2}\right)\frac{1}{A_j^{n+1}}\right] + \frac{5}{6\Delta t} + \frac{K}{2} + N\left\{\left(\frac{AS_j^{n+1}-AS_j^n}{2\Delta t}\right)\frac{1}{A_j^{n+1}}\right\} \tag{4-146}$$

$$\gamma_j^n = 0 \tag{4-147}$$

$$\delta_j^n = \left\{\frac{5}{6\Delta t} + \frac{1}{2\Delta x^2}\left[\frac{-E_j^nA_j^n}{A_{j-1}^n} - \left(\frac{E_j^n+E_{j-1}^n}{2}\right)\left(\frac{A_j^n+A_{j-1}^n}{2}\right)\frac{1}{A_j^{n+1}}\right] - \frac{u_{j-1}^n}{4\Delta x}\right\} * W_{j-1}^n + CQ_j^n - M\left\{\left(\frac{AS_j^{n+1}-AS_j^n}{\Delta t}\right)\frac{1}{AS_j^n}\right\} * WS_j^n \tag{4-148}$$

The coefficients for the flood tide are similar except that the advective flux terms now take account of the flushing return rate coefficient. Coefficients α_j^n and γ_j^n are unchanged, but β_j^n and δ_j^n become:

$$\beta_j^n = (2*\text{RETRT}-1)\,\frac{u_j^{n+1}}{4\Delta x} \qquad (4\text{-}149)$$

$$\delta_j^n = -(2*\text{RETRT}-1)\,\frac{u_j^n}{4\ x} \qquad (4\text{-}150)$$

The appropriate values of matrix coefficients for the two boundary segments are computed at each timestep. This therefore completes the matrix equation (4-123) and allows a solution vector to be determined.

4.2.4 Representation of Dispersion Processes

Dispersive flux terms entered into the governing equation for transport of contaminants as a result of spatial integration. The averaging process implied when reducing the three-dimensional equation down to two, and finally one-dimensional form, requires that consideration be given to so-called "cross product" terms. These terms take the form of:

$$\int_0^{-h} u'C'dz \qquad (4\text{-}151)$$

where u' = the variation of longitudinal velocity from its depth averaged mean $\bar{u}$,

c' = the variation of contaminant concentration from its depth averaged mean $\bar{c}$,

$-h$ = water depth

Variations described here generally result from frictional effects at the side and bottom boundaries of the channel.

A similar set of cross product terms result from lateral integration of the governing equations. The similarity of this process to molecular diffusion resulting from random motion of particles has led to common use of an analogy to the Fickian representation of diffusion. This analogy may be stated as follows:

$$\frac{1}{h}\int_{0}^{-h} u'C'dz \equiv E_{xz}\frac{\partial \overline{C}}{\partial x} \qquad (4\text{-}152)$$

where E_{xz} is a longitudinal (x direction) dispersion coefficient resulting from vertical (z direction) variation in velocity and concentration. Similarly, for lateral (y direction) variations:

$$\frac{1}{w}\int_{-w/2}^{w/2} u'C'dy \equiv E_{xy}\frac{\partial \overline{C}}{\partial x} \qquad (4\text{-}153)$$

If we consider the entire cross sectional area, the longitudinal dispersion process is represented by:

$$\frac{1}{A}\int_A u'C'dA \equiv E\frac{\partial \overline{C}}{\partial x} \qquad (4\text{-}154)$$

The classical work of G. I. Taylor on dispersion of salt in pipe flow demonstrated that the dispersion coefficient can be approximated by:

$$E = 10.1\, r_0 u^* \qquad (4\text{-}155)$$

where r_0 = pipe radius

$u^* = \sqrt{\tau_0/\rho}$ the friction velocity

τ_0 = shear stress at the pipe wall

ρ = density of water

By manipulation of the definition of friction velocity, it can be related to the Mannings roughness coefficient, n:

$$u^* = \frac{V_n}{1.49} \sqrt{g}\ R^{-1/6} \qquad (4\text{-}156)$$

where V = flow velocity

R = hydraulic radius

n = Mannings roughness coefficient

g = acceleration of gravity = 32.2 ft/sec^2

In English units, this results in the following formula for the dispersion coefficient in pipe flow:

$$E = CRu^* \qquad (4\text{-}157a)$$

Many investigators have derived alternative expressions for defining dispersion coefficients in natural channels. Frequently, these results are normalized by comparing them to the Taylor expression. This has led to a large volume of data in the form of coefficients for the following expression

$$E = C' V_n R^{5/6} \qquad (4\text{-}157b)$$

$$\text{Where } C' = \frac{\sqrt{g}}{1.49} * C = 3.808 * C \qquad (4\text{-}158)$$

In this form, coefficients may range from 100 to 10,000 depending on the flow conditions. These coefficients reflect not only frictional effects but also irregularities of the natural channels and the design of the measuring system. In the absence of better data, a value of approximately three times the Taylor formula coefficient is a reasonable starting point for a natural channel. Selection of a final value for a specific location requires application of field data on mixing rates in the channel.

When dispersion coefficients are estimated for average conditions over a period of time (such as a tidal cycle), additional factors must be considered. In addition to

spatial variations in velocity and concentration, temporal variation must be taken into account. Integration of the governing transport equations over time leads to terms such as:

$$\frac{1}{T}\int_0^T u''C''dt = \text{Diffusive Transport} \qquad (4\text{-}159)$$

where u" and c" are temporal variation of velocity and concentration from their time averaged means, respectively. Dispersion effects due to temporal variations in tidal channels have been shown to exceed those due to spatial variations by one or more orders of magnitude. The higher values of coefficients described above are those which deal with tidal cycle averaged conditions. These temporal effects are not considered in the water quality model because "instantaneous" values are computed at each timestep. However, computation of the tidal cycle averaged salinity gradient described previously in section 4.1.3 did employ a large coefficient to account for this effect.

For the tidal rivers of interest here, contaminant transport can also result from density driven circulation. Density driven circulation results when a strong longitudinal density gradient (due to longitudinal salinity variation) establishes a vertical stratification and vertical mixing is not sufficiently strong to destroy this

effect. Under these conditions, a net inward flow of denser water occurs at the bottom of the channel and a net outward flow of lighter water occurs at the surface. This results in additional variation of velocity from its vertically averaged mean and ultimately additional variation of contaminant concentration. These variations can again be related to an increased effective dispersion coefficient.

Previous work by Hansen and Rattray (1962) and Officer (1977) has produced analytical solutions for vertical velocity profiles in stratified estuary flow. For the case of a uniform longitudinal salinity gradient over the depth, and a bottom boundary condition of zero velocity, the tidal cycle averaged circulation velocity profile is given as:

$$v_x = \frac{gh^3}{48N_z}\frac{\lambda}{\rho}(1-9n^2+8n^3) + \frac{3}{2}v_0(1-n^2) \qquad (4\text{-}160)$$

The variation from the average velocity is therefore:

$$v' = v_x - v_0 = \frac{gh^3}{48N_z}\frac{\lambda}{\rho}(1-9n^2+8n^3) + \frac{3}{2}v_0(\frac{1}{3}-n^2) \qquad (4\text{-}161)$$

where h = depth of estuary

λ = longitudinal density gradient

ρ = density of water

N_z = vertical eddy viscosity coefficient

n = depth parameter z/h

z = vertical dimension

v_0 = net fresh water velocity

If we consider a steady state mass balance of salt in an elemental volume as shown in Figure 13, the most important flow processes are longitudinal advection and vertical turbulent diffusion. This leads to the following differential equation:

$$K_z\frac{\partial^2 S}{\partial z^2} = v_x\frac{\partial S}{\partial z} \qquad (4\text{-}162)$$

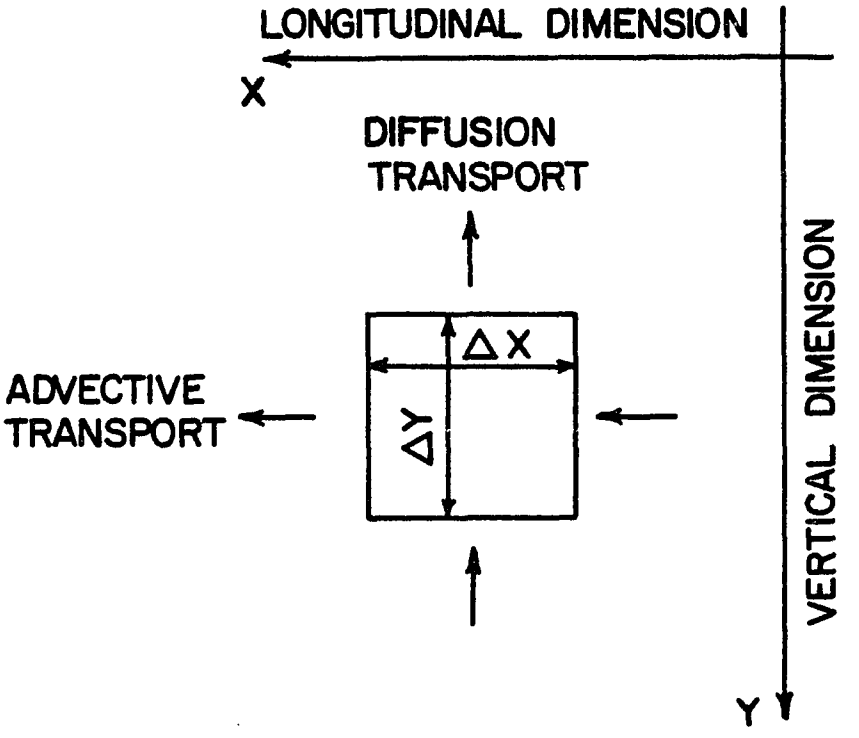

FIGURE 13

MASS BALANCE OF SALT FOR ELEMENTAL VOLUME

where K_z = vertical turbulent diffusion coefficient

v_x = longitudinal flow velocity

s = salinity

Integrating twice yields the vertical salinity profile:

$$S_z = \frac{1}{K_z} \frac{\partial S}{\partial x} \iint v_x \, dz \, dz + \int c_1 \, dz + c_z \qquad (4\text{-}163)$$

A boundary condition of $\partial S_z / \partial z = 0$ at $Z = 0$ gives $C_1 = 0$. Substituting for the vertical velocity profile:

$$S_z = \frac{1}{K_z} \frac{\partial S}{\partial x} \iint [v_S(1-9n^2+8n^3) + \frac{3}{2} v_0 (1-n^2)] \, dz \, dz + c_2 \qquad (4\text{-}164)$$

$$v_s = \frac{gh^3}{48N_z} \frac{\lambda}{\rho} \qquad (4\text{-}165)$$

where v_0 = net fresh water velocity.

Integratiion of this equation yields:

$$S_z = \frac{h^2}{K_z}\frac{\partial S}{\partial x}\left[v_S\left(\frac{n^2}{2} - \frac{3n^4}{4} + \frac{2n^5}{5}\right) + v_0\left(\frac{3n^2}{4} - \frac{n^4}{8}\right)\right] + C_2 \qquad (4\text{-}166)$$

Defining the average salinity by

$$S_{AVG} = \frac{1}{h}\int_0^h S_z \qquad (4\text{-}167)$$

$$S_{AVG} = \frac{h}{K_z}\frac{\partial S}{\partial x}\int_0^h \left[v_S\left(\frac{n^2}{2} - \frac{3n^4}{4} - \frac{2n^5}{5}\right) + v_0\left(\frac{3n^2}{4} - \frac{n^4}{8}\right)\right] dz + C_2 \qquad (4\text{-}168)$$

$$S_{AVG} = \frac{h}{K_z}\frac{\partial S}{\partial x}\left[\frac{1}{12}v_s + \frac{9}{40}v_0\right] + C_2 \qquad (4\text{-}169)$$

and subtracting $S_z - S_{AVG}$ gives the following expression for variation of salinity from its average:

$$S' = \frac{h^2}{K_z}\frac{\partial S}{\partial x}\left[v_S\left(\frac{n^2}{2} - \frac{3n^4}{4} + \frac{2n^5}{5} - \frac{1}{12}\right) + v_0\left(\frac{3n^2}{4} - \frac{n^4}{8} - \frac{9}{40}\right)\right] \qquad (4\text{-}170)$$

Recalling the definition of the dispersion coefficient:

$$E_{xz} = -\frac{1}{D\frac{\partial \bar{C}}{\partial x}}\int_0^h u'C'dz \qquad (4\text{-}171)$$

or for the tidally averaged salt dispersion coefficient:

$$E_S = -\frac{1}{h\frac{\partial S}{\partial x}}\int_0^h (v_x - v_0)S'dz \qquad (4\text{-}172)$$

and substituting for v_x and S' results in

$$E_S = \frac{-h}{K_z} \int_0^h [v_S(1-9n^2+8n^3) + v_0(\frac{1}{2} - \frac{3}{2} n^2)]$$

$$* [v_S(\frac{n^2}{2} - \frac{3n^4}{4} + \frac{2n^5}{5} - \frac{1}{12}) + v_0(\frac{3n^2}{4} - \frac{n^4}{8} - \frac{9}{40})] dz \qquad (4\text{-}173)$$

Carrying out this integration results in:

$$E_S = \frac{-h}{K_z} (.0302\, v_S^2 + .0369\, v_0 v_S + .0857\, v_0^2) \qquad (4\text{-}174)$$

where

$$v_s = \frac{gh^3}{48N_z} \frac{\partial\rho/\partial x}{\rho} \qquad (4\text{-}175)$$

Applying the approximation expression $\rho = 1 + .00075S$ for S defined in parts per thousand results in

$$v_s = \frac{gh^3}{48N_z} \frac{.00075 \frac{dS}{dx}}{1+.00075S} \tag{4-176}$$

Approximating the vertical eddy viscosity by an expression of the form of equation (4-157) with a coefficient K = 0.067 yields:

$$N_z = .255\ V_n R^{5/6} \tag{4-177}$$

and calculating the vertical turbulent diffusion coefficient by a similar expression with K = 0.034 yields:

$$K_z = .128\ V_n R^{5/6} \tag{4-178}$$

The circulation dispersion coefficient for salinity can therefore be calculated from equation (4-174) using density gradients described in Section 4.1.3. We now assume that mixing of contaminants in the water column will be identical to the mixing of salt. It is clear that this assumption is not correct for large particulate matter or materials adsorbed on these particles. However, for dissolved contaminants and fine or colloidal sized particulates the assumption is reasonable. One objective of the field studies described in Chapter 5 was to demonstrate the validity of this assumption.

The water quality model has now been completely described. Calibration and application runs of the model are described in Chapters 5 and 6. Further details of input and output data are given in Appendix A.

CHAPTER 5

FIELD DATA AND PARAMETER CALIBRATION

The analysis undertaken here includes several components, each requiring field data for adjustment of parameters. In some cases, extensive research has been done by others on the processes involved, and it was considered redundant to pursue these areas further in the limited context of this research program. This is particularly true of the hydrologic analysis, where parameters related to rainfall-runoff relationships and open channel flow in non-tidal streams were abstracted from the literature. In other cases, less work has been done, but complete investigation of these processes was not possible within this program and would be inconsistent with the objective of developing an economical, readily applied methodology. This is particularly true for the contaminant-generation processes on the land surface. Limited data in the literature was used for the analysis but was adjusted to best simulate field water quality data from the Durham Urban Runoff Project. In the case of estuarine processes, however, it is generally more difficult to assign proper values to important parameters. The complexity of these water bodies has prevented development of a universally applicable technique for assigning parameters. Therefore, a field program was

defined for gathering specific data on the Oyster River estuary. Calibration of the various model components for the Oyster River Basin and the method for synthesizing data for each is described in more detail below.

5.1 Hydrologic Analysis

Application of Soil Conservation Service hydrologic analysis techniques requires fairly extensive preliminary work. The basin must be divided into hydrologically similar sub-basins, the surface water system that interconnects these sub-basins must be identified, and important storage or flow control features located. These features of the Oyster River Basin were defined from USGS quadrangle and drainage maps obtained from the Town of Durham and the Strafford Regional Planning Commission. Using a 660-ft square grid system (10 acres), each element was assigned to one of approximately 100 minor sub-basins, and those containing a significant surface water feature were identified.

Due to the variety of land uses and soil types, these sub-basins were not necessarily hydrologically uniform. As described earlier, the problem of uniformity is handled by assigning SCS Runoff Curve Numbers, then allocating all areas to four CN values: 35, 71, 89 and 97. This results in approximately 400 hydrologic units to be considered in the analysis, a cumbersome and computationally prohibitive

number of sub-basins. Therefore, the 100 minor basins were aggregated into 26 sub-basins as shown in Figure 14. Sixteen of these, containing a total of 19.57 square miles, drain over the tide head dam. Five more containing 3.71 square miles drain to the upper reaches of the tidal river within a mile of the dam. The remaining five sub-basins, containing the balance of 7.36 square miles in the Oyster River Basin, drain directly to the lower reaches of the tidal river. Elevation data assigned to each grid element from USGS maps allowed the drainage pattern of the entire basin to be determined using the previously described data mangement system. This pattern is shown in Figure 15. Flow direction arrows contained in boxes are indicative of the presence of a surface water feature within the grid element. The data management program also calculated flow velocity (either overland or channel) for each grid element and sequentially summed the resulting travel times to produce travel time data from any point to the low point of the sub-basin. These were used, in turn, to assign the time of concentration for each sub-basin and the travel time (and velocity) through each stream reach. Results for the 26 sub-basins are given in Table 7. The allocation of areas to the four key Runoff Curve Numbers is given in Table 8.

This preliminary analysis produced all data required for the hydrologic analysis except the Antecedent Moisture Index. As indicated earlier, the Runoff Curve Numbers are

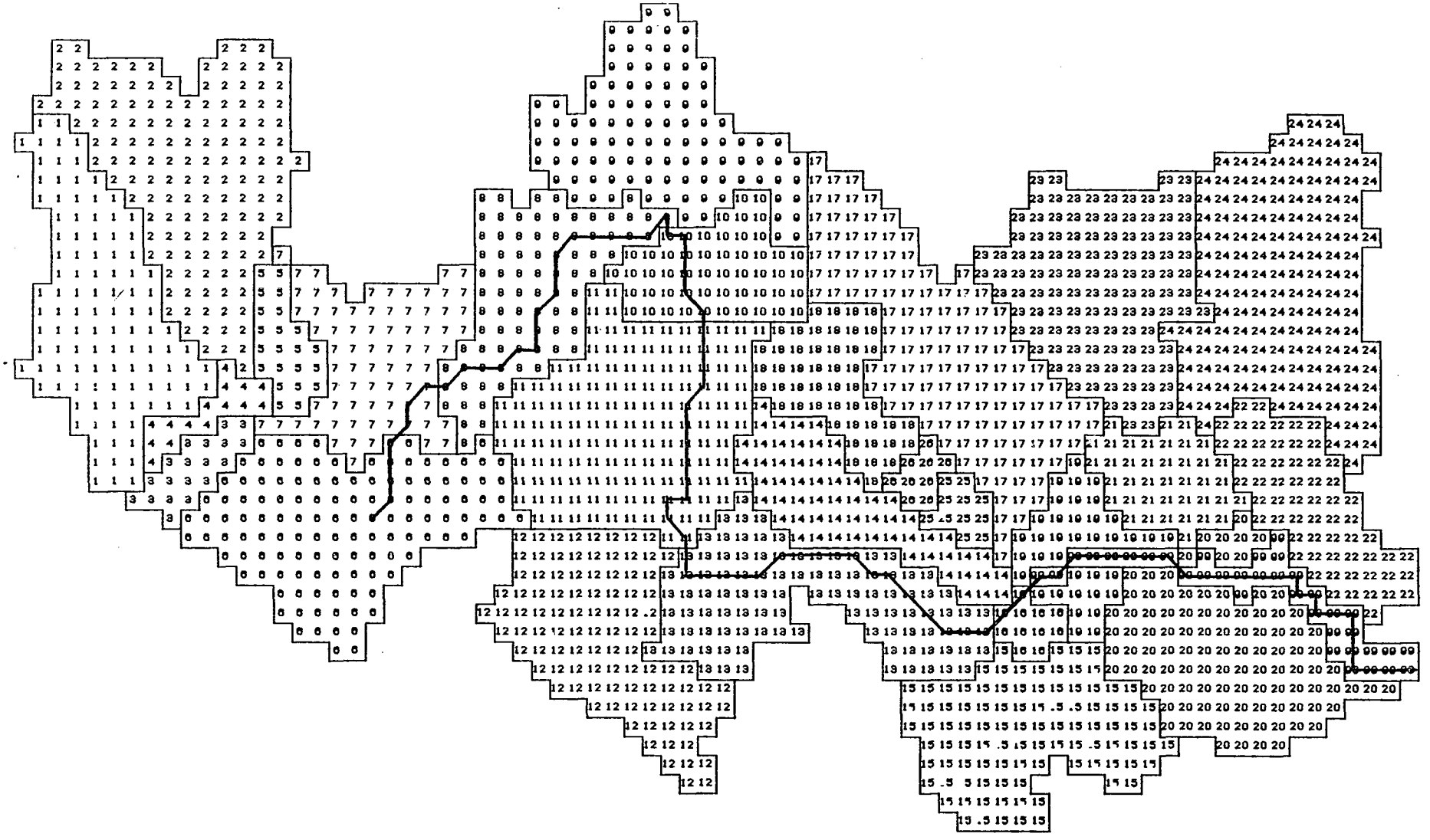

FIG 14 OYSTER RIVER SUB-BASINS

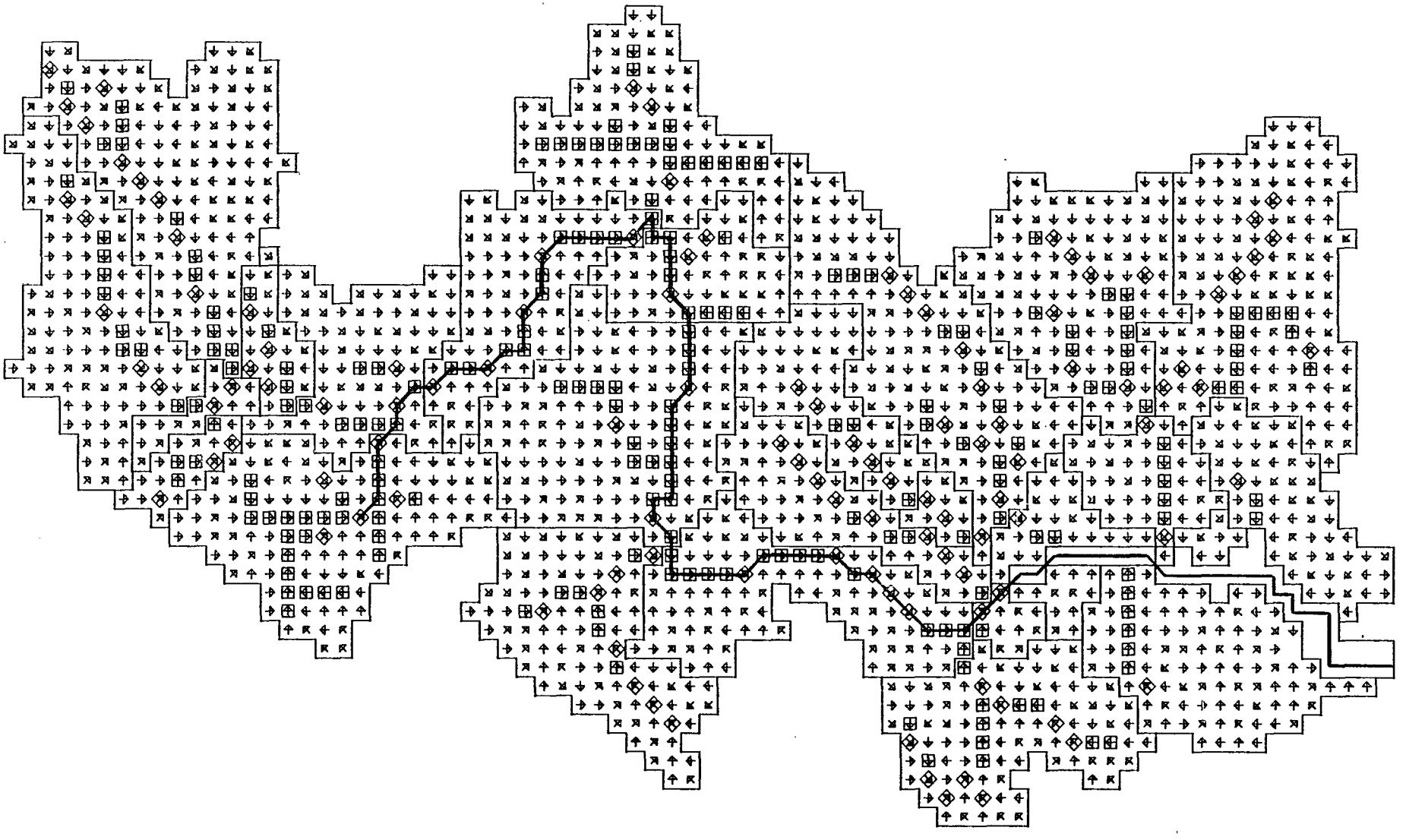

FIG 15 SURFACE DRAINAGE OYSTER RIVER BASIN

Table 7

Temporal Characteristics of the Oyster River Basin

SUB-BASIN	TIME OF CONCENTRATION (Hours)	STREAM TRAVEL TIME (Minutes)
1	3.06	47.68
2	15.17	80.75
3	1.35	39.11
4	2.28	8.54
5	0.80	15.20
6	5.05	78.25
7	5.33	48.05
8	2.27	48.52
9	5.37	47.33
10	5.06	25.25
11	4.27	47.69
12	3.33	80.05
13	4.09	41.78
14	3.28	44.26
15	2.13	52.45
16	1.35	7.29
17	4.57	58.94
18	5.29	21.09
19	3.68	2.96
20	8.38	40.91
21	2.85	29.12
22	4.91	17.25
23	2.88	35.61
24	7.58	63.45
25	0.42	7.69
26	1.33	4.64

Table 8

Runoff Curve Number Distribution in Oyster River Basin
(Areas in Acres)

SUB-BASIN	CN=35	CN=71	CN=89	CN=97
1	351	589	178	13
2	1175	209	25	0
3	165	14	11	0
4	72	68	10	0
5	132	69	12	8
6	421	522	227	100
7	462	179	101	16
8	325	378	106	3
9	24	820	196	0
10	56	398	67	0
11	432	719	211	0
12	180	637	176	1
13	144	519	347	0
14	12	325	245	16
15	22	611	336	0
16	0	67	43	0
17	137	911	265	13
18	60	329	91	0
19	9	234	116	11
20	30	726	271	10
21	25	301	73	0
22	61	460	98	0
23	513	479	133	0
24	450	836	206	1
25	0	44	63	3
26	0	58	32	0
TOTAL	5258 (26.8%)	10502 (53.6%)	3639 (18.6%)	195 (1.0%)

adjusted downward for dryer-than-normal and upward for wetter-than-normal conditions. The original SCS techniques allow for only three conditions: 1, 2, or 3. This was modified to allow an alternative range of 10 to 30 in increments of 1. When using the alternative range, a value of 10 is equivalent to the SCS 1 (dry condition), and 30 is equivalent to the SCS 3 (wet condition). The total volume of runoff is found to be quite sensitive to the assigned Antecedent Moisture Index. When simulating an actual storm, the results must be calibrated by adjusting this parameter. When predicting the impact of an individual future storm, it is likely that interest will focus on either an extreme condition or an average condition, so use of the SCS values 1, 2, or 3 will be entirely adequate. When considering a series of storms, judgment must be used in assigning values to the Antecedent Moisture Index for the second and successive storms.

The hydrologic model was calibrated for the storm of 25 October 1980 to demonstrate the model's ability to simulate flows in the Oyster River Basin. This major storm produced more than 2.5 inches of rain during a nine-hour period. Rainfall and stream flow data were available for the Pettee Brook gage of the Durham Urban Runoff Project. This gage receives drainage from sub-basins 18, 25, and 26, comprising approximately 1.1 square miles. Figure 16 presents a map of the general area modeled. Relatively dry conditions had prevailed before that storm, and the initial

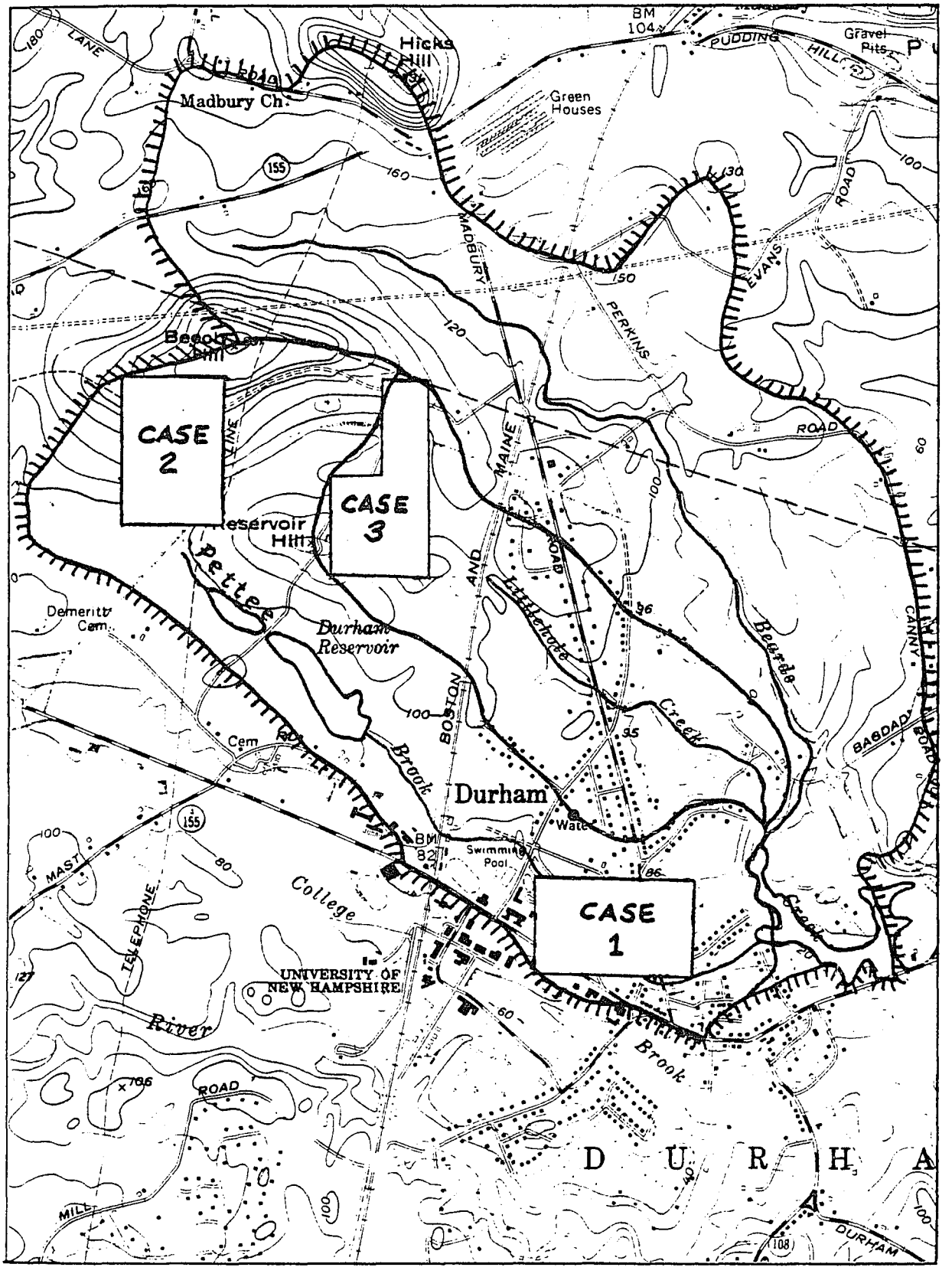

FIG 16 MAP OF PETTEE BROOK AND BEARDS CREEK

value used for calibration runs was 1 (dry condition). However, flow volumes predicted by the model still significantly overpredicted stream flow during the early hours of the storm. Reinvestigation of conditions of the basin led to the conclusion that the old Durham reservoir located near the headwaters of Pettee Brook delays discharge of a major portion of the sub-basin runoff and must be considered in the analysis. Inclusion of a reservoir with a large storage-to-outflow ratio improved the results of the analysis significantly. Initial flows using a dry antecedent condition were then found to underestimate actual flows. A number of additional runs led to selection of an antecedent moisture value of 1.3. Although this value produces a total storm flow somewhat below that observed, greater weight was given to predicting peak flows. Lower antecedent moisture values would increase the total flow, but the peak would depart further from the observed value. Furthermore, inspection of Figure 17 shows that at the end of the nine-hour period used for calibration, all AMI values gave flows above the observed flow. The deficiency in total flow is probably made up during later stages of the recession flow. Results for this condition and three other values are compared to observed runoff in Figure 17. This figure presents the observed hydrograph plotted as flow against minutes into the storm. Simulated hydrographs for Antecedent Moisture Indices 12, 13, 14 and 15 are plotted in the same figure,

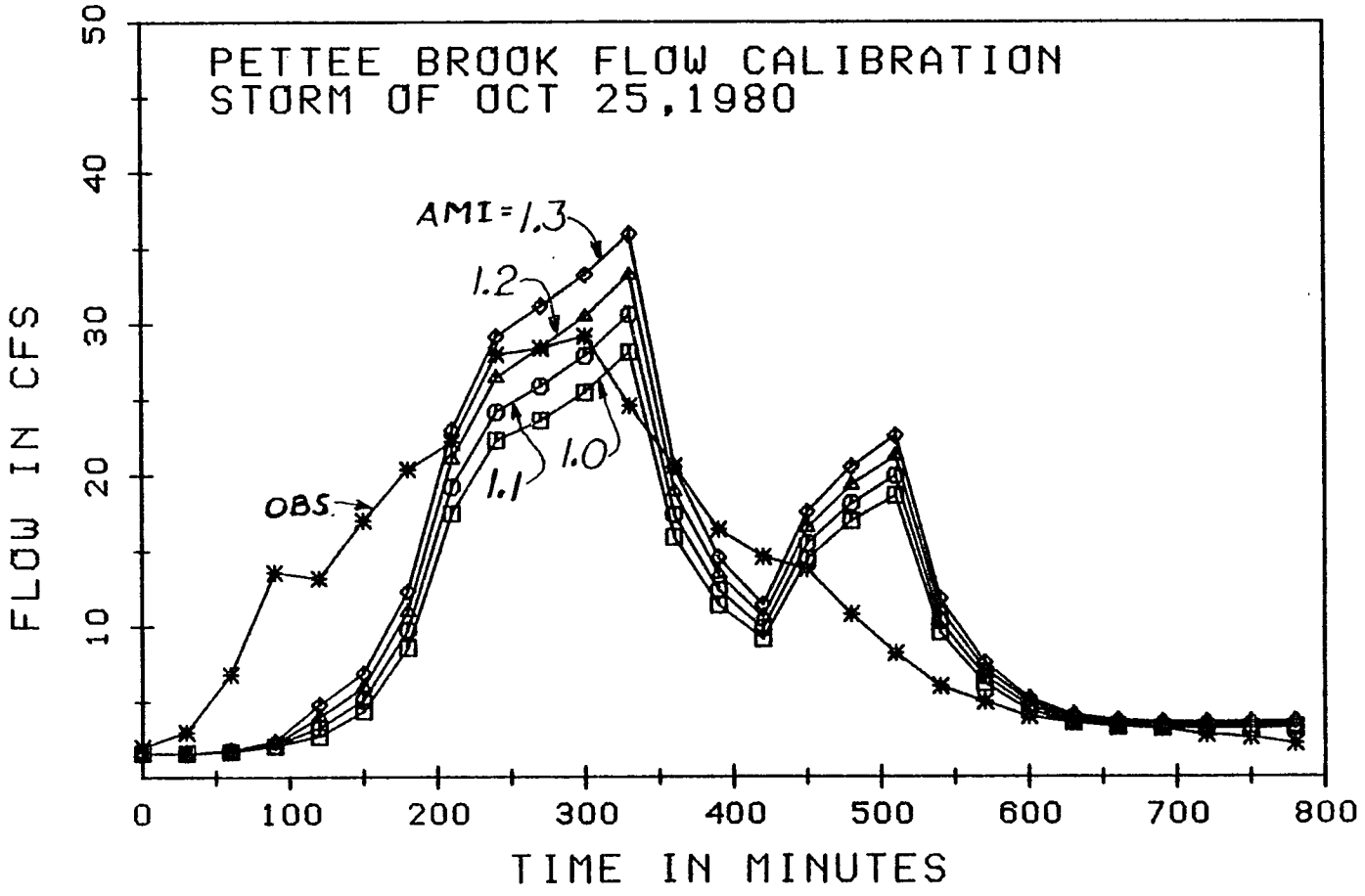

FIG 17 PETTEE BROOK FLOW CALIBRATION

Table 9

Hydrologic Model Calibration Results

LAND USE SCENARIO	STORM	TOTAL FLOW (CFS-HRS)	TOTAL BOD (LBS)
Base	2.6" Rain	4332.	22343.
Case 1	2.6" Rain	4380.	24317.
Case 2	2.6" Rain	4399.	24217.
Case 3	2.6" Rain	4412.	24992.
Base	2.6" Rain (Extended Time)	4344.	20644.
Base	0.6" Rain	288.	199.
Case 1	0.6" Rain	299.	267.
Case 2	0.6" Rain	301.	254.
Case 3	0.6" Rain	303.	272.
Base	0.6" Rain (Extended Time)	288.	199.

Note: In all cases, 2.6" rain storm started at 0.0 hrs, and 0.6" rain storm started at 120.0 hrs.

wih a base flow of 1.6 cfs superimposed.

Considering the lack of parameter adjustment required to produce the simulated hydrograph, agreement is quite good. However, it is clear that the precise shape of the hydrograph is difficult to simulate. As is commonly observed in rainfall-runoff simulations, this difficulty is likely to be due to the precision of rainfall data provided to the model. For this work, rainfall data are provided by a recording gage located at the Forest Sciences Laboratory near the intersection of Route 4 and Old Concord Road (see Figure 18). The gage is near the headwaters of Pettee Brook, but its ability to define rainfall precisely in the critical lower portion of the basin is questionable. More importantly, the recording system of the instrument is designed for continuous data over a period of a week. It is impossible to distinguish rainfall intensities for periods shorter than about fifteen minutes. Since instantaneous intensities can vary significantly within a fifteen-minute period, there is considerable systematic data smoothing built into the rainfall time series.

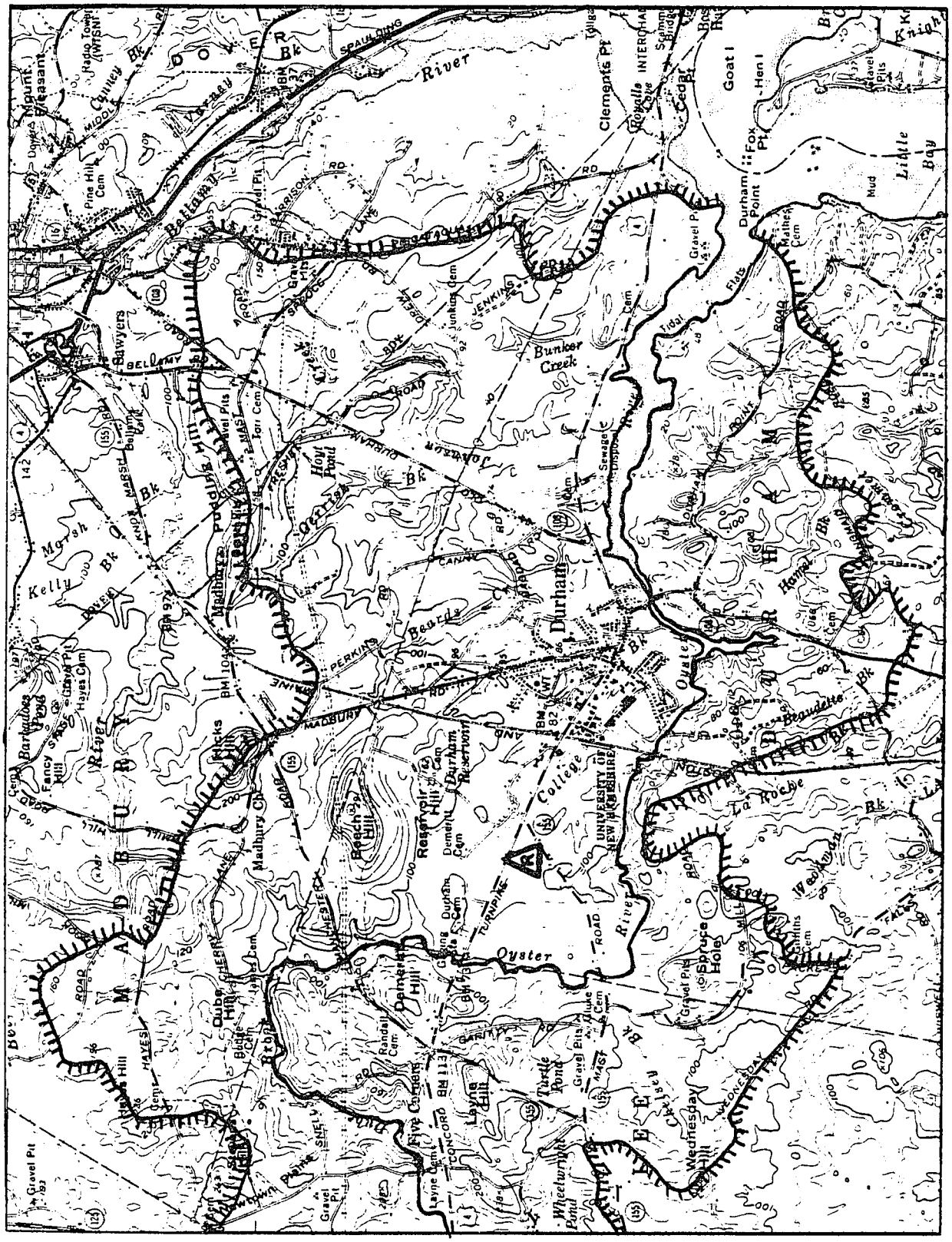

FIG 18 OYSTER RIVER BASIN MAP

Shows rain gage location ⚠

5.2 Contaminant Source Calibration

Calibration of the contaminant washoff model requires consideration of a number of adjustable parameters. As indicated previously, the model produces contaminant pollutographs by applying proportionality constants or potencies to the total sediment washoff at each timestep. Parameters may therefore be divided into sediment parameters and potency parameters. The processes modeled by the former group of parameters are assumed to be independent of land use type and other geographic variables, and hence one set of parameters is used for the entire basin. On the other hand, contaminant potencies have been found to be highly dependent on land use type. Therefore, these parameters are derived for each sub-basin as a function of land use mix. The two parameter types are grouped in Table 10.

As noted previously, much less work has been done on defining these parameters. In a limited sense, the Durham Urban Runoff Project and similar research efforts across the country are addressing this question. For the work described here and its application to planning studies, parameters will be selected from published studies of similar areas and will be adjusted to suit local conditions and locally available data. Since the contaminant algorithms were derived from the EPA Non-Point Source Model, parameter values are available for virtually all of the parameters in published studies using that model. The

Table 10

Contaminant Parameters

A. SEDIMENT PARAMETERS

1) KRER--SOIL FINES DETACHMENT CONSTANT (PERVIOUS AREA)
2) JRER--SOIL FINES DETACHMENT EXPONENT (PERVIOUS AREA)
3) KSER--SOIL FINES TRANSPORT CONSTANT (PERVIOUS AREA)
4) JSER--SOIL FINES TRANSPORT EXPONENT (PERVIOUS AREA)
5) KEIM--DUST/DIRT TRANSPORT CONSTANT (IMPERVIOUS AREA)
6) JEIM--DUST/DIRT TRANSPORT EXPONENT (IMPERVIOUS AREA)
7) OVFACT--OVERLAND FLOW PROPORTION FACTOR (PERVIOUS AREA)
8) REMI--DAILY DRY WEATHER SEDIMENT DECAY RATE ON IMPERVIOUS AREA
9) REMP--DAILY DRY WEATHER SEDIMENT DECAY RATE ON PERVIOUS AREA
10) ACCI--DAILY DRY WEATHER SEDIMENT ACCUMULATION ON IMPERVIOUS AREA
11) ACCP--DAILY DRY WEATHER SEDIMENT ACCUMULATION ON PERVIOUS AREA

B. CONTAMINANT POTENCY PARAMETERS

12) ARP(I)--ACRES OF PERVIOUS SURFACE IN SUB-BASIN I
13) COVER(I)--AVERAGE VEGATATIVE COVER IN SUB-BASIN I
14) FIRSTI(I)--INITIAL IMPERVIOUS AREA SEDIMENT LOAD IN SUB-BASIN I
15) FIRSTP(I)--INITIAL PERVIOUS AREA SEDIMENT LOAD IN SUB-BASIN I
16) PMP(I,N)--POTENCY OF CONTAMINANT N ON PERVIOUS AREA OF SUB-BASIN I
17) PMI(I,N)--POTENCY OF CONTAMINANT ON IMPERVIOUS AREA OF SUB-BASIN I

most complete analysis appears to be that done for the Third Fork Creek drainage basin in Durham, North Carolina, and hence basic parameter data were abstracted from that study.

The first six parameters define basic sediment-generation processes in response to rainfall intensity and runoff rate. Each of these was abstracted directly from the Third Fork Creek results. Parameter OVFACT, which is not used in the EPA model, was assigned a value of 1.0. This indicates that all overland flow on pervious portions of the basin is capable of transporting contaminants. These parameters were then modified so that the total washoff of sediment during the 25 October 1980 storm was simulated as closely as possible.

Before modifying these parameters, a sensitivity analysis was done to identify the best approach to calibration. Six cases were run to evaluate five of the parameters. The two parameters dealing with soil fines detachment were not considered because of the lack of data on this process. Case 1 was a base case for the parameter values of the Third Fork Creek. Cases 2 through 6 each employed a modification of one parameter: OVFACT, KSER, JSER, KEIM, and JEIM, respectively. Results of these sensitivity runs for each of the four key Runoff Curve Number values are given in Table 11. This table presents the sediment balance for each area in units of pounds/acre and reflects the net impact of the 25 October 1980 storm.

Table 11

Sensitivity Analysis of Sediment Parameters

	INITIAL	DUST & DIRT WASHOFF	FINAL	INITIAL	SOIL FINES DETACHMENT	WASHOFF	FINAL
CN=35							
1	1000.5	0	1000.4	515.9	66.8	0	581.6
2	1000.5	0	1000.4	515.9	66.8	0	581.6
3	1000.5	0	1000.4	515.9	66.8	0	581.6
4	1000.5	0	1000.4	515.9	66.8	0	581.6
5	1000.5	0	1000.4	515.9	66.8	0	581.6
6	1000.5	0	1000.4	515.9	66.8	0	581.6
CN=71							
1	1000.5	6.2	994.3	515.9	65.4	0	580.2
2	1000.5	6.2	994.3	515.9	65.4	0	580.2
3	1000.5	6.2	994.3	515.9	65.4	0	580.2
4	1000.5	6.2	994.3	515.9	65.4	0	580.2
5	1000.5	10.3	990.2	515.9	65.4	0	580.2
6	1000.5	3.6	996.8	515.9	65.4	0	580.2
CN=89							
1	1000.5	466.6	533.8	515.9	52.2	45.2	521.8
2	1000.5	466.6	533.8	515.9	52.2	13.0	554.0
3	1000.5	466.6	533.8	515.9	52.2	75.3	491.6
4	1000.5	466.6	533.8	515.9	52.2	33.7	533.3
5	1000.5	777.7	222.7	515.9	52.2	45.2	521.8
6	1000.5	441.8	558.6	515.9	52.2	45.2	521.8
CN=97							
1	1000.5	844.9	155.5	515.9	69.6	248.3	336.1
2	1000.5	844.9	155.5	515.9	69.6	71.3	513.1
3	1000.5	844.9	155.5	515.9	69.6	413.8	170.6
4	1000.5	844.9	155.5	515.9	69.6	222.7	361.6
5	1000.5	1000.4	0	515.9	69.6	248.3	336.1
6	1000.5	872.5	127.9	515.9	69.6	248.3	336.1

Initial conditions of 1000 lbs/acre and 500 lbs/acre were employed for a start time of zero hours (midnight of the previous night). These values were selected arbitrarily, but do not affect the mass balance unless the entire sediment reservoir becomes depleted. This occurred only for the impervious portion of the CN-97 area in case 5. All other runoff values are unaffected by the choice of initial conditions. The slight deviation from the 1000 and 500 lbs/acre initial values reflects sediment buildup and decay on the surface between midnight and the 3:00 PM (1500 hrs) start of the storm. Parameters employed for the buildup and decay processes are discussed in a later paragraph.

Results of the sensitivity runs demonstrated that virtually all of the sediment is generated on the higher curve number areas. This is primarily due to the much greater runoff rate from these less pervious locations. Furthermore, the dust and dirt component generated on the impervious portion is significantly greater than the soil fines component. Adjustment of parameter OVFACT from 1.0 to 0.5 made a large change in soil fines washoff (45.2 to 13.0 lbs on CN = 89, and 248.3 to 71.3 lbs on CN = 97), but the impact on total sediment load is small due to the lesser importance of soil fines.

Adjustment of the washoff constants KSER and KEIM from 0.3 to 0.5 resulted in a proportional change in the soil fines and dust/dirt transport. This linearity is

limited, however, in that the total washoff cannot exceed the available reservoir. Adjustment of washoff exponents from 1.8 to 2.0 resulted in a smaller change in net transport. The larger exponent generated less transport because the quantity being raised to this power, namely runoff during the timestep in inches, is less than 1.0.

As a result of these sensitivity studies, it is apparent that the most reasonable approach to calibrating total sediment loss is adjusting constants KSER and KEIM. In the absense of more detailed field data, both constants should be adjusted in the same ratio. In this manner total sediment washoff can be adjusted to fit the observed data. As will be noted below, the parameters from Third Fork Creek gave good results, and no adjustment was necessary.

The next parameters to be considered were REMI and REMP, representing daily decay rate of the sediment reservoirs, and ACCI and ACCP, representing daily sediment accumulation. The EPA analyses of Third Fork Creek employed daily accumulation rates between 30 and 80 lbs/acre. A middle value of 50 lbs/acre was selected for the Oyster River Basin. Decay parameters for the EPA study were 0.08 and 0.05 for impervious and pervious areas, respectively. Because very limited street sweeping is employed within the Oyster River Basin, the distinction between impervious and pervious areas was considered inappropriate. Therefore, a value of 0.05 was employed for both parameters.

The remaining six parameters all vary as a function of land use type and, therefore, must be calculated as an appropriately weighted average. Data were assigned for each land use type, and the data management computer program described previously was used to calculate the correctly weighted average for each key curve number area of each sub-basin.

Whenever possible and appropriate, parameter data were abstracted from the EPA study of Third Fork Creek. Parameter ARP(I) was developed from available data in that study. The number of acres of impervious surface was determined for each grid element by multiplying the total area (10 acres) by factor IMPKO of the EPA study. Since IMPKO was available for only four land use types, judgement was necessary to select appropriate values for other types. These values and their souce are listed in Table 12.

Parameter COVER(I) was also taken from the Third Fork Creek study. That study employed a value of 0.90 for all land uses except single family, which employed a value of 0.95. Because of the similarity of multi-family and institutional areas to single family land use, these were also assigned a value of 0.95 for this study.

Parameters FIRSTI(I) and FIRSTP(I), representing the initial value of the sediment reservoir on impervious and pervious portions of the area, have been mentioned above. They have no effect on the transport of sediment until the sediment reservoir has been entirely depleted. If the

Table 12

Impervious Area Proportions
for Land Use Types

LAND USE	IMPKO	DATA SOURCE
1) SINGLE FAMILY	.18	THIRD FORK CREEK STUDY
2) MULTI-FAMILY	.3	APPROX 1.5 x SINGLE FAMILY
3) COMMERCIAL	.55	THIRD FORK CREEK STUDY
4) INDUSTRIAL	.75	THIRD FORK CREEK STUDY
5) RECREATIONAL	.1	APPROX 2 x OPEN LAND
6) AGRICULTURAL	.05	SAME AS OPEN LAND
7) OPEN	.05	THIRD FORK CREEK STUDY
8) FOREST	.02	APPROX 1/2 x OPEN LAND
9) INSTITUTIONAL	.15	APPROX 1/2 x MULTI-FAMILY

model were run over a long period of time, any error in initial conditions would eventually be obscured as accumulation, decay and washoff of sediment increase in magnitude. As noted in Section 3.2.3, during a long dry period the pre-storm sediment reservoir will converge asymptotically to a value of ACCI/REMI or ACCP/REMP. Since the storm of 25 October was preceded by a relatively dry month, this equilibrium value was selected for all subsequent analyses. The accumulation and decay rates given above result in an initial sediment reservoir of 1000 lbs/acre for both pervious and impervious areas.

The final parameters to be assigned are the contaminant potencies PMP(I,N) and PMI(I,N). The Oyster River Basin study has focused on analysis of BOD, dissolved oxygen and suspended solids. Therefore, two potency factors are required for the pervious and impervious portion of each sub-basin. Once again, values are assigned to each land use type, and the data management computer program is used to compute the correctly weighted average potency values for each curve number area of each sub-basin. Preliminary potency values were selected from the Third Fork Creek study. Unfortunately, however, only a single value was used in that study for each contaminant. That study employed a BOD potency value of 0.04 and a suspended solids potency value of 0.71 for all land uses. Since this effort is directed toward evaluating the impact of alternative land use decisions, such an approach is

clearly unsatisfactory. Considerably more data on the relative strength of contaminant sources in different land use areas is available in the Storm Water Management Model of EPA and other similar studies. The most convenient form of such data was found in a report on a Simplified Stormwater Management Model by EPA (1976a). Table 13 gives values for contaminant loads (lbs/acre-inch of rainfall) for a number of land uses as presented in that report. By using these values, a relative land use weighting factor was developed as shown in the table. This weighting factor was applied to the potency values given above to determine an appropriate potency factor for each land use. Where data was not available for a given land use type, the value for the most similar land use was used. This results in the contaminant potencies given in Table 14.

From the above discussion of calibration, it is clear that the extent of available field data will affect the effort required. Complete calibration should begin with the hydrologic model. Adequate results can be obtained by adjustment of a single parameter, the Antecedent Moisture Index. After selection of this value, the sediment washoff simulation should be considered. As shown on Table 10, as many as eleven parameters can be adjusted to calibrate the sediment algorithms. However, it was shown that in the absence of extensive field data, adjustment of the two transport constants, KSER and KEIM, would assure most of the required error reduction. Finally, if extensive

Table 13

Contaminant Loads for Land Use Types

LAND USE	BOD		SUSPENDED SOLIDS	
	FACTOR	RELATIVE WEIGHT	FACTOR	RELATIVE WEIGHT
Residential	0.799	0.46	16.3	0.72
Commercial	3.20	1.84	22.2	0.99
Industrial	1.22	0.70	29.1	1.29

Table 14

Contaminant Potency Factors

LAND USE	BOD	SUSPENDED SOLIDS
Single Family	.018	.51
Multi-family	.018	.51
Commercial	.074	.70
Industrial	.028	.92
Recreational	.018	.51
Agricultural	.028	.92
Open land	.018	.51
Forest	.018	.51
Institutional	.018	.51

contaminant data are available for the area of interest, the contaminant potency factors abstracted from the literature can be adjusted.

For the calibration of the Oyster River Basin against the October 25 storm, an initial run was made using the Third Fork Creek parameters, the modified contaminant potencies described above, and an Antecedent Moisture Index of 1.3. Results were compared to composite samples taken at the Madbury Road sampling station. Because of limitations in that data, the following approach was employed.

The sampler capacity was limited and became full before the end of the storm. Out of a total storm flow of 649,200 cubic feet measured at the gage, the sample was representative of the first 302,400 cf. Of this, 20,131 cf was calculated as base flow, leaving 282,269 cf of storm flow. For this sample, a total BOD loading of 225 lbs or 12.8 mg/l was calculated. For solids, only a total solids concentration of 402 mg/l was available, with no data on suspended solids. Fortunately, both total and suspended solids data were available for the Alumni Center sampling station at the upper end of the sub-basin. At this station total solids and suspended solids loads were 5253 lbs and 3843 lbs, respectively. Assuming that the same ratio would apply to the Madbury Road station, a calculated suspended solids concentration of 294 mg/l was determined.

In the model results, a flow of 288,846 cf was

calculated for the first 6.5 hours of the storm. For this same period, simulated BOD and suspended solids loads were 220.68 lbs and 5647.23 lbs, respectively. These resulted in concentrations of 12.3 and 313 mg/l, respectively. The comparison to observed data is shown in Table 15.

On the basis of the close agreement between observed and simulated contaminant data, no adjustments were made in the initial set of parameters. While it is unlikely that every set of field data would be simulated as closely as this, proper use of published contaminant parameters and a reasonably accurate hydrologic simulation have been shown to produce meaningful results.

5.3 Hydrodynamic Model Calibration

Calibration of the hydrodynamic model involves four sets of output data: channel velocity, channel cross sectional area (or water surface elevation), the density-driven circulation velocity, and tidal cycle averaged salinity distribution. The first two data sets are used to calibrate a single group of parameters, the friction coefficients. The final two are used to calibrate those parameters defining the circulation mixing coefficients, namely salinities S_{MAX} and S_{1000}, vertical mixing factor VMF, and the tidal mixing parameter ETM.

Table 15

Contaminant Model Calibration Results

	OBSERVED	SIMULATED
STORM FLOW (CF)	282,269	288,846
BOD: LOAD (lbs)	225	220.68
CONC (mg/l)	12.8	12.3
SUSP. SOLIDS: LOAD (lbs)	----	5647.23
CONC (mg/l)	294*	313

*Calculated from total solids concentration and Alumin Center sampling station data.

5.3.1 Friction Coefficient - Sensitivity Analysis and Calibration

The limited adjustment for simulating velocity and elevation is both a blessing and a curse in calibrating the hydrodynamic model. Clearly, the effort involved in calibrating the model is minimized when only one parameter can be adjusted for each river segment. However, the ability of the one-dimensional model to accurately simulate the point values of measured field data is limited. With the complex geometry of the Oyster River, channel dimensions and resulting velocities can vary dramatically in both longitudinal and cross-channel directions. The probability of selecting a measuring location that is exactly representative of average velocity along a 750-ft segment for even a single timestep is small. The likelihood that even such an idealized point would be representative of all velocities over a tidal cycle is even more remote. A further complication is pointed out by Shanley (1972) in his evaluation of velocity data at five stations in the Oyster River. He notes that while the assumption that all longitudinal flow is concentrated in a central deep channel is reasonable at low tide, at times near high tide significant longitudinal flow occurs over the shallow shore zones of the cross-section. For all these reasons, adjustment of the friction coefficient on the basis of field velocity data was not considered.

This leaves water surface elevation data as the only

feasible basis for selecting the appropriate friction coefficients. Once again, the situation is complicated by consideration of the real physical setting. To some degree the complex geometry affects local variations in surface elevations. To a much larger extent, wind velocities can cause a "set-up" or tilting of the longitudinal surface profile. Furthermore, the net effect of longitudinal salinity gradients is to impart a net upward surface slope from mouth to head of the estuary. A rather significant field program including two or more tide gages, a wind speed and direction sensor, and salinity measurement would have to be undertaken over several tidal cycles. Before embarking on such a program, a sensitivity analysis of the hydrodynamic model was undertaken. This analysis was directed toward evaluating the precision and scope required for a sampling program to define the friction coefficients. The analysis employed a range of friction coefficients from 0.02 to 0.04 and also considered the impact of different flows and salinity gradients. Results were obtained by extracting the values of each term of the governing equations at a number of timesteps of a tidal cycle together with complete output of surface elevation variations. Five representative cases are described in Table 16.

Additionally, velocity data was evaluated for each case. Although calibration against field velocity has been dismissed, the importance of this data should not be

Table 16

Sensitivity Analysis of Hydrodynamic Model Friction

CASE NUMBER	FRESH WATER FLOW	FRICTION COEFFICIENT	OCEAN SALINITY RANGE
1	10	.02	0.2-30.0
3	10	.04	0.2-30.0
4	100	.02	0.2-30.0
6	100	.04	0.2-30.0
7	100	.02	0.2-0.2

underestimated. The objective of the overall effort has been stated to be calculation of contaminant distribution in the estuary. Regardless of whether the hydrodynamic model precisely simulates observable instantaneous conditions in the estuary, the results of the contaminant computations depend on a consistent set of velocity data which describe average advective transport in each river segment and at each timestep.

Evaluation of the various processes affecting hydrodynamic computations and sensitivity of the model to parameter selection is summarized in Figures 19 through 23 and Table 17. The five figures illustrate the variation of surface elevation over a tidal cycle for points near the mouth and head of the estuary (stations 3 and 19, respectively). Each case clearly reveals the expected sinusoidal stage variation at both stations and also the phase lag for the tidal wave to reach the head of the estuary. Also apparent is the small but perceptible amplification of the wave at the head end. Comparison of cases 1 to 3 and 4 to 6 reveals the effect of increased friction on tidal heights. A higher friction coefficient has little effect on maximum elevation of the surface, but raises the lowest point of the curve for the head end of the estuary. This results from the "holdup" of water near the head during an ebb tide. Even more dramatic is the effect on phase lag from mouth to head. Doubling the friction coefficient results in a significant delay of the

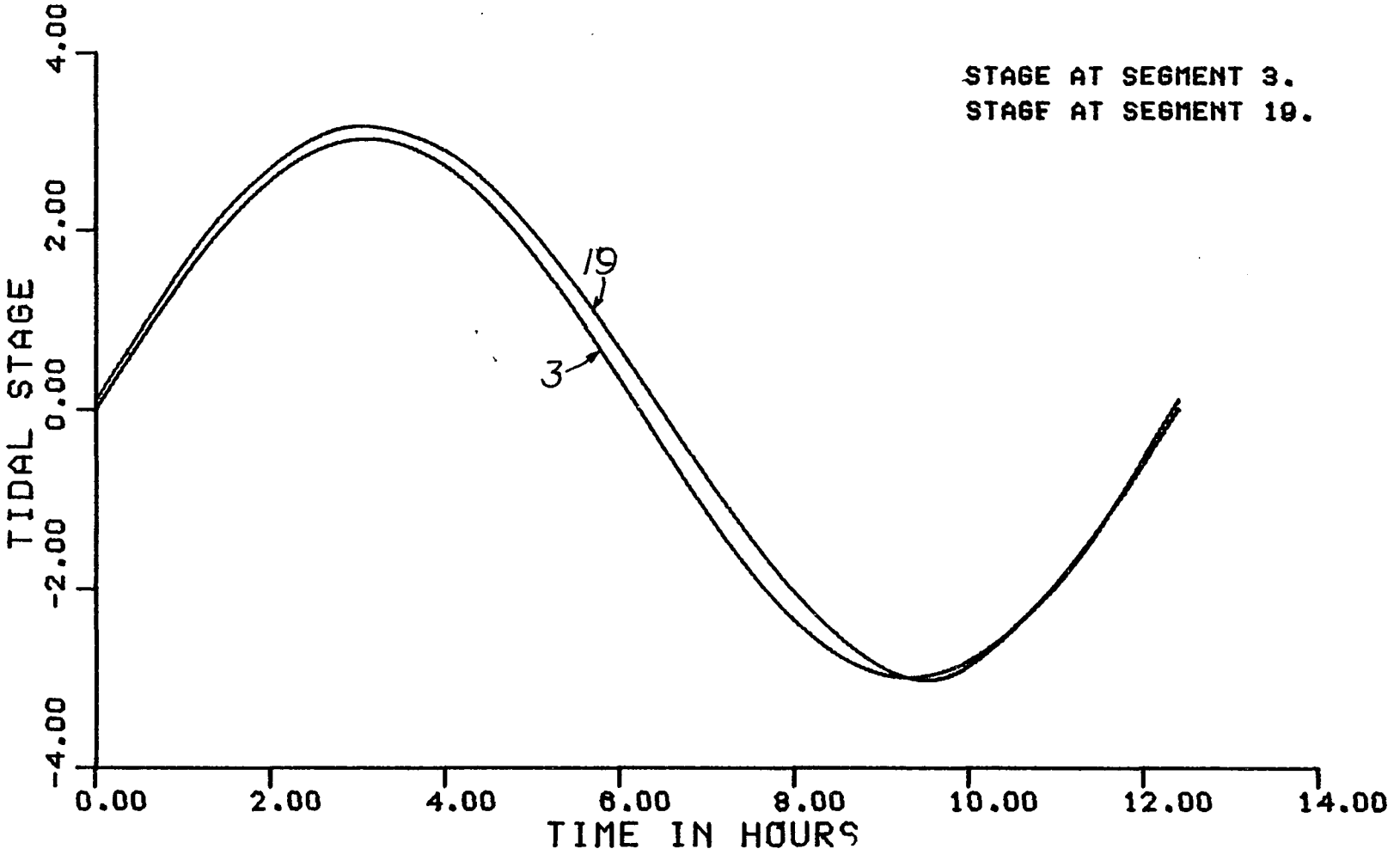

FIG 19 TIDAL STAGE CALIBRATION CASE I

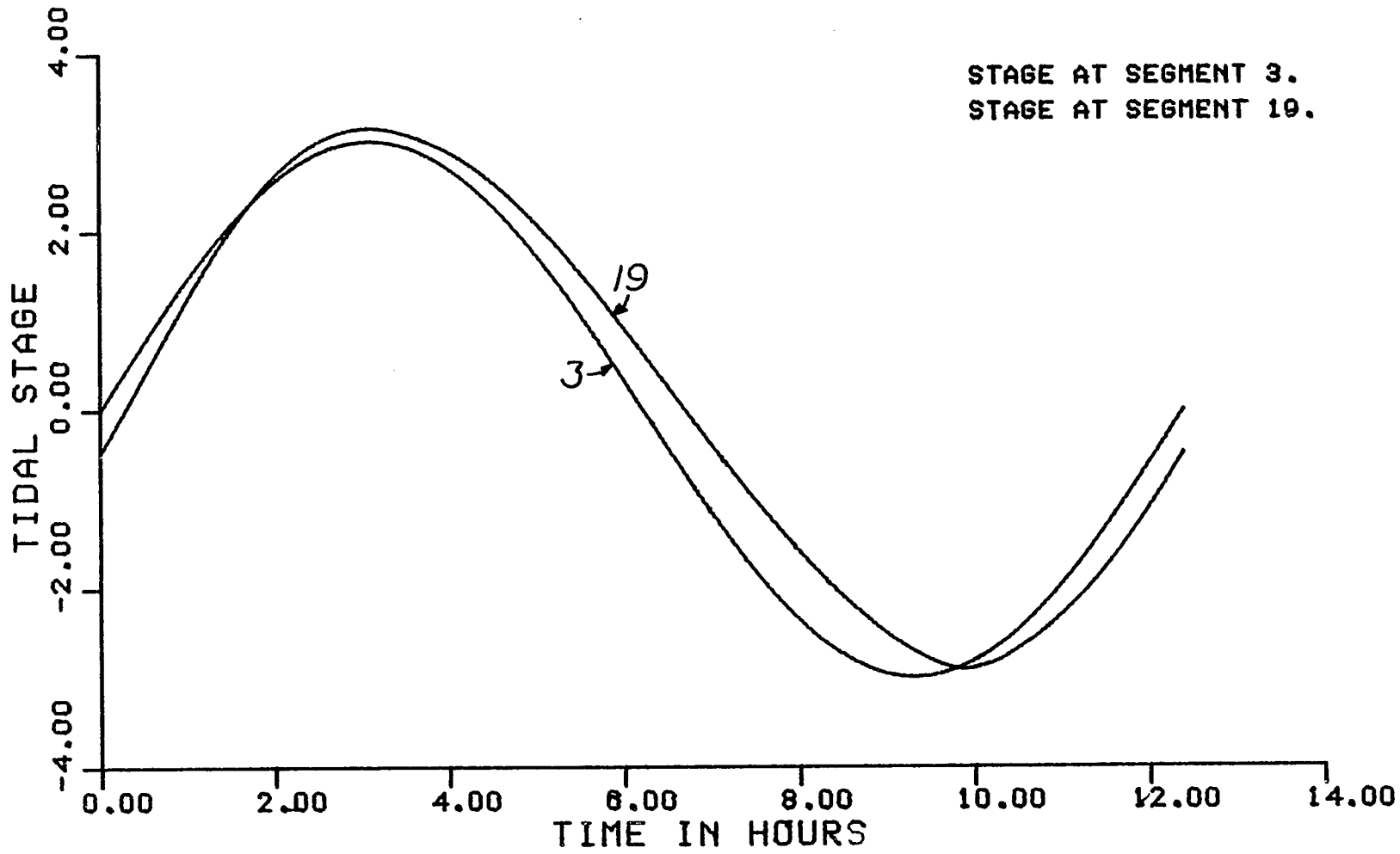

FIG 20 TIDAL STAGE CALIBRATION CASE 3

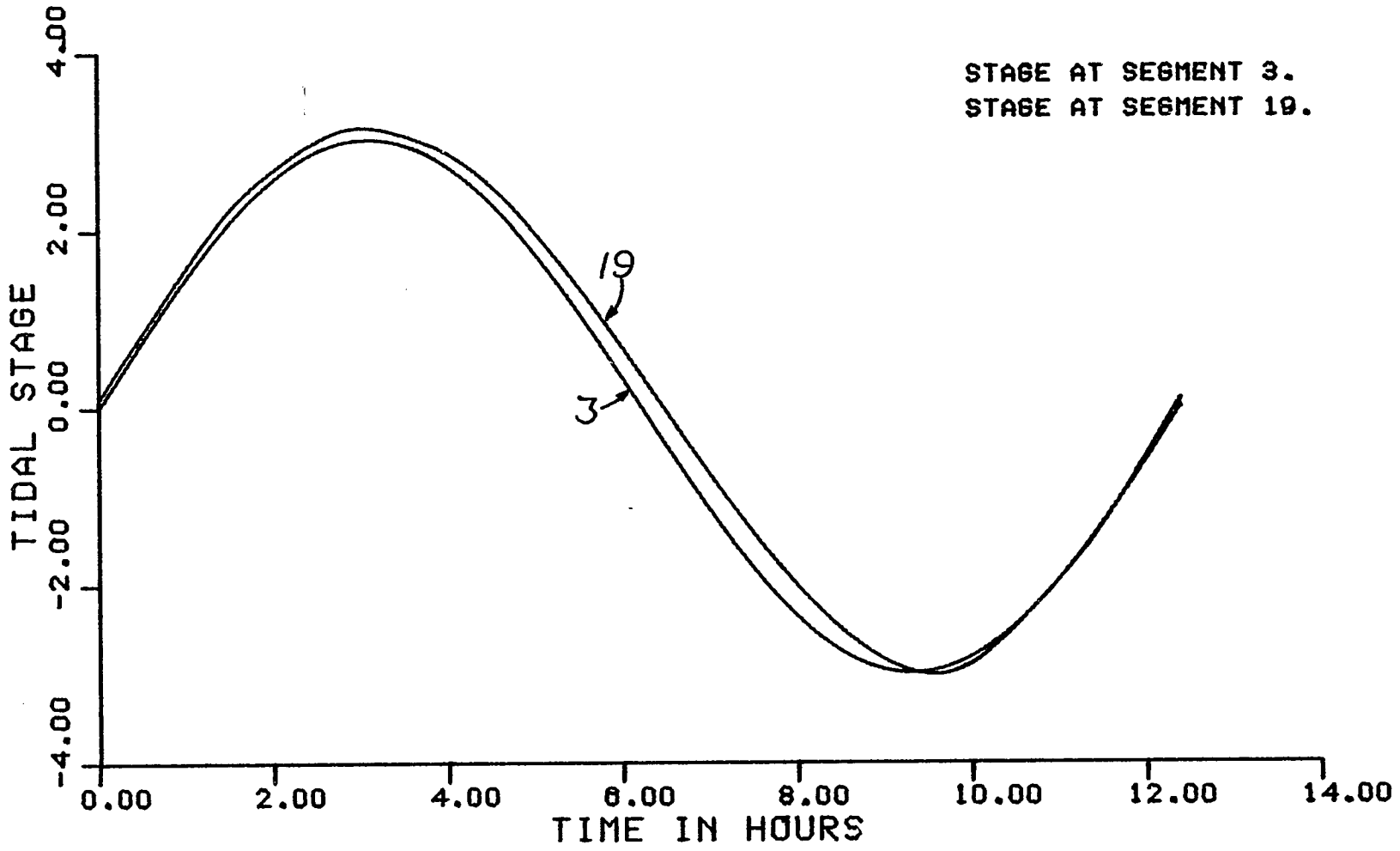

FIG 21 TIDAL STAGE CALIBRATION CASE 4

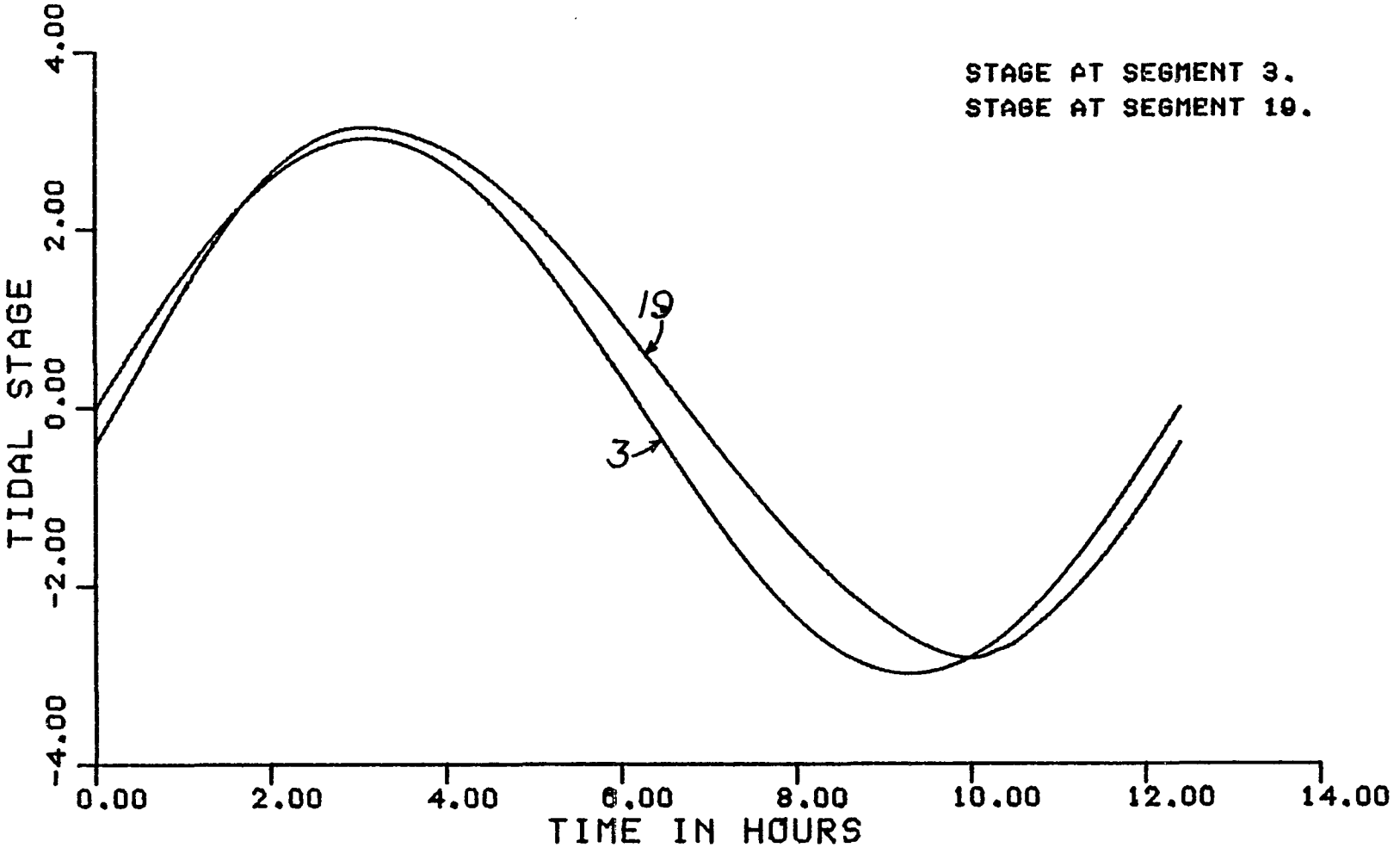

FIG 22 TIDAL STAGE CALIBRATION CASE 6

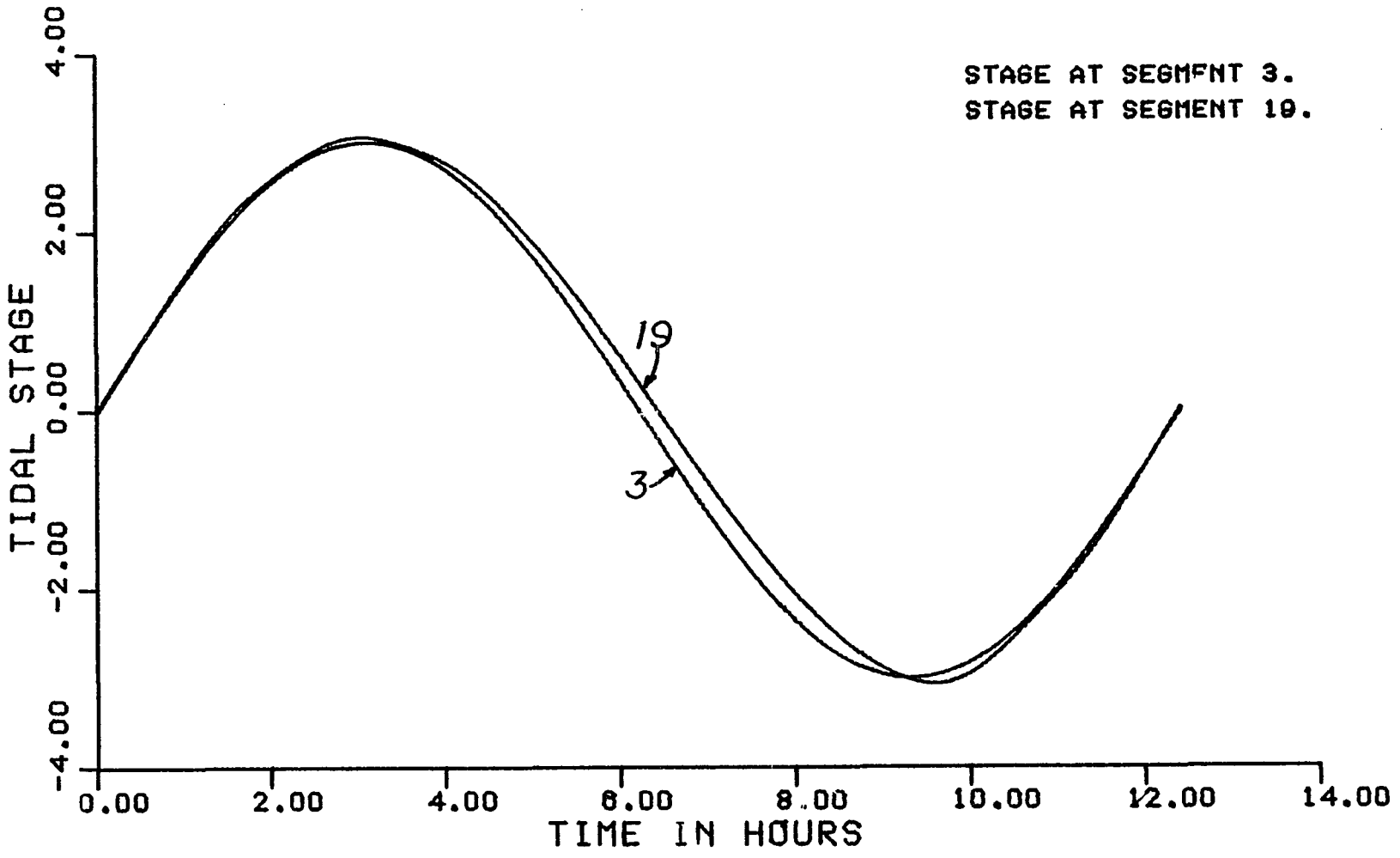

FIG 23 TIDAL STAGE CALIBRATION CASE 7

Table 17

Sensitivity Analysis for Hydrodynamic Parameters

	CASE 1		3		4		6		7	
	STA 4	STA 20	STA 4	STA 20	STA 4	STA 20	STA 4	STA 20	STA 4	STA 20
VELOCITY MAX	.915	1.037	.922	1.038	.912	.899	.903	.877	.908	.898
TIME OF MAX	12.058	11.657	0.239	0.200	12.045	11.774	.213	.278	12.058	11.785
VELOCITY MIN	-.899	-.915	-.876	-.802	-.912	-1.052	-.887	-.915	-.908	-1.052
TIME OF MIN	6.349	7.227	6.426	7.382	6.349	7.395	6.426	7.537	6.349	7.408
SPEED MEAN	.583	.624	.577	.607	.582	.637	.573	.613	.584	.637
SPEED STD DEV	.279	.284	.276	.270	.278	.293	.276	.264	.280	.293
STAGE MAX	3.018	3.166	3.018	3.168	3.015	3.147	3.015	3.135	3.005	3.069
TIME OF MAX	3.100	3.035	3.100	3.100	3.113	3.035	3.100	3.087	3.100	3.048
STAGE MIN	-2.991	-3.030	-2.995	-2.909	-3.000	-3.021	-3.000	-2.826	-3.005	-3.068
TIME OF MIN	9.300	9.507	9.300	9.894	9.300	9.571	9.300	9.998	9.300	9.571
LOCAL ACCEL MEAN	.478	.059	.477	.062	.476	.059	.474	.060	.474	.058
LOCAL ACCEL STD DEV	.243	.039	.237	.054	.253	.043	.233	.050	.250	.043
ADV ACCEL MEAN	.529	.242	.522	.229	.527	.240	.520	.220	.525	.239
ADV ACCEL STD DEV	.376	.164	.371	.165	.375	.162	.370	.145	.373	.161
SLOPE MEAN	2.162	.397	2.175	.704	1.758	.401	1.890	.739	.800	.329
SLOPE STD DEV	.985	.243	1.615	.390	.921	.277	1.520	.522	.469	.273
FRICTION MEAN	.286	.171	1.120	.630	.286	.180	1.112	.649	.283	.181
FRICTION STD DEV	.209	.118	.789	.433	.201	.134	.784	.418	.200	.135
DENS GRAD MEAN	1.621	.136	1.614	.137	1.206	.078	1.234	.079	.016	.001
DENS GRAD STD DEV	.328	.076	.327	.075	.244	.043	.250	.042	.003	.000

tidal wave. Finally, comparison of case 7 to case 4 shows that inclusion of a salinity gradient has essentially no effect except a slight elevation of the water surface toward the head of the estuary.

Table 17 quantifies these effects. For example, it can be seen that increased friction at a 10 cfs fresh water flow raises the low point of the stage curve 0.121 ft (4%) but has virtually no effect on the high point. At the 100 cfs flow, the low point is raised 0.195 ft (6.5%). At the lower flow, increased friction has little effect on the phase lag for high water but increases the low water lag by 0.387 hours. The corresponding number for a 100 cfs flow is 0.427 hours.

The balance of Table 17 summarizes the effect of friction changes on velocity and a comparison of the various components of force acting on water masses. As with surface elevation, the primary effect of increased friction on velocity occurs on the ebb tide. For a 10 cfs flow, minimum velocity (greatest ebb velocity) is raised from -0.915 to -0.802 ft/sec near the head of the estuary. For 100 cfs, the increase is from -1.052 to -0.915 ft/sec. Velocities near the mouth of the estuary and during flood tide at all stations are much less affected. In spite of the modification of peak ebb velocities, the mean speed over a tidal cycle is not affected greatly. For a 10 cfs flow, increased friction reduces the mean speed near the head end by only 2.7 percent. For the 100 cfs flow, the

reduction is 3.8 percent. Finally, regarding the timing of maximum and minimum velocities, little change occurs in the time of greatest ebb velocity. However, the time of greatest flood velocity is changed significantly when friction is increased. Near the head end, increased friction delays the time of maximum flood velocity by almost one hour. In summary, the effect of increased friction on velocity is primarily a reduction of peak ebb velocity and a delay in time of peak flood velocity. The effect on overall flow conditions as represented by mean speed is small.

The reason for the relatively minor effect on velocities of changing friction coefficients is illustrated in the lower portion of Table (17). These data were developed by extracting each force term of the governing momentum equation separately. Data are presented in units of ft^3/sec^2 . They can be converted to pounds per foot of channel length by multiplying by the mass density, approximately 2 $Slugs/ft^3$. The five terms relate to local acceleration, advective acceleration, surface slope force, friction force, and density gradient force. The mean and standard deviation have been calculated for the absolute value of each term, so their relative magnitudes can be compared. Given their proper signs, the sum of these terms adds to zero at each timestep.

Again, comparison of case 1 to case 3 and of case 4 to case 6 allows the impact of increased friction

coefficients to be assessed. Clearly, only two terms are affected significantly--namely, the surface slope force and the friction force. For the 10 cfs flow, doubling the friction coefficient raises the mean of the slope term at the head end from 0.397 to 0.704. While the mean of the slope term is not changed dramatically at the mouth of the estuary, the variability over a tidal cycle, as measured by its standard deviation, increases from 0.985 to 1.615. Similar changes occur for the 100 cfs flow cases.

A final point to be extracted from this table is the effect of density gradient on the force terms. Cases 4 and 7 differ only in that a density gradient exists for case 4 but not for 7. Here the changed terms are surface slope force and density gradient force. No other terms are affected. Clearly, the only effect of salinity or density gradients on the one-dimensional hydrodynamic variables is to raise the slope and, hence, surface elevation at interior locations of the estuary.

These sensitivity analyses allow selection of the optimum field program for calibration of the hydrodynamic model friction coefficients. Clearly, velocity measurements cannot produce adequate data for this purpose. Isolated measurement of tidal stage at a single point is also inadequate. The most useful data would be obtained by simultaneous measurement of tidal stage at two points of the estuary. Phase lag at the lowest elevation would give a clear indication of the magnitude of friction effects.

To ensure reliable data, observations should be carried out over several tidal cycles.

These analyses also pointed out an important aspect of the hydrodynamic computations. Within a reasonable range of friction coefficients, average velocities at any point are not changed significantly. Apparently, for a short tidal river such as the Oyster River, velocity results are predicated primarily on proper definition of river geometry. An uncalibrated hydrodynamic analysis can be improved only slightly by selection of optimum friction coefficients. For the overall program undertaken here, precise calibration of hydrodynamic results is unnecessary. Only the net water flux will have a significant effect on computation of water quality parameters. Under the conditions of limited field study resources, it was deemed unnecessary to proceed further with calibration of the friction coefficient. A value of 0.02 was selected for all subsequent computations.

5.3.2 Calibration of Circulation Parameters

The remaining parameters of the hydrodynamic model all relate to computation of the density-driven circulation. Salinities S_{MAX} and S_{1000} are used to define salinity at the mouth of the estuary as a function of fresh water flow in the river. Their relationship to flow rates is illustrated in Figure 24.

A similar relationship is postulated for boundary concentrations at the head of the estuary, except that the response to increased flow would be more rapid. That is, at increased flow, the head-end salinity falls more quickly than at the mouth due to the smaller area and its proximity to the source of fresh water. Furthermore, it is assumed that groundwater flow and base flow over the dam will prevent head-end salinity from ever reaching the maximum salinity at the estuary mouth. Selection of parameters to represent these boundary conditions was based on limited available field data. Data was plotted on semi-log paper, and values for S_{MAX} and S_{1000} were selected from a best-fit line.

These computations are illustrated in Figure 25. Best-fit lines were developed from the observed data in the following way. Logarithms of salinities were computed, and a least squares regression was performed against fresh water flow. In the case of salinity at the mouth of the river, the regression was constrained to pass through a salinity of 30 ppt at zero fresh water flow. This

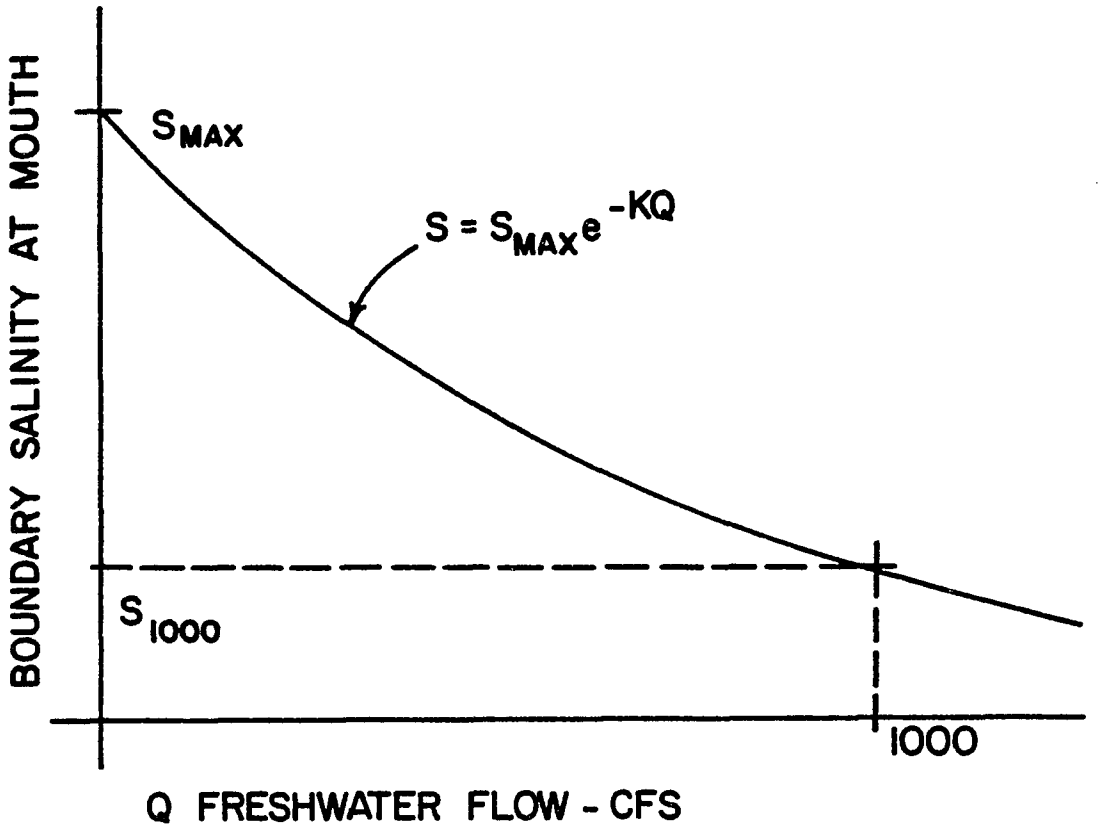

FIGURE 24

GENERAL RELATIONSHIP OF BOUNDARY SALINITY TO FLOW

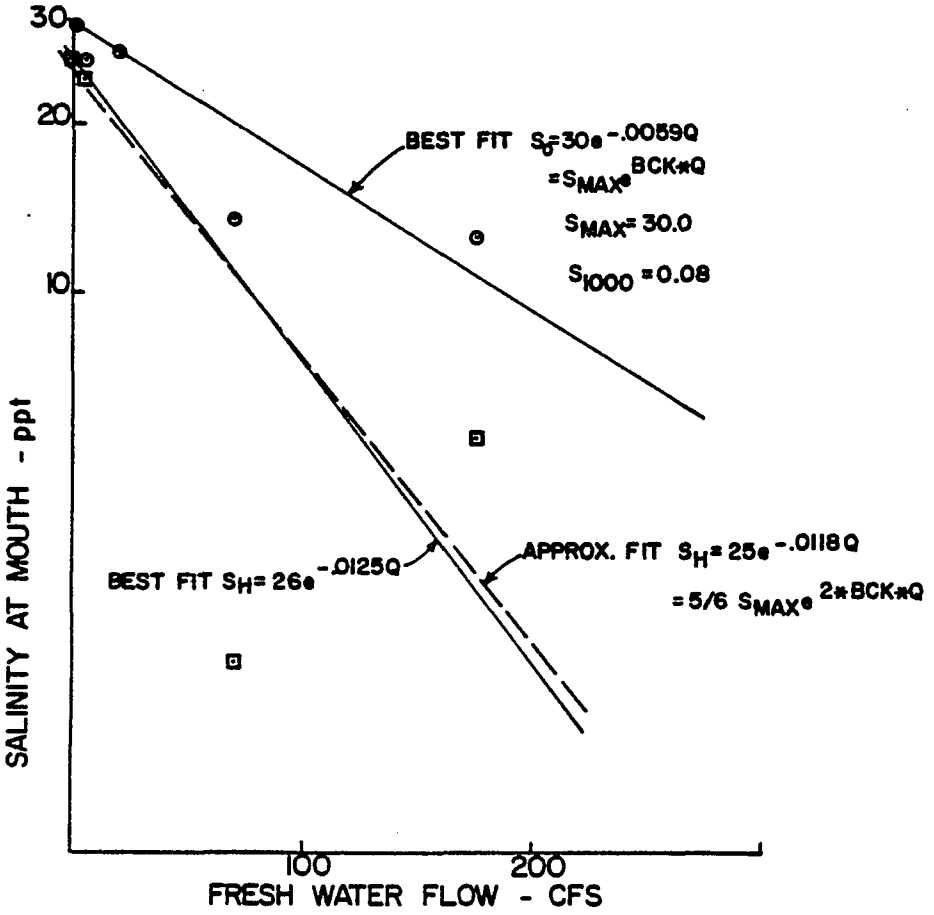

FIGURE 25

SALINITY BOUNDARY CONDITION ANALYSIS

constraint was imposed so that observed salinities in Little Bay would be approximated. The regression for head-end salinity was not constrained.

As shown on the sketch, best-fit lines are:

$$S_{Mouth} = 30*\exp(-.0059Q) \qquad (5\text{-}1)$$

$$S_{Head} = 26*\exp(-.0125Q) \qquad (5\text{-}2)$$

For convenience, the head-end regression line was adjusted slightly to take advantage of its apparent relationship to the regression line at the mouth. The slope of the head-end line is very nearly twice the slope of the mouth-end regression line. Using this factor results in an approximate fit.

$$S_{Head} = 25*\exp(-.0118Q) \qquad (5\text{-}3)$$

Defining

$$S_{MAX} = 30 \tag{5-4}$$

$$SLOPE = BCK = -.0059 \tag{5-5}$$

leads to

$$S_{MOUTH} = S_{MAX}\, e^{BCK*Q} \tag{5-6}$$

and

$$S_{HEAD} = \frac{5}{6}\, S_{MAX}\, e^{2*BCK*Q} \tag{5-7}$$

These relationships are used to compute boundary salinities in the model.

Parameter BCK is related to the previously described parameter S_{1000} by this expression:

$$BCK = .001*Ln\ (\frac{S_{1000}}{S_{MAX}}) \qquad (5\text{-}8)$$

For the regression expressions described above, the value of S_{1000} is calculated from this equation to be 0.08. All subsequent analyses used these values: S_{MAX} = 30.0 and S_{1000} = 0.08. For other rivers, both the values of S_{MAX} and S_{1000} together with the factors 5/6 and 2 used to compute S_{HEAD} would have to be adjusted to suit available field data.

Parameter ETM was calibrated by comparing the longitudinal salinity profile predicted by the analytical solution to observed field data. In each case, the predicted profile was obtained by running the hydrodynamic model to equilibrium for a specified fresh water flow. Tidal cycle averaged salinity distribution is contained in the model output. Five different ETM values were applied to four flow conditions for a total of 20 calibration runs.

The four flow conditions resulted from fresh water inflows of 5, 20, 70, and 175 cfs. In all cases, a six-foot harmonic tide was imposed at the mouth. The four

flow rates correspond to the following field data sets:

5 cfs - April 1979 dye study

20 cfs - Shanley average flow conditions (Shanley,1972)

70 cfs - Shevenell salinity data (from Shanley,1972)

75 cfs - September 1979 dye study

For the two dye studies, salinity data represents near-surface readings taken with a conductivity instrument at six stations. Data from approximately six sampling runs were averaged to get the appropriate values. For the Shanley data and Shevenell's data (reproduced by Shanley in his thesis), the data is abstracted from figures showing isohalines on a longitudinal section along the Oyster River. In each of these cases, near-surface and near-bottom salinities were averaged for each of four phases of the tide at twelve locations. The four depth averages at each point were then averaged to get a value representative of the entire tidal cycle.

Data for 20 runs employing ETM values between 15 and 750 are compared in Table 18 to field observations. Evaluation of the data to select a best fit was done as follows. For each model run a standard error of predicted salinity was calculated by:

$$S.E. = \sqrt{\frac{\Sigma(S_F - S_M)^2}{n}} \qquad (5\text{-}9)$$

Table 18

Sensitivity of Salinity Model to Tidal Mixing

	SHANLEY LOW FLOW	SEPT DYE STUDY	ETM 15	ETM 25	ETM 75	ETM 300	ETM 750	SHANLEY AVG FLOW	ETM 15	ETM 25	ETM 75	ETM 300	ETM 750
FLOW (CFS)	1.0	5.0	5.0	5.0	5.0	5.0	5.0	19.6	20.0	20.0	20.0	20.0	20 0
S-24		24.0	24.1	24.1	24.1	24.1	24.1	0.8	5.1	5.3	5.7	5.9	5.9
S-22	26.8		24.4	24.4	24.4	24.4	24.4	1.5	7.5	8.0	8.8	9.4	9.5
S-20	27.6	24.4	24.6	24.6	24.6	24.6	24.7	10.8	10.1	10.8	11.8	12.4	12.6
S-18	28.1		24.8	24.8	24.8	24.9	24.9	16.5	12.8	13.4	14.5	15.1	15.3
S-16	28.4	25.0	25.0	25.0	25.0	25.0	25.0	22.5	15.3	15.9	16.9	17.5	17.6
S-14	28.7		25.1	25.1	25.2	25.2	25.2	22.7	17.7	18.2	19.0	19.6	19.7
S-12	29.0	25.3	25.3	25.3	25.3	25.3	25.3	23.4	19.8	20.2	20.9	21.4	21.5
S-10	29.1		25.4	25.4	25.4	25.4	25.4	24.1	21.8	22.1	22.6	23.0	23.1
S-8	29.2	25.4	25.5	25.5	25.5	25.5	25.5	25.6	23.5	23.7	24.1	24.4	24.5
S-6	29.7		25.6	25.6	25.6	25.6	25.6	25.1	25.0	25.1	25.4	25.6	25.6
S-4	29.9		25.7	25.7	25.7	25.7	25.7	26.2	26.3	26.4	26.5	26.7	26.7
S-2			25.8	25.8	25.8	25.8	25.8		27.5	27.5	27.5	27.6	27.6
STANDARD DEVIATION		.110	.110	.110	.110	.110	.148		3.963	3.739	3.546	3.500	3.494

	SHEV-ENELL	ETM 15	ETM 25	ETM 75	ETM 300	ETM 750	APRIL DYE STUDY	ETM 15	ETM 25	ETM 75	ETM 300	ETM 750
FLOW (CFS)	70.0	70.0	70.0	70.0	70.0	70.0	175.0	175.0	175.0	175.0	175.0	75.0
S-24	2.2	4.0	4.0	4.1	4.2	4.3	5.5	5.1	5.1	5.3	5.4	5.5
S-22	5.5	5.0	5.1	5.4	5.7	5.8		5.6	5.6	6.0	6.3	6.5
S-20	8.5	6.2	6.3	6.6	6.9	7.1	6.0	6.3	6.3	6.7	7.2	7.4
S-18	8.5	7.3	7.5	7.7	8.1	8.3		7.2	7.1	7.5	8.0	8.2
S-16	10.5	8.5	8.6	8.8	9.2	9.3	7.9	8.2	7.9	8.4	8.8	8.9
S-14	10.9	9.5	9.6	9.8	10.1	10.2		9.1	8.8	9.1	9.5	9.6
S-12	11.2	10.5	10.5	10.7	10.9	11.0	6.7	9.9	9.6	9.8	10.1	10.2
S-10	11.9	11.4	11.4	11.5	11.7	11.8		10.6	10.3	10.5	10.7	10.7
S-8	12.3	12.1	12.1	12.2	12.3	12.4	10.3	11.2	10.9	11.0	11.2	11.2
S-6	12.8	12.8	12.8	12.8	12.9	12.9		11.7	11.5	11.5	11.6	11.6
S-4		13.3	13.3	13.3	13.4	13.4	11.5	12.1	11.9	12.0	12.0	12.0
S-2		13.8	13.8	13.8	13.8	13.8		12.4	12.3	12.3	12.3	12.3
STANDARD DEVIATION		1.302	1.238	1.113	.961	.922		1.399	1.237	1.362	1.575	1.647

where:

SE = standard error

SF = salinity observed in field

SM = model results

n = number of data points

These standard errors are listed in Table 18. For each flow condition the standard errors were then normalized to the standard error at the middle value of ETM = 75. This normalized standard error was then plotted against the ETM values for each flow condition on Figure 26. As shown in the figure, no simple relationship between standard error and the value of ETM exists. However, it is clear that, for all but the lowest fresh water flow rate, increasing ETM above 750 has little effect. Only the 5 and 175 cfs flow rates exhibited a clear minimum standard error. This occurred at ETM values of about 75 and 25, respectively. Flows of 20 and 70 cfs seemed to tend asymptotically to a minimum at high values of ETM. The highest flow rate, 175 cfs, appeared to have least error at low values of ETM. Subjective evaluation of Figure 26 led to a choice of ETM = 250, although any value between about 100 and 400 would give similar error. A more refined selection of ETM would require better field data.

Having selected the value of ETM, attention focused on parameter VMF which relates to suppression of vertical mixing. Increased fresh water flow results in stronger stratification and less vertical mixing. As noted

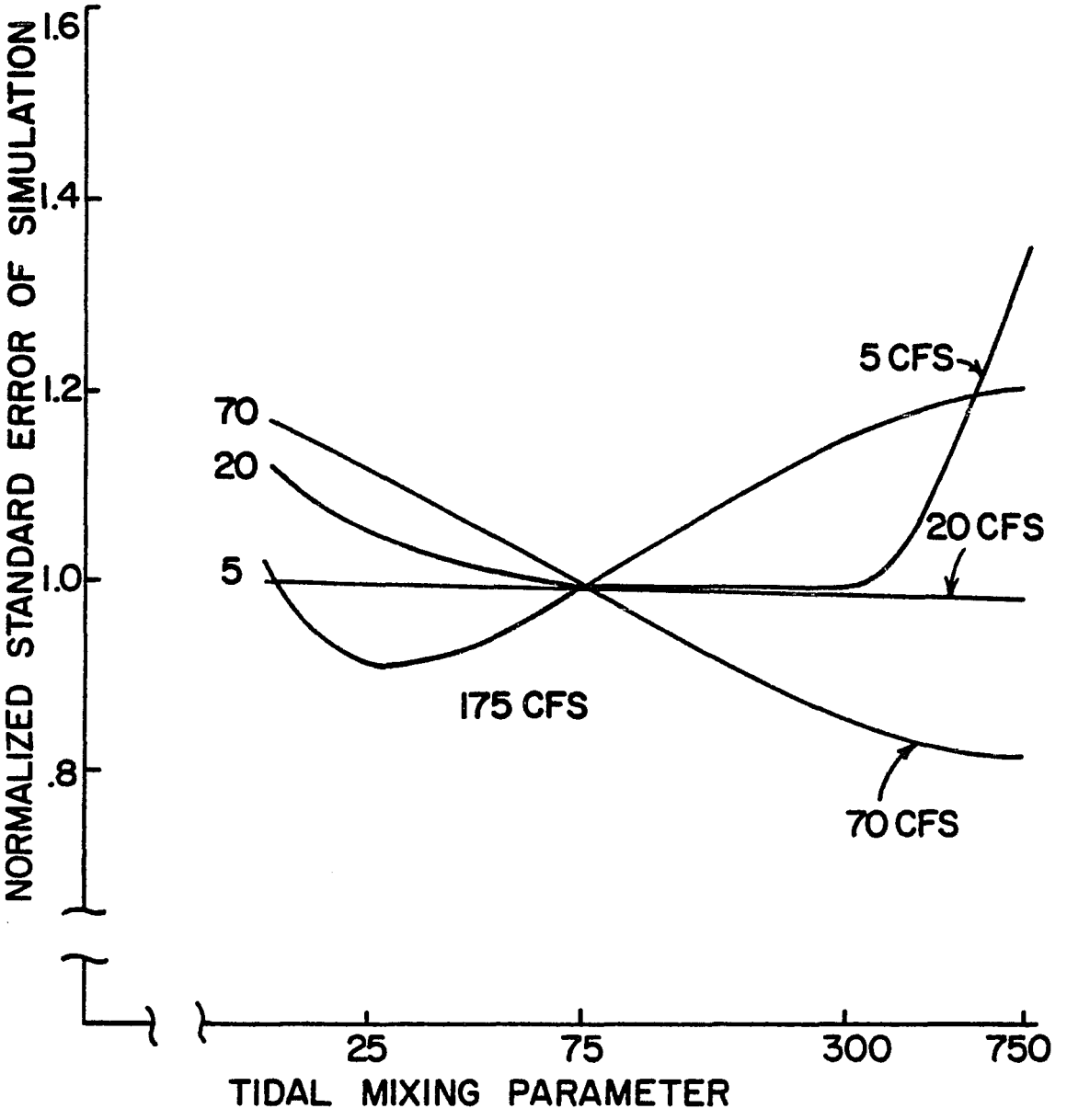

FIGURE 26

ANALYSIS OF TIDAL CYCLE MIXING

previously, VMF represents that flow rate for which vertical mixing is reduced half way from its maximum. Higher values result in a more gradual decrease. The adjustment of parameter VMF manifests itself in changing values for the density driven circulation velocity and hence the density driven dispersion coefficient.

In his thesis, Shanley presented results of a field program to measure the density driven circulation velocity. For a fresh water flow of just under 20 cfs, he presents an observed velocity profile in his Figure 28. Extrapolation of his curve to the surface gives a velocity of 9 cm/sec or 0.295 ft/sec.

Several additional runs of the hydrodynamic model were made to provide data for calibration of parameter VMF. The results are summarized in Table 19.

The table presents data for three locations of the estuary: mouth, middle and head end (segments 2, 12 and 24). In addition to the surface circulation velocity, the table includes average fresh water velocity, circulation dispersion coefficient and other data for each run. The surface circulation velocity near the mouth is plotted against parameter VMF in Figure 27. On this basis, a best-fit value of VMF = 9.3 was selected.

Table 19

Calibration Results for
Vertical Mixing Factor

	CASE 1	CASE 2	CASE 3	CASE 4
Flow Rate (CFS)	20	20	20	20
VMF	15	13	11	9
SEGMENT 2				
Salinity (ppt)	27.58	27.58	27.58	27.57
Gradient (ppt/ft)	-0.00058	-0.00058	-0.00059	-0.00059
Vs (ft/sec)	-0.192	-0.215	-0.250	-0.307
Vf (ft/sec)	-0.001	-0.001	-0.001	-0.001
Ec (ft^2/sec)	72.0	100.6	156.8	285.3
SEGMENT 12				
Salinity (ppt)	21.36	21.35	21.32	21.27
Gradient (ppt/ft)	-0.00114	-0.00114	-0.00115	-0.00115
Vs (ft/sec)	-0.094	-0.105	-0.121	-0.147
Vf (ft/sec)	-0.004	-0.004	-0.004	-0.004
Ec (ft^2/sec)	7.5	10.4	15.9	28.2
SEGMENT 24				
Salinity (ppt)	5.87	5.87	5.86	5.85
Gradient (ppt/ft)	-0.00243	-0.00243	-0.00242	-0.00241
Vs (ft/sec)	-0.284	-0.317	-0.364	-0.440
Vf (ft/sec)	-0.012	-0.012	-0.012	-0.012
Ec (ft^2/sec)	172.0	236.7	358.3	629.0

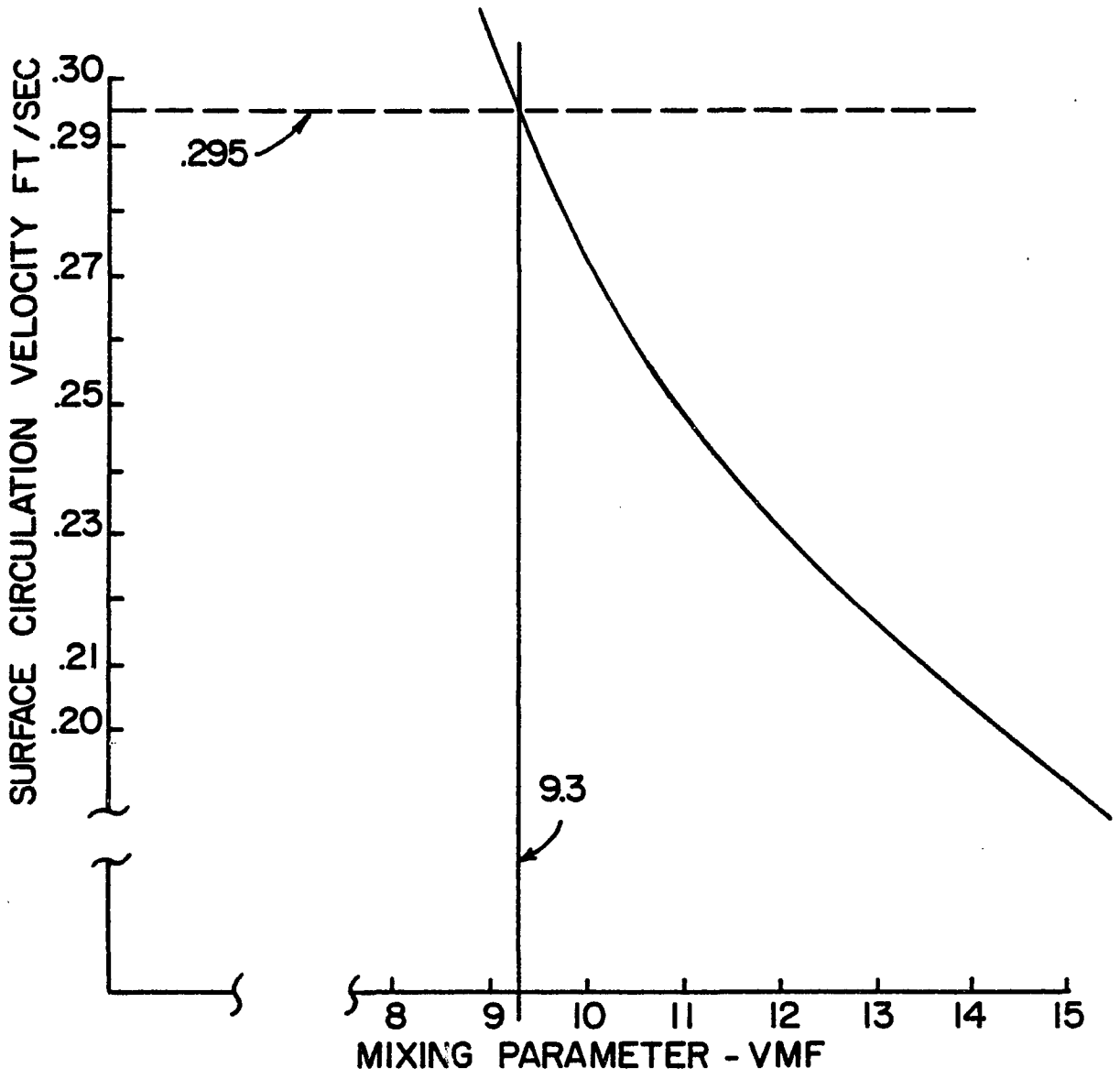

FIGURE 27

RELATIONSHIP OF CIRCULATION VELOCITY TO VERTICAL MIXING

5.4 Dispersion Model Calibration

Calibration of the dispersion model involves adjustment of dispersion coefficient multipliers EFACT(I), supplemental dispersion coefficients EZERO(I), and the return rate at the estuary mouth RETRT. Previously published data on salinity distribution in the Oyster River was employed unsuccessfully for this purpose. Therefore, dye study results were utilized to adjust these parameters and to optimize the ability of the model to predict contminant concentrations.

5.4.1 Calibration for Salinity Distribution

The initial effort to calibrate parameters of the dispersion model employed salinity data published by Shanley (1972) and credited to Shevenell. A complete set of isohalines for three tidal phases and a fresh water flow of about 70 cfs was given in Figure 6 of Shanley's thesis.

The hydrodynamic model was used to produce required flow and cross sectional area data for the dispersion model. Quasi steady state data for a flow of 70 cfs was developed using the following model parameters:

Q = 70 cfs

n = 0.02

AMP = 3.0 ft

VMF = 9.3

ETM = 250

T = 44,640 sec.

For purposes of developing the analytical solution for density gradients, the normal calculated boundary salinities were not used. Rather, tidal cycle averaged salinities at the mouth and head were specified in the data as 14.0 and 3.5, respectively. These values were taken from the salinity data described above.

Model results are summarized in Table 20 for three locations along the estuary--mouth, middle and head end. The resulting flow data file was then used to run the dispersion model. Friction coefficients used to calculate the dispersion coefficients were again specified as 0.02. Parameter EFACT, used to scale the computed dispersion coefficients, was specified as 3.0 for each segment. In the absence of wind data or information on other sources of extraneous dispersion, parameter EZERO was set to zero for all segments.

The dispersion model was then run in the following way. First, a state of quasi-equilibrium was attained using a constant boundary condition of 14.0 ppt salinity at the mouth. Then a sequence of four dynamic tidal cycles were run with a time varying boundary condition specified by

$$S_{MOUTH} = 14.0 + 1.0*SIN\ (\frac{2\pi n}{48}) \qquad (5\text{-}10)$$

Table 20

Results of Salinity Model Calibration

	STATION 2	STATION 12	STATION 24
Avg. Tidal Speed (ft/sec)	0.467	0.605	0.165
Avg. Salinity (ppt)	13.8	10.9	4.2
Avg. Gradient (ppt/ft)	-0.000274	-0.000519	-0.000984
Surface Circulation Velocity (ft/sec)	-0.400	-0.187	-0.378
Fresh Water Vel (ft/sec)	-0.004	-0.014	-0.043
Circulation (ft^2 / sec) Dispersion Coeff.	1369.0	137.0	1108.0

where n is the timestep index. This boundary condition simulates the variability over a tidal cycle observed in the published field data. By the end of four dynamic cycles, salinity variation was repeating itself within a 1% bound.

Results of this run are summarized in Figures 28 and 29. This gives the longitudinal salinity profile at four stages of the tidal cycle and an average profile over the entire cycle. In each figure, salinity in the main flow channel is plotted as a solid line, and salinities in the near-shore storage zone (mudflat areas) are shown by a series of asterisks. Available field data for three phases of the tide are also plotted on Figures 28 and 29. The two data points at each location represent near-surface and near-bottom salinities taken from Shevenell's data.

Several important features of the model results are evident in these figures. Comparison of the four tidal phase profiles shows the advective motion of isohalines into and out of the river during the tidal cycle. The results also illustrate the time delay for mass transport into and out of the shore storage zones. During a flooding tide, shore salinity, as shown by the asterisks, lags behind the main channel salinity. Conversely, on an ebbing tide, as fresher water moves down river, the shore zone salinities are higher than those in the flow zone.

An effort was then made to optimize the value of parameter EFACT by several additional runs of the model.

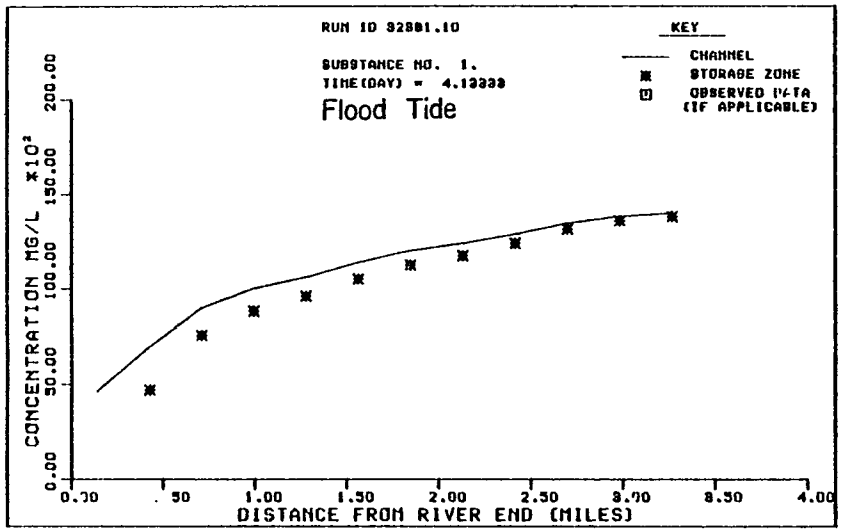

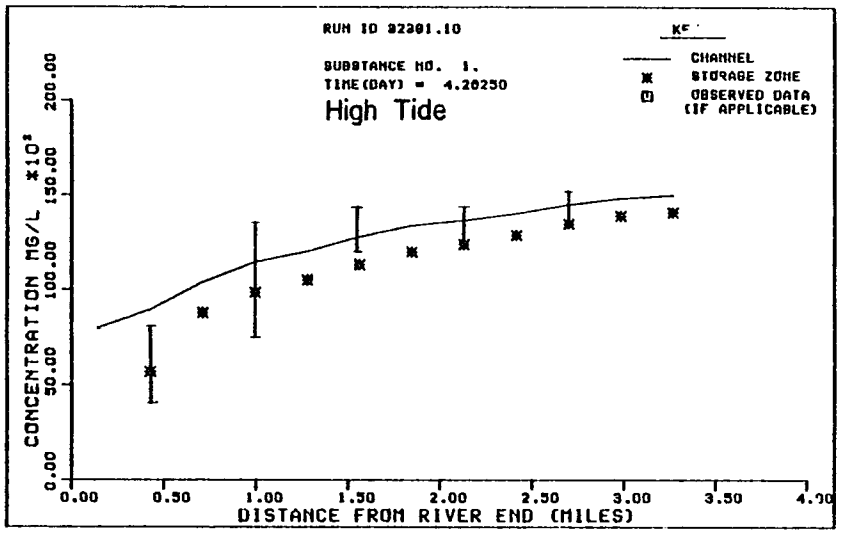

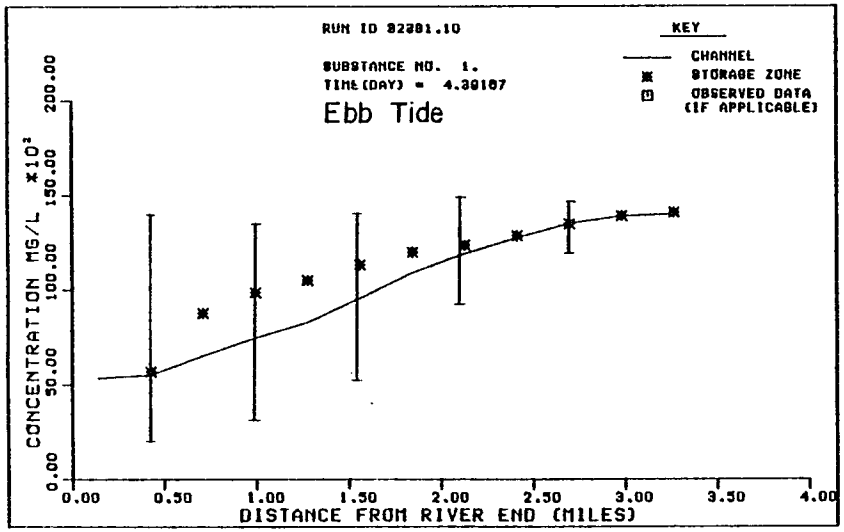

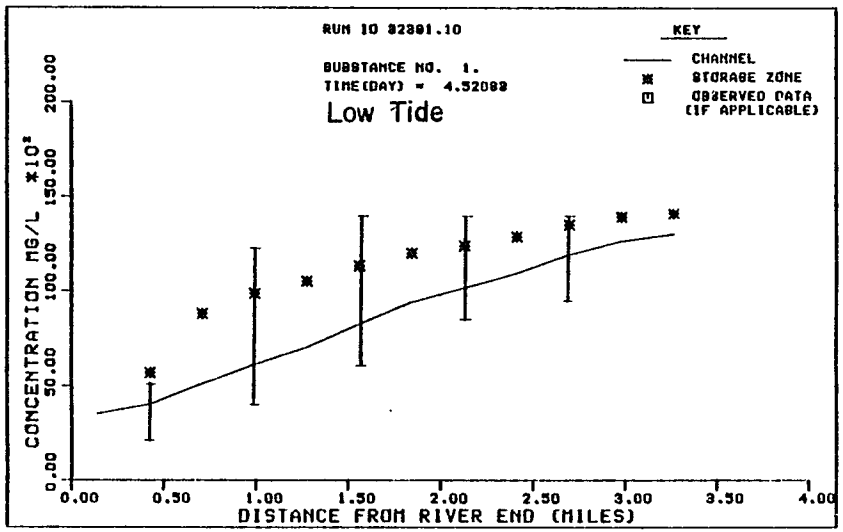

FIG 28 SALINITY STAGES FOR 20 CFS FLOW

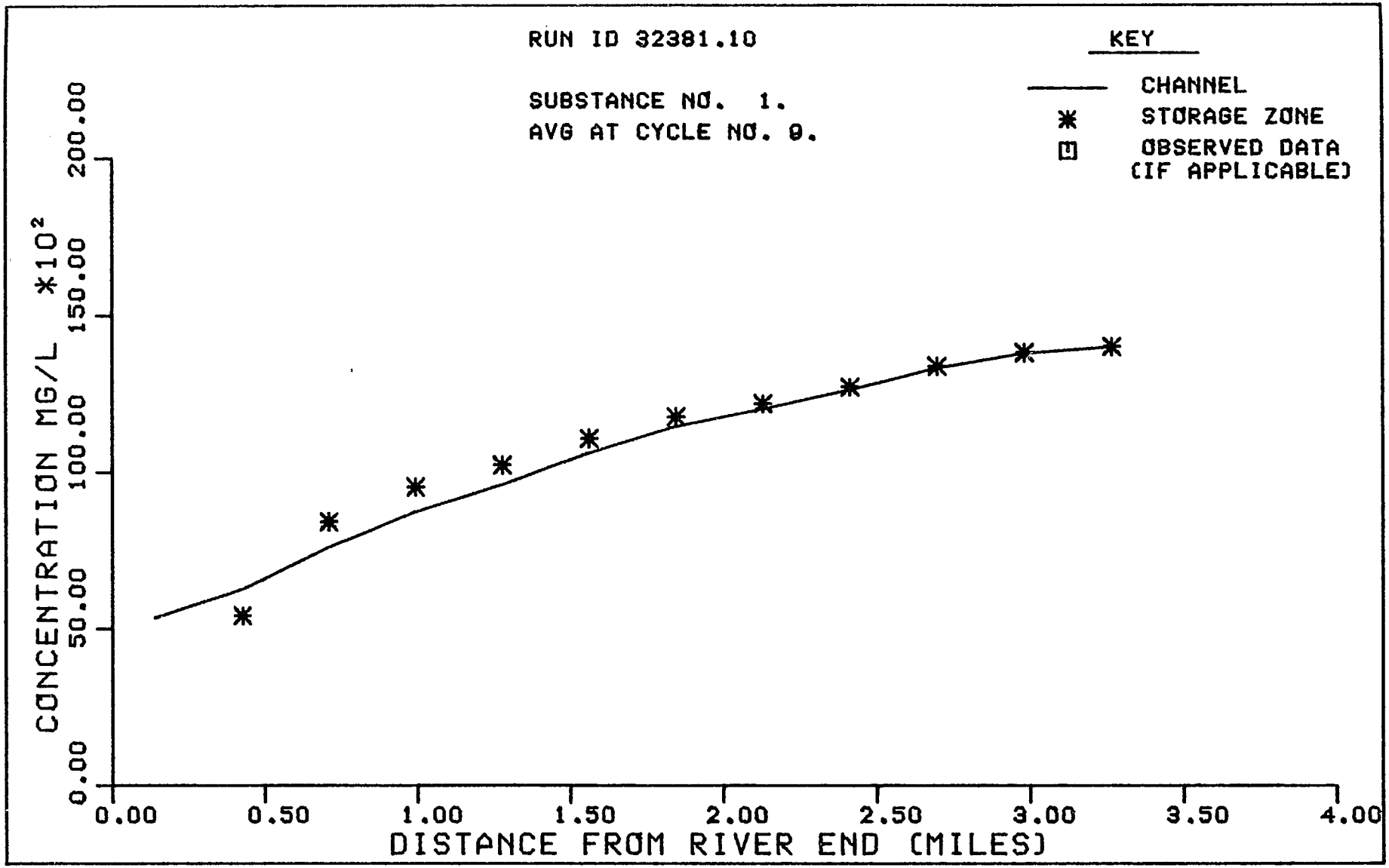

FIG 29 TIDAL CYCLE AVERAGED SALINITY FOR 20 CFS FLOW

It became evident that this parameter has little effect on the equilibrium salinity profile. For example, results for a run with EFACT = 0.3 (an order of magnitude decrease) were found to plot almost identically to those described above. While the large dispersion parameter had some impact on rate of convergence, the final equilibrium profile was virtually unaffected.

Increasing the value of EFACT by one order of magnitude to 30.0 had a more significant effect. The head-end salinities were raised approximately 0.5 ppt at all phases of the tide as a result of the increased dispersion. However, the maximum change resulting from a two order of magnitude adjustment of EFACT (0.3 to 30.0) was only 0.75 parts per thousand (ppt).

Comparison of field data to predicted salinities revealed that small upward changes in head-end salinity does not necessarily improve the fit. In particular, the simulated head-end salinity at high slack water exceeds the observed value at all values of EFACT. Further increases in EFACT would only serve to worsen the fit here. For other phases of the tide the conclusion is not as obvious, but it became apparent that optimization using salinity data is not reasonable.

Further consideration of the physics of the dispersion process and the magnitude of the components of this process served to explain the small role of this parameter. First, the Fickian representation of dispersion

employs a product of the dispersion coefficient and the contaminant (or salinity) gradient. At equilibrium these gradients have been reduced to a minimum, and the relative importance of dispersion declines. Quantitatively, the relative magnitude of the several components of the dispersion coefficient used here is revealing. In this model, four different components are encompassed in the dispersion coefficient. These are: 1) cross section variability of velocity and concentration due to friction and geometric irregularities; 2) net circulation due to density gradients; 3) temporal variability of velocity and concentration due to tides; and 4) extraneous dispersion due to wind or other factors. These may be represented as:

$$E = E_f + E_C + E_T + E_0 \qquad (5\text{-}11)$$

Parameter EFACT enters into the first component. The magnitude of this component can be estimated using typical values for computing E_f :

$$E_f = EFACT*77*n*U*R^{5/6} \qquad (5\text{-}12)$$

For EFACT = 3.0, n = 0.02, U = 0.5 ft/sec., and R = 10 ft., the resulting value is $E_f = 15.7\ ft^2/sec$. By comparison, the values of E_C were shown to be on the order of 1000. For an ETM of 250, tidal cycle mixing represented by E_T is also on the order of 1000. For these analyses the value of E_0 was selected as 0. Using these values, an order of magnitude increase in CORFA increases the total dispersion effect from approximately 2015 to 2150 ft /sec, an increase of only 6%. For the small gradients present at equilibrium, no change in longitudinal profile should be expected.

On the other hand, when large gradients exist due to rapid introduction of contaminants into the estuary, dispersion effects are significantly more important. Furthermore, when the analysis is examining transport occurring on a time scale significantly shorter than a tidal cycle, term E_T does not enter into the analysis.

This term results from the averaging of velocity and concentration over a tidal cycle and does not enter into instantaneous dispersion. Therefore, it is more reasonable to calibrate parameter EFACT using transient conditions. Proper selection of the dispersion parameters required field data on continuously varying transient concentrations. The most effective way to obtain such data is introduction of a readily measured artificial water tracer.

5.4.2 Field Studies of Dye Dispersion

Two field dye dispersion studies were undertaken to provide the required transient data. Design of the field studies included consideration of the eventual model application to storm flow transported contaminants. Therefore, the dye release point was located near the tide head dam and the dye was discharged gradually over several hours to simulate a storm flow. Furthermore, the impact of varying flow rate on the flow regime of the tidal river was considered. As a result, the dye studies were scheduled for a high fresh water flow period in April and a low flow period in late summer.

In both cases, dye was diluted to a volume of approximately five gallons (approximately 10:1) and released through a plastic hose below the Route 108 bridge

in Durham. The location is identified on Figure 30. Flow rate was limited to approximately 0.02 gallons/minute by an oriface placed at the end of the hose. The release was timed to end near the time of high slack water in each case. Details of the two dye releases are given in Table 21. For the spring dye study, dye concentration measurements were initiated immediately after completing the dye release. However, it became clear that this is not the optimum procedure for data collection. The plume was concentrated in a narrow stream of fresh water. Meandering of the narrow plume made it quite difficult to obtain a meaningful pattern of dye dispersion during the first few hours of sampling.

Later in the sampling program, however, the plume began to spread enough that better data was obtained. To avoid this difficulty, release of dye for the second study was scheduled for the evening preceding field sampling. This allowed an entire tidal cycle of mixing to occur before measurements were made.

The April sampling program was designed for intensive evaluation of dye plume dispersion during the first few tidal cycles after release. It was correctly postulated that the high fresh water flow rate would rapidly carry the dye out of the river. Two Turner model 10 fluorometers were mounted in boats and operated with flow-through systems for dye analysis.

An instrument owned by the New Hampshire Water Supply

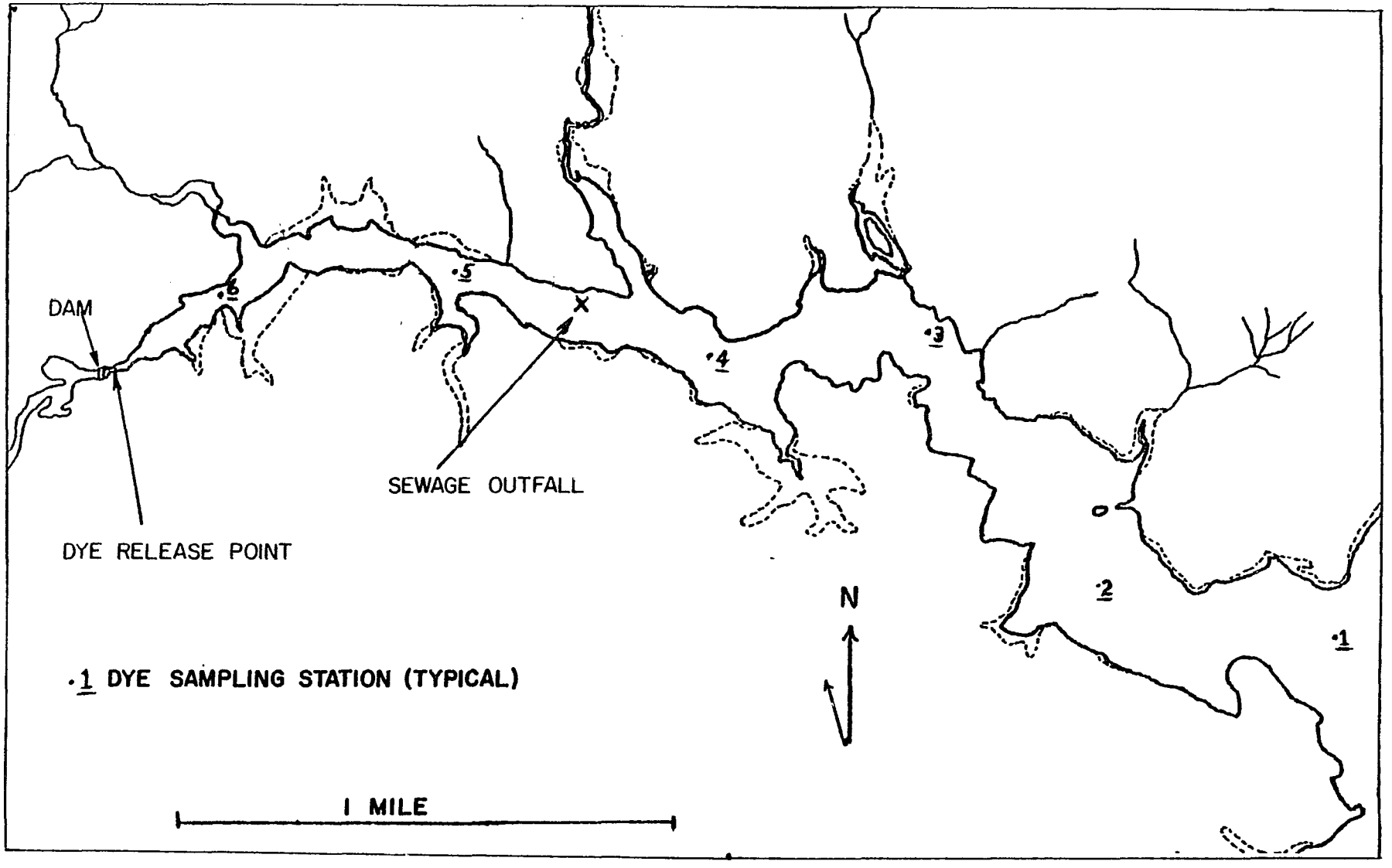

FIG 30 OYSTER RIVER ESTUARY MAP

Table 21

Dye Study Descriptions

	SPRING DYE STUDY	SUMMER DYE STUDY
DATE OF RELEASE	4 April 1979	12 Sept 1979
TIME OF HIGH WATER*	0738 Hrs	1853 Hrs
RELEASE INITIATED	0440 Hrs	1640 Hrs
RELEASE COMPLETED	0655 Hrs	1825 Hrs
TOTAL WT OF DYE SOLUTION**	5.12 lbs	7.75 lbs
AVERAGE FLOW RATE	0.038 lbs/min	0.074 lbs/min
ESTIMATED RIVER FLOW	175 CFS	3-5 CFS

*Estimated from Boston tide tables

**Gross weight of 20% solution Rhodamine weight

and Pollution Control Commission (NHWSPCC) had previously been calibrated by the manufacturer for Rhodamine dye. A UNH instrument identical to this one was calibrated against it by pumping dye solution through both instruments connected in series. The UNH instrument was found to have an extraneous signal equivalent to 1.5 ppb of Rhodamine dye. All data from this instrument must, therefore, be reduced by this value to get true concentrations. The UNH instrument was operated from a fourteen-foot outboard motorboat owned by the New Hampshire Water Supply and Pollution Control Commission. Water was pumped to the fluorometer through plastic hose by a submersible bilge pump with a capacity of 4 gallons/minute. Power for both the instrument and the pump was taken from the boat's 12-volt DC system. A battery powered strip chart recorder was used to record data, and several sample bottles were filled for later laboratory analysis and confirmation of the dye concentration readings. The second instrument, owned by the New Hampshire WSPCC, was mounted in their lobster boat, MV Vose. A small centrifugal pump drew water to the instrument and a Rustrak recorder gave a continuous recording of dye concentrations.

Sampling proceeded as follows. The MV Vose made several longitudinal transects through the length of the Oyster River. Continuous measurements were made, and the instrument was operated in an automatic mode which allows it to select from the most appropriate of four instrument

ranges. The smaller boat made lateral transects across the channel at six marker buoys previously placed in the river and at several identifiable intermediate locations. This instrument was operated in a manual mode where range changes are made only when selected by the operator.

A great deal of strip chart data was recorded during the first day. Unfortunately, the previously mentioned problem--following a narrow, invisible plume of dye meandering through the river--made much of the longitudinal transect data useless. The problem was compounded by the use of the automatic mode. As the sampling probe passed in and out of the plume, the instrument continuously hunted for the best range. Time lags inherent in both the hydraulic system and the instrument electronics made it virtually impossible to identify meaningful data points. More useful data was obtained from the lateral transects, although this too was not ideal. Generally, the strip chart traces showed a single narrow peak of dye concentration, but some transects exhibited several peaks or a more diffuse dye pattern. The traces are not reproduced in this report, but Table 22 summarizes the time and peak concentration for lateral transects made throughout the first day of sampling.

Maximum observed concentrations just after completion of the dye release were around 70 ppb near the release point. Dilution of the average dye release rate of 0.038 lbs/min by 175 cfs of fresh water would result in a

Table 22

Dye Concentrations
during High Flow Study

Time	Location	Peak Concentration
0710	Old Landing	70
0713	Marker 5	49-63
0723	Marker 4	0
0729	Sewage Trtmt Plant	>30
0740	Marker 5	65
0742	Jackson Landing	30-54
0746	Marker 6	38
0752	Old Landing	64 (Localized Pocket of Dye)
0800	Marker 6	26
0806	Jackson Landing	43
0810	Marker 5	38
0813	Sewage Trtmt Plant	19
0818	Marker 4	15
0834	Sewage Trtmt Plant	25
0840	Marker 5	33
0845	Marker 6	40
0850	Old Landing	50 (Localized Pocket of Dye)
1006	Marker 3	13
1020	Marker 4	10
1026	Sewage Trtmt Plant	13
1030	Marker 5	21
1035	Jackson Landing	11
1050	Marker 5	14
1055	Marker 4	13
1100	Marker 3	9
1110	Marker 2	9
1130	Marker 1	5.4
1302	Marker 1	4.8
1330	Marker 3	7.8
1447	Marker 4	6.6
1505	Marker 2	3.3
1545	Marker 5	7.2
1552	Marker 6	2.6
1655	Marker 3	5.4
1705	Marker 2	2.7
1815	Marker 3	4.3
1820	Marker 4	4.6
1825	Marker 5	7.2

concentration of 58 ppb. Hence, it is apparent that the initial readings represent direct observation of dye as it entered the estuary. It is clear that the dye was moved rapidly through the river, with some reaching the mouth at Marker 1 within the first tidal cycle.

By the time of the first low tide, the dye had been diluted well below 10 ppb at all locations. Some dye apparently returned to--or never left--the upper end of the river, but by the afternoon of the first day dye could be observed at almost any location along the river. Sampling was concluded at about 1900 hours at the end of one complete tidal cycle.

On the following morning sampling was initiated using a single instrument aboard the MV Vose. During the night, rainfall had begun which continued through the morning. It is likely that this resulted in some dye dilution at the surface. A somewhat different strategy was adopted for the second day of sampling. Emphasis was now placed on the vertical distribution of dye in the water column. Observations of both dye concentration and salinity were made at 0.1, 0.5, 1.0 and 1.5 meter depths at each of the Marker stations. These data were grouped into sets representative of a single run either up or down the river and are plotted in Figures 31 through 35.

On this second day of sampling, maximum dye concentrations had fallen to approximately 2 ppb and were fairly uniformly distributed throughout the river.

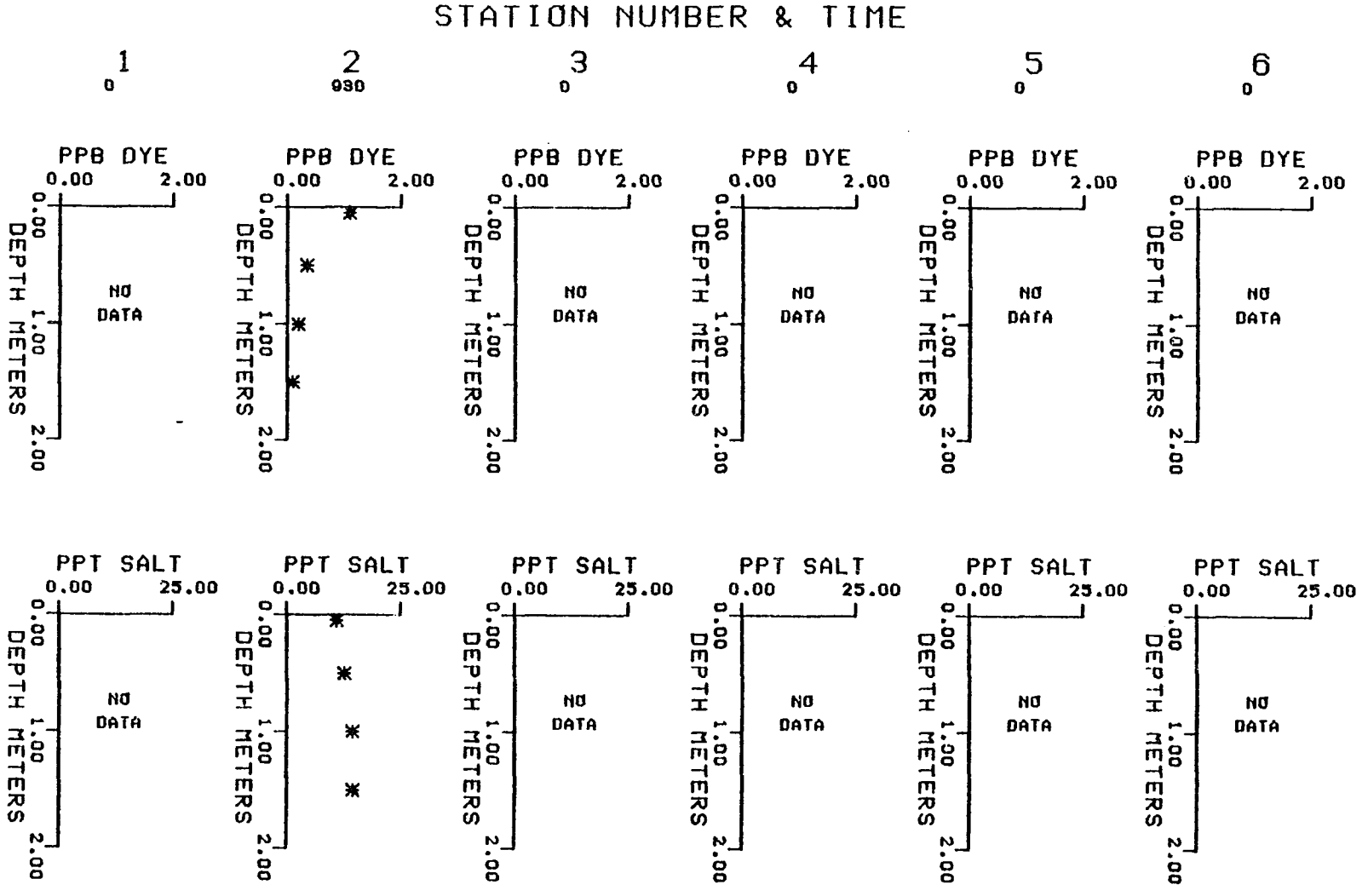

FIG 31 HIGH FLOW DYE PROFILE 0930

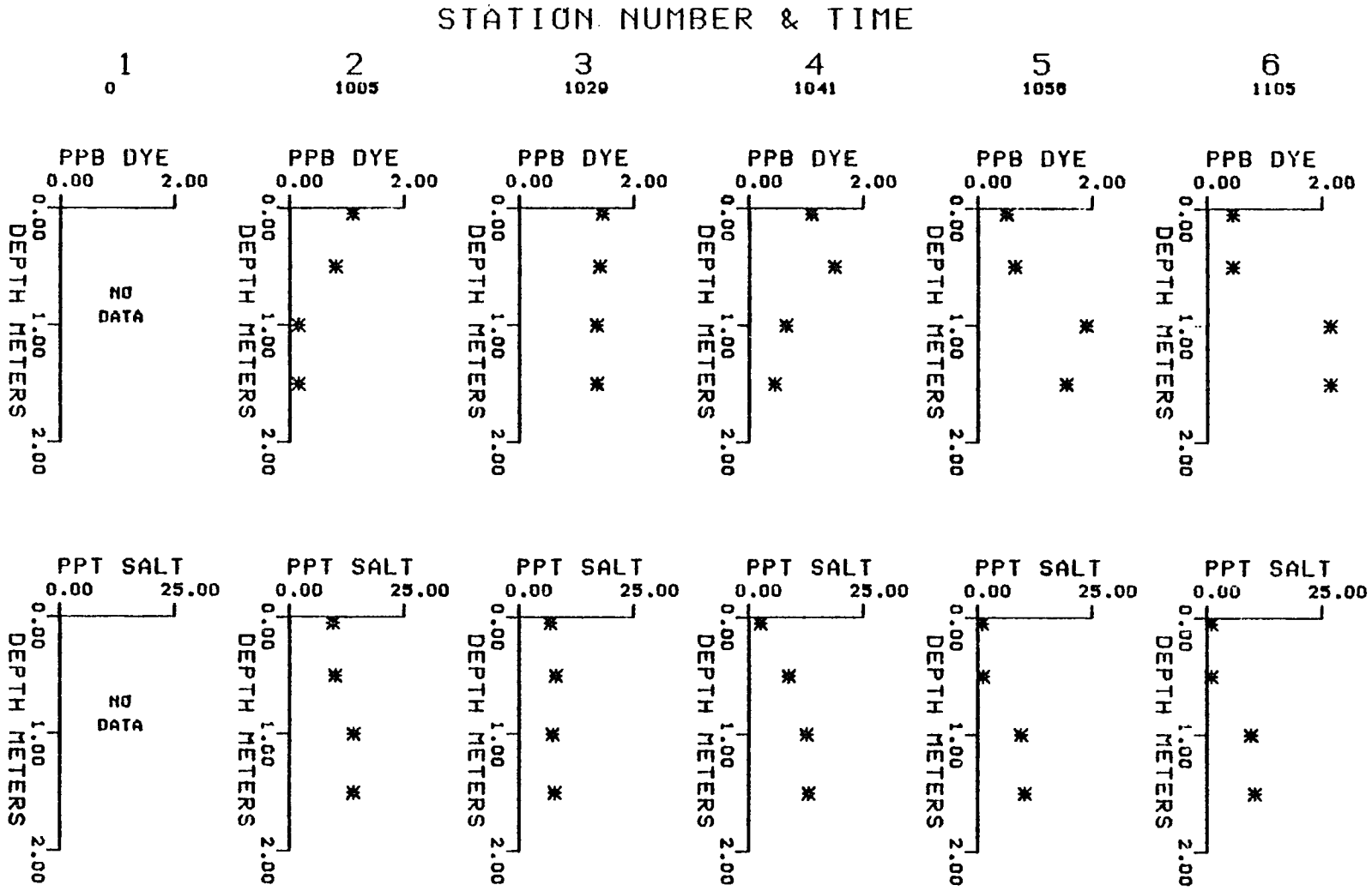

FIG 32 HIGH FLOW DYE PROFILES 1005-1105

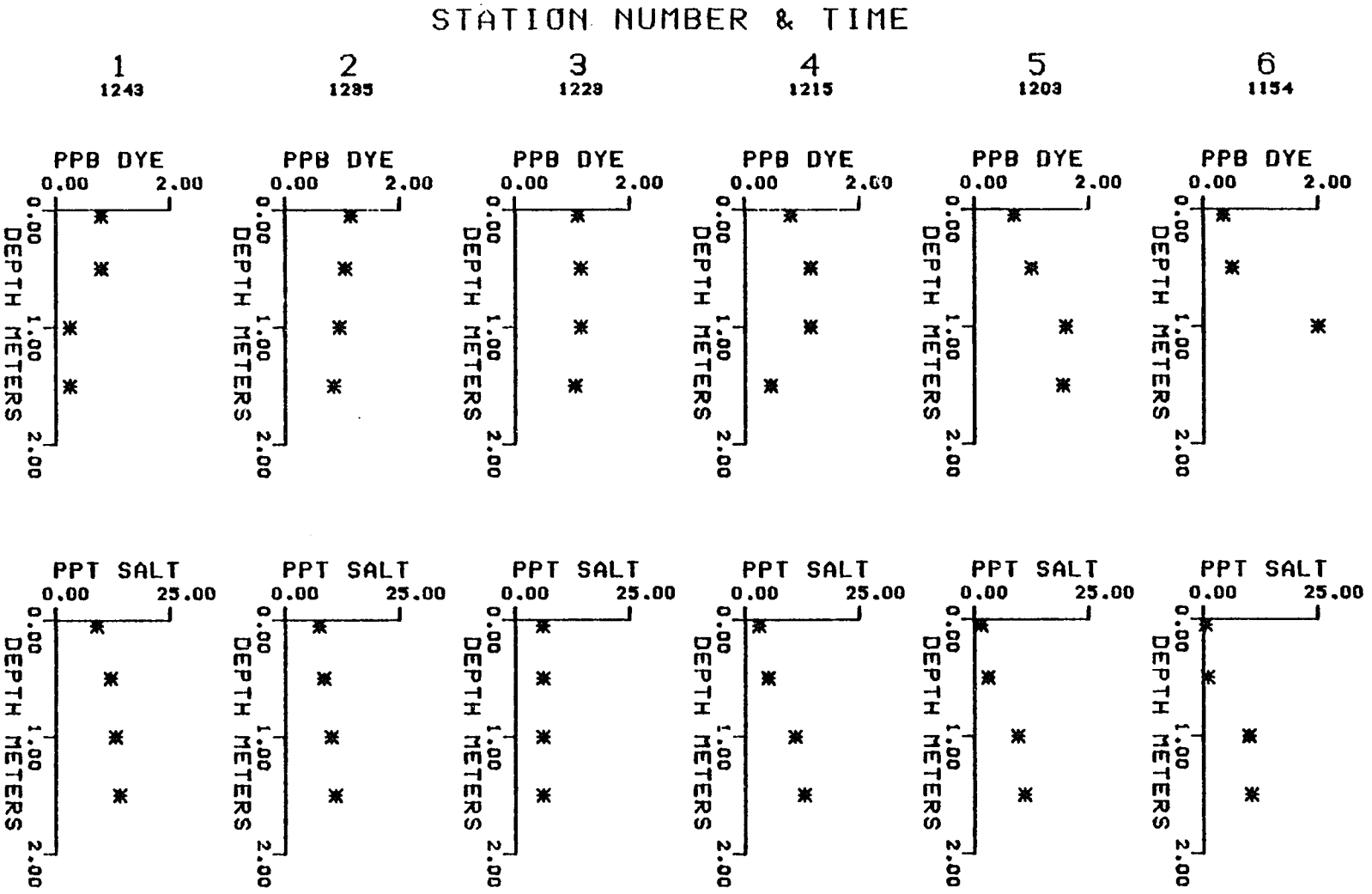

FIG 33 HIGH FLOW DYE PROFILES 1154-1243

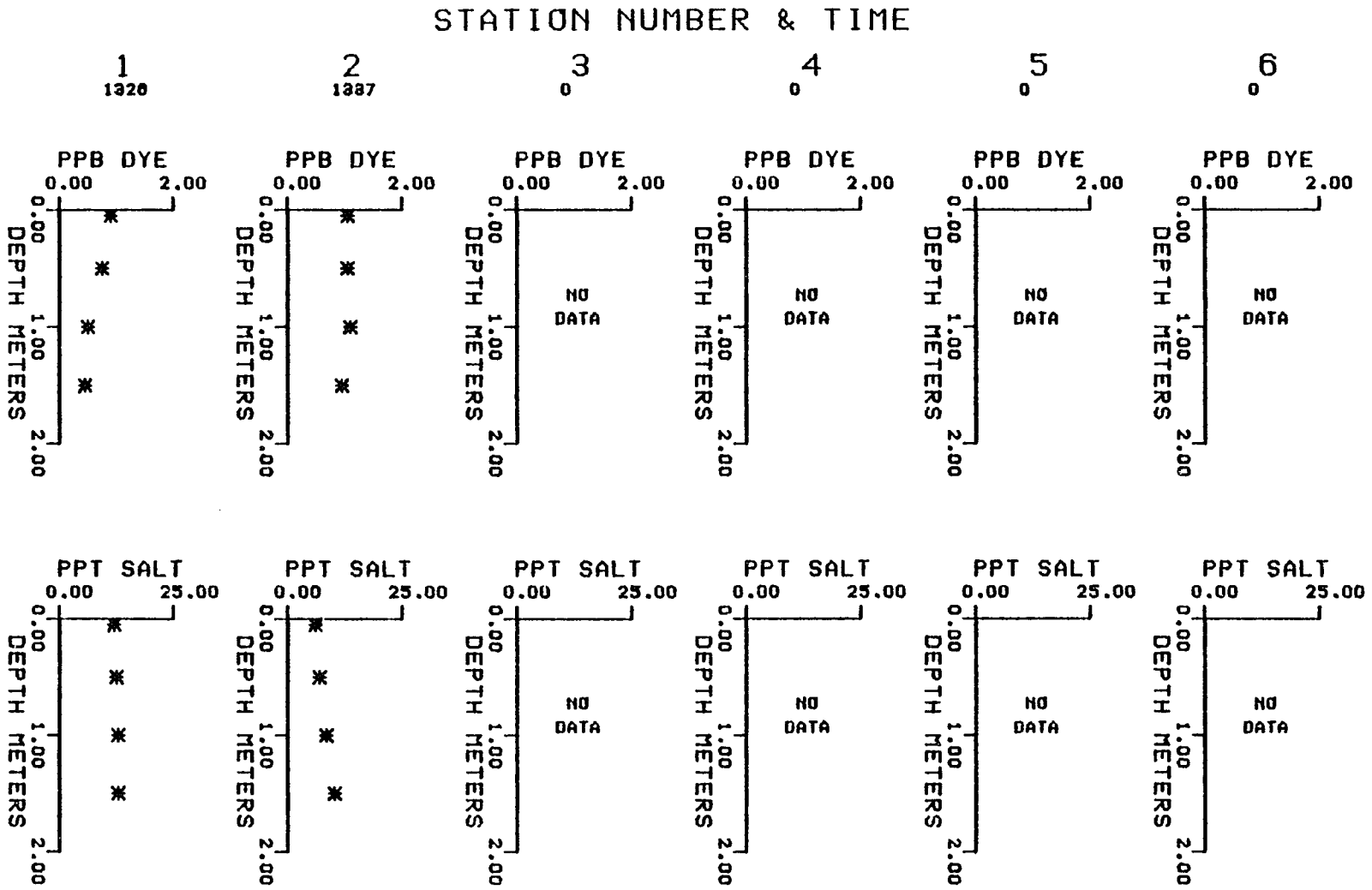

FIG 34 HIGH FLOW DYE PROFILES 1326 - 1337

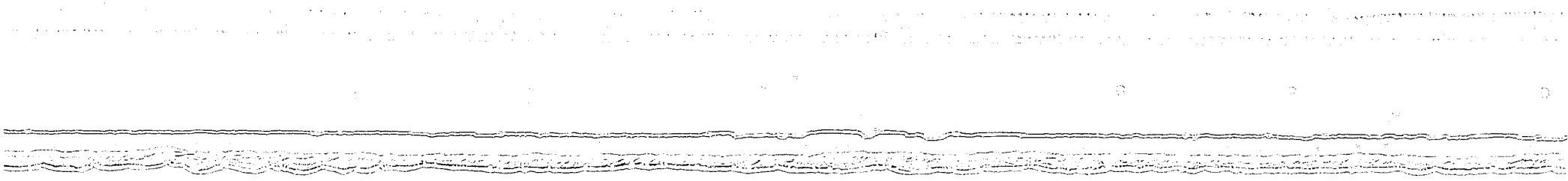

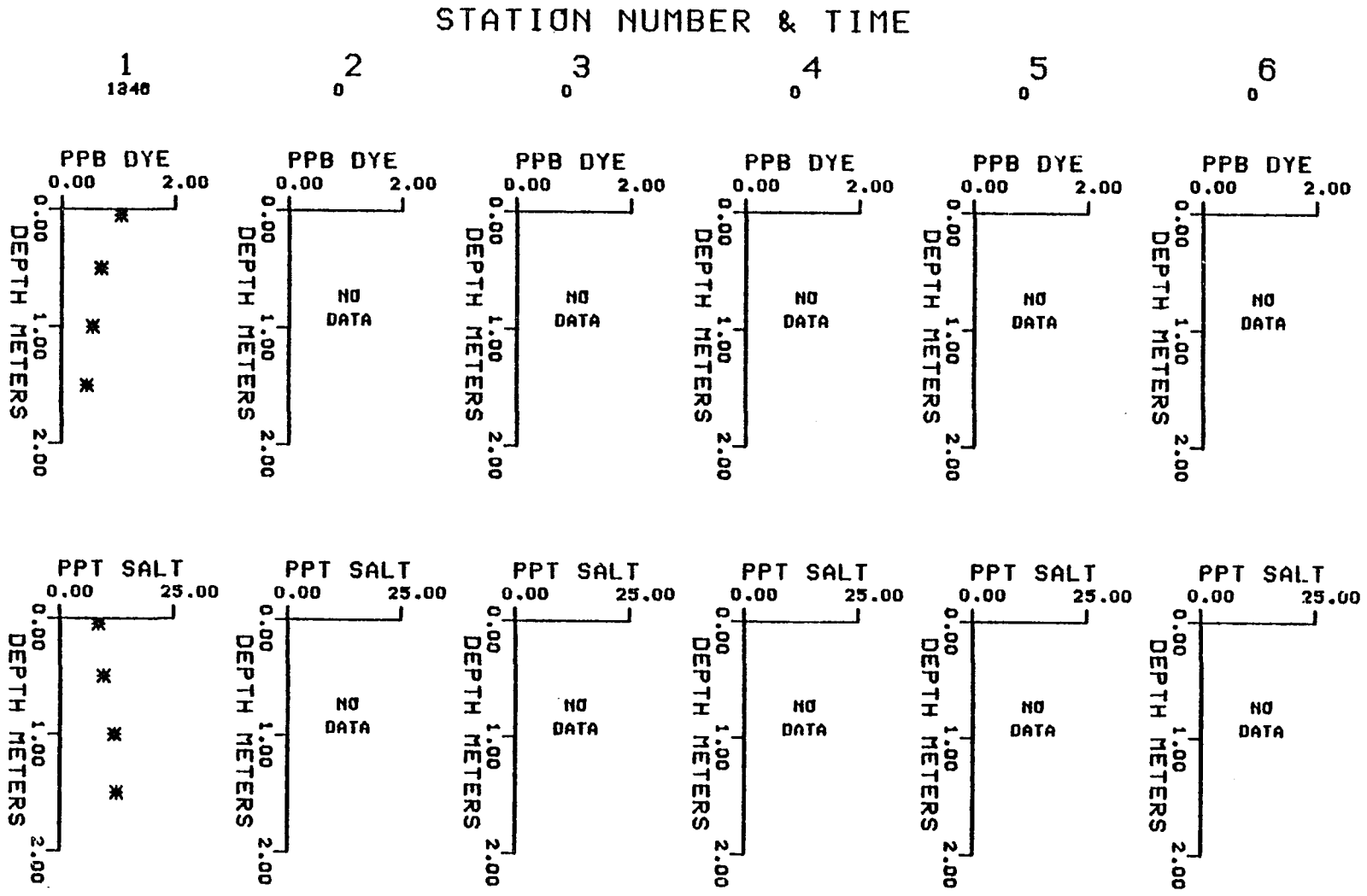

FIG 35 HIGH FLOW DYE PROFILES 1346

Inspection of the dye profiles reveals the stratification known to exist in the river. They also show that near the mouth of the river dye concentration and salinity vary inversely, but near the head end (higher marker numbers) they vary directly with each other. This interesting observation leads to the following hypothesis regarding mixing of water masses in the river.

The dye may be visualized as residing in a distinct water mass which oscillates longitudinally with the tide and continuously expands by mixing with adjacent water. At the downstream end of the mass (toward the mouth), its lower density allows it to ride over the heavier water mass containing higher salinity and lower dye concentrations. Conversely, at its upstream end fresher water introduced after completion of the dye release rides up over the water mass containing dye. As dilution occurs at both ends of this water mass, concentrations are reduced and lines of equal concentration continuously grow outward.

The dilution process was further evaluated by plotting the relationship of dye concentration to salinity observed at each sampling location. This technique, first developed by Boyle (1974), is used to determine whether contaminants carried by a freshwater flow are mixing conservatively with ambient salt water. If data points plot as a straight line, conservative mixing can be shown to exist. The end points of the line provide an indication of the contaminant concentration in the fresh and salt

water components. Data from the fifteen vertical transects are plotted in this form on Figure 36. It is obvious that no single straight line can adequately represent this data. However, if the data is separated into two sets, a useful result is obtained. In Figure 37, data points identified by triangles are taken from stations 3, 5, and 6 where dye profiles are parallel to salinity profiles. Data points identified by asterisks are taken from stations 1, 2 and 4 where dye and salinity profiles vary inversely. A linear least squares regression results in two straight lines having correlation coefficients of 0.947 and -0.844, respectively.

This analysis shows quantitatively the extent to which conservative mixing can describe the dye dispersion process. It also demonstrates that dispersion processes affecting salinity are similarly affecting the fresh water component carrying the dye. This observation justifies the use of circulation dispersion coefficients derived from salinity analyses for other materials dissolved in, or moving with, the water mass.

The September dye study was designed to evaluate dispersion conditions when low flow prevails. It was postulated that flushing would be slow and dye would remain in the estuary for a much longer period of time than in the previous study. The sampling program was therefore less intensive but extended over a period of almost two weeks. As discussed previously, dye was released one tidal cycle

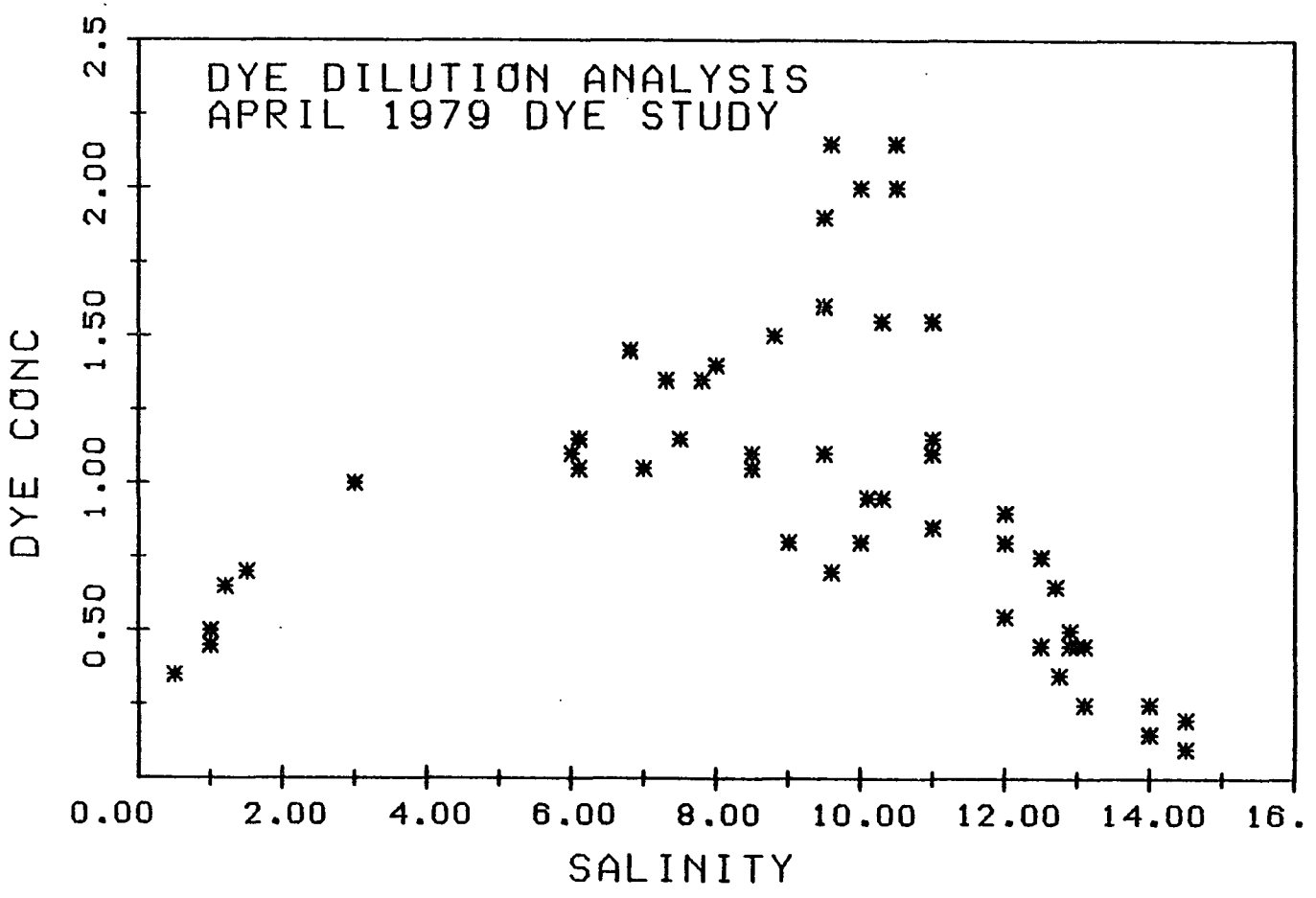

FIG 36 HIGH FLOW DYE/SALINITY DATA

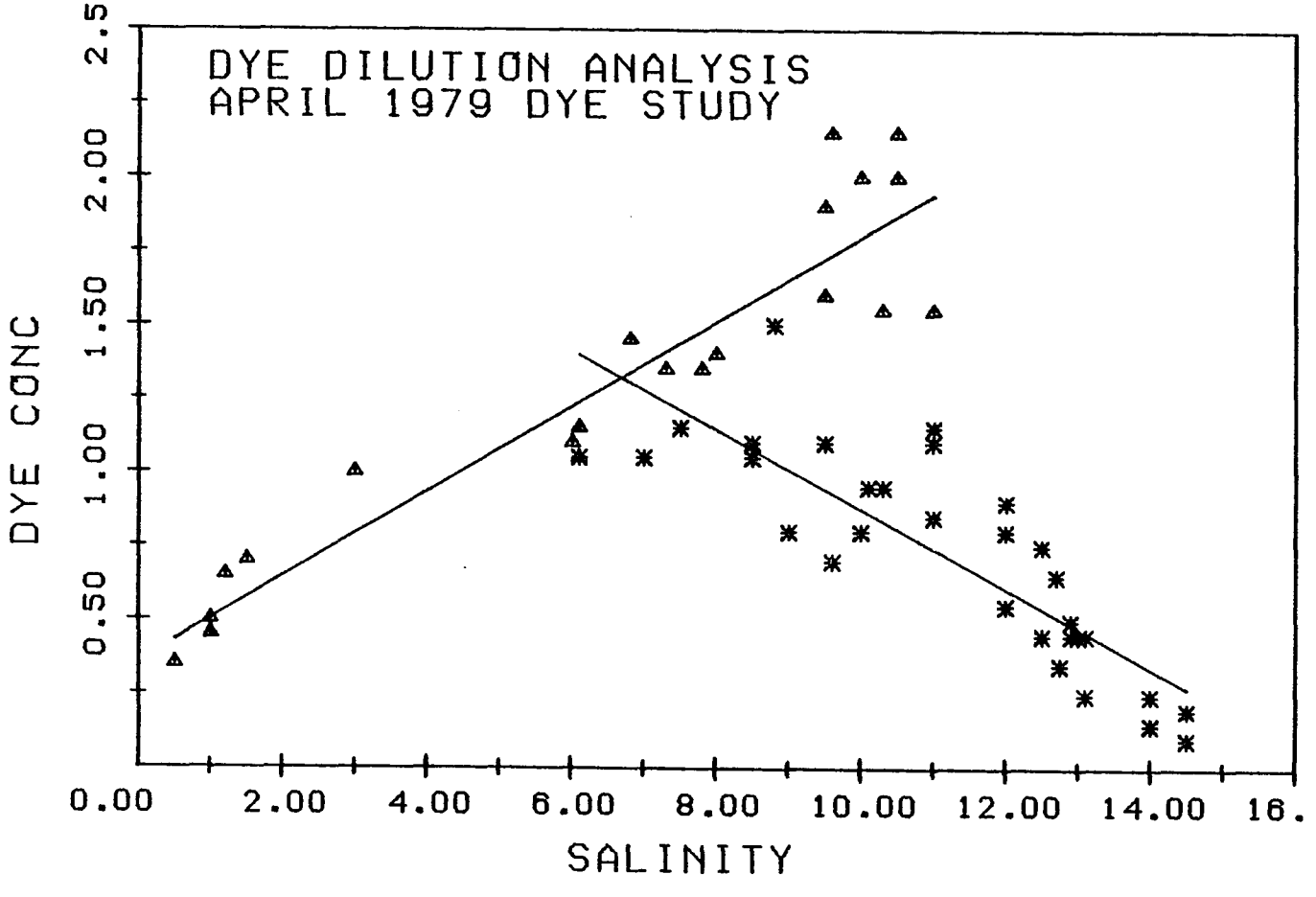

FIG 37 DYE DILUTION ANALYSIS

before sampling began. The NHWSPCC Turner 10 fluorometer was mounted in their fourteen-foot outboard boat, and the 4-gpm pump was used to draw water from depths of 0 to 2 meters. Once again, the battery- operated strip chart recorder was used to record continuous data. This system was operated for two days (daylight hours only) after release of the dye. Subsequent data was obtained by filling sample bottles which were returned to the laboratory for analysis on the UNH Turner 10 fluorometer. From day 3 through 6, sampling was done at six stations at the morning high tide and the afternoon low tide. Dye bottles were filled at depths of 0.1 meter and 1.0 meter. Additionally, salinity was measured at these depths in situ using a YSI model 33 conductivity instrument. From day 7 through 10, this sampling was reduced to twice daily surface dye samples at a single station.

Data from lateral transects made on the first day are plotted in Figures 38 thru 43. Comparison to data for the spring dye study shows the effect of fresh water flow rate on flushing of contaminants from the river. During the second tidal cycle after dye release, none was observed at the mouth of the river. At station 2, the highest observed concentration was less than 2 ppb. Furthermore, concentrations at the head of the river fell much more gradually than during the spring dye study. After one tidal cycle, a peak of 42 ppb was observed at station 6, compared to a maximum of about 5 ppb at station 5 for the

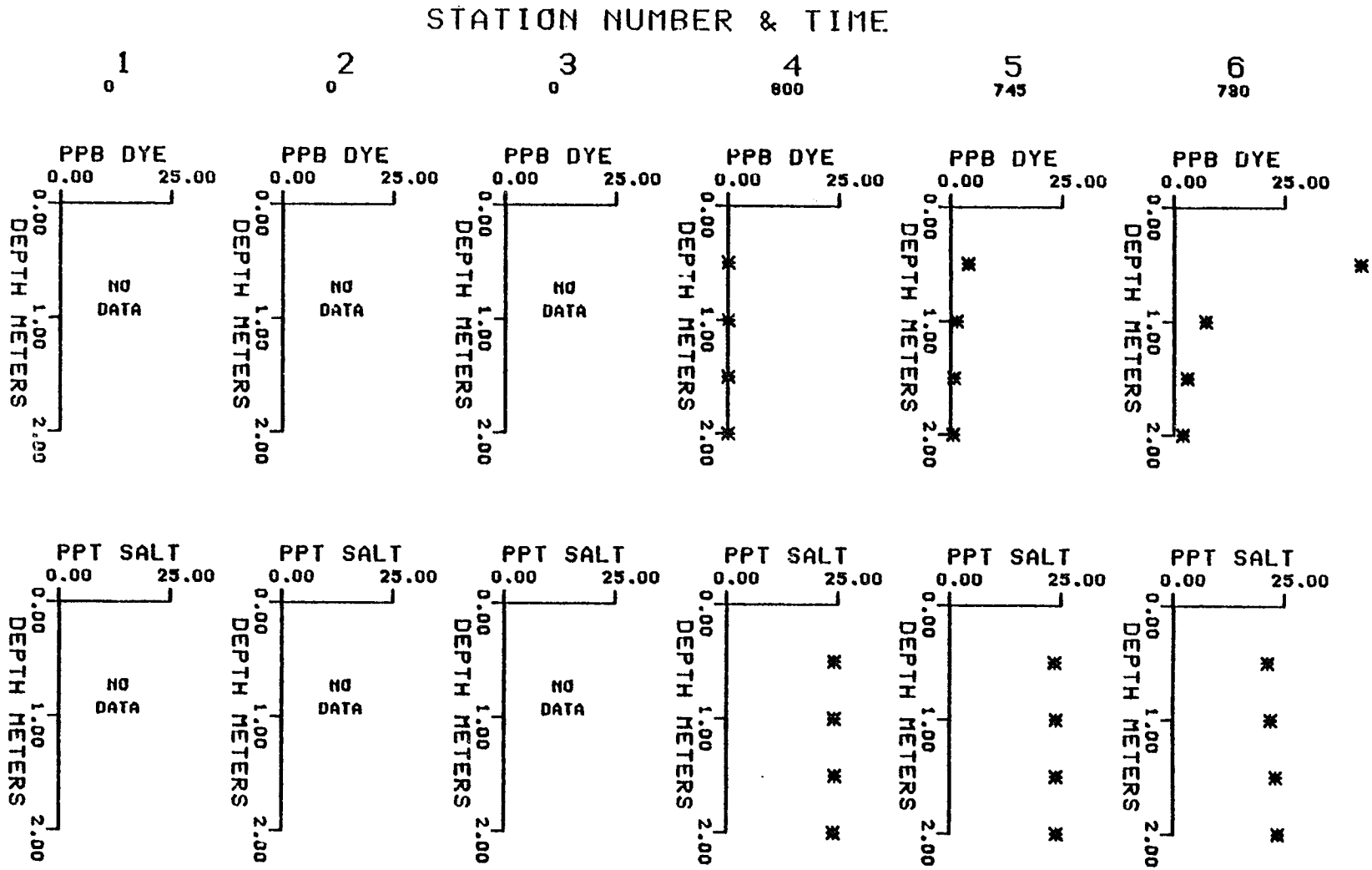

FIG 38 LOW FLOW DYE PROFILES 0730 - 0800

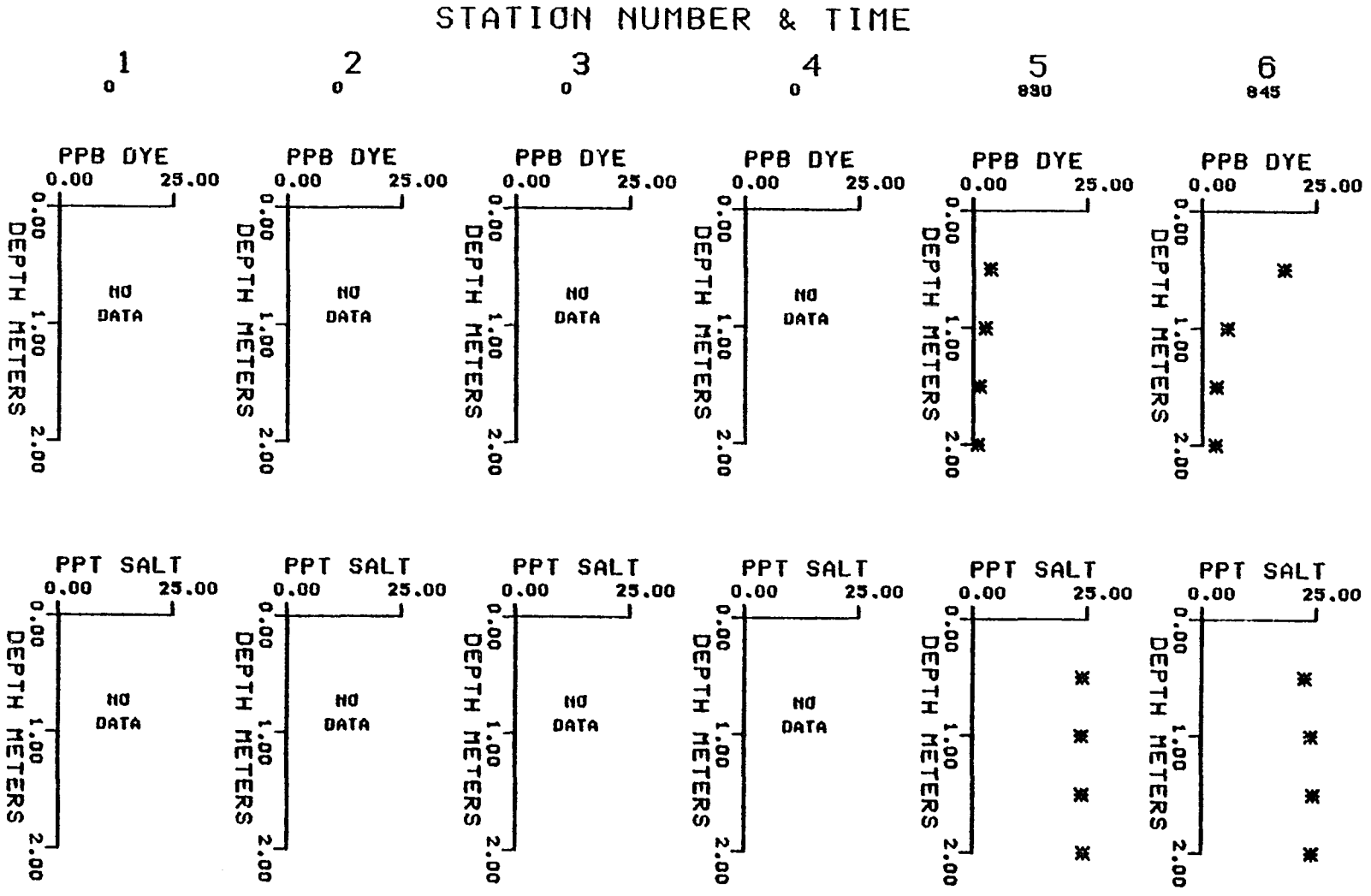

FIG 39 LOW FLOW DYE PROFILES 0830 - 0845

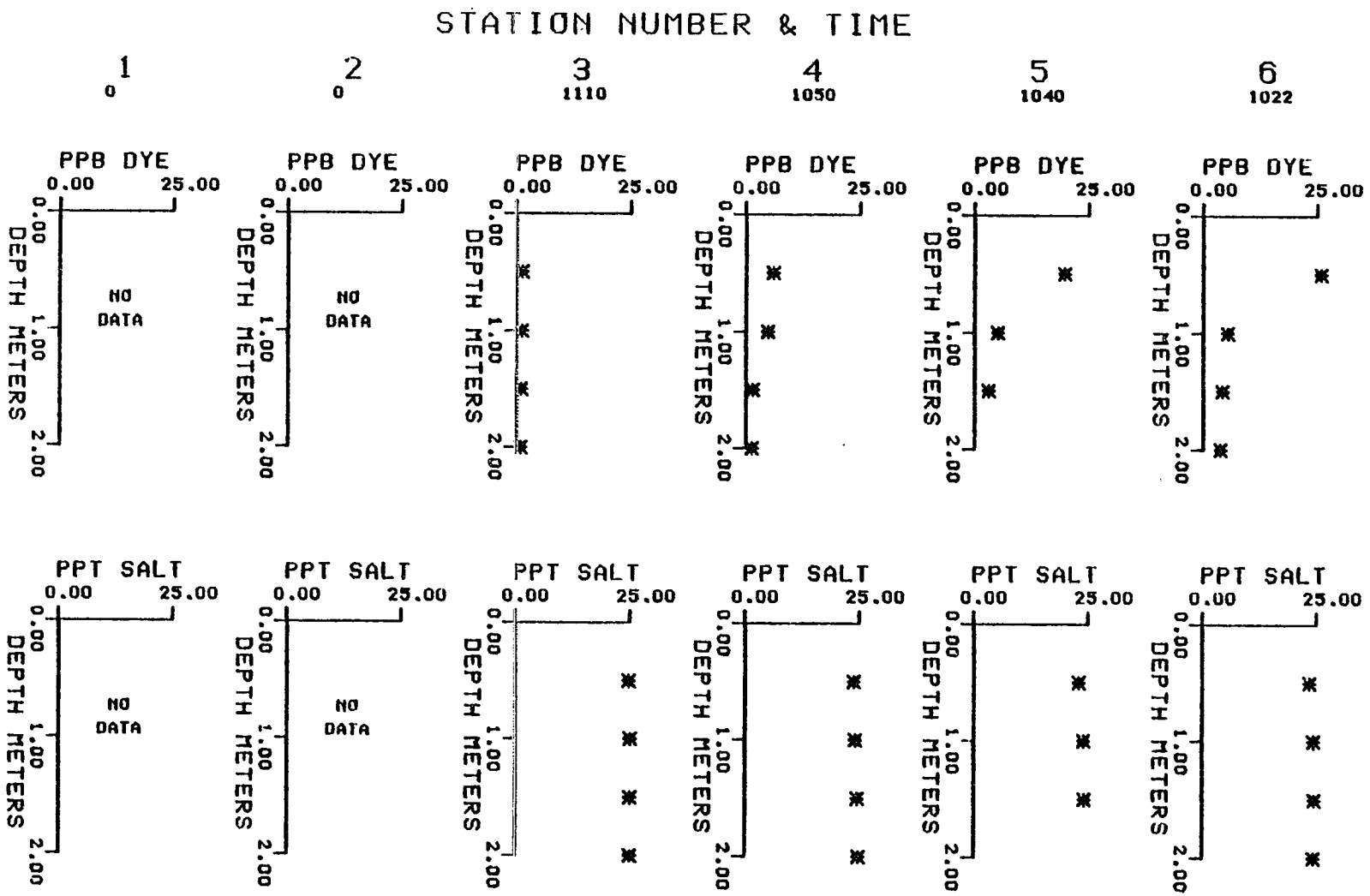

FIG 40 LOW FLOW DYE PROFILES 1022 - 1110

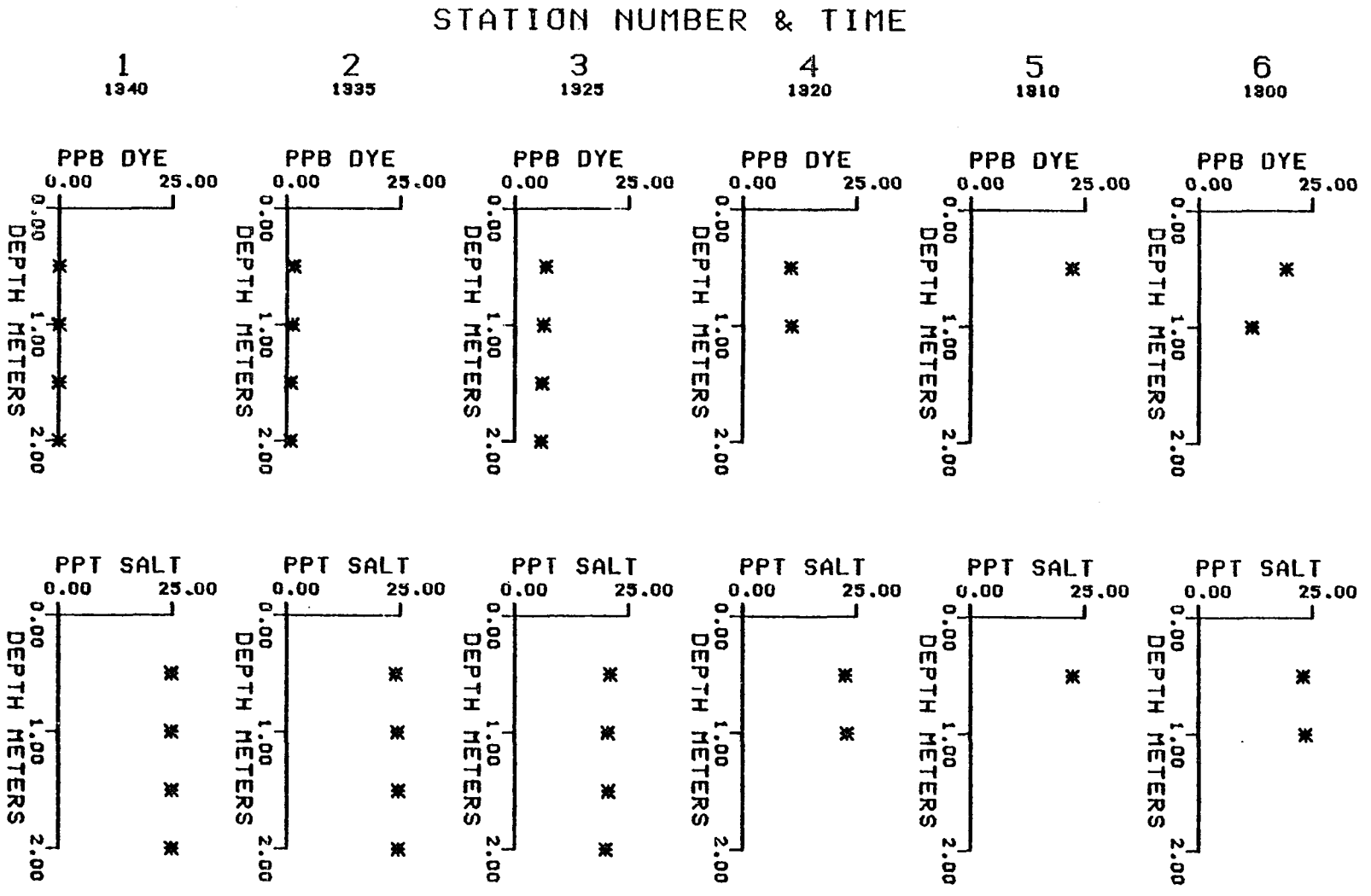

FIG 41 LOW FLOW DYE PROFILES 1300-1340

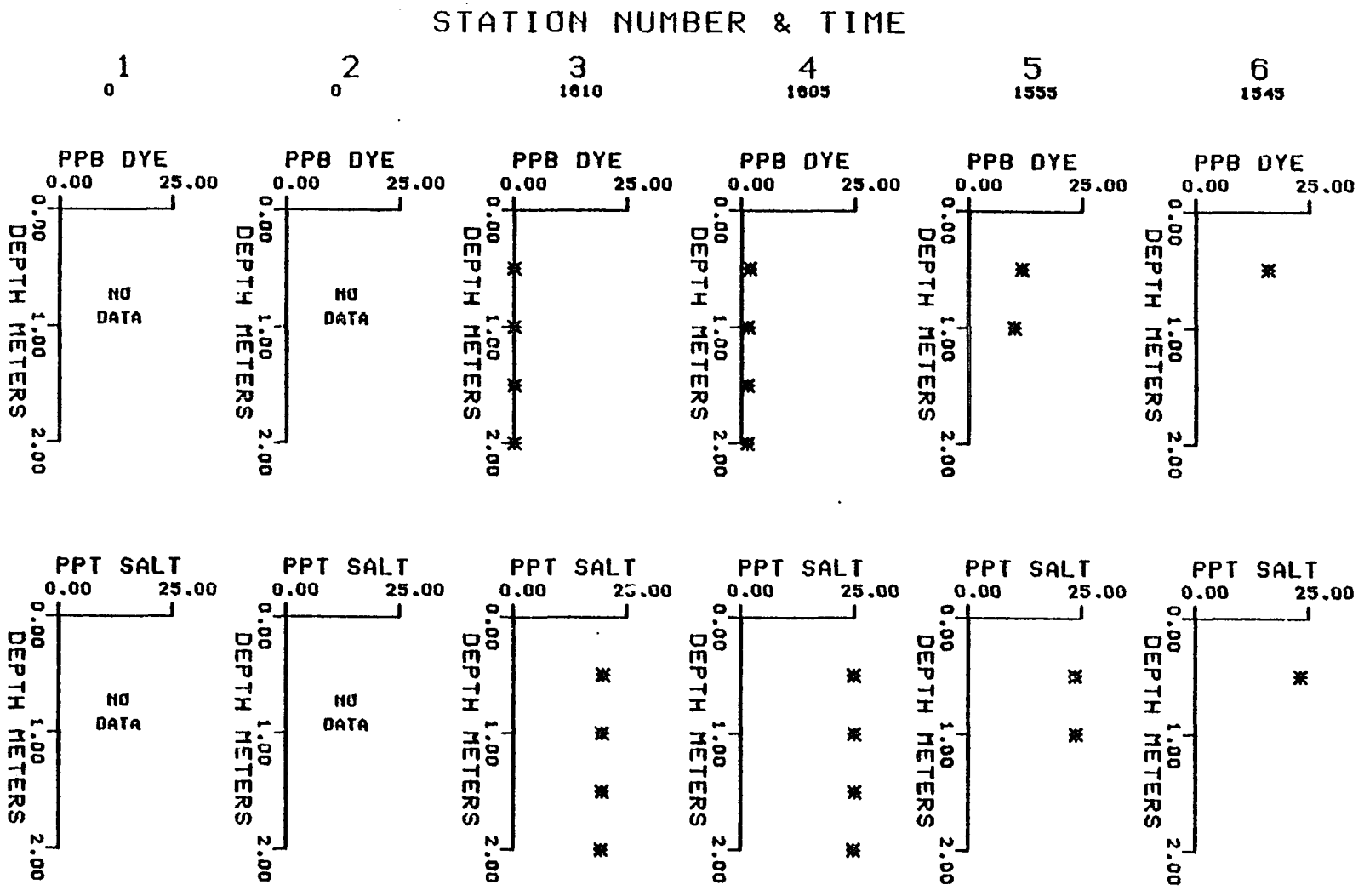

FIG 42 LOW FLOW DYE PROFILES 1545-1610

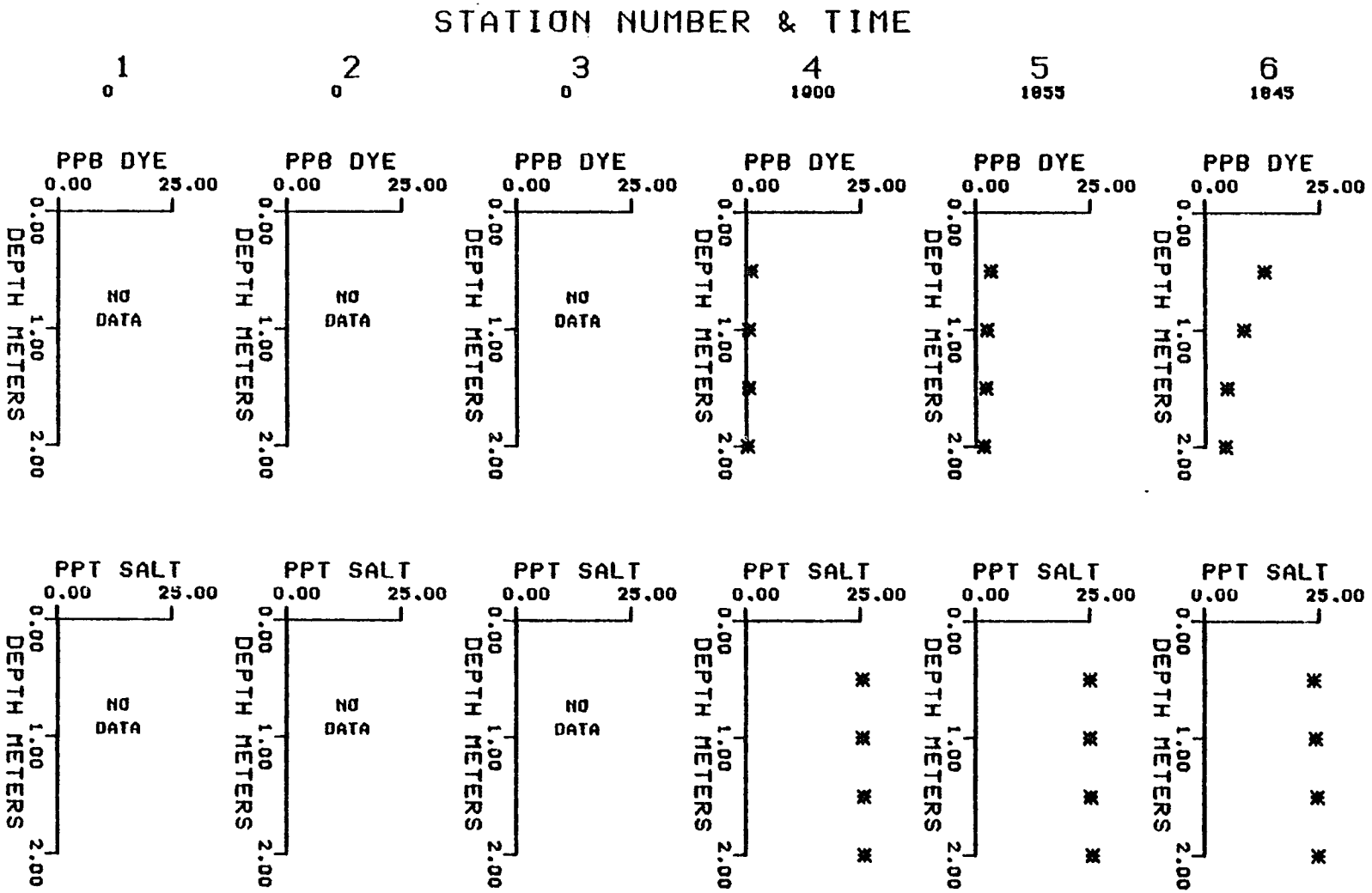

FIG 43 LOW FLOW DYE PROFILES 1845-1900

spring study. Even after adjustment for the 50 percent greater weight of dye, the peak concentration is more than five times higher. After two tidal cycles, a concentration of 13 ppb could still be observed at station 6.

The gradual dispersion and flushing of dye over a six day period is illustrated in Figure 44. This figure presents high and low tide dye concentrations at the surface and at 1.0 meter depth for each sampling station along the river. The longitudinal advection of the plume between high and low tide and the reduction of peak concentrations by dispersion are clearly evident in the data.

5.4.3 Calibration for Dye Distribution

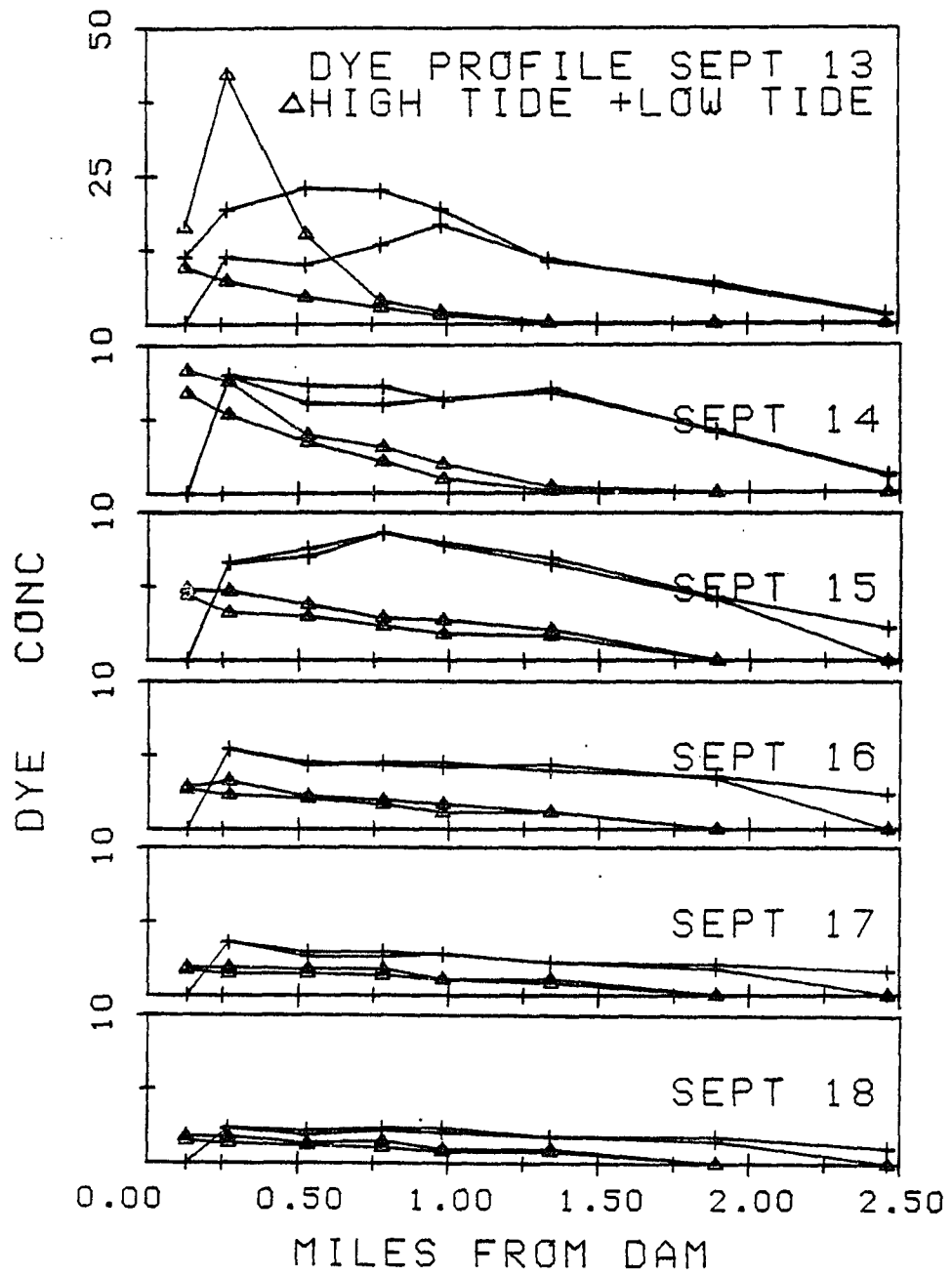

FIG 44 LONGITUDINAL DYE DISTRIBUTIONS -LOW FLOW STUDY

Note: Surface and bottom concentrations in PPB

The field data from these two dye studies was then used to calibrate the remaining dispersion model parameters, EFACT and RETRT. A great deal of dye concentration data was available for this calibration process. Therefore, an iterative process was employed to converge on a preliminary best choice of parameters. While such a trial and error procedure lacks the strict objectivity of statistical analysis or curve fitting procedures, it is believed that judgmental interaction in this case leads to better results. The final selection was then based on an error minimization technique.

The preliminary procedure was as follows. A large number of complete program runs were made to simulate conditions of the two dye studies. Output was generated in the form of dye concentrations at quarter points of each tidal cycle. Adjustment of parameter EFACT modifies the magnitude of dispersion due to instantaneous flow velocity. It encompasses effects of both friction and geometric irregularities of the channel. These effects are most significant when concentration gradients are large. Therefore, the early tidal cycles of the dye studies were most useful in selecting EFACT. Parameter RETRT has no effect until the first flood tide after dye reaches the river mouth. After that time, the parameter can dramatically affect the decay of dye concentrations due to loss through the boundary. Adjustment of RETRT was based on the later tidal cycles of the low flow dye study and on

the second day of the high flow dye study.

While it was intended that dye study data be used only for adjustment of these final parameters, it was found that other improvements in model results could also be made. These will be described first, since final adjustment of EFACT and RETRT employed the model improvements.

It was observed that model simulations held the dye in the most upstream segment of the river much longer than observed in the field. This was particularly true for the low flow dye study when advective transport in this segment was very small. During the dye studies, it was evident that dye was carried over the surface of the ambient water at a relatively high velocity. In effect, the active water depth near the head of the estuary is small. Advective transport is limited to this thin surface layer. For this reason, a water depth of 1.0 ft was selected for this first segment. This significantly improved the rate at which dye entered the main portion of the estuary.

It was also observed that simulated peak concentrations for the high flow dye study were suppressed much more quickly than observed in the field. This can be attributed to excessive dispersion in the model. Reduction of parameter EFACT was found to give insufficient decreases in the dispersion coefficients. It was therefore obvious that at high flows, the predicted circulation dispersion coefficient was too large. The primary parameter

controlling circulation dispersion is VMF, the vertical mixing factor. This parameter was determined by comparison to a single data set at a flow of 20 cfs. Extrapolation to a flow of 175 cfs was clearly inadequate. The relationship between the vertical mixing parameter and the fresh water flow rate resulting from the previously described calibration procedure is given in Figure 45.

When extrapolated to a flow of 175 cfs, this curve produces circulation dispersion coefficients ranging from 188 ft^2/sec at segment 4 to 10.35 ft^2/sec at segment 24. Since the calibration process for VMF involved only one set of data, a family of curves exists which will produce identical VMF values at the calibration flow of 20 cfs. These curves are characterized by differing asymptotes. Any asymptote value less than 0.3027 could produce the required value at a flow of 20 cfs. An alternative selection of an asymptote equal to 0.25 results in a new equation for VMF.

$$UMF = 0.25 + 0.75*\exp(-.13277Q) \qquad (5\text{-}13)$$

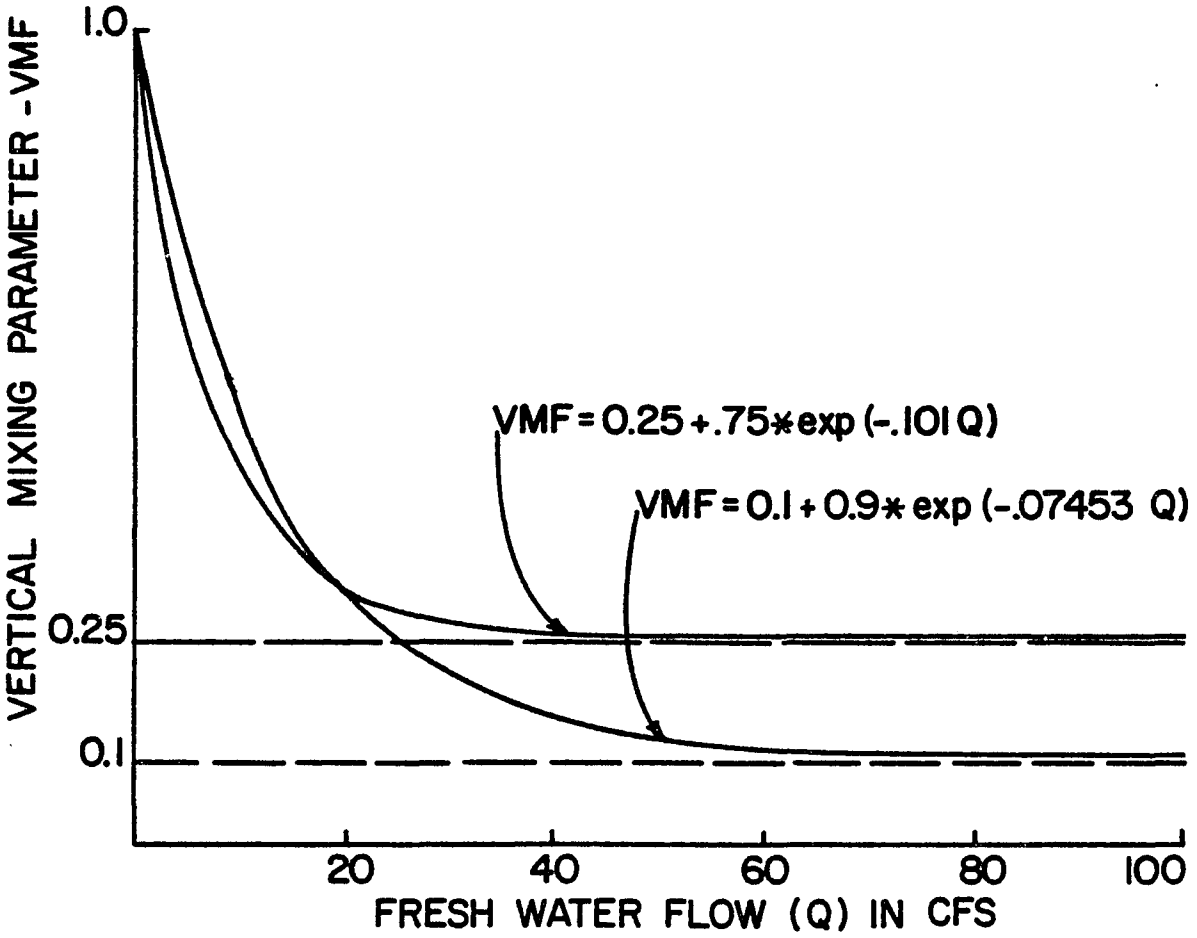

FIGURE 45

RELATIONSHIP OF VERTICAL MIXING

TO FRESH WATER FLOW

This new relationship for the vertical mixing coefficient produces significantly lower circulation dispersion coefficients at a high flow of 175 cfs. These values are 39 ft^2/sec at segment 4 and 96 ft^2/sec at segment 24. The reduced circulation dispersion coefficients decreased the rate at which peak concentrations dropped and allowed more accurate simulation of high flow conditions. From Figure 45, it is clear that VMF (and hence the circulation dispersion coefficients) are changed insignificantly at the low flow rate of 5 cfs.

The final general observation regarding dye study simulations was that the advective velocity of the dye peak lagged behind that observed in the field. It is likely that the main core of flowing water is narrower than the hydrographic data predicts. Friction along the sides of the channel tends to reduce the effective width. Since the model employs hydrographic data directly, the effect is not included. To compensate for this discrepancy, the channel width was reduced by 25 ft throughout the upper 6000 ft of its length. This rather minor adjustment reduces the total volume of the estuary at high tide by slightly over 1 percent. It has essentially no effect on overall dye concentration levels, but does serve to propel the dye plume to the middle reaches of the river more quickly. Having made these adjustments, the final calibration runs for EFACT and RETRT were performed. Final adjustment employed the error minimization technique described below.

A representative summary of field data was assembled for use in the calibration process. These data are shown in Table 23. Measuring stations are related to segment numbers used in the model. The designations 1-2 and 2-3 indicate that measuring stations 6 and JL fall between model segments. In all cases where vertical dye profiles were available, the data shown in the table is the average of surface and 1.5 meter depth dye measurements. If subsurface data was unavailable, the surface value was adjusted as follows. For ebbing tides, surface values were reduced by 25 percent to take account of expected lower concentrations at depth. For flood tides, the surface data was used directly. The resulting data is believed to be representative of depth-averaged dye concentrations and hence comparable to the model results. No effort was made to take account of lateral variability of dye concentrations because of the lack of sufficient data and the likelihood that great variation will exist in lateral profiles from point to point in the estuary. The tabular values are most representative of the lateral peak of dye concentrations. During the early hours after initial dye release, model results would be expected to be lower than these measured values.

Dye concentration data was abstracted from the model results for the time of each field data point. This results in a total of 23 data pairs for a low flow dye study simulation and 35 data pairs for a high flow dye

Table 23

Dye Concentration Data
for Model Calibration

Field Data for Low Flow Dye Study

STATION	OL	6	JL	5	TP	4	3	2	1
SEGMENT	1	1-2	2-3	3	4	5	7	9	11
1.25 PERIODS	-	24.6	9.7	3.2	1.6	0.1	-	-	-
1.75 PERIODS	-	15.2	16.3	17.8	17.9	10.6	6.5	1.5	-
3.25 PERIODS	-	6.5	3.7	2.6	1.5	0.3	-	-	-
3.75 PERIODS	-	-	6.7	6.6	6.4	6.9	4.2	1.2	-

Field Data for High Flow Dye Study

0.25 PERIODS	-	27.4	30.4	47.6	25.1	-	-	-	-
0.50 PERIODS	-	-	7.1	14.6	8.6	6.4	8.6	-	-
0.75 PERIODS	-	-	-	-	-	-	4.7	-	2.5
1.0 PERIODS	-	0.8	-	4.3	-	-	-	1.4	-
1.25 PERIODS	-	-	-	4.3	-	2.3	2.1	-	-
2.25 PERIODS	-	0.7	1.5	1.6	2.0	1.6	0.6	0.6	-
2.5 PERIODS	-	1.3	-	1.2	-	1.0	1.4	0.6	-
2.75 PERIODS	-	1.2	-	1.1	-	1.0	1.1	1.0	0.5

NOTE: All values are average of surface and 2m depth readings except first day data for high flow when 2m reading was not available. For each of these data sets, the surface reading was multiplied by .75 to compensate for assumed lower subsurface values.

study simulation. A normalized standard error of these pairs was defined in the following way:

$$E = \sqrt{\frac{\sum_{n} \left(\frac{E-M}{F}\right)^2}{n}} \qquad (5\text{-}14)$$

where:

E = normalized standard error

F = field data

M = model result

n = number of data points

This statistic was evaluated for each calibration run. Minimization of the normalized standard error was used as the criterion for selecting optimum parameters.

Many computer runs were made for both the high and low flow conditions for the purpose of optimizing parameter EFACT. The effect of RETRT on this optimization process was also evaluated preliminarily so that the most realistic results could be obtained. For the low flow simulations RETRT values of both 0.50 and 0.90 produced larger errors than a value of 0.75. Therefore, the 0.75 value was used in subsequent low flow runs. For high flow simulations, larger values of RETRT produced continuous improvement of error. Therefore, a value of 0.95 was used for these

calibration runs.

For each flow condition, a constant EFACT parameter throughout all river segments was employed first. The effect of varying the value at different locations was then evaluated. Results for constant EFACT are summarized in Figure 46. It is clear from this figure that very large values of EFACT (over 20) result in large increases in error. Attention was therefore focused on values below 20. For low flow conditions, a distinct error minimum occurs at a constant EFACT of 10. A very slight further improvement in the error was achieved by increasing the dispersion parameter in the lower river reaches while holding the value at 10 in the upper reaches. However, this improvement was not significant and does not appear to warrant variation of the parameter.

For high flow conditions the picture is not as clear. Changing the value of EFACT results in rather minor changes to the normalized standard error. Furthermore, the reduction of error improves at smallest values of EFACT. Both this and the earlier observation that high values of RETRT give least errors lead to the same conclusion. Under high flow conditions, the model is flushing contaminants downstream more rapidly than it should. The most likely source of this is excessive circulation driven dispersion. As noted previously, calibration of the circulation analysis was based on a single velocity profile measured by Shanley. This data point may result in an excessively high

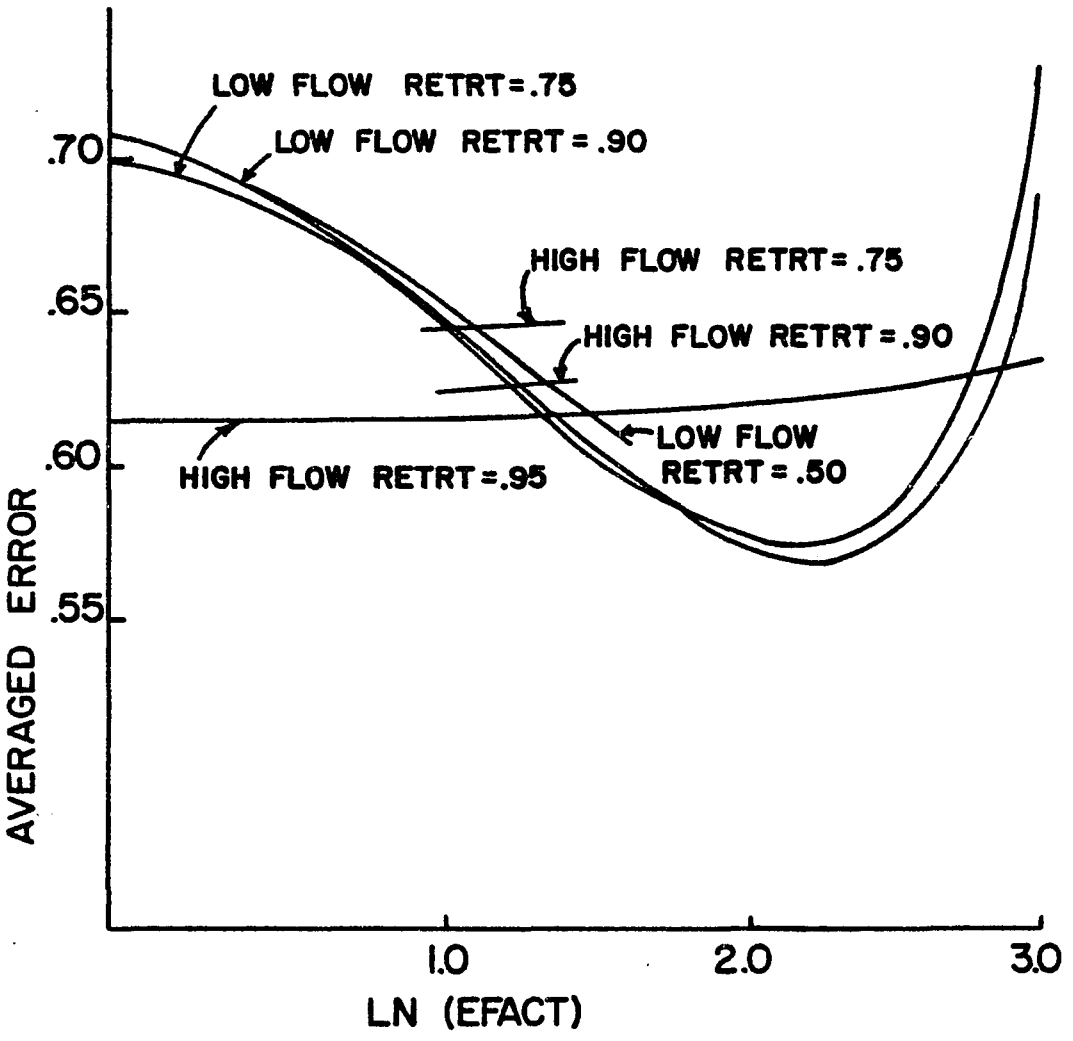

FIGURE 46

OPTIMIZATION OF DISPERSION MAGNITUDE PARAMETER EFACT

dispersion coefficient. Furthermore, the extrapolation to much higher fresh water flows is questionable. For these reasons, greater weight was given to the low flow simulations, and a uniform value of EFACT = 10 was selected.

Final calibration runs were oriented toward refining the value of parameter RETRT by using field data for later tidal cycles of the dye studies. Since the high flow sampling was terminated after only three tidal cycles, emphasis was placed on cycles 3 through 10 of the low flow case. A number of cases were run using values of RETRT from 0.50 to 1.2.

Results from these runs are summarized in Table 24. This table compares simulated dye concentrations to observed concentrations averaged over tidal cycles 6, 8 and 10 following dye release. Clearly the higher values of RETRT produce better results until values significantly over 1.0 are reached. In all cases, the simulated concentrations are below the values observed in the field. Larger values of RETRT increase concentrations by reintroducing larger amounts of dye into the mouth of the estuary on a flood tide. The effect is most pronounced at the lower end of the estuary (near the mouth) and much smaller at the upper end. The lower simulated concentrations are to be expected for two reasons. First, and most importantly, the model produces average values within a river segment. Field data taken in mid-channel

Table 24

Results of Calibrating Boundary Flushing Parameter RETRT

	STATION	OL	6	JL	5	STP	4	3	2	1
	SEGMENT	1	1-2	2-3	3	4	5	7	9	11
FIELD DATA	TIDAL CYCLE									
	6	4.6	4.4	3.9	3.5	3.3	3.0	2.3	1.2	-
	8	2.9	3.1	2.5	2.3	2.1	1.7	1.3	0.8	-
	10	1.2	1.9	1.9	2.0	1.7	1.4	1.1	0.6	-
RETRT = .50	6* (3.22)	.63	.86	1.08	1.07	.90	.81	.65	.42	.24
	8 (1.94)	.35	.49	.63	.63	.53	.48	.39	.25	.15
	10 (1.16)	.20	.29	.37	.37	.31	.28	.23	.15	.09
RETRT = .75	6 (3.70)	.64	.89	1.13	1.13	.96	.88	.73	.49	.30
	8 (2.37)	.37	.53	.69	.69	.60	.55	.46	.31	.19
	10 (1.49)	.22	.32	.43	.43	.37	.34	.29	.19	.12
RETRT = .90	6 (4.41)	.65	.92	1.20	1.20	1.04	.97	.83	.58	.39
	8 (3.05)	.39	.57	.77	.78	.69	.65	.56	.40	.27
	10 (2.07)	.25	.38	.51	.52	.46	.43	.38	.27	.19
RETRT = .99	6 (5.29)	.67	.96	1.25	1.27	1.11	1.06	.94	.71	.51
	8 (4.00)	.42	.63	.87	.89	.79	.76	.69	.53	.40
	10 (2.98)	.29	.45	.62	.64	.58	.55	.51	.39	.30
RETRT = 1.0	6 (NA)	.67	.96	1.27	1.29	1.13	1.07	.96	.73	.53
	8 (NA)	.42	.64	.88	.90	.81	.78	.71	.55	.42
	10 (NA)	.29	.46	.64	.66	.60	.58	.53	.41	.32
RETRT = 1.05	6 (NA)	.68	.99	1.33	1.35	1.20	1.15	1.07	.85	.67
	8 (NA)	.44	.70	.98	1.01	.92	.90	.85	.70	.57
	10 (NA)	.33	.53	.76	.79	.73	.71	.68	.57	.47
RETRT = 1.25	6 (23.67)	.95	1.52	2.13	2.18	2.08	2.22	2.64	3.14	3.83
	8 (40.54)	1.39	2.13	2.97	3.08	3.07	3.40	4.28	5.34	6.71
	10 (69.20)	2.42	3.51	4.80	4.99	5.04	5.63	7.21	9.10	11.52

* $_{(3.22)}^{6}$ Indicates 3.22 lbs. of dye remaining in estuary after six tidal cycles.

are likely to be the peak concentration. In this model, as with all such numerical models, both lateral and longitudinal spreading tends to exceed observed conditions due to numerical dispersion. This artificial dispersion results from the instantaneous averaging within an entire segment and prevents direct modeling of peaks. Additionally, the difficulty of zeroing the dye measuring instrument mentioned previously may have been a source of extraneously high readings.

On the basis of these observations the most reasonable choice for parameter RETRT is 1.0. In effect, this choice assigns a negligible concentration gradient across the boundary during flood tide. It does not, however, prevent loss of dye through the boundary, since non-zero dispersive flux will occur at all times, and during ebb tide a significant advective flux occurs across the boundary. The overall flushing of dye from the estuary resulting from this selection is summarized in Figure 47. This figure illustrates the average weight of dye within the river during each of the first 10 tidal cycles.

The final result of the complete calibration process is illustrated in Figure B1 through B5 for the high flow conditions and Figures B6 through B12 for the low flow case. Figures designated with a prefix "B" are found in Appendix B. These figures present longitudinal dye concentration profiles for quarter points of the initial tidal cycles, and tidal cycle averages for later cycles of

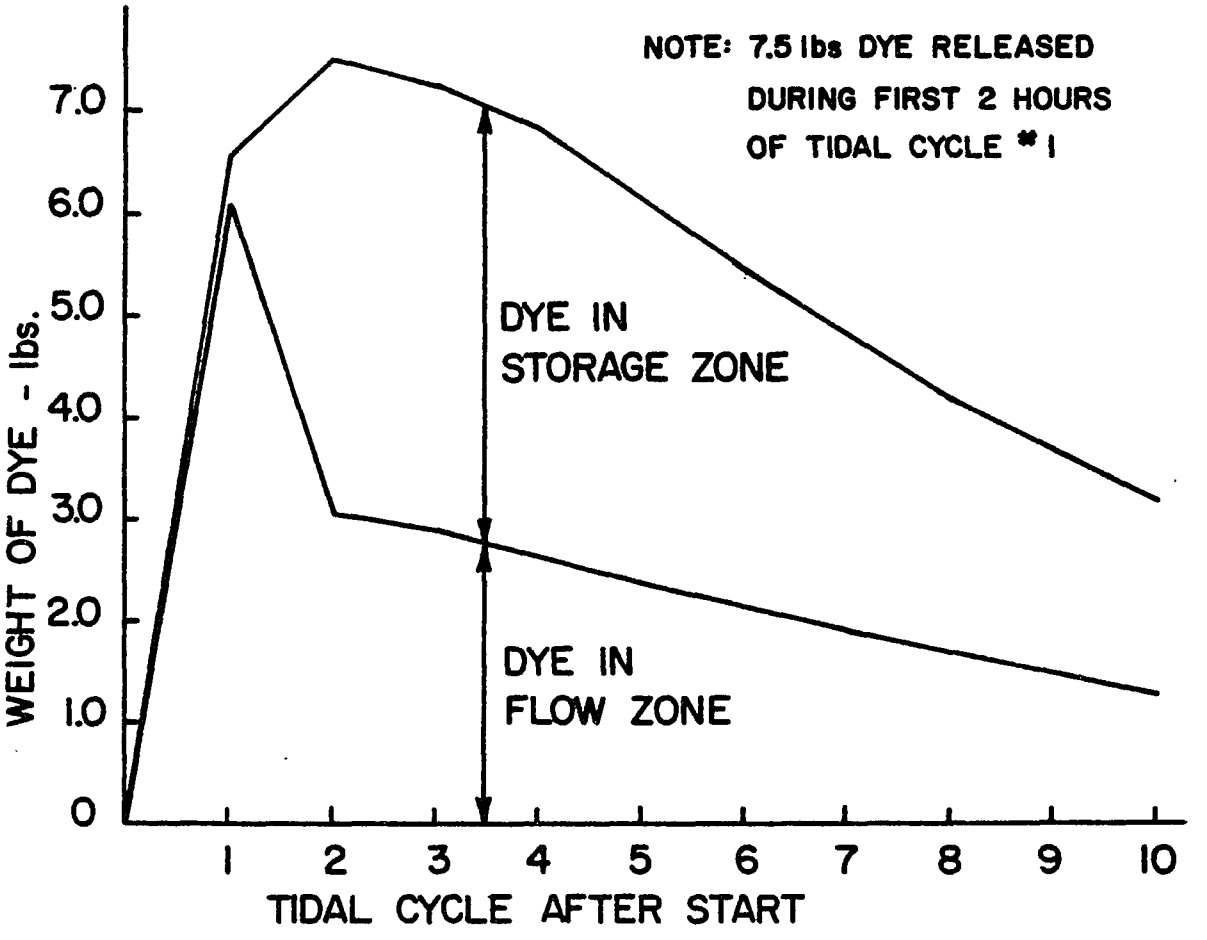

FIGURE 47

SIMULATED FLUSHING OF DYE FOR LOW FLOW STUDY

each dye study.

CHAPTER 6

INVESTIGATION OF WATER QUALITY IMPACTS IN THE OYSTER RIVER ESTUARY

The objective of this portion of the work was to investigate the impact which storm water and non-point source contaminants have on the Oyster River Estuary. The investigation was performed through application of the calibrated models of upland and estuary processes. The specific questions considered were:

1) What is the present impact of runoff on water quality of the estuary?
2) What effects do differences in storm characteristics have on water quality?
3) What effect does a change in land use have on water quality?
4) To what degree does the location of modified land use change the water quality impact?

It is, of course, impossible to investigate all possible alternatives in studying these questions. However, a carefully devised set of analyses was used to gain maximum insight with a reasonable effort. The models are capable of investigating a wide range of specific questions, and other applications can be performed as necessary in the future.

These investigations employed the concept of key

indicators of general water quality. Specifically, BOD, dissolved oxygen, and suspended solids were used. Both real and synthetic storms were considered so that a range of conditions could be evaluated. A total of ten storm-land use scenarios were investigated, and six different estuary water quality analyses were undertaken encompassing up to two weeks of dynamic analysis (25 tidal cycles). The various components of these analyses are described below.

6.1 Description of the Modeling Study

6.1.1 Storm Characteristics

The large storm observed October 25, 1980 was used to represent an extreme condition. This storm produced in excess of 2.5 inches of rainfall within an eight-hour period. While larger storms can occur in southeastern New Hampshire, this amount of rainfall would not normally be exceeded more than once a year. Data was available from the recording raingage located at the Forest Sciences Laboratory in Durham. The applicability of this data has been previously discussed in the chapter on model calibration.

The effect of storm intensity (as opposed to total rainfall volume) was investigated by modifying the timestep of the October 25 data. By doubling the timestep used for analysis, the 2.5 inches of rainfall was spread over

sixteen hours.

A moderate storm was simulated by applying 0.6 inches of rain over a five hour period. This amount of rainfall would be expected to occur frequently in this area and might be observed in almost any month of the year. Based on the results of this size storm, no smaller storms were selected for analysis.

6.1.2 Land Use Characteristics

The basic data used for upland analysis was that obtained from town and regional land use maps. Data is generally representative of conditions prevalent in 1975, but some updating has been done for the town of Durham. Land use data is presented in Figure 48. The land use types represented by each number were described in Table 2.

The impact of land use modification was investigated by simulating development of a 60-acre tract for commercial use. This would be representative of a shopping mall with adjacent businesses or a rather major "strip type" commercial development. Location of the land use change is significant for several reasons. First, the degree of change is affected by what use existed previously at the site. Second, natural conditions of slope, soil type and surface drainage features will affect the degree of impact. Finally, the proximity of the site to the estuary would be expected to influence the water quality impacts. Three

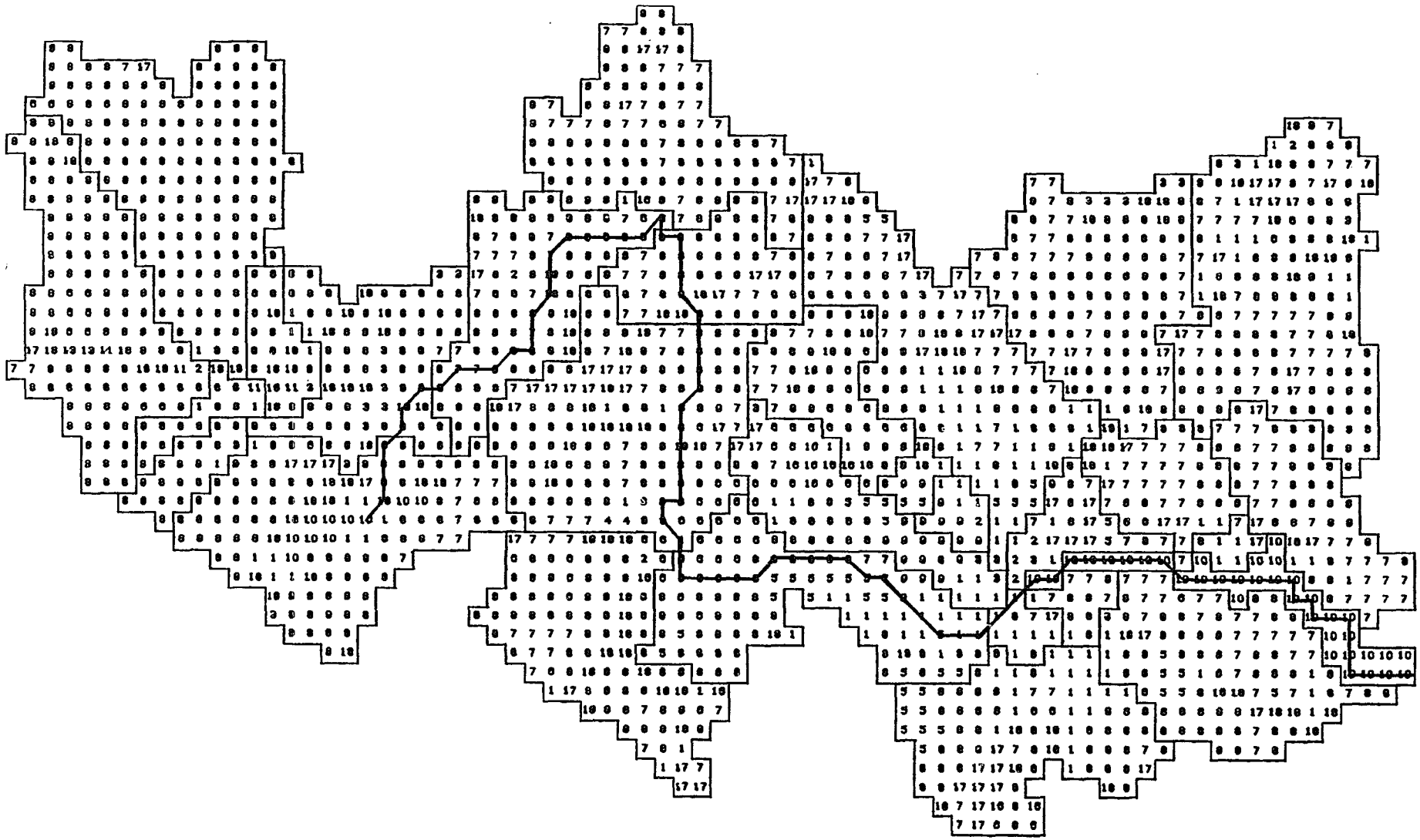

FIG 48 LAND USE GRID - OYSTER RIVER BASIN

Note: See text for decription of symbols

different locations were considered, as shown on Figure 16.

Case 1 considered increased development in the lower Pettee Brook area adjacent to the present business district of Durham. The conversion involved 20 acres previously shown as single family land use, 10 acres previously multifamily, and 30 acres of institutional land use. The changes encompassed here are probably representative of long-term trends started several years ago and which may continue in the future.

Cases 2 and 3 considered large unused areas along the Route 4 bypass. They were so located as to drain to different sub-basins. Case 2 modified the land use of 60 acres which drain overland to Littlehale Creek and then to Beards Creek. Previous land use included 30 acres of forest land, 20 acres of agricultural land, and 10 acres of open land. It was assumed that after conversion to commercial land use, a semi-improved natural channel would carry drainage to Littlehale Creek. Case 3 was located only about one quarter mile west of Case 2 but drains to the Old Durham Resevoir and upper Pettee Brook. Previous land use here was 40 acres of forest land and 20 acres of open land.

6.1.3 Estuary Characteristics

For all estuary analyses, a baseflow of 10 cfs into the uppermost segment of the tidal river was assumed. A

six-foot tidal range was imposed at the river mouth, and a tidal period of 12.4 hours was used. The hydrodynamic model was run to quasi-steady state at these conditions before the start of each case. Storm water hydrographs produced by the upland analyses were then imposed, and dynamically varying flow conditions were calculated.

Background water quality of the river was based on an assumed BOD loading from the Durham wastewater treatment plant. Based on a flow of 1.5 million gallons/day and a BOD concentration of 30 mg/l, a uniform BOD load of 0.004 lbs/sec was established. For each case, analysis was preceded by a quasi-steady state condition for this load. The output BOD time series from upland analysis was then employed for dynamic water quality analysis. Based on typical published values for rivers and estuaries, a BOD decay coefficient of 0.5 per day and a re-aeration coefficient of 0.2 per day were employed for all runs.

6.2 Stormwater and Contaminant Discharge for Different Scenarios

The combination of conditions for the various analyses are summarized in Table 25. For all runs, the drainage basin was divided into three parts. The largest portion drains to the non-tidal reaches of the Oyster River above the Route 108 tide head dam. All hydrologic and contaminant conditions of this major portion were held

Table 25

Scenarios for Evaluating
Non-Point Source Impacts

RUN	LAND USE	STORM(S)	ESTUARY LOADING
1	-----	-----	Wastewater Flow Only
2	Base	2.6" at 0.0Hrs +0.6" at 120.0Hrs*	Wastewater + Storm Flow
3	Case 1 (Lower Pettee Bk)	2.6" at 0.0Hrs +0.6" at 120.0Hrs	Wastewater + Storm Flow
4	Case 2 (Littlehale Cr)	2.6" at 0.0Hrs +0.6" at 120.0Hrs*	Wastewater + Storm Flow
5	Case 3 (Upper Pettee Bk)	2.6" at 0.0Hrs +0.6" at 120.0Hrs*	Wastewater + Storm Flow
6	Base +0.6" at 120.0Hrs*	Extended storm at 0.0Hrs	Wastewater + Storm Flow

*Note: Antecedent moisture condition for the second storm was assumed to be 2 - normal soil moisture.

constant for all analyses. Only the applied rainfall was varied. The second portion includes all land which drains to Beards Creek, or the tidal reaches of the Oyster River between Beards Creek and the tide head dam. This portion was analyzed separately for each of the cases described above. The hydrographs and contaminant time series for the upper Oyster River were added to the appropriate computational node of the upland analysis, and the final results were used directly as total input to the tidal river. The third portion of the drainage basin, which flows directly to the lower reaches of the tidal river, was not included in the analysis. The neglected contaminant and freshwater flow is minor and invariant among the various analyses.

Results of the upland hydrologic and non-point source analysis are summarized in Table 26 and Figure 49. A number of conclusions can be drawn directly from the table. Clearly, the most significant variable with respect to both stormwater volume and weight of contaminant discharged to the estuary is total rainfall. While the larger storm is only about four times the size of the smaller one, the storm's runoff water volume is approximately fourteen times as great, and contaminant load is 90 to 100 times as great.

Neither the 60-acre land use change nor the increased storm duration had a significant impact on total storm flow. This would be expected because the 60 acres represents only 0.5 percent of the total drainage basin

Table 26

Results of Hydrologic
and Non-Point Source Analysis

SCENARIO	TOTAL FLOW (CFS-HRS)	BOD LOAD (LBS)
2.6" Storm, Base Land Use	4331.5	22,343
2.6" Storm, Case 1	4379.9	24,317
2.6" Storm, Case 2	4399.5	24,217
2.6" Storm, Case 3	4412.4	24,992
Extended Storm, Base Land Use	4343.5	20,644
0.6" Storm, Base Land Use	288.4	199
0.6" Storm, Case 1	298.9	267
0.6" Storm, Case 2	301.2	254
0,6" Storm, Case 3	302.7	272

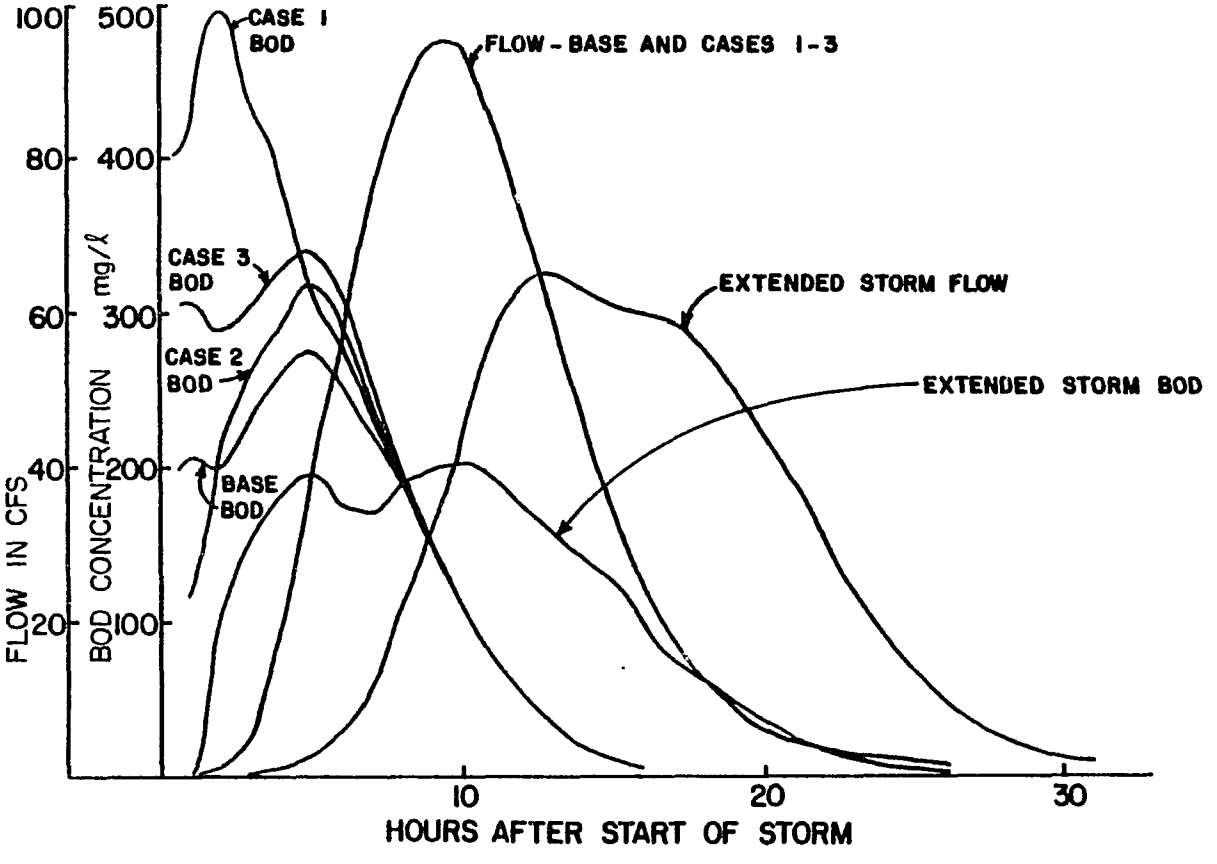

FIGURE 49

BOD SOURCE LOAD FOR OCT 25 STORM

considered, and the storm duration has no effect on total volume of water available. On the other hand, both the 60-acre land use change and the storm duration affect the total contaminant flow. Changing only 0.5 percent of the area from rural type land uses to commercial land use increased contaminant flow by almost ten percent. It is obvious that major changes in land use could have a significant impact on total weight of contaminants reaching the estuary. The effect of storm duration was almost as great as that from changing land use. The decreased intensity reduced total contaminant load by approximately eight percent when compared to the base case with the 2.6-inch storm.

For the small storm, contaminant loading is much less, but the percent increase due to land use changes is larger. The BOD load was from 27 to 35 percent larger when only 60 acres was changed to commercial land use. This difference results from the greater role played by impervious portions of the basin during smaller storms. Pervious areas and those having low SCS Runoff Curve Numbers are capable of abstracting all of the small storm rainfall with no resultant runoff.

It is interesting to note that in three cases where land use was changed, each produced approximately the same total contaminant runoff. As would be expected, location of the commercial growth does not affect the total contaminant load produced but does alter the timing of

impacts. Further insight into temporal characteristics of these three cases can be gained from Figure 49. The stormwater flow curves for the base case and three modified land use cases are virtually indistinguishable from one other. On the other hand, the concentration of contaminants changes dramatically.

As shown in the figure, contaminant concentration for the base case peaks around 275 mg/l BOD at approximately five hours into the storm. This can be compared to the timing of the stormwater flow peak around 9.5 hours and illustrates this commonly observed relationship between flow and concentration. Case 1 involves increased contaminant loading only 3/4 mile from the discharge point into the tidal river. The 60 acres is immediately adjacent to a natural drainage channel (Pettee Brook). For these reasons, BOD concentrations peak earlier (at about three hours) and higher (at about 500 mg/l).

Both case 2 and case 3 involve increased contaminant loading at sites more than twice as far from the tidal river. They are also separated from the natural surface water channels. The outcome is a peak at about the same time as predicted for the base condition. Case 3 produces slightly higher BOD concentrations due primarily to differences in the prior land use at the two sites. The maximum predicted concentrations are about 315 mg/l and 340 mg/l, respectively, for cases 2 and 3.

In all three cases, the contaminant concentrations

converge to the base case concentrations after about nine hours. This clearly illustrates the transient nature of increased impact due to intensified land use. It also suggests the greater importance of controlling contaminant discharges from such developments during the early stages of a major storm flow event. The time series of BOD for these five cases, given in Figure 49, illustrates the variation and duration of contaminant flows for a typical two-storm sequence.

The output file from these analyses also provides data on the net production and loss of sediment during and between the storms. A mass balance for pervious and impervious portions of Lower Pettee Brook having Runoff Curve Numbers of 35, 71, 89, and 97 is given in Table 27 for the sequence of two storms used in this analysis. These numbers are typical of the changes expected in other portions of the basin. However, somewhat different values occur on each sub-basin due to differences in such parameters as the cover coefficient and the relative proportion of pervious and impervious land surface.

6.3 Estuary Water Quality Impact of Different Scenarios

The hydrographs and contaminant time series from these upland runs were used as input to the estuary hydrodynamic and water quality analysis. The first case represents equilibrium conditions which would prevail at a base flow

Table 27

Sediment Mass Balance for Simulated Storm

AREA TYPE	2.6" RAINFALL BEGINNING AT 0.0 HRS					0.6" RAINFALL BEGINNING AT 120.0 HRS			
	INIT'L LOAD-ING	STORM GEN-ERATED	STORM WASH-OFF	FINAL LOAD-ING	ACCUMU-LATION AND DECAY	INIT'L LOAD-ING	STORM GEN-ERATED	STORM WASH-OFF	FINAL LOAD-ING
CN-35 PERVIOUS	1000	+216	0	1216	-19	1197	+7	0	1204
CN-35 IMPERV.	1000	---	0	1000	+25	1025	---	0	1025
CN-71 PERVIOUS	1000	+212	-2	1210	-19	1191	+7	0	1198
CN-71 IMPERV.	1000	---	-273	727	+81	808	---	0	808
CN-89 PERVIOUS	1000	+169	-153	1016	+31	1047	+6	-9	1044
CN-89 IMPERV.	1000	---	-966	34	+216	250	---	0	250
CN-97 PERVIOUS	1000	+225	-477	748	+77	825	+8	-3	830
CN-97 IMPERV.	1000	---	-1000	0	+193	193	---	-39	193

of 10 cfs with contaminant input from the wastewater treatment plant only. The other five cases represent water quality impact of the five scenarios described in Table 25 which include both storm flows and the treatment plant effluent.

The impact of stormwater flow on advective velocity is illustrated in Table 28. As would be expected, the additional flow reduces flood tide velocities and enhances ebb velocities. The effect is much greater at the head of the estuary than near the mouth because of the smaller cross sectional area of the channel. At station 2, located about 0.43 miles from the dam, the peak ebb velocity during the first transient cycle of storm flow is over 1.6 ft/sec compared to only 0.44 ft/sec before the storm. On the other hand, at station 12 near the river mouth, the increase is only 0.03 ft/sec, from 0.72 to 0.75 ft/sec. As the storm hydrograph falls, the impact is rapidly reduced so that by the third tidal cycle peak velocities have returned to their pre-storm values.

Of much greater significance is the effect which increased fresh water flow has on the density gradient and hence contaminant dispersion. At the relatively low base flow rate of 10 cfs, circulation plays a comparatively small role in total dispersion. However, as the storm hydrograph increases to several hundred cfs, it becomes the dominant component of the dispersion coefficient. This is illustrated in Table 29 which compares the total dispersion

Table 28

Impact of Stormwater on Estuary Velocities

	QUASI-STEADY STATE		TRANSIENT CYCLE 1		TRANSIENT CYCLE 2		TRANSIENT CYCLE 3	
STATION	MAX	MIN	MAX	MIN	MAX	MIN	MAX	MIN
2	0.480	-0.442	0.408	-1.615	0.460	-0.521	0.475	-0.448
3	1.040	-0.915	0.905	-1.560	1.024	-0.973	1.036	-0.919
4	1.504	-1.335	1.320	-1.923	1.488	-1.394	1.501	-1.339
5	1.565	-1.419	1.384	-1.879	1.552	-1.468	1.562	-1.423
6	1.413	-1.307	1.290	-1.566	1.406	-1.340	1.411	-1.310
7	0.969	-0.912	0.927	-1.028	0.968	-0.930	0.969	-0.914
8	0.723	-0.688	0.699	-0.757	0.722	-0.699	0.723	-0.689
9	0.903	-0.867	0.877	-0.938	0.903	-0.879	0.903	-0.868
10	0.973	-0.945	0.954	-1.004	0.974	-0.955	0.974	-0.946
11	0.912	-0.895	0.903	-0.940	0.914	-0.903	0.913	-0.896
12	0.732	-0.721	0.726	-0.752	0.734	-0.727	0.733	-0.722

Note 1: Positive velocity for flood tide

Negative velocity for ebb tide

Note 2: Maximum/minimum velocities in ft/sec

Table 29

Contribution of Circulation to Dispersion Coefficients

	STATION 2		STATION 7		STATION 12	
FLOW	CIRCULATION DISPERSION	TOTAL DISPERSION	CIRCULATION DISPERSION	TOTAL DISPERSION	CIRCULATION DISPERSION	TOTAL DISPERSION
10 CFS*	.002	.018	.002	.056	.020	.085
255	.086	.122	.056	.115	.143	.210
103	.039	.059	.023	.080	.360	.427
14	.007	.023	.008	.062	.109	.154
12	.004	.020	.003	.057	.030	.095
11	.003	.019	.002	.056	.027	.092

*Quasi-steady state condition

Note: All dispersion coefficients are in units of square miles per day

coefficient to that portion resulting from density driven circulation. In each case, coefficients are averaged over a tidal cycle and compared at three stations along the estuary.

At the steady state flow of 10 cfs, circulation contributes between 4% and 24% of the total dispersion coefficient. However, at a tidal cycle averaged flow of 255 cfs in transient cycle 1, the contribution increases to a range of 49% to 70% of the total. At the second transient cycle, circulation decreases at the upper end of the estuary due to decreasing freshwater flow. However, at the mouth, circulation still contributes a maximum of 84% of the total dispersion coefficient.

As a result of this increased circulation, the dispersion coefficient at the mouth rises from 0.085 square miles/day to 0.427 square miles/day, or approximately 400%. In the third transient tidal cycle, net circulation still contributes significantly, but by the fifth cycle, when fresh water flow has fallen to about 11 cfs, its contribution again becomes small.

The impact of the six scenarios on water quality of the estuary was assessed by analyzing dissolved oxygen depletion (DOD). Water quality runs began with convergence to quasi-steady state for wastewater discharge only and then a total of fifteen transient tidal cycles. The major storm which produced 2.6 inches of rainfall was timed to begin at midflood of the first transient tidal cycle. The

smaller storm containing 0.6 inches of rainfall began 120 hours later, or about low slack water of the ninth transient tidal cycle. Peak concentrations of BOD and dissolved oxygen deficit for the six cases are given in Table 30.

The most dramatic observation from this table is the impact of storm induced contaminant flow over steady state conditions. The maximum BOD concentration is increased over 100-fold for case 3, and dissolved oxygen deficit increased by 17 times. These increases are as indicative of low impact from the wastewater treatment plant effluent as they are of the magnitude of storm effects. Not apparent from this table is the spatial and temporal variation of these impacts.

Figures B13 through B34 illustrate the longitudinal profiles of BOD and dissolved oxygen deficit during the four phases of the first tidal cycle, and tidal cycle averages over the first three cycles for the steady state condition of wastewater effluent only and for the five land use scenarios. Clearly, the increased BOD loading is highly localized in the upper end of the tidal river and dissipates quickly downstream. On the other hand, dissolved oxygen deficit reaches relatively high concentrations over a large portion of the river length. Furthermore, the deficit is maintained over these three tidal cycles and requires many cycles to rebound to its equilibrium value.

Table 30

Water Quality Impacts
of Non-Point Source Contaminants

	BOD PEAK			DOD PEAK		
	CONC (mg/l)	LOCATION (STATION)	TIME (TRANS. CYCLE)	CONC (mg/l)	LOCATION (STATION)	TIME (TRANS. CYCLE)
STEADY STATE	0.51	2	0.75	.069	3	0.75
BASE STORM	50.5	1	1.50	1.06	4	2.00
CASE 1	51.7	1	1.50	1.08	3	4.00
CASE 2	56.6	1	1.50	1.12	5	2.00
CASE 3	61.0	1	1.50	1.19	5	2.00
EXTENDED STORM	38.6	1	1.75	0.91	3	4.00

The temporal variability of BOD and dissoved oxygen deficit is illustrated in Figures 50 and 51. These figures clearly indicate the rapid dissipation of BOD but the very gradual decrease of dissolved oxygen deficit after reaching its peak. The second set of BOD and DOD peaks after tidal cycle 10 results from the more moderate impact of the second storm. Comparison of the dissolved oxygen deficit plots for stations 3 and 5 also illustrates the effect of tidal flushing on these concentrations. At station 5, dissolved oxygen deficit peaks earlier and in some cases slightly higher than at station 3. However, at later tidal cycles station 3 maintains a large impact for a longer time period.

The relative impact of the different storm flow scenarios can also be abstracted from the previous table and figures. As indicated earlier, all three cases of modified land use produced similar total BOD loads. Case 1, with commercialization of lower Pettee Brook, produced earlier and much higher BOD concentrations in the storm discharge. On the other hand, the peak estuarine concentration of BOD, and hence dissolved oxygen deficit, is higher for both case 2 and case 3. This apparent contradiction results from the timing of stormwater discharges. For case 1, the proximity of lower Pettee Brook to the tidal river produces a peak much earlier than the peak discharge from the balance of the Oyster River drainage basin. Discharge from commercialized areas for

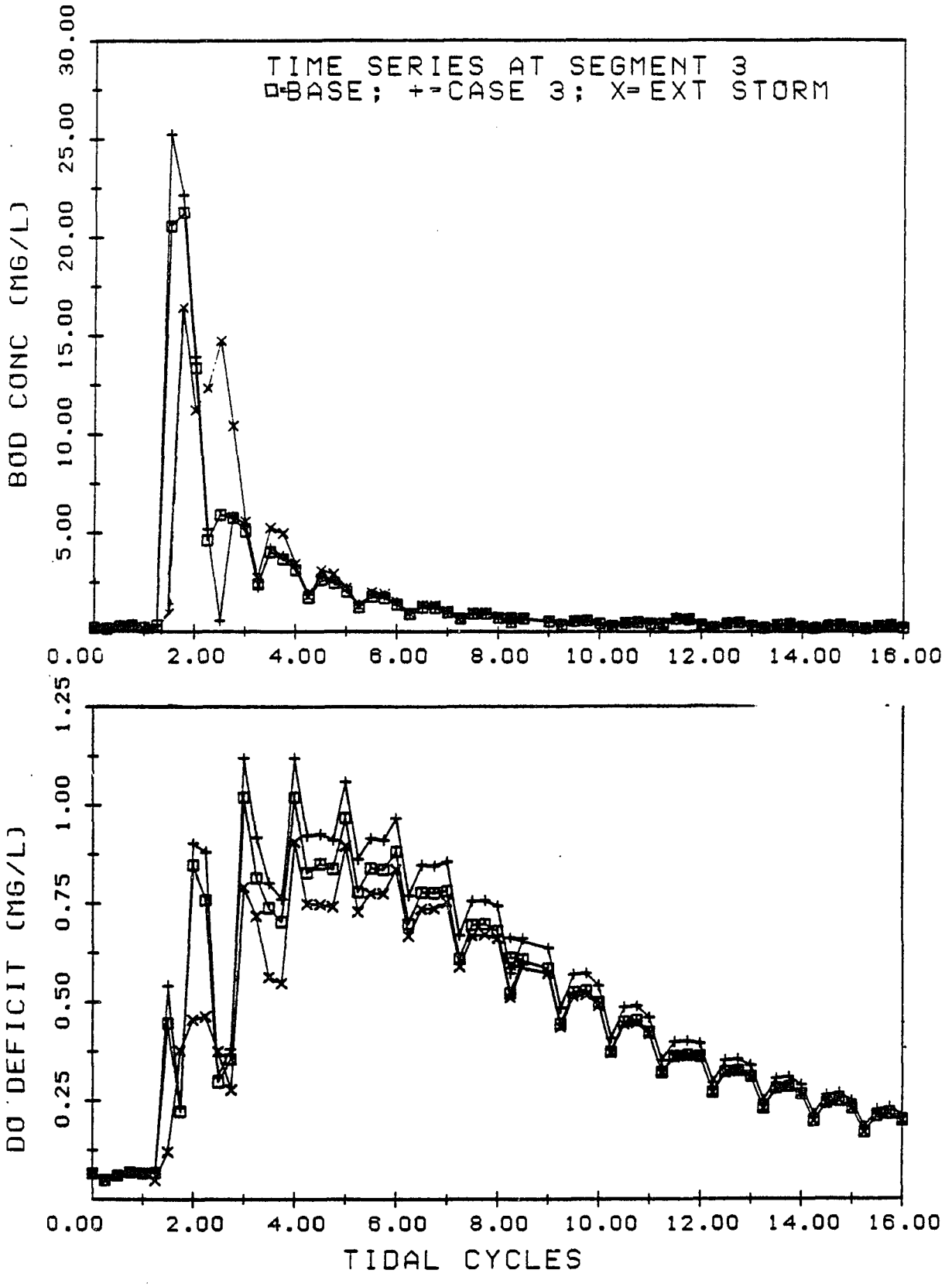

FIG 50 BOD AND DO TIME SERIES - SEG 3

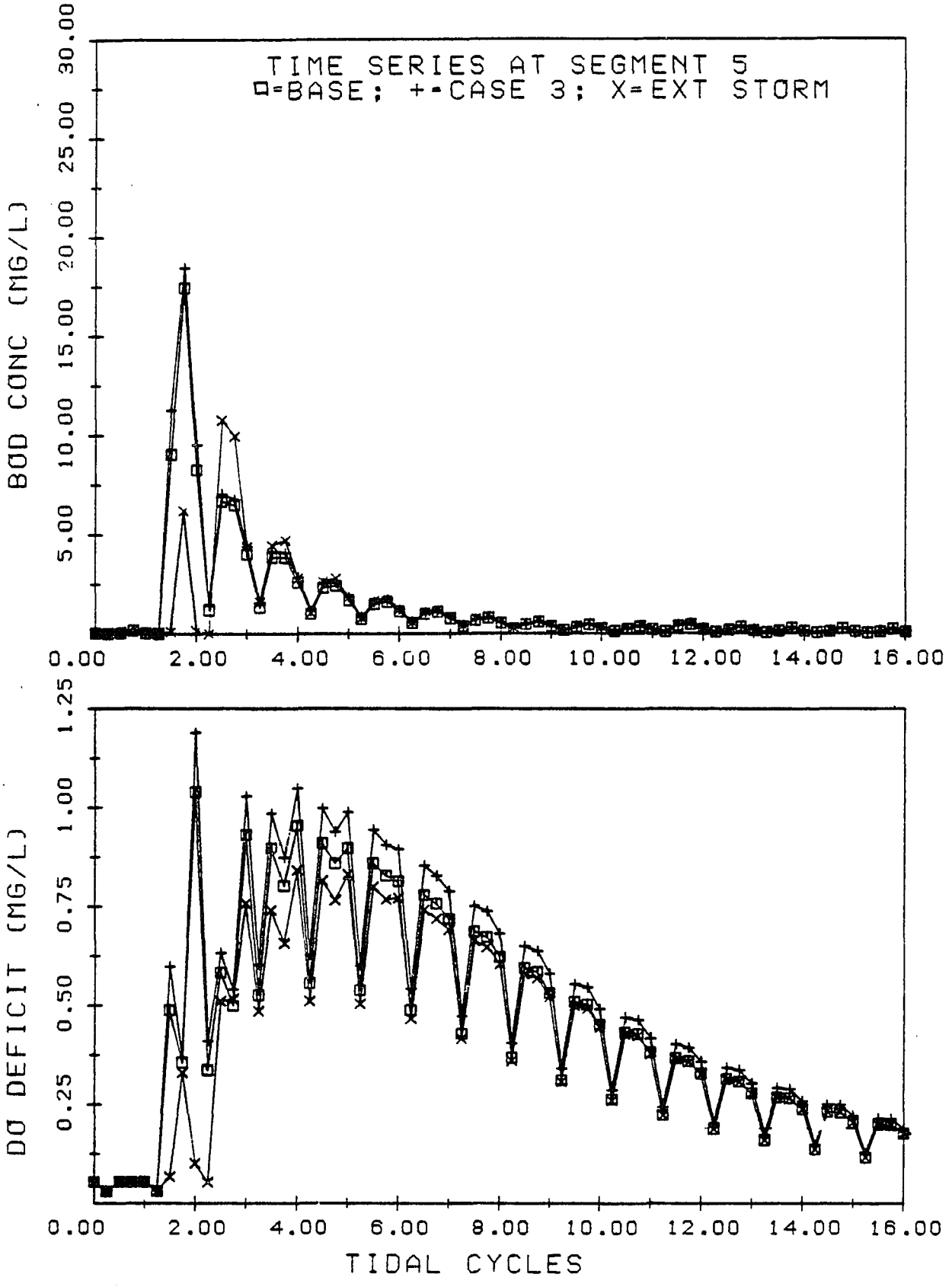

FIG 51 BOD AND DO TIME SERIES - SEG 5

cases 2 and 3 is later and coincides more closely with the peak of other areas of the basin. In effect, the water quality impact is induced over a longer time for case 1, and the resulting peak impact is closer to the base condition.

A final observation from these data relates to the effect of storm duration. Clearly, the impact of the extended storm is significantly less than the base case. Peak BOD concentration is only 76% of the base condition, and dissolved oxygen deficit is 86%. While reducing the intensity of rainfall reduced total BOD discharge by about 8%, the water quality impact reduction is two to three times as great.

CHAPTER 7

SUMMARY OF CONCLUSIONS

The objectives of this research program fell into two catagories. These were: development of an appropriate general modeling technique, and an analysis of impacts in small tidal rivers from non-point source contaminants. Included in the development objective was use of field data to ensure proper representation of processes and calibration of model parameters. The second objective employed simulation runs of the modeling techniques for both observed conditions and postulated changes in a portion of the Oyster River drainage basin. Conclusions presented here will be similarly separated into modeling considerations and impact analysis results. In each catagory, needs for further research will also be identified.

7.1 Conclusions of the Model Development Program

It is reasonable to conclude that the modeling objective has been met in that operational computer programs are available, and their application to the Oyster River has produced results comparable with observed field data. The important attributes of the techniques, and limitations which must be considered in further

applications, are summarized below:

1) The non-linear response of runoff to rainfall can be adequately simulated through application of the partial-area theory of surface hydrology. Separation of each unit area of land surface into five independent sub-areas characterized by a single surface condition or curve number provides adequate resolution to simulate the non-linearity.

2) Subdivision of a large drainage basin into ten-acre units allows localized land use variations or changes to be represented in the model. Aggregation into a workable number of sub-basins allows computation of runoff and contaminant production without losing the spatial relationship of different portions of the drainage basin. Sub-basins may be defined for small areas of interest and can be integrated into a coarse representation of the balance of the basin.

3) The precision of travel time estimates for a large basin is enhanced by using a 660-foot square grid system. Specification of elevations and land use types for each grid element allows use of a computerized grid data management system to produce key data for simulation of the temporal response to rainfall events.

4) Hydrologic simulation is accomplished with adjustment of only one parameter, the Antecedent Moisture Index (AMI). Since this index incorporates the effect of

soil moisture and water balance prior to the storm of interest, selection of a proper value is not trivial. Great care must be exercised in assigning the AMI to each storm, particularly when multiple storms are considered in sequence. Further research is warranted to develop a technique for selecting this parameter and possible development of stochastic or deterministic models relating Antecedent Moisture Index to rainfall records, air temperature, insolation, season of the year, etc.

5) Adequate hydrologic simulation requires careful attention to the geometry and topography of the basin. For example, surface storage features are found to have a major impact on the ability to correctly simulate observed stream flow.

6) A characteristic of all hydrologic simulation is the importance of adequate rainfall data, both temporally and spatially. One or more raingages must be located in or near the basin. Hourly data is not adequate for developing representative hydrographs due to the potential variability within an hour. Fifteen-minute, or better yet five-minute, observations should be considered when planning a data program for use in a modeling study.

7) Calibration of parameters for the contaminant generation algorithm demonstrated that most of the sediment, and hence contaminants, are generated on areas of least permeability. This is due primarily to the much greater runoff generated in these areas, and secondarily to

the greater intensity of use which characteristically causes the reduced permeability. That is, a higher proportion of paved area occurs in those areas where man's activities are most intense.

8) Among the seven parameters used for computation of sediment washoff, two are most effective in calibrating results. Transport constants KSER and KEIM are most important to the calibration process. These two constants are linear proportionality factors for transport of soil fines and dust/dirt from pervious and impervious areas, respectively. These two should be adjusted so that total sediment washoff over the duration of a storm is simulated. If more detailed data on variation during the storm is available, other parameters may be refined. In the absence of adequate field data, literature values from a hydrologically similar area can be used for these and other constants.

9) With respect to hydrodynamic modeling of a small tidal river such as the Oyster River, the primary calibration parameter is the friction coefficient. It was found that sensitivity to a reasonable range of Manning's n is small. Increased friction causes a reduction in maximum ebb velocity and delays the time of peak flood velocity. However, the overall effect on average transport velocities is small. Analysis of the balance of forces acting on water masses showed that the primary balance is between friction and surface slope. Additional friction elevates

the surface but has little effect on acceleration terms and, hence, velocities.

10) Longitudinal density gradient also has little effect on velocities. Salinity at the mouth of the river has the primary effect of elevating the water surface at points upstream. More important, however, is its effect on the vertical profile of velocity. Large changes occur in the magnitude of velocity variation over the water column when the longitudinal salinity gradient is increased.

11) Calibration of the hydrodynamic model clearly demonstrated the hierarchy of physical processes affecting dispersion of contaminants. Using dispersion due to friction-induced velocity profiles in the water column as a basic unit, other processes are related as follows. Turbulent mixing due to short term temporal velocity variation is at least an order of magnitude less than friction-induced dispersion. Dispersion due to lateral variation of velocity across the channel cross section is approximately one-half to one order of magnitude larger than friction-induced dispersion. Dispersion due to tidal cycle variation of velocity is at least two orders of magnitude larger than friction-induced dispersion. Dispersion due to density driven circulation is highly variable, ranging from the same magnitude as friction-induced dispersion up to two or more orders of magnitude higher. Maximum circulation dispersion occurs at high fresh water inflow rates, in boundary reaches of the

estuary where longitudinal salinity gradients are high, and near the mouth where deeper water results in greater hydrostatic driving forces at the bottom.

12) Several sets of longitudinal salinity profiles at different fresh water flows were adequate for calibration of the boundary salinity expression and the tidal cycle averaged mixing coefficient. However, the quality of this data was not documentable, and a large variability was present. Future programs for calibration of the hydrodynamic model should incorporate a carefully planned sequence of salinity measurement cruises.

13) Calibration of the very important parameter which defines the strength of vertical eddy diffusion (VMF) was based on a single set of circulation velocity data. This parameter should receive greater attention in future calibration-oriented field studies. Furthermore, additional research should be undertaken to define a phenomenological basis for the strength of vertical mixing as it relates to density differences in the water column, fresh water flow, and other hydraulic factors.

14) Results from the two dye studies clearly demonstrated that salinity and artificially introduced contaminants are affected by the same mixing processes. Salinity-dye concentration analysis revealed that their distributions can be equated to a conservative mixing process. This important result confirms the validity of applying salinity-derived circulation dispersion

coefficients to other materials.

15) Dye study data also revealed the major role of fresh water flow rate in contaminant dispersion. The effect of fresh water flow is modeled by an analytical solution for a circulation driven dispersion coefficient at each segment of the estuary. This technique was found to satisfactorally represent extremes of both high and low fresh water flow.

7.2 Conclusions of Model Application to Non-Point Source Water Quality Investigations

The second category of objectives related to an analysis of receiving water body impacts due to non-point source contaminants. Work described in this dissertation demonstrated the utility of the general modeling technique for assessing water quality impacts. Furthermore, these investigations revealed important information about the general nature of the water quality problem. These conclusions are summarized below:

1) Both storm water volume and contaminant weight discharged to the Oyster River Estuary have a non-linear relationship to rainfall volume. The functional relationships among these variables cannot be defined in closed form. However, it is clear that an exponential relationship exists. Furthermore, the rate of increase for

contaminant discharge is much greater than the increase of runoff as rainfall volume increases. Therefore, large and intense storms will generate significantly higher contaminant concentrations at the point of discharge to the estuary.

2) Modification of land use on a small portion of the drainage basin will have a minor effect on storm water volume. However, for a basin such as the Oyster River drainage basin characterized by relatively low levels of development, the impact on contaminant flow can be great. Simulations demonstrated that changing land use on less than one percent of the land area can increase contaminant discharges by more than 10%. As larger tracts of land are developed, both storm water volume and contaminant weight will increase proportionately.

3) Contaminant loading from small storms is much less than that from large storms. However, this smaller load is more sensitive to increased intensity of land use. Since many more small storms occur than large storms, the increase in total load over a period of a year or more may be even greater than the 10% observed for a single large storm.

4) Evaluation of contaminant and runoff time series demonstrated that contaminant concentration peaks significantly before the higher storm water discharge. This confirms the characteristic commonly referred to as first flush. However, closer examination of the simulation

results show that while contaminant concentration peaks early, the mass flow rate peak is much closer to the runoff peak.

5) The impact of stormwater flow on average advective velocities in the upper reaches of the Oyster River can be significant. For the major 2.6-inch storm, velocities within one-half mile of the tide head dam were increased by almost 300% during the first tidal cycle after the storm. As storm flow receded, the effect was rapidly dissipated during successive cycles.

6) Dynamically varying stormflow has a great effect on dispersion processes in the estuary. Increased stratification due to the higher flow causes density driven circulation to dominate dispersion for several tidal cycles after a major storm. Although the mouth of the estuary is remote from the source of stormwater, the effect of increased circulation is greatest there due to the depth of water.

7) The impact of stormwater contaminants on water quality of the Oyster River Estuary as measured by BOD and dissolved oxygen is small. Even the worst case evaluated (a 60-acre commercial development) produced maximum BOD concentrations of only 61.0 mg/l and dissolved oxygen deficits of only 1.2 mg/l. However, if these impacts are weighed against the impact of sewage discharged by the Durham wastewater treatment plant, their significance must be re-evaluated. Water quality impacts of the sewage

discharge are about 1% to 6% of those caused by the stormflow. Although the duration of the stormwater-induced impacts is short, the impacts may be significant. Further research may therefore be justified on the problem of cost-effectiveness of water quality improvement techniques. Stormwater discharges may warrant increased priority relative to municipal wastewater treatment.

In completing this research program and dissertation, it is appropriate to consider the future potential of the resulting modeling techniques. A useful tool is available for assessing water quality implications of land development in the Oyster River drainage basin. As a result of the extensive model development, data gathering, and calibration effort, results of further simulations and different land development scenarios can be obtained quickly and at minimal cost. It is hoped that this potential is not overlooked and that other investigators will take advantage of these results. In a broader sense, the techniques have been intended to be readily transferred to other similar drainage basins and tidal rivers. While a larger data effort would be required for this purpose, the scope is not prohibitive, and the results may prove to have significant value. A one-year project within a governmental agency, university or consulting firm could produce a meaningful water quality analysis for potential development in any of dozens of small drainage basins along

the New England coastline.

LIST OF REFERENCES

LIST OF REFERENCES CITED

Betson, R.P., "What is Watershed Runoff?" Journal of Geophysics Resources, Vol 69, pp 1541-1552, 1964.

Boyle, E., Collier, R., Dengler, A.T., Edmond, J.M., Ng, A.C. and Stellard, R.F., "On the Chemical Mass Balance in Estuaries," Geochemica et Cosmochemica Acta, Vol 38, pp 1719-1728, 1974.

Christodoulou, G.C., Connor, J.J., and Pearce, B.R., "Mathematical Modeling of Dispersion in Stratified Waters," Ralph M. Parsons Laboratory, MIT, Report No. 219, 1976.

Connor, J.J. and Wang, J.D., "Finite Element Modeling of Two Dimensional Hydrodynamic Circulation in Shallow Water Masses," Ralph M. Parsons Laboratory, MIT, Report No. 172, 1973.

Crawford, N.H. and Linsley, R.K., "Digital Simulation in Hydrology: Stanford Watershed Model IV," Department of Civil Engineering, Stanford University, Stanford, California, Technical Report No. 39, 1966.

Donigan, A.S. Jr. and Crawford, N.H., "Modeling Nonpoint Pollution from the Land Surface," EPA-600/3-76-083, 1976.

Dunne, T., and Black, R.D., "Partial-Area Contribution to Storm Runoff in a Small New England Watershed," Water Resources Research, Vol 6, pp 1296-1311, 1970.

Elder, J.W., "The Dispersion of Marked Fluid in Turbulent Shear Flow," Journal of Fluid Mechanics, Vol 5, Part 4, pp 554-560, 1959.

Engman, E.T., "Partial Area Hydrology and Its Application to Water Resources," Water Resources Bulletin, Vol 10, pp 512-521, 1974.

Field, R. and Turkeltaub, R., "Urban Runoff Receiving Water Impacts," in Proceedings of National Conference on Urban Stormwater and Combined Sewer Overflow Impact on Receiving Water Bodies, Orlando, Florida, November 26-28, 1980.

Fisher, H.B., "Dispersion Predictions in Natural Streams," Journal of the Sanitary Engineering Division, ASCE, Vol 94, No. SA5, pp 927-943, 1968.

Fisher, H.B., "A Lagrangian Method for Predicting Pollutant Dispersion in Bolinas Lagoon, Marin County, California," U.S. Geological Survey, Geological Survey Professional Paper 582-B, 1972.

Freeze, R.A., "Role of Subsurface Flow in Generating Surface Runoff, 2, Upstream Source Areas," Water Resource Research, 8(5), pp 1272-1283, 1972.

Frere, M.H., Onstad, C.A. and Holtan, H.N., "ACTMO, An Agricultural Chemical Transport Model," U.S. Department of Agriculture, publication ARS-H-3, 1975.

Garrison, K.M., "Development of a One Dimensional Finite Difference Dispersion Model," M.S. Thesis, University of New Hampshire, 1979.

Greenberg, M.D., Foundations of Applied Mathematics, Prentice-Hall Inc., 1978.

Haith, D.A. and Dougherty, J.V., "Non-Point Source Pollution from Agricultural Runoff," Journal of the Environmental Engineering Division, ASCE, Vol 102, No. EE5, 1976.

Hansen, D.V. and Rattray, M., "Gravitational Circulation in Straits and Estuaries," Journal of Marine Research, Vol 23, No. 2, pp 104-122, 1965.

Harleman, D.R.F., in Estuary and Coastline Hydrodynamics, Ippen, A.T., ed., pp 507-509, McGraw Hill Book Company, 1966.

Harleman, D.R.F. and Ippen, A.T., "Two Dimensional Aspects of Salinity Intrusion in Estuaries: Analysis of Salinity and Velocity Distributions," prepared for Committee on Tidal Hydraulics, U.S. Army Corps of Engineers, Technical Bulletin 13, 1967.

Harleman, D.R.F. et al, "The Computation of Tides and Currents in Estuaries and Canals," prepared for Committee on Tidal Hydraulics, U.S. Army Corps of Engineers, Technical Bulletin 16, 1969.

Hess, K.W., "A Three-Dimensional Model of the Estuary Circulation and Salinity in Narragansett Bay," Estuarine and Coastal Marine Science, Vol 4, pp 325-338, 1976.

Holley, E.R., Harleman, D.R.F. and Fisher, H.B., "Dispersion in Homogeneous Estuary Flow," Journal of

the Hydraulics Division, ASCE, No. HY8, pp 1691-1709, 1970.

James, L.D., "An Evaluation of Relationship Between Streamflow Patterns and Watershed Characteristics Through the Use of OPSET," University of Kentucky, Water Resources Institute, Report No. 12, 1970.

Kuo, E.T.Y., "Analytical Solution for 3-D Diffusion Model," Journal of Environmental Engineering Division, ASCE, Vol 102, No. EE4, pp 805-820, 1976.

Lee, C.K., "One-Dimensional Analysis of Estuary Water Quality," Ph.D. Dissertation, Massachusetts Institute of Technology, 1970.

Leendertse, J.J., "Aspects of a Computational Model for Long Period Water Wave Propagation," Rand Corporation Memorandum RM-5294-PR, 1967.

Leendertse, J.J., "A Water Quality Model for Well Mixed Estuaries and Coastal Seas, Vol I, Principles of Computation," Rand Corporation Memorandum RM-6230-RC, 1970.

Leendertse, J.J. and Lire, S.K., "A Three-Dimensional Model for Estuaries and Coastal Seas: Volume II, Aspects of Computation," Rand Corporation Report R-1764-OWRT, 1975.

Leimkuler, W.F., Christodoulou, G., Connor, J.J., Sundgren, S.L. and Wang, J.D., "A Two-Dimensional Finite Element Dispersion Model," Sea Grant Report MIT-SG-1975, 1975.

Loder, T.C. and Glibert, P.M., "Great Bay Estuarine Field Program, 1975, Data Report Part 3: Nutrient Chemistry," University of New Hampshire Sea Grant Report No. UNH-SG-159, 1977.

Metcalf & Eddy Inc., University of Florida, and Water Resources Engineers Inc., "Storm Water Management Model, Volumes 1-4," U.S. Environmental Protection Agency Report No. 11024DOC, 1971.

Meyer, L.D. and Wischmeier, W.H., "Mathematical Simulation of the Process of Soil Erosion by Water," Transactions of American Society of Agricultural Engineers, 12(6), pp 754-762, 1969.

Muir, L.R., "Unsteady Flow in Networks of Open Channels," Ocean and Aquatic Sciences, Central Region, Canada,

Manuscript Report Series No. 1, 1975.

Niemeyer, G., "Numerical Methods for the Simulation of Hydrodynamic and Ecological Processes," Hawaii Institute of Geophysics, Report No. HIG-78-1, 1978a.

Niemeyer, G., "Solution of Coupled Nonlinear Ecosystem Equations," Journal of Environmental Engineering Division, ASCE, Vol 104, No. EE5, pp 849-861, 1978b.

Officer, C.B., "Longitudinal Circulation and Mixing Relations" in Estuaries, Geophysics and the Environment, National Academy of Science, Washington, D.C., 1977.

Reichard, R.R., "The Vertical Structure of Estuarine Tidal Currents," Ph.D. Dissertation, University of New Hampshire, 1980.

Reichard, R.R. and Celikkol, B., "Application of a Finite Element Hydrodynamic Model to the Great Bay Estuary System, New Hampshire," in Hydrodynamics of Estuaries and Fjords, Nihoul, J.D.J., ed., Elsevier Scientific Publishing Co., Amsterdam, 1978.

Roesner, L.A., Monser, J.R. and Evenson, D.E., "Computer Program Documentation for the Stream Water Quality Model, QUAL-II," Water Resources Engineers, Inc., Walnut Creek, California, 1973.

Sayre, W.W. and Chang, F.M., "A Laboratory Investigation of Open Channel Dispersion Processes for Dissolved, Suspended and Floating Dispersants," U.S. Geological Survey, USGS Professional Paper 433E, 1968.

Schmidt, E.J., Unpublished Correspondence with Normandeau Associates Inc., 1979.

Schmidt, E.J., "Dispersion Studies of the Piscataqua River," University of New Hampshire Sea Grant Report No. UNH-SG-167, 1980.

Schmidt, E.J., Unpublished branched model development and correspondence to C. Vorosmarty at Complex Systems Research Center, University of New Hampshire, 1981.

Shanley, G.E., "The Hydrography of the Oyster River Estuary," M.S. Thesis, University of New Hampshire, 1972.

Soil Conservation Service, U.S. Department of Agriculture, "National Engineering Handbook - Section 4,

Hydrology," 1966.

Soil Conservation Service, U.S. Department of Agriculture, "Computer Program for Project Formulation," Technical Release No. 20, 1965.

Soil Conservation Service, U.S. Department of Agriculture, "Urban Hydrology for Small Watersheds," Technical Release No. 55, 1975.

Strafford Regional Planning Commission, Personal Communication with E.J. Schmidt, 1981.

Stone, H.L. and Brian, P.L.T., "Numerical Solution of Convective Transport Problems," Journal American Institute of Chemical Engineers, Vol 9, No. 5, 1963.

Swenson, E., Brown, W.S. and Trask, R., "Great Bay Estuarine Field Program, 1975, Data Report Part I: Currents and Sea Levels," University of New Hampshire Sea Grant Report No. UNH-SG-157, 1977.

Taylor, G.I., "The Dispersion of Matter in Turbulent Flow Through a Pipe," Proceedings - Royal Society A, Vol 223, pp 446-468, 1954.

Taylor, R.B., "Dispersive Transport in River and Tidal Flows," Proceedings of the Fifteenth Coastal Engineering Conference, Vol 4, pp 3336-3357, 1976.

Texas Water Development Board, "QUAL-I, Simulation of Water Quality in Streams and Canals: Program Documentation and User's Manual," Austin, Texas, 1970.

Thatcher, M.L. and Harleman, D.R.F., "A Mathematical Model for the Prediction of Unsteady Salinity Intrusion in Estuaries," Ralph M. Parsons Laboratory for Water Resources and Hydrodynamics, MIT, Report No. 144, 1972.

U.S. Army Corps of Engineers, "A Model for Evaluating Runoff Quality in Metropolitan Master Planning," ASCE Urban Water Resources Research Program, Technical Memorandum No. 23, 1974.

U.S. Environmental Protection Agency, "Development and Application of a Simplified Stormwater Management Model," Municipal Environmental Research Laboratory, EPA Report No. EPA-600/2-76-218, 1976a.

U.S. Environmental Protection Agency, "Modeling Pesticides

and Nutrients on Agricultural Land," Environmental Research Laboratories, EPA, Publication EPA-600/2-76-043, 1976b.

U.S. Environmental Protection Agency, "Modeling Non-Point Pollution from the Land Surface," Environmental Research Laboratory, EPA report No. EPA-600/3-76-083, 1976c.

Wanielista, M., Yousef, Y. and McLellon, W., "Non-Point Source Effects on Water Quality," J. Water Pollution Control Federation, 49:441, 1977.

Ward, G.H. and Espey, W.H., Introduction in Estuarine Modeling: An Assessment, Tracor, Inc., 1971.

Ward, P.R.B., "Measurements of Estuary Dispersion Coefficients," Journal of the Environmental Engineering Division, ASCE, Vol 102, No. EE4, pp 855-859, 1976.

Webster and Martin, Inc. and Ebasco Services, Inc., "Hydrographic Studies Report - The Piscataqua River," Internal Report of Public Service Company of New Hampshire, 1969.

Wilson, J.R. Jr., "Fluorometric Procedures for Dye Tracing," Chapter 12 of Techniques of Water Resources Investigations, U.S. Geological Survey, 1968.

Yeh, G.T. and Tsai, Y.J., "Analytical Three-Dimensional Transient Modeling of Effluent Discharges," Water Resources Research, Volume 12, No. 3, pp 533-540, 1976.

Yotsukura, N., Fisher, H.B. and Sayre, W.W., "Measurement of Mixing Characteristics of the Missouri River," U.S. Geological Survey, Geological Survey Water Supply Paper 1899-G, 1970.

APPENDIX A

INPUT/OUTPUT DATA FORMATS FOR MODELS

APPENDIX A

INPUT/OUTPUT DATA FORMATS FOR MODELS

The entire non-point source impact analysis employs up to seven separate computer programs. Four of these relate to manipulation of new data files and generation of input data for computations. The other three perform all computations of the hydrologic, non-point source, hydrodynamic and water quality analysis. The seven programs are described briefly below.

1) INPUT.FOR - interactive program to create data files RIVER.DAT, GEOM.DAT, and WQ.DAT used by the estuary analysis models.

2) INNP.FOR - interactive program to create data file D NONP used by the upland analysis model.

3) MAP.FOR - program to manipulate hydrologic and contaminant data and assign appropriate aggregated parameters and area data used when running INNP.FOR.

4) TTIME.FOR - program to mainpulate hydrologic data to produce time parameters used when running INNP.FOR.

5) NONP.FOR - hydrologic and non-point source analysis program which produces a ime series of basin discharge and contaminant flow rates for a sequence of up to seven specified storm events separated by

dry periods.

6) MUDFLT.FOR - hydrodynamic analysis of intra and inter tidal cycle variations of flow velocity and water surface elevations.

7) WQMF.FOR - water quality analysis of single or multiple contaminant systems in a tidal river due to either varying contaminant discharges or ocean boundary contaminant concentrations.

The operation of these computer programs is described in more detail in the following pages. These descriptions emphasize requirements for data input and format of the output. They are not intended to replace the necessary technical background and knowledge of the processes and numerical analysis techniques. Neither will they allow an inexperienced modeler to simply pick up the models and begin to run sophisticated analyses. It is intended, however, that sufficient information be presented to ensure proper input of data and a basic understanding of the results.

Data Formatting Programs INPUT and INNP

1) General - Much of the data used by the numerical models must be provided in formatted data files located on the user's disc area. To simplify the preparation of these

lengthy files and ensure proper formats, programs INPUT.FOR and INNP.FOR were developed. It is not essential that these programs be used for simple cases, since the required files can be created by key-punching or can be input at a terminal. However, for large, complex systems, their use will simplify the work.

2) Data files - No data files are necessary as input to these programs. Program INPUT.FOR creates three files. File GEOM.DAT contains cross-sectional dimensions of the tidal river at each segment, and RIVER.DAT contains all other dimensions, parameters, and data required by the hydrodynamic analysis. File WQ.DAT contains data required by the water quality model including parameters and options, boundary conditions and constant source data. Data files containing additional input for the water quality model are created by the other computational models and will be described under those models. Program INNP.FOR creates a single file D-NONP used for input of all data to the hydrologic and non-point source analysis.

3) Operation of the programs - Most data to be typed in at the terminal is simply passed through for input to the computational models. These data are described in more detail under the model descriptions. Before running INNP.FOR, the data management programs described below should be run to aggregate hydrologic and contaminant data needed here. In addition, it is important that the topology of the drainage system be carefully defined and an

appropriate sketch be prepared. A typical topological sketch of a drainage basin is shown in Figure A1.

This network illustrates all components necessary to develop a complete drainage basin description. It is defined by the nineteen nodes identified by circles. Four types of node may occur as follows:

Designation	Type	Node Numbers
1	Runoff	1,2,4,5,10,11,13,14
2	Reach	9,18
3	Reservoir	8
4	Add	3,6,7,12,15,16,17,19

Runoff nodes are the starting points of the system where rainfall is converted into a runoff hydrograph and one or more contaminant pollutographs. Data required for each node includes the drainage area in acres, the Runoff Curve Number and the time of concentration in hours. Additionally, all contaminant parameters must be specified. Runoff nodes always appear in groups of four (e.g., 1, 2, 4, 5) representing the four Runoff Curve Number groups employed in the analysis (35, 71, 89, 97). Hydrographs and pollutographs from two areas are added together at the "ADD" nodes. No data is required for these nodes. The remaining two types of nodes represent routing conduits. Reservoir nodes are employed when the storage volume of the surface water feature is large by comparison to flow, and

reach nodes when the storage volume is comparatively small. Reservoir nodes are specified by their storage-flow characteristics given elsewhere in the data file. Reach nodes require input of the channel length and an SCS routing coefficient.

When running the INNP.FOR program, topology is specified by sequential input of the node type and the node number to which it drains. The nodes are renumbered in the program algorithm so the input numbers do not have to be in order. However, the first node should be a "RUNOFF" node and the last node should be an "ADD" node. The program reassigns node numbers in proper sequence for use in the hydrologic analysis and displays the new numbers at the terminal. These should be recorded on the sketch because results will be identified with these node numbers. All other information required by the program is self-explanatory and should be available after running MAP.FOR and TTIME.FOR.

Operation of program INPUT.FOR requires that the discretization of the estuary be known. This simply requires that the one-dimensional channel be divided into equal length segments. The number of segments should be a multiple of 4 so that the water quality analysis which uses half as many segments will have an even number. Cross-sectional data requirements have already been described. All other data is again self-explanatory. However, care must be exercised in choosing the number of

timesteps of the tidal cycle for the hydrodynamic computation. The timestep must be short enough to meet the Courant condition described previously. The total number of steps should be a multiple of 4 plus one additional. The timestep of the water quality model is less critical, but there is a loss of accuracy if it exceeds the shortest advective travel time through any segment of the system.

Data Management Programs MAP and TTIME

1) General - The data management system consists of two computer programs, MAP.FOR and TTIME.FOR., These programs make use of a number of primary data files to produce data required by the hydrologic and non-point source contaminant program NONP.FOR. Data requirements, program operation, and descriptions of input and output are given below.

2) Data files - Five data files in ASCII format must be available on disc in order to run the program. One data value is given for each grid cell in the rectangular grid. If a grid cell falls outside the basin of interest, a data value of zero may be assigned. In all cases the data is listed in integer format. Since the programs read the data with an unformatted read statement, the data can be filed with any number of values on a line, each separated by a blank space. The first record in the file lists the number

of rows (NROW) in the data grid (note: not the number of lines of data in the file) and the number of columns in the data grid. These values should be identical for all data files. Each subsequent record lists NCOL data values for a single row of the grid. The total number of records in each file is therefore NROW + 1.

The five data files are as follows:

a) LNDUSE.DAT - positive integer data value of 1 to 19 representing land use type for the grid cell.

b) SOIL.DAT - positive integer data value of 1 to 99 representing soil classification number as assigned to soils shown on the SCS map.

c) BASIN.DAT - positive integer data value of 1 to 99 representing the identification number of the sub-basin where that grid cell falls.

d) RTYPE.DAT - positive integer data value of 1 to 10 representing the type of surface water feature found in that grid cell. If none is present, a value of zero is assigned.

e) ELEV.DAT - positive integer data value representing the elevation above sea level in feet. To represent an elevation in tenths of a foot, a negative integer value is used (e.g., 143.6 is represented by -1436).

3) Program operation - Programs MAP.FOR and TTIME.FOR are operated interactively from a computer terminal. In

addition to the five data files described above, additional information must be provided at the terminal.

After initiating operation of MAP.FOR, the user will be asked to type six plot options. The computer prompts the user with a self-explanatory message. Each requested plot will result in a plot produced on the CALCOMP plotter at a scale of 0.25" per grid cell (2 inches equals 1 mile). The plotting routine allows a maximum grid size of 10 miles (80 grid cells wide) by 5-1/2 miles (50 grid cells). These limits may be easily modified in the program.

The program will then prompt the user whether the sub-basins should be regrouped. Typing option 1 will result in a further prompt to type in 100 new sub-basin identification numbers. These numbers must be in the range of 0-100 and should be typed in order of the present (old) basin numbering system (e.g., if old basin 1 becomes 15 and old basin 2 becomes 20, the first 2 numbers would be 15, 20). Any number of values can be typed per line, but each must be separated by blank spaces. Typing option 2 will result in reading a data file RENUM.DAT. This file should contain the same renumbering data which would be typed at the terminal. If option 2 is selected, a RENUM.DAT file must be available to avoid an error message.

At this point the program has all data to produce the requested plots and write an output file CN.LPT containing information on quantity parameters for the hydrologic and contaminant models.

Several important sets of default values are contained within the program. These values may be changed for specific applications through use of a program editor. The variables having such default values are listed below:

(a) AMPROP - A data statement beginning on line 14 of the program lists 20 values of proportion impervious area for each land use.

(b) COVER - A data statement beginning on line 17 of the program lists 20 values for the proportion of exposed soil surface for each land use.

(c) NGROUP - A data statement beginning on line 24 of the program lists 100 soil type identifiers. These have values of 1 to 7 corresponding to SCS soil types A, A/B, B, B/C, C, C/D, and D. They relate numerical identifications of SCS soil classifications to the soil types used in selecting SCS Runoff Curve Numbers.

(d) NCURV - A data statement beginning on line 30 of the program lists nineteen set of seven Runoff Curve Numbers. The seven values correspond to curve numbers for the seven soil types and for each of the nineteen land use types.

(e) PMP,PMI - The first group of executable statements in the program assigns values for pervious and impervious contaminant potency factors. These are identified by two indices, the first representing land use type, and the second representing contaminant type. The current

default values of contaminant type are: 1 - BOD, 2 - SUSPENDED SOLIDS, 3 - NOT USED, 4 - NOT USED.

Program TTIME.FOR is initiated to produce time-related data for the models. Once again, the user is prompted for plot and sub-basin renumbering options. At this point, the program has data to produce the requested plots and to write files TIME.LPT and CUMTIM.LPT containing all time-related output data.

Because of the complexity of the slope and flow direction analyses and the potential for erroneous or inconsistent elevation data, a number of error messages have been included in the program. If a data problem exists, one of the messages will be printed at the terminal but this will not stop operation of the program. Error messages fall into two categories. The first group relates to individual data points, the second to the sequencing of grid cells when tracking flow from a grid cell to the sub basin outlet. These are explained below.

Data point errors:

(a) "Grid number xx,xx is not the low point but drains to xx,xx." This message will be printed if a grid cell drains to another sub-basin. An exception is when the grid cell is the low point, then it must drain out of the sub-basin and no error message is printed.

(b) "No drainage from point xx,xx." This message is printed if all points surrounding a grid cell are at the same or a higher elevation.

Sequencing errors:

(a) "More than 75 grids between ends for xx,yy." It is assumed that no sub-basin is so large that more than 75 grid cells must be traversed to reach the discharge point. If an unterminated or very long loop occurs within the data, this message will be printed.

(b) "Error at point xx,yy, ran outside of grid when N = nn . . . I = xx J = yy." This message occurs if drainage from grid cell I, J progresses across N grid cells until it reaches a point outside of the grid. This message does not occur if the drainage reaches the low point of the sub-basin. Point xx,yy is the grid cell where the error occurred.

(c) "Travel time from row ii, column jj terminates at row xx, column yy." This message is printed when a drainage sequence reaches a cell where no further drainage can occurr. Its occurence is related to data point error (b) above.

Default values are also used in TTIME.FOR which may be modified for a specific application. These values are as follows:

(a) HYRAD - A data statement in subroutine RIVER assigns ten values of hydraulic radius in feet for the ten river types. The values are those shown in Table 3.

(b) FRIC - A data statement in subroutine RIVER assigns ten values of Manning's "n" coefficient for the ten river types. The values are those shown in Table 3.

(c) VI,VI0 - Data statements in subroutine OLAND assign ten values of overland flow velocity in ft/sec for slopes of one percent and ten percent for each of 20 land use types. These values were selected from data shown in Figure 3-1 of SCS publication TR-55.

4) Input and output of data - All input data requirements have been described above. Output data is found on three files which are described below.

(a) CN.LPT is generated by program MAP.FOR and contains all dimensional data generated for the hydrologic and contaminant models. Output is as follows:

(i) Area distributions - For each sub-basin, the total acreage is printed followed by the distribution of area to the five curve number groups. This latter data is in units of number of grid cells. It can be converted to acres by multiplying by 10.

(ii) Contaminant parameters - For each sub-basin and each curve number group, the following are printed:

- total area in acres
- impervious area in acres
- proportion of unexposed soil surface
- pervious (POLP) and impervious (POLI) contaminant potency factors for each of four contaminants.

(b) TIME.LPT is generated by TTIME.FOR and contains time parameters for the hydrologic and contaminant analysis. For each sub-basin (as renumbered) the file lists time of concentration in seconds and maximum cumulative travel time through streams or rivers of the sub-basin in seconds. To ensure that time of concentration is not controlled by a few remote poorly drained segments, the twenty longest travel times are printed out for each sub-basin. The program selects a time of concentration which ignores the worst five percent of the travel times. However, since the twenty longest times are printed out, the user may select a different value if it is desirable.

(c) CUMTIM.LPT is also generated by TTIME.FOR and contains additional time parameters as follows:

(i) For each (renumbered) sub-basin the grid cell location of the low point is identified.

(ii) The cumulative travel time from any grid cell to the low point of its sub-basin in minutes is printed. The first two columns of this table identify the grid cell row number, and the grid cell column number of the first data point in that row of the table.

Hydrodynamic Model MUDFLT.FOR

1) General - The hydrodynamic model utilizes geometric data, fresh water input rates and a tidal height forcing function to predict flow velocities and water surface elevations throughout the tidal river. A variety of options may be specified regarding boundary conditions, inflow characteristics, and duration of the analysis. For this research, the primary objective of hydrodynamic analysis is to develop velocity and cross-sectional flow areas for input to the water quality analysis.

2) Data files - Two data files are required for running the model and a third is used only when transient variation of fresh water flow is considered. The files must be resident on the user's disk space and have the

following names: GEOM.DAT, RIVER.DAT and PUNCH.DAT. The first and last are straightforward and are described in narrative form below. File RIVER.DAT incorporates a number of options, and for clarity a flow chart of data input has been employed.

File GEOM.DAT contains cross-sectional dimensions of the tidal river at each segment. Four optional cross section types have been described in Chapter 4, and reference is made to Figure 8 for the meaning of the dimensions. The file contains the following lines of formatted data:

A - For CASE = 1

One line of data for each cross section, each including D(J), Z0(J), B(J) where J is an index. The required format is (10X, 2F10.5, F10.1). Segment J = 1 is to be located at the mouth of the estuary as shown in Figure 7.

B - For CASE = 2

One line of data for each cross section, each including D(J), Z0(J), B(J), BS(J), DS(J), BM(J). Index J is used in the same way as in Case 1. The required format is (10X, 2F10.5, 2F10.1, F10.5, F10.1).

C - For CASE = 3

The first line contains a value for parameter SLOPE

in (I3) format. A value of 1 indicates that side slopes for all sections are the same and will be set equal to the side slope at section 1. A value of 2 indicates a variable side slope as read in for each section. Following this parameter is one line of data for each cross section including D(J), Z0(J), SS(J), SS(J), BB(J). Data format should be (10X, 4F10.5).

D - For CASE = 4

The first two lines contain values for KB and BO, the decay parameter and the constant which define an exponential variation of channel width. Data formats are (E10.3) and (F10.5) respectively. The width is defined by the following function:

$$B(J) = BO * EXP(-1 * KB * (J-1) * DX)$$

Following these two lines of data is one line for each cross section, including D(J), Z0(J) in format (10X,2F10.5).

File PUNCH.DAT is an optional data file used when a time series of freshwater flows (hydrograph) at the tide head dam is specified. It is only used when parameter NTRANS is greater than zero. This file can be created directly by the hydrologic/non-point source model or can be typed at the terminal. The file can contain hydrograph information alone or both hydrographs and pollutographs.

It can also encompass more than one storm or runoff period, so the timing of flows must be keyed to the start time of transient tidal cycles.

The first line of the file contains a title which is read in (20A4) format. Time series data is then grouped to represent one storm hydrograph or pollutograph. Each set of data contains the following lines.

The first line of data in each set is a hydrograph number NHYD which identifies the type of data. When NHYD is 7, the time series is read as a hydrograph. Values of 14, 21 and 28 represent contaminant pollutographs not used by the hydrodynamic model. The format for NHYD is (15X,I2). The next data line contains variable START and DTHYD representing the starting time of the hydrograph in hours relative to mid-flood of the first transient tidal cycle and the timestep of the time series in hours. The format for these variables is (12X,2F12.4).

The next group of data lines contain the hydrograph flow rates in preceded by an identifying index. If the line contains additional data, an index value of 8 is followed by five flow values. After all data points have been read, a data line containing an index value of 9 is added. Each of these lines is read in (I2,10X,5F12.2) format.

As indicated above, hydrographs and pollutographs can be interleaved in this file and more than one of each can be used. All hydrographs should have the same timestep and

must be referenced to the same beginning time of the transient analysis. For the array dimensions used in the program, the total time of all sequential hydrographs should not encompass more than 365 timesteps including dry periods between storms. If necessary, this dimension can be changed.

File RIVER.DAT contains all other data for operation of the hydrodynamic model. Figure A1 illustrates the flow of data input. Variable names are shown on the chart along with the required formats. Where data is contained on more than one line, the format specification is also split into multiple lines.

The definition of each variable is given in the following list in the order of appearance in the flow chart.

MCMAX - number of cases to be included in this data file.

IJOB - title of the current case.

ICASE - description of the current case.

ITYPE - upstream boundary type; always use type 1 - closed end.

JMAX - total number of equal length segments used to discretize the tidal river.

NMAX - number of timesteps per tidal cycle plus one (must be a multiple of 4, plus one).

CHLEN - total length of channel.

CASE - index for type of cross sectional geometry (refer

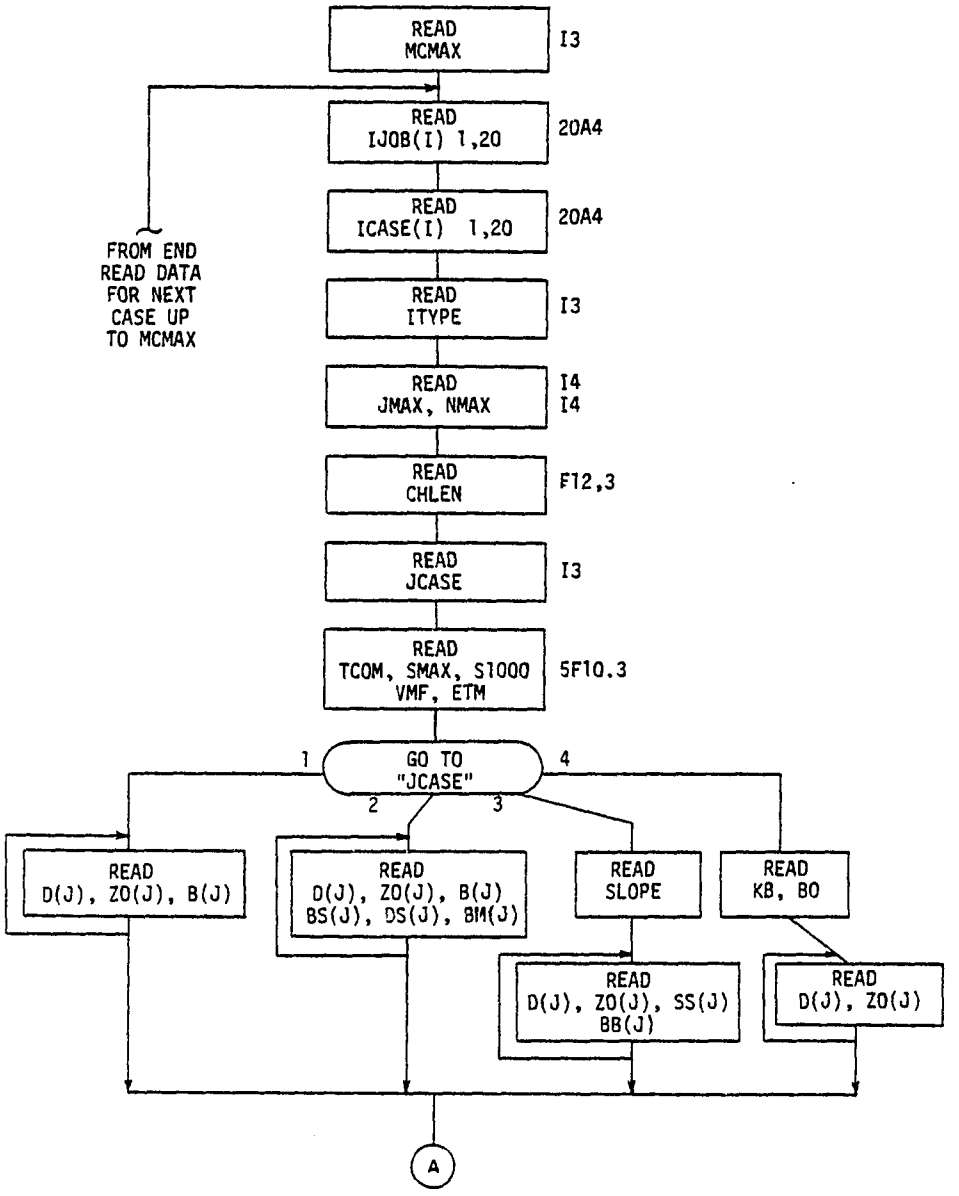

FIGURE A1 HYDRODYNAMIC MODEL INPUT DATA

SHEET 1 OF 3

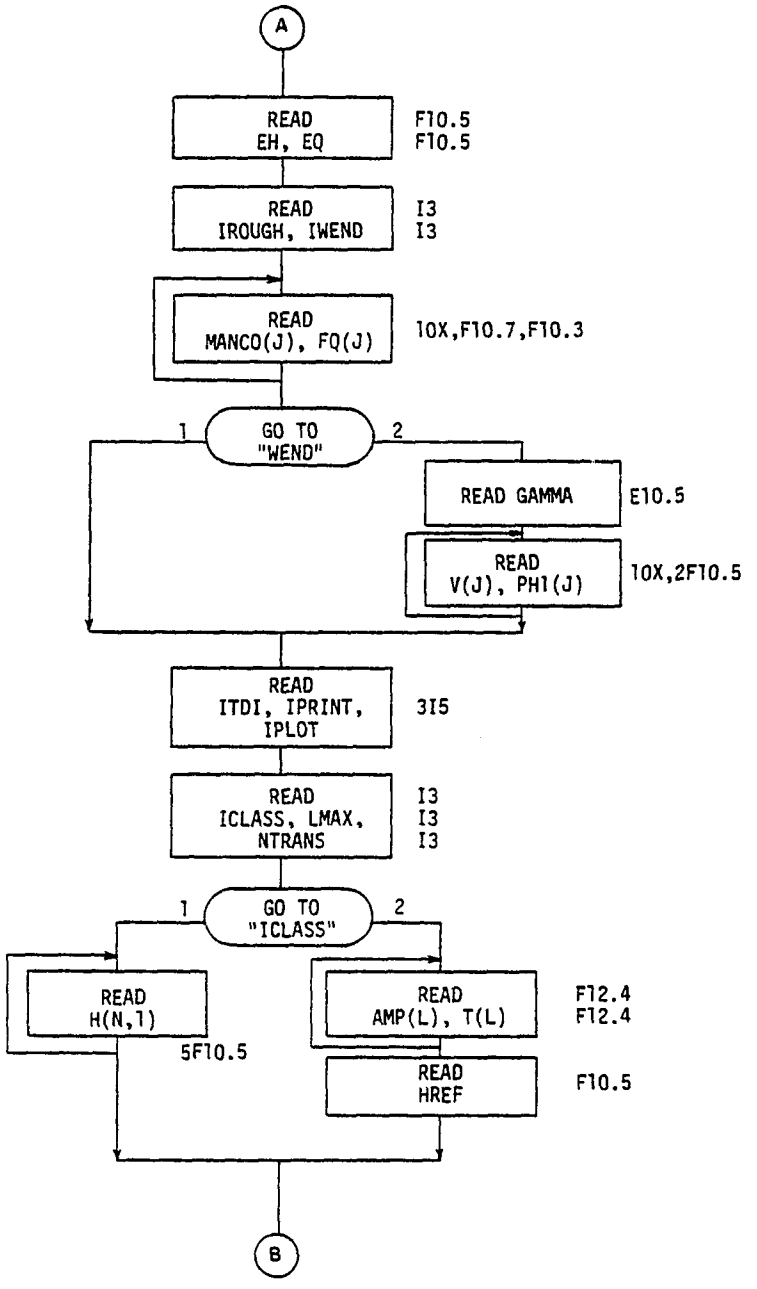

FIGURE A1 HYDRODYNAMIC MODEL INPUT DATA

SHEET 2 OF 3

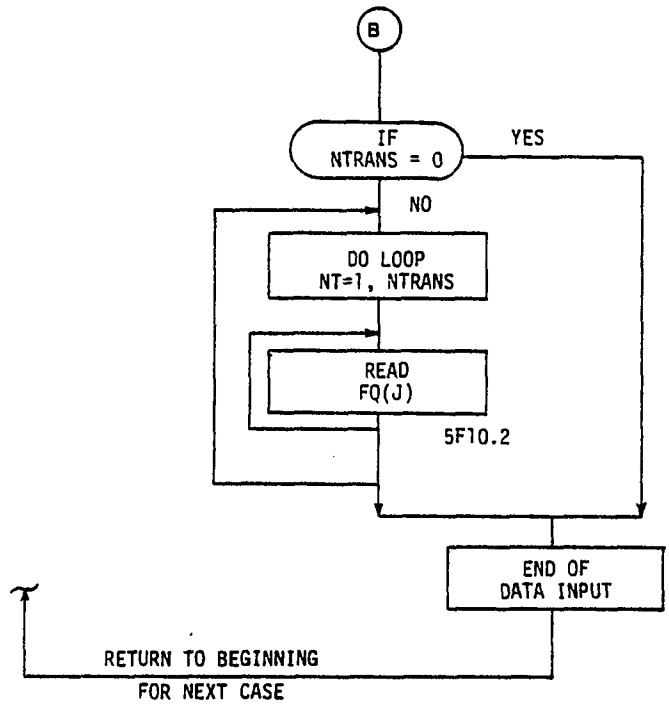

FIGURE A1 HYDRODYNAMIC MODEL INPUT DATA

SHEET 3 OF 3

to Figure 8).

TCOM - total length of one tidal cycle in seconds.

SMAX - When NTRANS = 0, this is the tidal cycle averaged salinity at the mouth. If transient flow conditions are to be run, then this is the maximum salinity observed at the mouth when fresh water flow is essentially zero.

S1000 - When NTRANS = 0, this is the tidal cycle averaged salinity at the head end. If transient flow conditions are to be run, then this is the salinity expected at the mouth when fresh water flow is 1000.

VMF - the vertical mixing factor, physically related to the fresh water flow rate, which reduces vertical mixing halfway to its minimum value.

ETM - tidal cycle mixing factor which represents the ratio of dispersion due to averaging over a tidal cycle to dispersion predicted by the "Taylor" formula.

EH - convergence criterion for quasi-steady state water surface elevations (in feet).

EQ - convergence criterion for quasi-steady state tidal flows.

IROUGH - roughness parameter if 1, the Mannings n is constant along the channel and equal to the value at segment 1. If equal to 2, n varies.

IWEND - wind option if 1, then no wind is considered; if

2, wind stress on the water surface is to be included.

MANCO(J) - Mannings coefficient at segment J.

FQ(J) - constant lateral inflow at segment J.

V(J) - wind velocity at segment J in feet per second.

PHI(J) - wind direction at segment J in degrees from the positive flow direction (into the estuary).

ITDI - number of sets of output data per tidal cycle (as required by the water quality model).

IPRINT - print options; if 0, only basic input data is echoed; if 1, a summary of velocity and elevation is also printed; if 2, a complete set of velocity, flow, and elevation data at each time-step is printed. (Option 2 is not generally used except for troubleshooting).

IPLOT - plotting options; if 0, no plots are made; if 1, longitudinal profiles of elevation and velocity for each twelfth timestep, and a time series of height variation at three longitudinal points are plotted.

ICLASS - ocean boundary condition; if 1, tidal height variation is input; if 2, a harmonic tide is used.

LMAX - for a harmonic tide, the number of harmonics included.

NTRANS - the number of transient tidal cycles with varying fresh water in flow to be analyzed.

H(N,1) - ocean boundary tidal height at timestep N.

AMP(L) - amplitude of tidal harmonic L in feet.

T(L) - period of tidal harmonic L in seconds.

HREF - the mean elevation of the harmonic tide measured in feet above the reference elevation of the channel cross sections.

FQ(J) - lateral inflow at segment J for the current transient tidal cycle (in CFS).

3) Program operation - The hydrodynamic analysis may be used to produce a quasi-steady state analysis only, or quasi-steady state followed by transient tidal cycles. The entire analysis employs a continuously repeating tidal height boundary condition. However, when transient cycles are specified, fresh water flow at the tide head dam may be varied continuously, and flow into each other river segment can be varied at each tidal cycle.

A variety of printing and plotting options may be specified as identified above. When calibrating or troubleshooting the analysis, these options may be employed, and the extensive files created by them can be printed. However, a production run does not usually warrant such detailed output. In fact, if all options are selected, a run encompassing many tidal cycles (say 25 or more) can produce large enough files to exceed available disk space limits on the DEC-10. On the other hand, if the minimal options are selected, the only file of significance

is that containing data required by the water quality analysis. A much more limited range of data is produced in the other files, and no plots are produced.

4) Output of data - The majority of output data is written onto file HYDRO.LPT. In addition to echoing the input data, this file will contain a summary of circulation related data at every other river segment, and calculated circulation dispersion coefficients. If option 1 is selected, a summary of tidal height, flow and velocity data is also printed. This summary contains the range of values over a tidal cycle and the time of maximums and minimums. Following the summary, the flow and cross-sectional area data developed for the water quality analysis is printed. If option 2 is selected, the file also includes the complete listing of tidal height, flow, and velocity at each river segment for each timestep of the analysis. Since each variable is calculated at up to 1000 timesteps of each cycle, this option can produce very large files.

File TERMS.LPT contains a breakdown of the relative magnitude of physical processes encompassed in the momentum equation. The breakdown is given at three stations along the estuary and at approximately fifteen-minute increments of time throughout the tidal cycle. This file is only used during the model calibration process to identify the sensitivity of results to changes in various adjustable parameters.

File FLOW.DAT is the most important file from the

standpoint of a complete analysis of water quality impacts. It contains velocity, cross-sectional area, and circulation dispersion coefficient data for each timestep of the water quality analysis. For economy of data storage, the file is written in binary form and therefore cannot be printed out. If it is necessary to review these data, the appropriate option should be selected to print the data in file HYDRO.LPT.

Output data is also found in one other place. Certain information is immediately printed at the terminal when running interactively or on the log file when running in a batch stream. This includes output or dispersion and flow data at each tidal cycle as the model iterates to a quasi-steady state solution. If a poor choice of parameters is causing a slow convergence, this information is useful in troubleshooting. A summary of relative magnitudes of the momentum equation terms at the head and mouth of the river is also output in this way as an aid in calibration.

Water Quality Model WQMF.FOR

1) General - The water quality model utilizes flow and cross sectional area data from a hydrodynamic analysis to simulate the variation of contaminant concentrations along a tidal river. Usually hydrodynamic data is

developed from the companion model, but other data sources or analyses can be used. Contaminant sources may be direct discharges to any river segment or material at the downstream boundary, or may be generated internally by chemical reaction of other materials. The analysis can be either steady state or dynamic. Three types of chemical system can be represented by the model--single contaminant, BOD-dissolved oxygen system, or cyclic system of inter-related contiminant species. The single contaminant system can include either conservative or non-conservative materials. The BOD-dissolved oxygen analysis considers artificially introduced BOD which decays and depletes available dissolved oxygen. Re-aeration is included as a first order decay of dissolved oxygen deficit. The cyclic chemical system allows any number of chemical species of a contaminant to be analyzed. However, the system is limited to species which undergo first order decay into the next species of the cycle only. No "feedback" or more complex interactions among the species can be considered in the present version of the model.

2) Data files - Two data files are required for running the model, and a third is used only when transient variation of contaminant inflow at the most upstream river segment is used. The files must be resident on the user's disk space and have the following names: FLOW.DAT, WQ.DAT and PUNCH.DAT. As with the hydrodynamic model, the second file is complex, and a flow chart will be employed to

describe input via this file.

File FLOW.DAT contains hydrodynamic data for each timestep of the water quality analysis. For a typical timestep of a quarter hour, 48 sets of data are required for each tidal cycle. When freshwater flow is constant and ocean tidal heights repeat for each cycle, a single set of data is sufficient. When conditions vary continuously, each tidal cycle must be specified.

For each tidal cycle of data the first set of lines contains computed circulation dispersion coefficients in ft^2 /sec. They are written in unformatted binary form beginning with the most upstream river segment (head end). This is followed by two sets of data for each timestep of the tidal cycle. The first of these contains velocities in ft/sec for each segment also written in unformatted binary form. The second set contains three pieces of data for each segment, again in unformatted binary form. The three are cross sectional flow area in feet, the hydraulic radius of the flow cross section in feet, and the ratio of total cross section area (including the mudflat regions) to the area of the flow cross section.

File PUNCH.DAT is the same file used by the hydrodynamic model. The format is described completely in that section. When the hydrograph number NHYD has a value of 14, 21 or 28, that portion of the data file contains contaminant flow rates in pounds per hour. In all cases NHYD = 14 is used for BOD data. Values of 21 or 28 may be

used for any other contaminant.

File WQ.DAT contains all other data for operation of the water quality model. Figure A2 illustrates the flow of data input. Variable names are shown on the chart along with the required formats in a similar manner to Figure A1 for the hydrodynamic model. Definitions of each variable are given below in the order of their use in the chart.

MCMAX - number of complete cases to be run.

RUNID - generally, the date followed by a single identification integer. This number appears on any plots made during the run.

MTYPE - the type of system; if 1, then single contaminant; if 2, then BOD-dissolved oxygen system, if 3, then cyclic contaminant system.

MTMAX - number of contaminant species in a cyclic computation.

ISUB(IS) - name of contaminant IS.

ITITLE - title for this case.

IDESCR - description of this case.

KTS - duration option; if 1, transient cycles only; if 2, converge to quasi-steady state; if 3, transient cycles following quasi-steady state.

QSS - convergence criteria in pounds of contaminant number 1 (for KTS equals 2 or 3 only).

II - number of equal length river segments (even

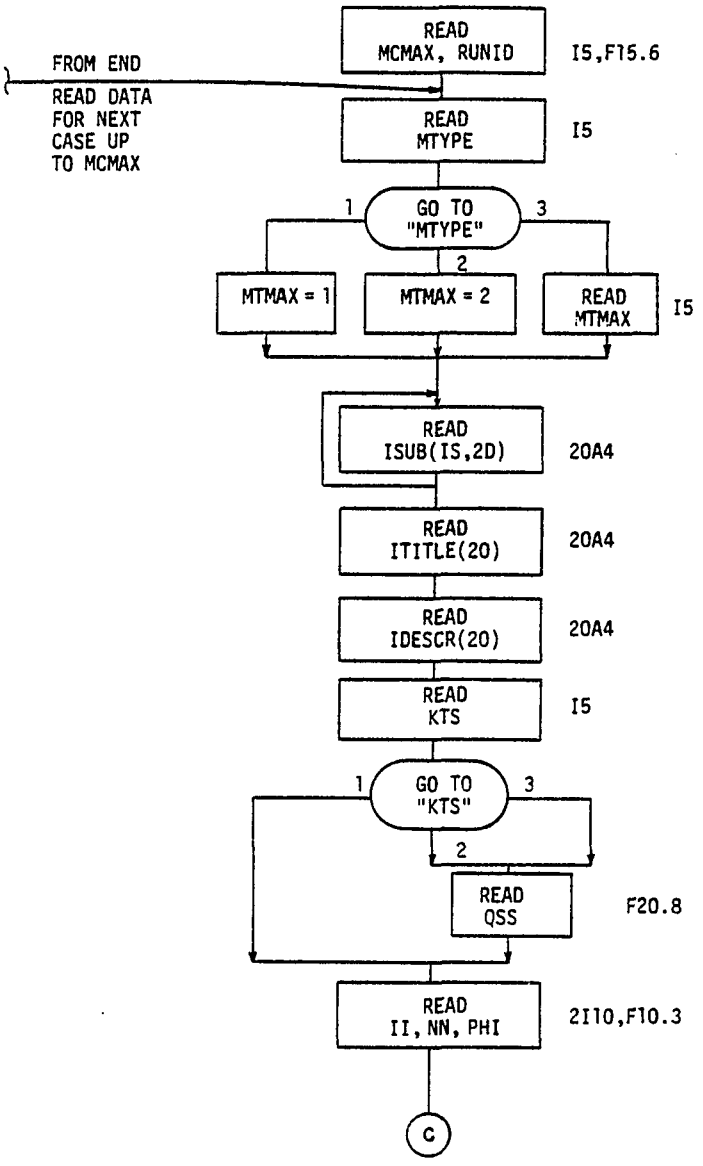

FIGURE A2 WATER QUALITY MODEL INPUT DATA

SHEET 1 OF 6

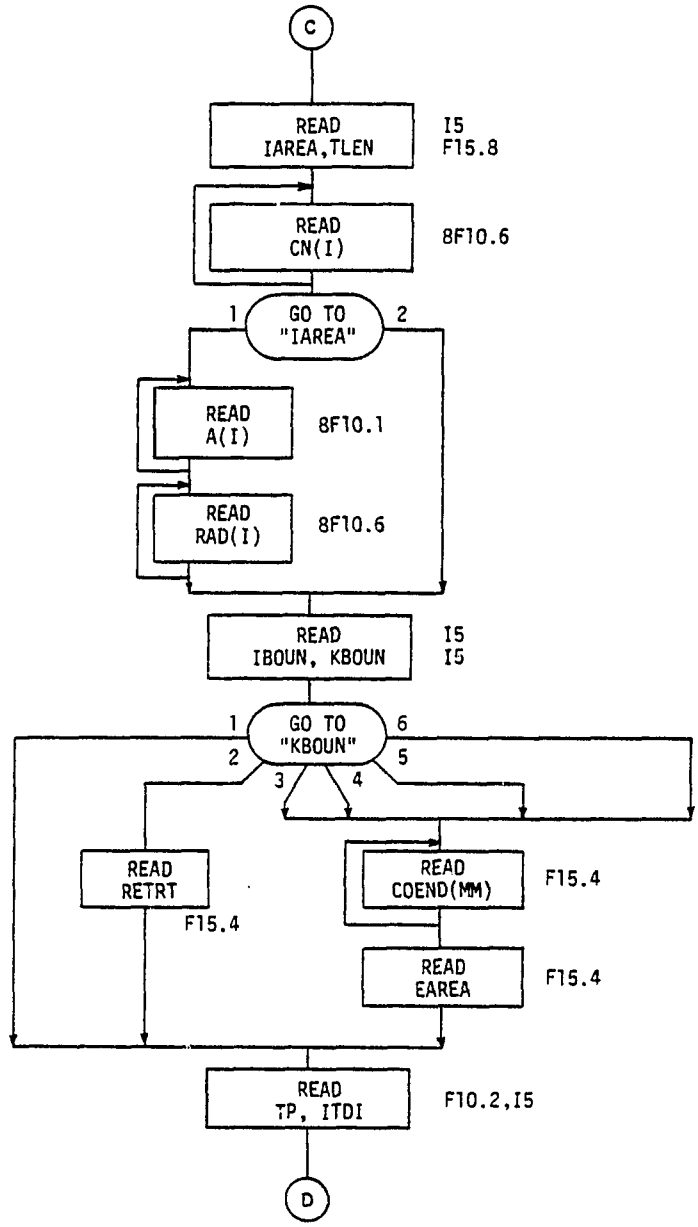

FIGURE A2 WATER QUALITY MODEL INPUT DATA

SHEET 2 OF 6

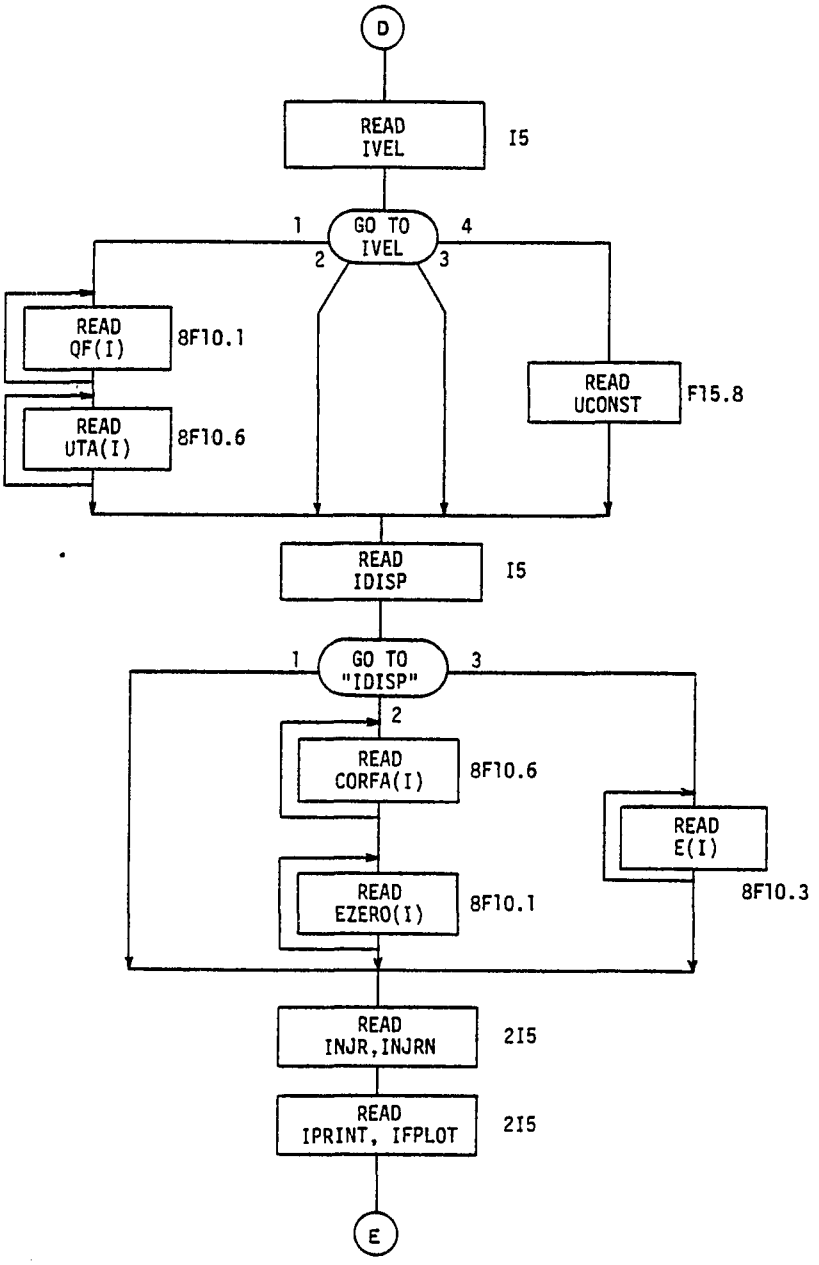

FIGURE A2 WATER QUALITY MODEL INPUT DATA

SHEET 3 OF 6

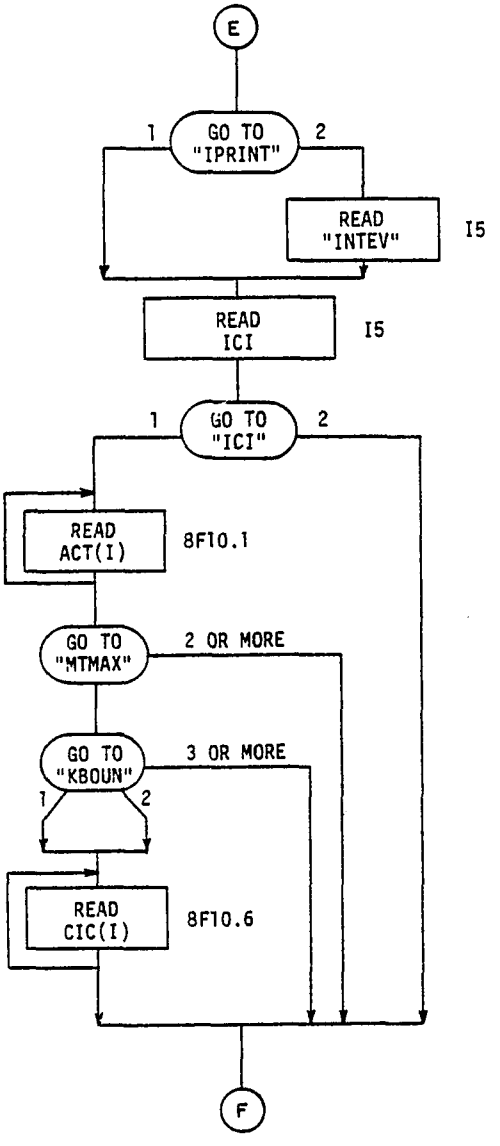

FIGURE A2 WATER QUALITY MODEL INPUT DATA

SHEET 4 OF 6

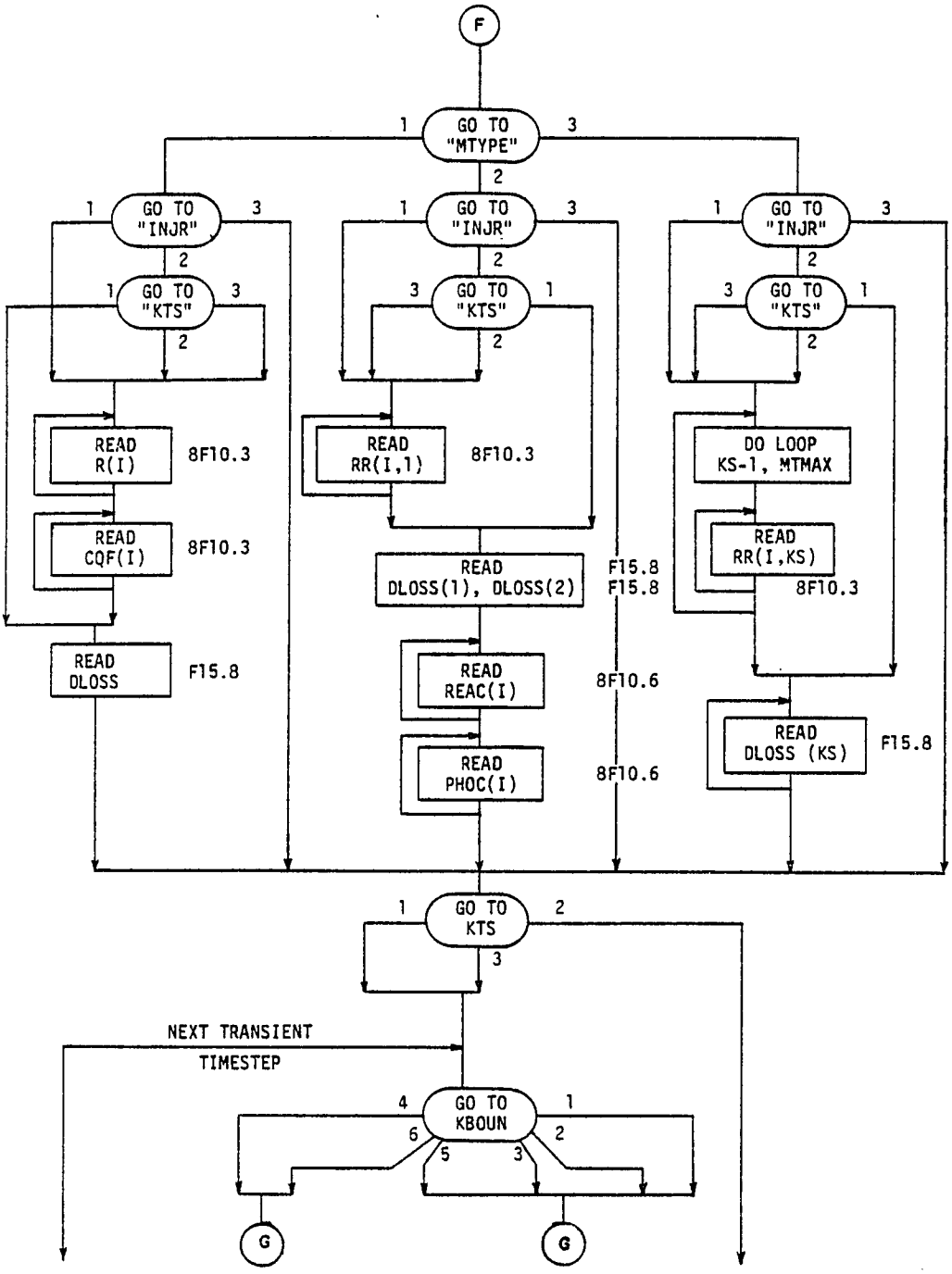

FIGURE A2 WATER QUALITY MODEL INPUT DATA

SHEET 5 OF 6

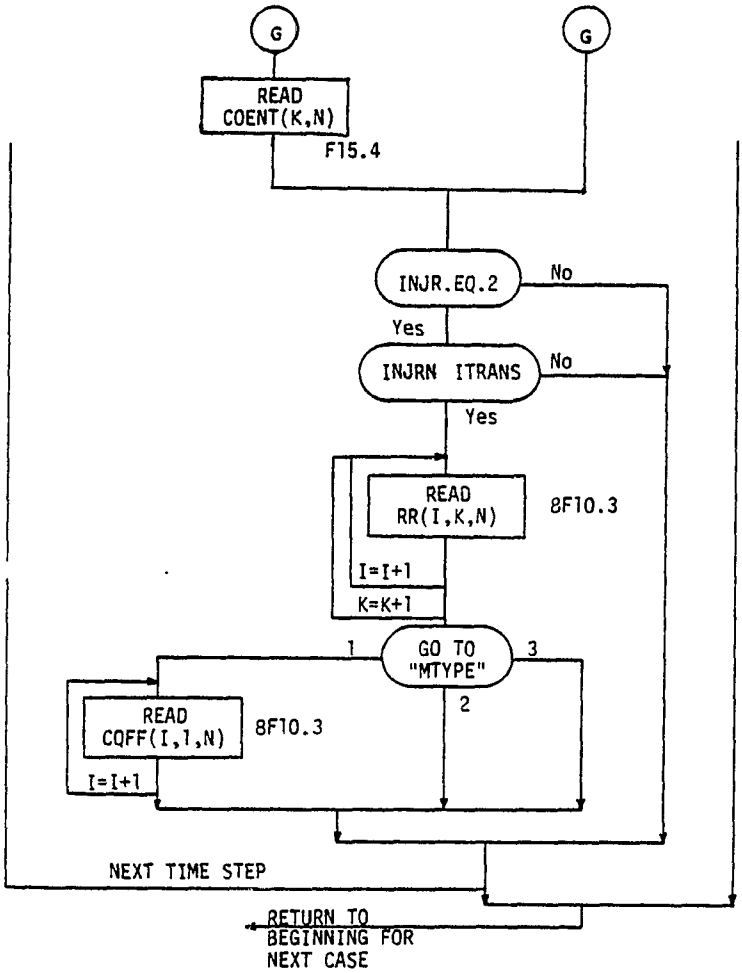

FIGURE A2 WATER QUALITY MODEL INPUT DATA

SHEET 6 OF 6

number).

NN - total number of timesteps to be run; must include both iterative tidal cycles up to quasi-steady state and transient cycles. Generally, it is best to use a large number since the run will terminate at the end of data input regardless of whether all timesteps are used.

PHI - a weighting factor to modify the relative weight of present and future timesteps in the finite difference operator. Generally, a value of 0.5 should be used, and it can be no less than this.

IAREA - cross section option; if 1, area varies with X but is constant in time; if 2, area varies with both X and time.

TLEN - channel length in miles.

CN(I) - Mannings coefficient at segment I.

A(I) - constant cross-sectional area at segment I (for IAREA = 1).

RAD(I) - constant hydraulic radius at segment I (for IAREA = 1).

IBOUN - river boundary option; if 1, open end; if 2, closed end. Option 2 should always be used here.

KBOUN - ocean boundary (mouth) option; if 1, open end with no contaminant return; if 2, open on ebb

and return of contaminant on flood tide based on RETRT; if 3, constant salinity at boundary; if 4, variable salinity; if 5, constant concentration of all contaminants at boundary; if 6, variable concentration of all contaminants at boundary.

RETRT - flushing return rate at mouth (for KBOUN = 2).

COEND(MM) - initial concentration of contaminant MM at the mouth (for KBOUN = 3, 4, 5 or 6).

EAREA - initial cross-sectional area at last segment (river mouth) used to convert initial concentrations to weight units.

TP - tidal period in seconds.

ITDI - number of timesteps per tidal cycle.

IVEL - velocity option; if 1, velocity varies as a sine wave over a tidal cycle; if 2, transient velocities read from file FLOW.DAT; if 3, quasi-steady state (repeating) velocities read from FLOW.DAT; if 4, a constant velocity is applied to all segments.

QF(I) - fresh water flow rate in for segment I (for IVEL = 1).

UTA(I) - amplitude of velocity variation in ft/sec at segment I (for IVEL=1).

UCONST - uniform and constant velocity (for IVEL = 4).

IDISP - dispersion coefficient option; if 1, E = 3 * ET; if 2, E = EFACT * ET + EZERO; if 3,

dispersion coefficients are read in. In all cases circulation coefficients are added to these values. (ET is the "Taylor" dispersion coefficient).

EFACT(I) - dispersion coefficient multiplier at segment I.

EZERO(I) - supplemental dispersion coefficient at segment I in ft^2/sec.

E(I) - dispersion coefficent (exclusive of circulation effects) at segment I in ft^2/sec.

INJR - source option; if 1, all external sources are constant; if 2, sources vary at each timestep; if 3, no external sources exist. For options 1 or 2, additional transient inflow of contaminants at segment 1 may be provided through file PUNCH.DAT.

INJRN - number of timesteps of vauable source input after which all sources are zero (for INJR=2).

IPRINT - print option; if 1, concentrations are printed at each timestep; if 2, concentrations are printed at quarter points of selected tidal cycles.

IFPLOT - plotting option; if 0, no plots are produced; if 1, plots of average concentration at each tidal cycle are produced; if 2, plots of averages and also quarter point concentrations for the selected tidal cycles are produced.

INTEV - the interval between tidal cycles when quarter point printing and plotting is done.

ICI - initial condition option; if 1, beginning concentrations at all segments are read in; if 2, all initial concentrations are set to zero.

ACT(I) - initial area of segment I in ft for converting initial concentration to initial weight (for ICI=1).

CIC(I) - initial concentration in segment I in parts per bilion (PPB) (only when MTMAX=1).

R(I) - source rate for single contaminant in segment I in lbs/sec.

CQF(I) - internal rate of generation for single contaminant in segment I in lbs/sec.

DLOSS - first order decay coefficient for single contaminant in units of 1 /sec.

RR(I,KS) - source rate for contaminant KS in segment I in lbs/sec.

DLOSS(1) - first order BOD decay rate in units of 1/sec (for MTYPE=2).

DLOSS(2) - first order reaeration coefficient in units of 1/sec (for MTYPE=2).

REAC(I) - supplementary aeration in segment I.

PHOC(I) - photosynthetic oxygen production in segment I.

COENT(K,N) - variable contaminant concentration at ocean end for contaminant K and timestep N in PPB.

RR(I,K,N) - variable source rate for contaminant K into

segment I at timestep N in PPB.

CQFF(I,1,N) - internal generation rate for single substance in segment I at timestep N in lbs/sec.

In considering the flow of data in this chart, several loops must be carefully followed. The major loop which returns from the end to the top of the chart allows multiple cases to be run with a single data file. At many points data is read for each segment and a small local loop is used. When transient tidal cycles are employed, data may be entered through several nested loops at the end of the chart. If ocean boundary conditions 4 or 6 are used, a boundary concentration must be specified for each contaminant at each timestep. Additionally, if transient source loading is considered, the source flow rate must be provided for each timestep. However, after a specified number of timesteps is completed (INJRN), no additional source data is required. When this variable source is used with a single contaminant, an internal generation rate may be used, and data must be read (use zeros if no internal generation). If a transient source exists at segment 1 only, the data requirements here may be replaced by providing data through file PUNCH.DAT as described above. It is also possible to use both of these source data methods simultaneously.

3) Program Operation - As described in the above paragraphs, the water quality program may be used in a wide

variety of ways. Options exist for various contaminant systems, source/sink terms, dynamic or equilibrium cases, etc. It is unlikely that an inexperienced modeler can simply pick up the program and produce immediate results. Great care must be taken in defining the problem, selecting the proper program options and properly formatting the files. However, once this is done, modification of the data to consider alternatives is quite easy, and due to the relative economy of the one-dimensional model many tidal cycles or many different cases can be run with minimal computer cost.

4) Output of data - All contaminant concentration data is contained in file CONCEN.LPT. The data is presented in tabular format for each timestep or each quarter point of a tidal cycle as requested. At each river segment, the table gives dispersion coefficient, velocity, source/sink, area and hydraulic radius data. Contaminant results are listed as CSTIME(I), CTIME(I), CPPB(I) AND CAVE(I). These represent weight of contaminant in storage and flow zones, raw contaminant concentration and smoothed contaminant concentration in the flow zone. This final quantity results from a longitudinal data-smoothing process which eliminates localized fluctuations inherent in the numerical solution technique. It represents the most useful of the output data for comparison to field observations or for evaluating water quality impacts.

In addition to these tables, at each timestep or

quarter point the total contaminant weight in the flow zones and storage zones is printed out. Average raw and smoothed flow zone and storage zone concentrations are also printed out for each tidal cycle of the analysis. Under the control of plotting option IFPLOT, plots of the concentraton data described above may also be produced. Each plot presents a longitudinal profile of smoothed flow zone concentrations and a data point at each segment representing smoothed storage zone concentrations. Care must be exercised in selecting plotting and printing options to avoid generation of excessive numbers of plots.

Hydrologic and Non-Point Source Model

1) General description - This model, called NONP.FOR, produces an analysis of both storm water runoff and contaminant washoff. The primary data is a time series of rainfall intensity. These data are applied to a discretized representation of the drainage basin to calculate individual runoff hydrographs for sub-basins and to route them downstream for ultimate integration into a single outflow hydrogaph. Sediment on the surface due to initial loading or generated by raindrop impact is washed from each sub-basin to produce a sediment washoff time series. Application of contaminant potencies then produces pollutographs which are routed downstream and integrated as for the hydrographs.

The model considers individual storms only, but up to

ten storms may be analyzed in a single run. Proper selection of start times for each storm allows a longer term flow series to be simulated. Since the model does not incorporate a complete moisture accounting system or a continuous analysis of contaminant accumulation, conditions occuring between storms must be incorporated into the subsequent initial conditions. Soil moisture at the beginning of a storm is handled by an Antecedent Moisture Index. Sediment loading at the beginning of a storm is calculated using a linear accumulation function and a first order decay function applied to the time between beginning of successive storms.

As many as three contaminants may be analyzed in a single model run. For consistency with data required by the estuary water quality model the first contaminant must always be biochemical oxygen demand (BOD). The second is usually suspended solids but may be another contaminant. The third may be any contaminant whose concentration (or mass flow rate) can be directly related to sediment washoff.

2) Data files - All data is contained in a single formatted file. The name for this file is optional since the model will request the file name at the users terminal when running the program. The data file may be considered in four sections, although they follow sequentially without separation in the file. The four are: 1) Contaminant source data; 2) Tabular data on rainfall and hydraulic

characteristics or flow control structures; 3) Sequential instructions to generate and route hydrographs and pollutographs; 4) Operational instructions to run a case with specified rainfall for all or part of the basin. (These may be repeated for multiple cases.)

a) Contaminant source data - The first line of the file contains several options used in the hydrologic model. For use in the complete non-point source analysis, these items are always written in the following FORTRAN format: ('JOB', 17x, 'ECON1', 5x, 'FULLPRINT PASS=001', 5x, I3). The number shown as a three digit integer at the end of this statement should be the number of contaminants to be considered in the analysis.

The second line contains the following variables:

NUMCON - number of contaminants again;

NUMAR - number of runoff areas (equals number of sub-basins times four);

NSECT - total number of node points in the basin topology;

AKRER - fines detachment coefficient;

AJRER - fines detachment exponent;

AKSER - fines runoff coefficient;

AJSER - fines runoff exponent;

AKEIM - dust/dirt runoff coefficient;

AJEIM - dust/dirt runoff exponent.

These variables should be in the following format: (3I3, 1x, 6F10.3).

The third line contains the overland flow contaminant

transport factor OVFACT in F8.3 format. The fourth line contains sediment decay and accumulation factors REMI, REMP, ACCUMI and ACCUMP in 4F8.3 format.

This is followed by NUMAR lines giving data for each runoff area. Each line contains the following:

NI(I) - node identification number;

A(I) - total acreage of the runoff area;

ARP(I) - number of pervious acres in this area;

COVER(I) - cover coefficient for raindrop impact shielding;

FIRSTI(I) - initial dust/dirt loading on impervious portion in pounds/acre;

FIRSTP(I) - initial soil fines loading on pervious portion in pounds/acre.

The next NUMCON lines contain the names of the contaminants, each in 12A2 format. This is followed by another NUMAR lines giving contaminant potency data for each runoff area. Each line contains:

PMP(1) - potency factor of contaminant 1 on pervious portion;

PMI(1) - potency factor of contaminant 1 on impervious portion;

PMP(2) - potency factor of contaminant 2 on pervious portion;

PMI(2) - potency factor of contaminant 2 on impervious portion;

PMP(3) - potency factor of contaminant 3 on pervious

portion;

PMI(3) - potency factor of contaminant 3 on impervious portion;

PMP(4) - potency factor of contaminant 4 on pervious portion;

PMI(4) - potency factor of contaminant 4 on impervious portion.

The final line contains identification data for the analysis including an identificaton number, the date and the title of the run. Format is (4x, 3A2, 3x, 3A2, 1x, 26A2).

b) Tabular data - This includes rainfall data, channel cros section data (when routing coefficients are calculated by the program) and flow control structure data.

Each line of tabular data includes an index and/or code word to identify the type of data found on that line. In the description below, these are found as a single ASCII string in the formats.

Rainfall data for each storm (up to 7) is presented as follows: The first line gives the storm number (must be 3 thru 9) and timestep of the rainfall data in hours. Format is (1x, 5 RAINFL', 1x, I1, 13x, F12.3). The next group of lines give cumulative rainfall totals in inches. The format is (1x, '8', 10x, 5F12.3). When all data for the storm is completed an "END OF TABLE" line is inserted. Format is (1x, '9 ENDTBL').

Optional channel cross secton data is presented as

follows: The first line contains identification data including cross secton number for the stream reach and drainage area in square miles. Format is (1x, '2 XSECTN', 3x, I3, 9x, F12.3).

The next set of lines contain a series of water surface elevations in feet, flow rates in CFS, and cross sectonal flow areas in square feet. These are used in computing the flow velocity and channel routing coefficient using average storage flow. The format of each line is (1x, '8', 22x, 3F12.3). After all data is completed an "END TABLE" line is inserted as before.

Optional flow control structure data is presented as follows. The first line contains the cross section number where the flow control is located. Format is (1x, '3 STRUCT', 6x, I2). The next set of lines contains a series of water surface elevations in feet, flow rate over the control structure in CFS and storage volume of the impoundment in cubic feet. Format is (1x, '8', 22x, 3F12.3). Once again an "END OF TABLE" line is used to close the data set.

c) - Sequential instructions - This rather lengthy set of data lines contains all instructions for hydrologic and contaminant generation computaions. They follow in the sequence which would be used to aggregate sub-basin flows if manual computations were performed. Reference should be made to the previous section on data management and in particular Figure A3 which illustrates discretization of

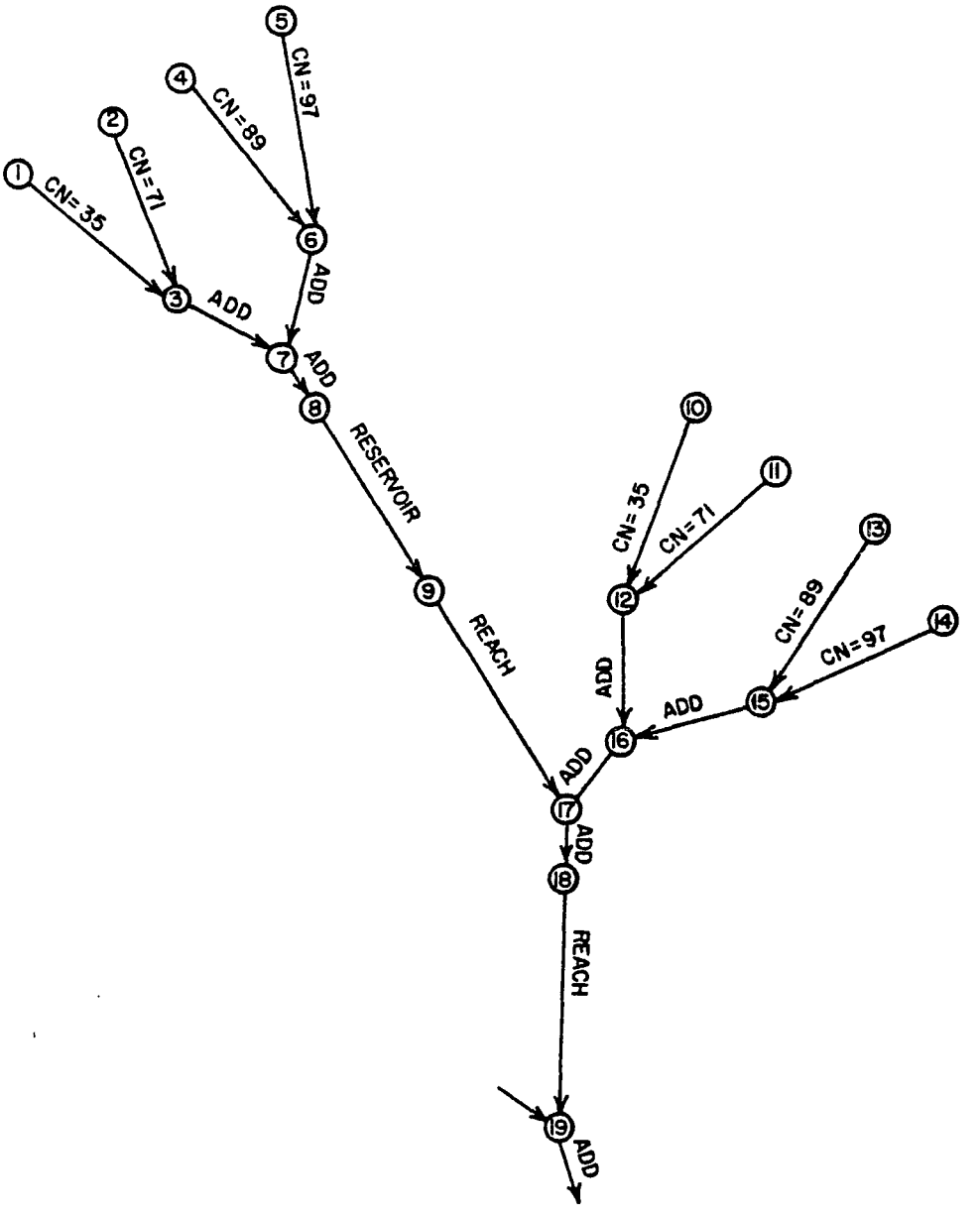

FIGURE A3

EXAMPLE DRAINAGE BASIN SCHEMATIZATION

the drainage basin.

Computations are performed in the following manner by the computer model. First rainfall data is applied to a runoff area to produce a hydrograph for an entire storm. This series of up to 300 flow rates is then stored in one of seven hydrograph storage areas numbered 1 through 7. Next, a contaminant flow time series is produced for the same area and same storm for each contaminant of interest. The time series for contaminant 1 is stored in a hydrograph whose number is 7 larger than the storm flow hydrograph. Contaminant 2 is stored with a number 14 higher. The 28 available storage sets (with current dimensioning of variables) are therefore assigned as follows: 1-7 storm flow hydrograph; 8-14 contaminant 1 time series; 15-21 contaminant 2 time series; 22-28 contaminant 3 time series.

These hydrographs and contaminant time series are then routed downstream and added to other hydrographs and contaminant time series until the aggregation of all sub-basins is complete. Hence only 7 hydrographs or 7 times series for each contaminant may be retained in storage at any one time. Great care must be taken in assigning storage location numbers to prevent over-writing on a data set still needed for further routing or addition. Keeping track of these location numbers is facilitated by being able to reassign a hydrograph or contaminant time series to a different location number. This is done by an

instruction called "SAVMOV." A typical sequence of instructions for a sub-basin containing 2 runoff areas, a single reach of a stream and a reservoir would require the following instructions:

1) RUNOFF - produces runoff hydrograph and contaminant time series for first area;

2) SAVMOV - reassigns storage location number for hydrograph;

3) SAVMOV - reassigns storage location number for a contaminant (repeat for others);

4) REACH - routes hydrograph;

5) SAVMOV - reassigns storage location for hydrograph;

6) REACH - routes contaminant 1 time series (repeat for others);

7) SAVMOV - reassigns storage location for contaminant 1 time series (repeat for others);

8) RUNOFF - produces new runoff hydrograph and contaminant time series for second area;

9) SAVMOV - reassigns storage location number for hydrograph;

10) SAVMOV - reassigns storage location number for a contaminant (repeat for others);

11) ADDHYD - adds hydrographs from 2 areas;

12) SAVMOV - reassigns hydrograph number;

13) ADDHYD - adds contaminant time series (repeat);

14) SAVMOV - reassigns contaminant time series storage location (repeat);

15) RESVOR - routes hydrograph thru reservoir;

16) REACH - routes contaminant series thru reservoir using channel routing methods.

An actual drainage basin analysis will therefore incorporate a large number of instructions. For example, the Upper Oyster River basin containing 16 sub-basins requires 64 runoff areas and 135 nodes which generate 682 instruction lines for a complete run. Data required for each of the 5 types of instruction line are given below:

1- RUNOFF The variables required are:

NUM	node number for the instruction
NHYD	storage location number of resulting hydrograph
AREA	drainage area in square miles
CURVNO	SCS runoff curve number
TMCONC	time of concentration in hours
IOOPT	input/output options (described below)

The format for these data is (1x, '6 RUNOFF 1', 1x, I3, 6x, I2, 1x, 3F12.4, I9).

2- REACH The variables required are:

NUM	node number for the instruction
NH	storage location number of input hydrograph or contaminant time series
NHOUT	storage location number of output hydrograph or contaminant time series
ALNGTH	length of river reach in feet
COEF	routing coefficient for SCS convex channel routing equation

IOOPT input/output options (described below)

The format for these data is (1x, '6 REACH 3', 1x, I3, 2x, I2, 1x, 2F12.4, 12x, I9).

3- RESVOR The variables required are:

NUM node number for the instruction

NH storage location number of input hydrograph or contaminant time series

NHOUT storage location number of output hydrograph or contaminant time series

ELEV starting elevation of reservoir in feet

IOOPT input/output option (described below)

The format for these data is (1x, '6 RESVOR 2', 4x, I2, I2, 2x, I2, 1x, F12.4, 24x, I9).

4- ADDHYD The variables required are:

NUM node number for the instruction

NHYD storage location of first input hydrograph or contaminant time series

IHYD storage location of second input hydrograph or contaminant time series

NHOUT storage location of output hydrograph or contaminant time series

IOOPT input/output option (descended below)k

The format for these data is (1x, '6 ADDHYD 4', 1x, I3, 2x, I2, I2, I2, 37x, I9).

5- SAVMOV The variables required are:

NUM node number for the instruction

NN storage location of input hydrograph or

contaminant time series

NHYD storage location of output hydrograph or contaminant time series

The format for these data is (1x, '6 SAVMOV 5', 1x, I3, 2x, I2, 2x, I2).

Following input of all lines of instruction, an end command must be provided. The format for this line is (3x, 'ENDATA'). At this point a group of data lines are entered which relate the numbering system of the contaminant data to the numbering system of the instruction set. All output data is keyed to the node numbers used in the instruction lines. If the contaminant data numbering system is different, the correct output node number is listed at this point for each contaminant node number in sequence. When all numbers are identical to their original identification numbers, this set of lines will simply list numbers 1 thru NUMAR in 20I3 format. These lines of data must be provided in all cases

Each of the first 4 instruction types made use of a variable called IOOPT. The nine integers of this variable contain 5 output option digits which may be either 0 or 1. The 1 indicates this option is desired, the 0 indicates it is not desired. The five optional outputs are:

PEAK output the peak discharge, its time and, when applicable water surface elevation.

HYD output the complete hydrograph time series.

ELEV output the water surface elevation time series

at this point.

VOL output total volume of water or contaminant weight for the hydrograph or contaminant time series

PUNCH write this hydrograph or contaminant time series on to output file DSK.PUNCH.

Within the 9 digits the 5 options are located in the following format (I1, 4(1x,I1))

4 - Operational instructions - The first line of operational instructions is an optional listing of the input data. If this is desired a LIST command is provided in format (1x, '7 LIST'). The next group of lines is an optional insertion of a hydrograph or contaminant time series. This option is particularly useful when a basin must be broken into two or more pieces due to limits on the size of a single run. A hydrograph input at this point is added into the hydrologic analysis by inclusion of an additional ADDHYD instructon in the sequencial instructons described above. The format of the input data is identical to the format of data output to file DSK.PUNCH described previously. By simply deleting the title and correcting the hydrograph numbers on DSK.PUNCH to correspond with the ADDHYD instruction, the file can be inserted directly at this point of the new data file.

The next 3 lines are the commands for actually performing the analysis using the sequential instructons.

The first line assigns the time increment of the output hydrogaphs in hours. The format of this line is (1x, '7 INCREM 6', 1Bx, F12.3).

The second line is optional and assigns a new baseflow to be employed in each successive hydrograph. Care must be taken that a non-zero baseflow is applied only to the appropriate hydrographs and not repetitively added to the system. It may be neccessary to run only a small part of the basin for a non-zero baseflow, then insert a new baseflow of zero for use in the balance of the basin. The format of this line is (1x, '7 BASFLO 5', 13x, f12.3).

The final line contains all other data for the run including:

NS1	first node number of the analysis
NS2	last node number of the analysis
START	start time of the analysis in hours
DEPTH	depth multiplier for rainfall (usually 1.0)
RAINDU	duration multiplier for rainfall (usually 1.0)
NTBL	identification number of the rainfall data series to be used here
IMOIST	antecedent moisture index (either 1, 2, or 3, or any integer between 10 and 30)

The format is (1x, '7 COMPUT 7', 1x, I3, 3x, I3, 3x, 3F12.3, 4x, I1, 2x, I2). The COMPUT line is followed by an end of computation line in the following format (3x,

'ENDCMP 1').

If additional cases are to be run an additional set of lines may be used for each. Each set should begin with an INCREM line and end with an ENDCMP line. Following the last set of computation instructions, an end of job line should be inserted in the following format (3x, 'ENDJOB').

The rather extensive data requirements of the model necessitate keypunching or formatted typing of many lines of data. To reduce the effort required to prepare a run of this model an interactive data file preparation computer program was developed. This program, called INNP.FOR, was described in an earlier section of this appendix. If the requirements given above are understood, operation of INNP.FOR at an interactive terminal should greatly simplify data file preparation.

C - Program Operation - The NONP.FOR program is operated interactively from a computer terminal. After initiating execution, the model will ask for names of the input data file and output file. After recieving these names, the program will perform the analysis described by each set of operational instructions. The model will employ the appropriate set of sequential instructions to perform the hydrologic and contaminant source computations. Each set of operational instructions may employ a different set of rainfall data, different input hydrographs and different portions or all of the sequential instructions as dicatated

by the starting and ending node numbers. By sequencing several storms with successive starting times and appropriate antecedent moisture indexes, a long period of time encompassing up to 7 storms can be analyzed. The output data from this group can all be written to file DSK.PUNCH for further evaluation or use in an estuary analysis.

D - Output files - The major output file named when running the program contains all data requested by the LIST instruction or by the IOOPT options on the sequential instructions. All contaminant data is also echoed onto this file. This rather extensive output file can contain the hydrograph and contaminant time series at every node of the drainage basin. If also contains summary data on total runoff volume, sediment generation and washoff and total weight of contaminant discharged at each point.

File DSK.PUNCH contains only those hydrographs and contaminant time series specifically requested in the last option of variable IOOPT. Generally, this file will be used only for the total outflow at the low point of the basin for each storm. When used in this way it provides data directly to the estuary hydrodynamic and water quality analysis models.

APPENDIX B

LONGITUDINAL CONCENTRATION DISTRIBUTION FIGURES

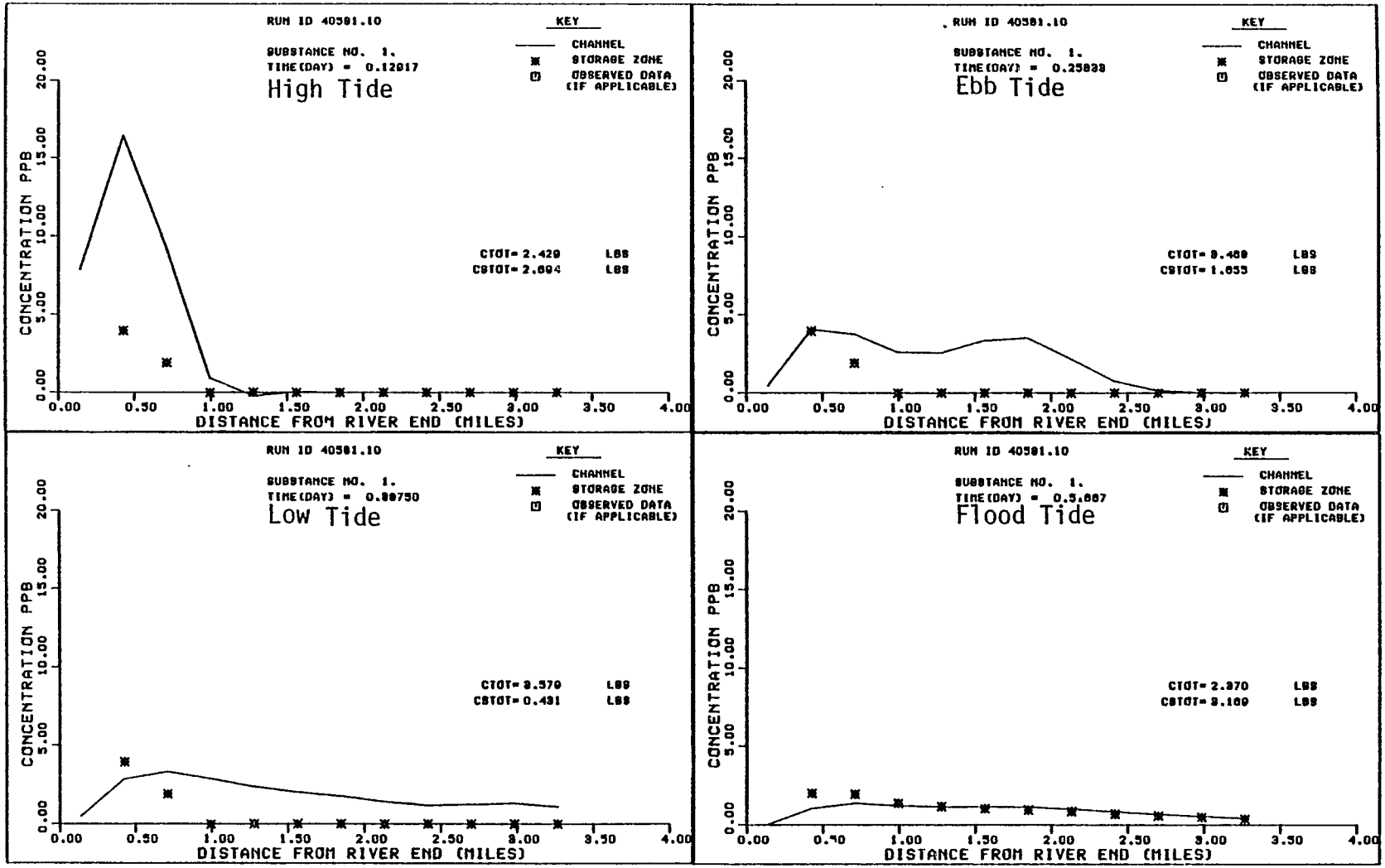

FIGURE B1 HIGH FLOW DYE STUDY--TIDAL CYCLE 1

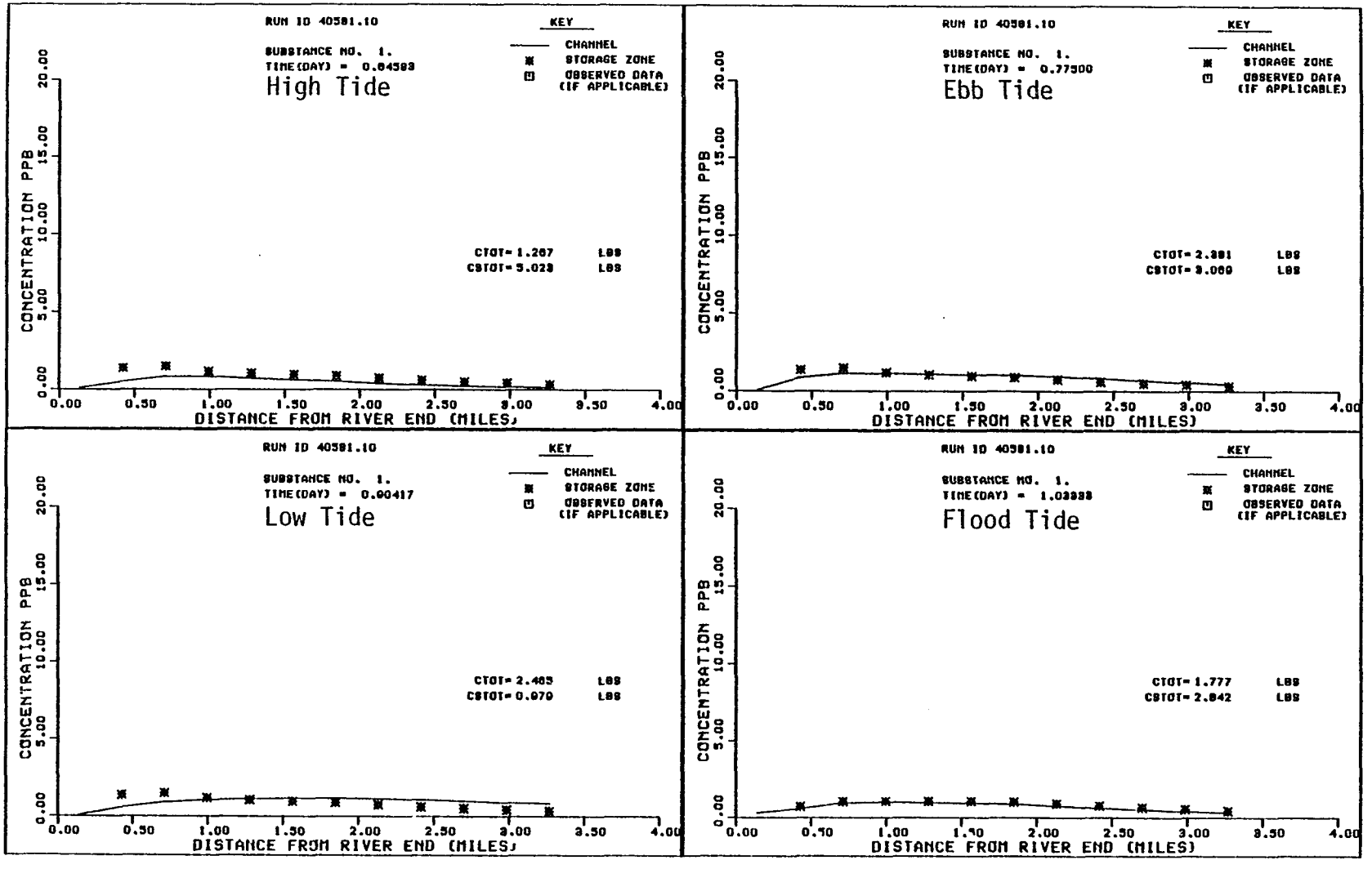

FIGURE B2 HIGH FLOW DYE STUDY--TIDAL CYCLE 2

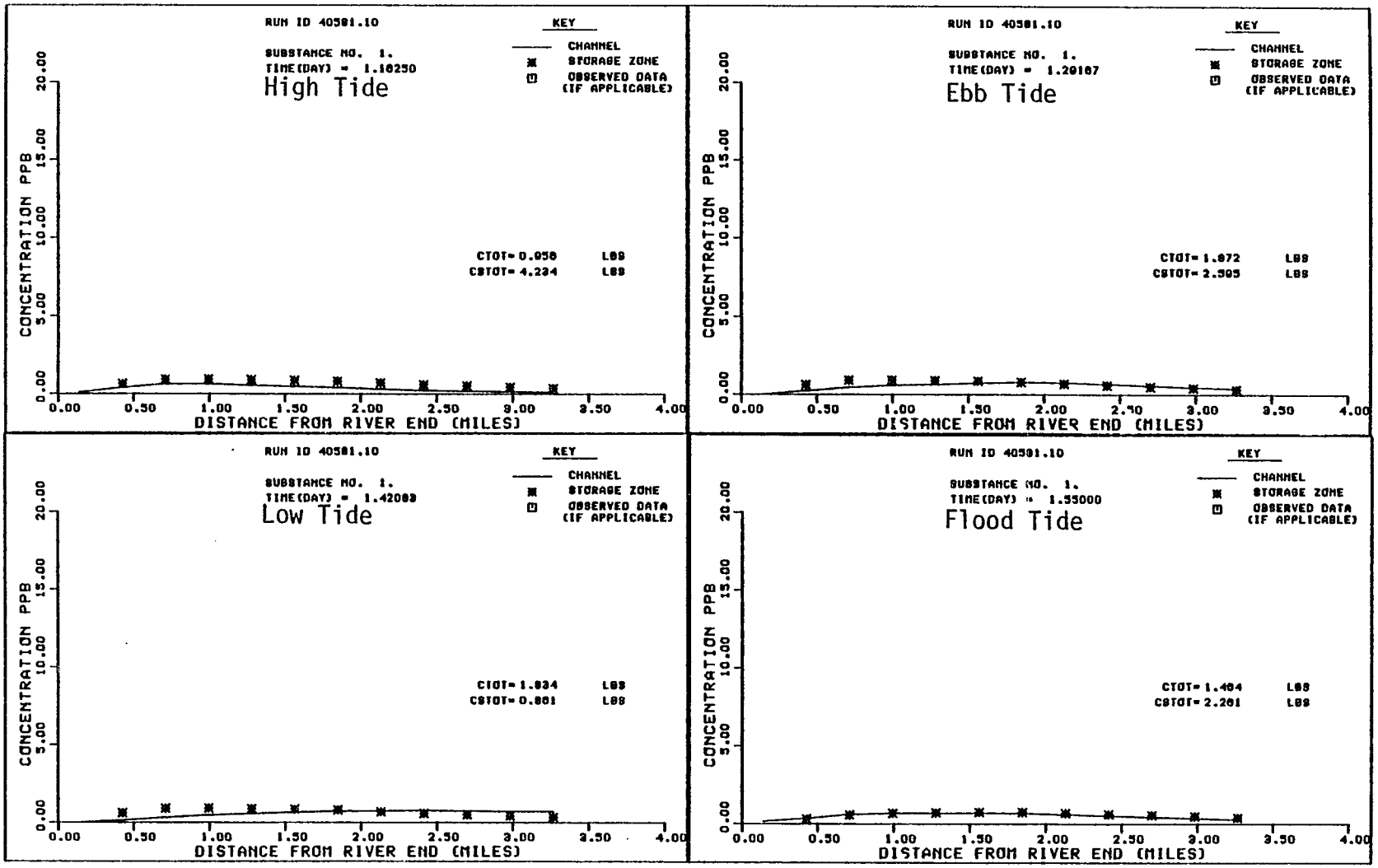

FIGURE B3 HIGH FLOW DYE STUDY--TIDAL CYCLE 3

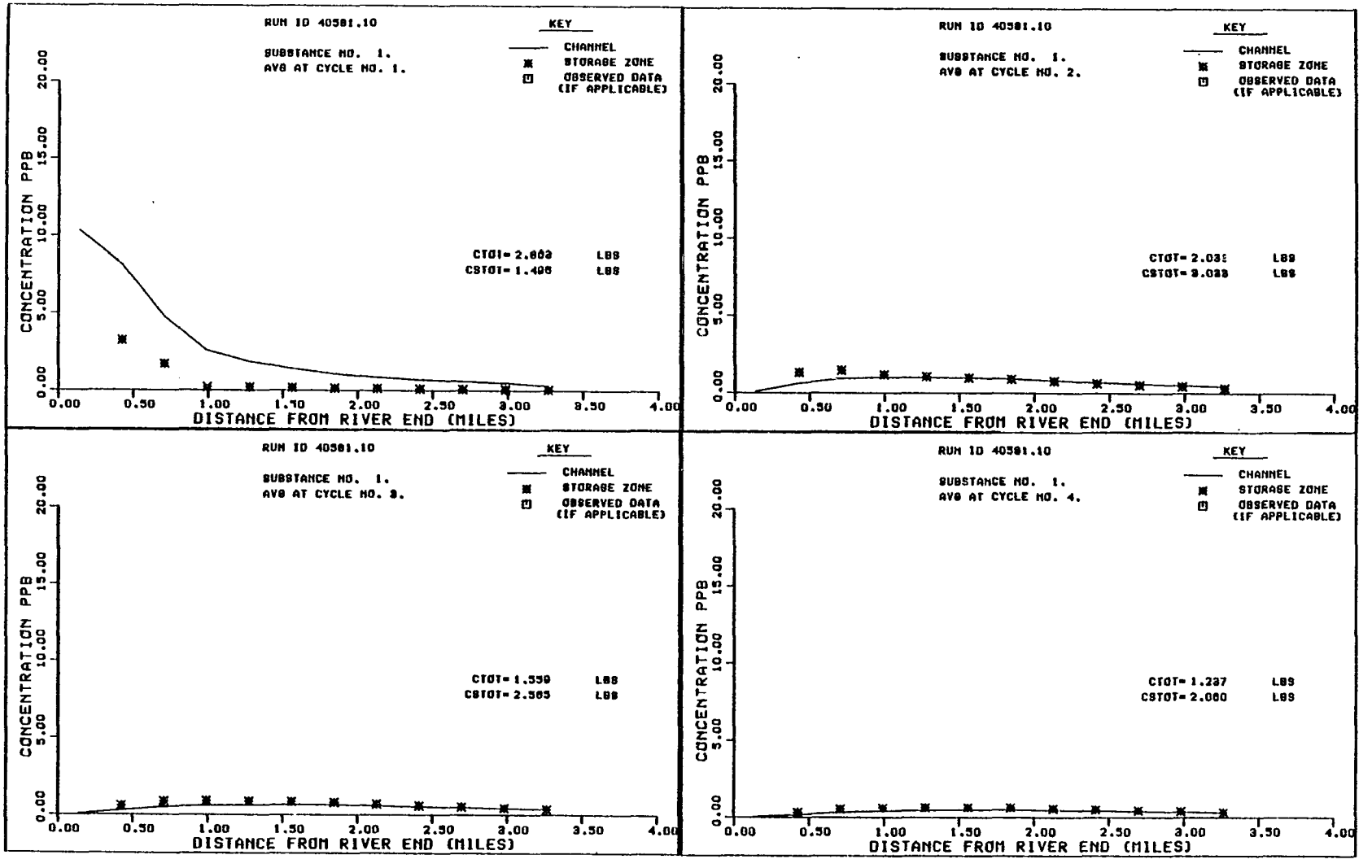

FIGURE B4 HIGH FLOW DYE STUDY--AVERAGES

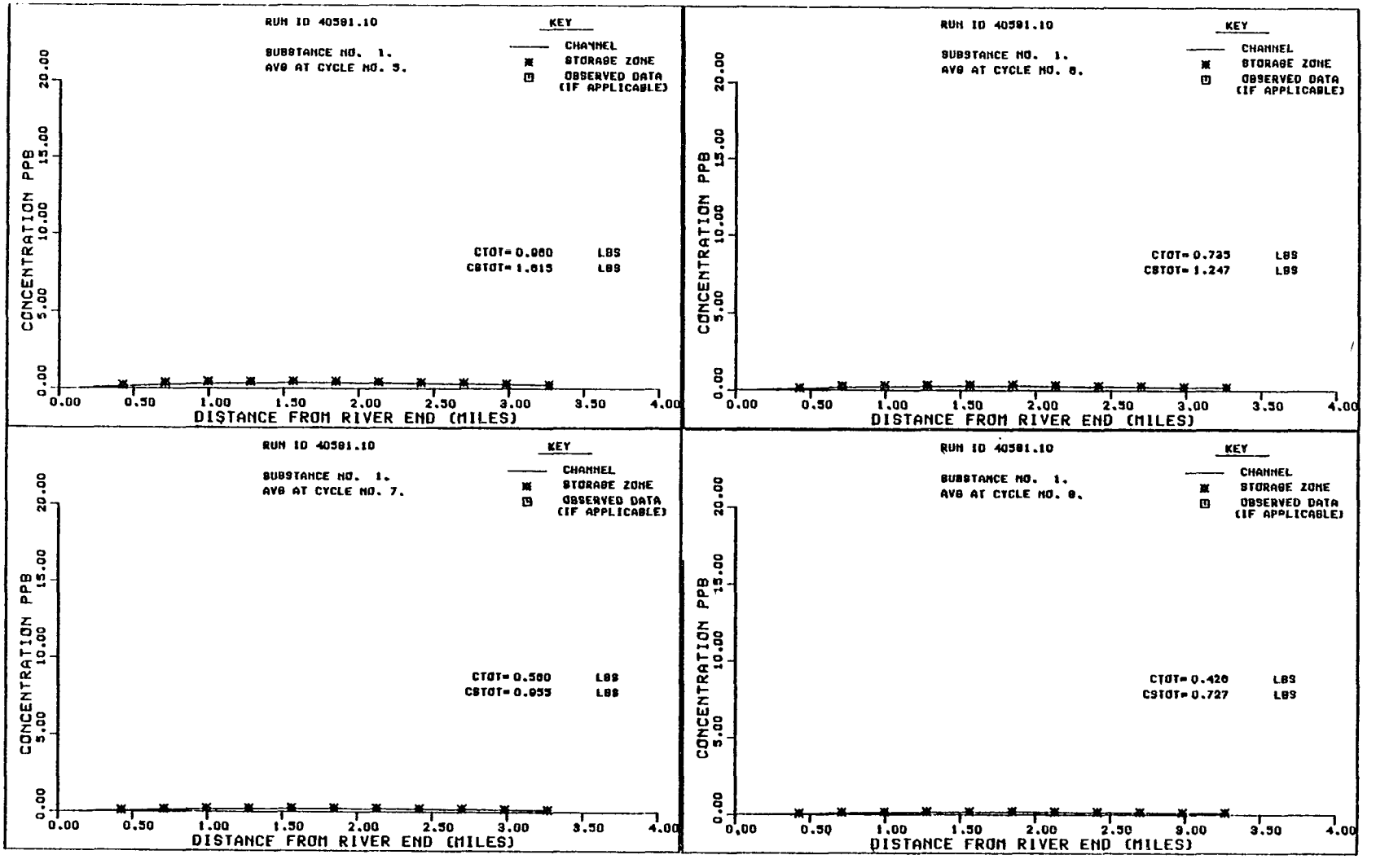

FIGURE B5 HIGH FLOW DYE STUDY--AVERAGES

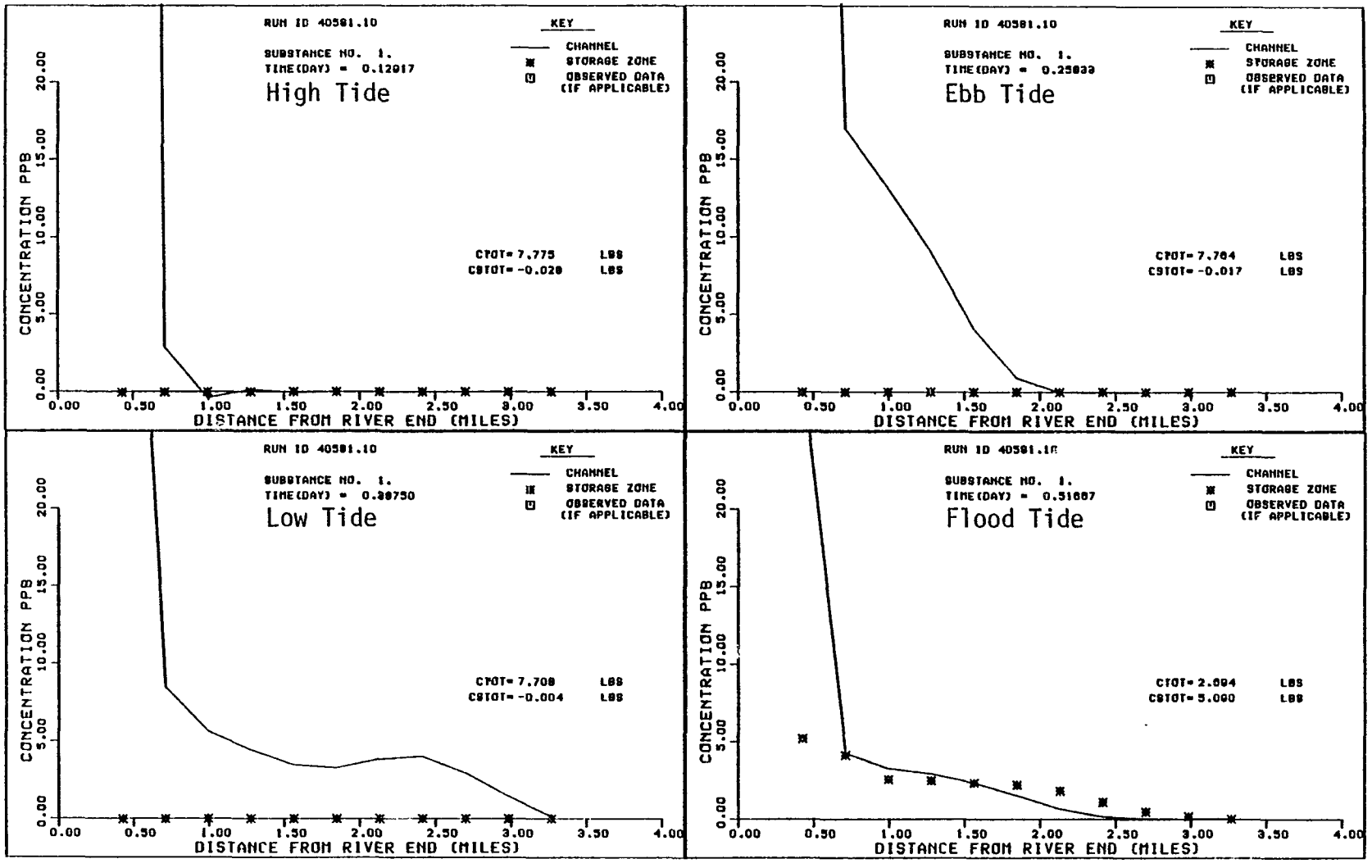

FIGURE B6 LOW FLOW DYE STUDY--TIDAL CYCLE 1

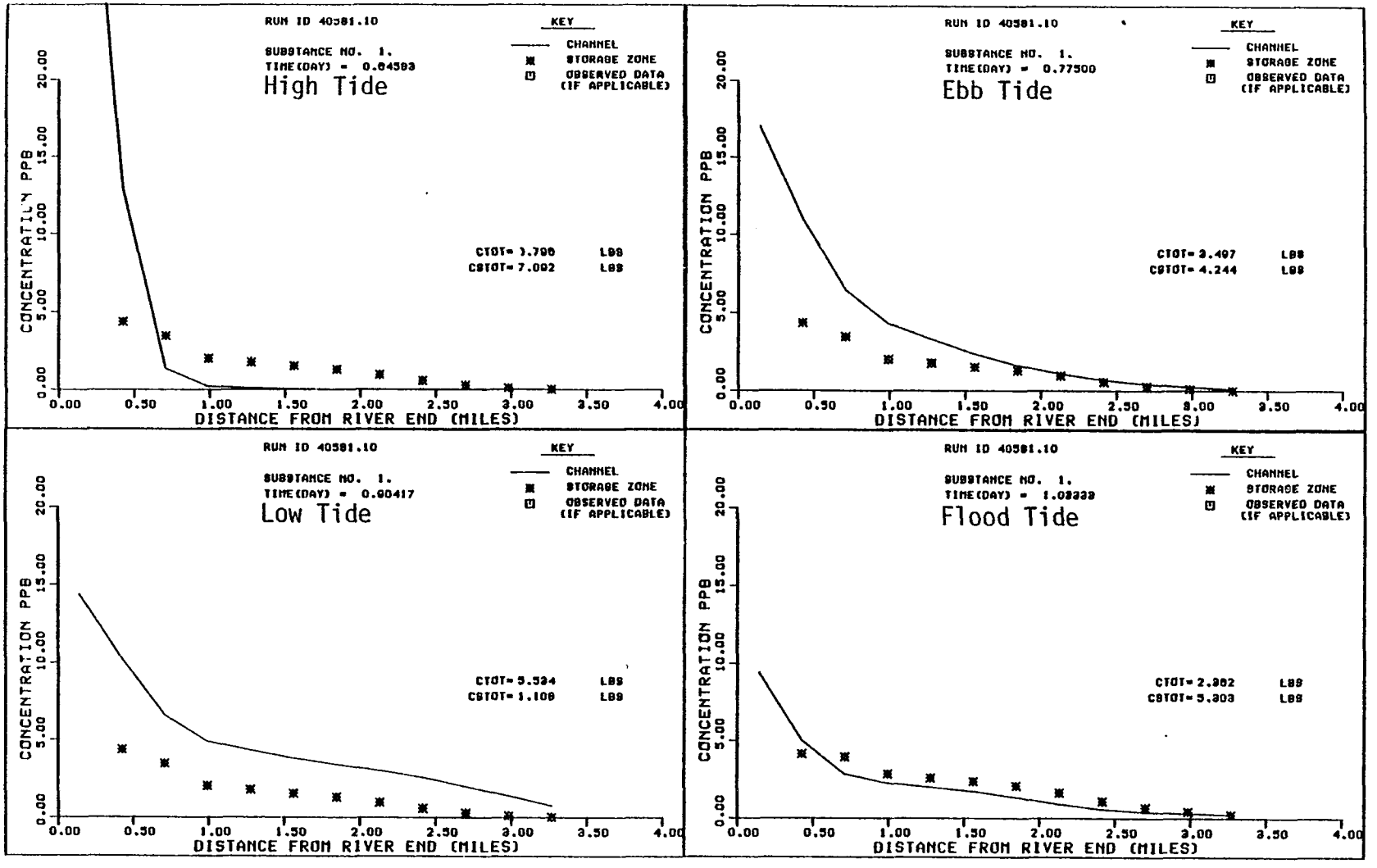

FIGURE B7 LOW FLOW DYE STUDY--TIDAL CYCLE 2

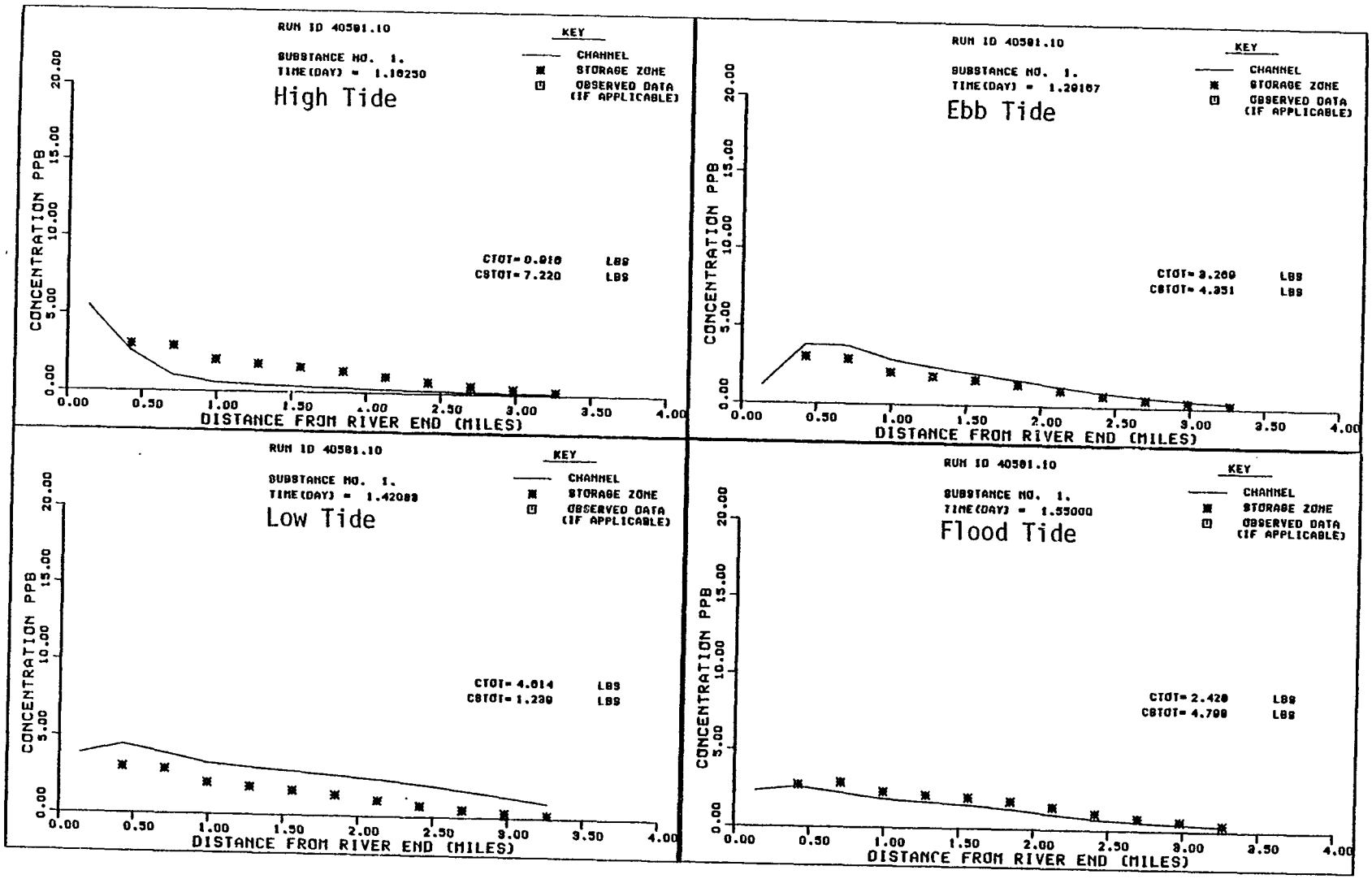

FIGURE B8 LOW FLOW DYE STUDY--TIDAL CYCLE 3

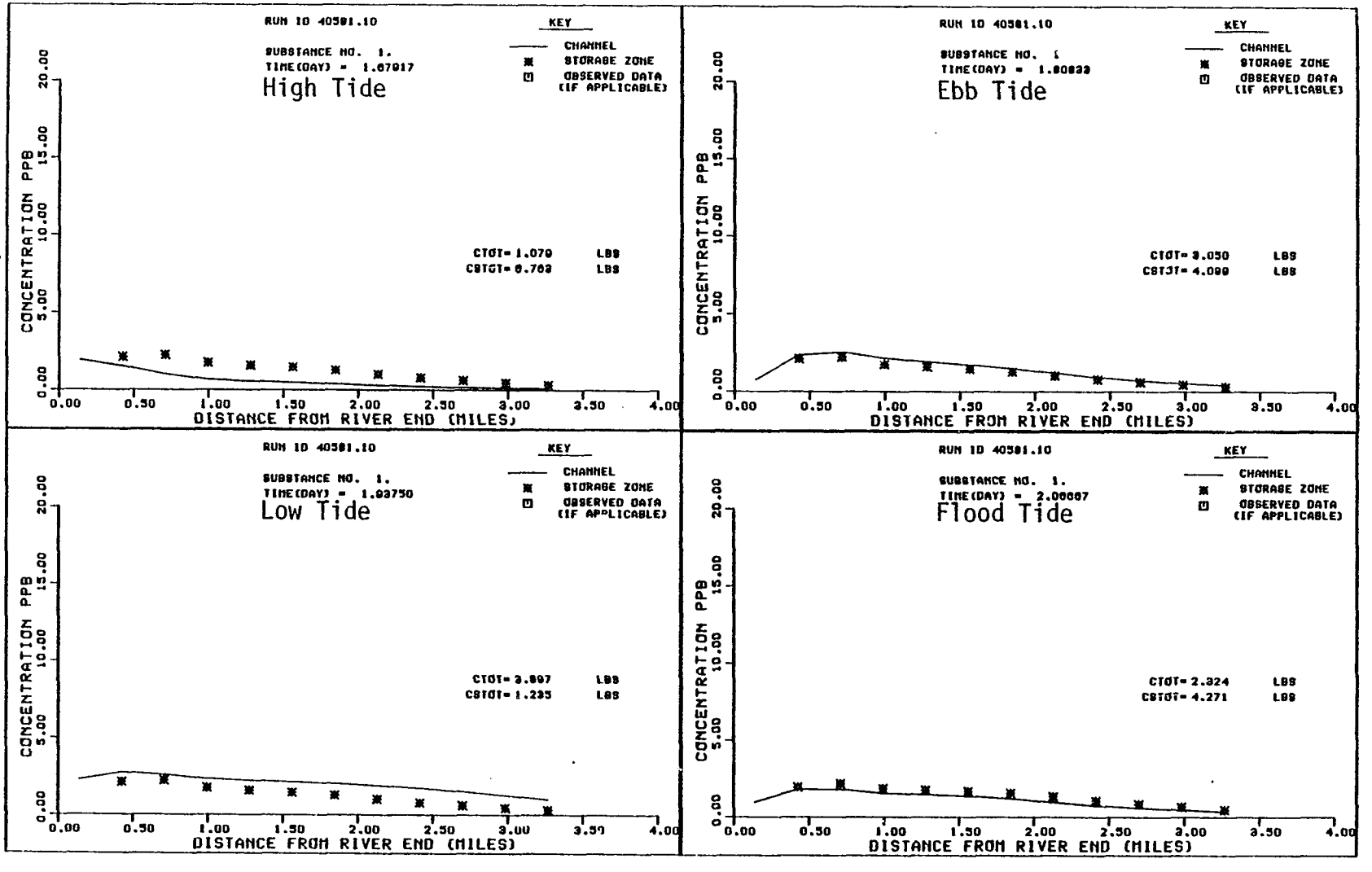

FIGURE B9 LOW FLOW DYE STUDY--TIDAL CYCLE 4

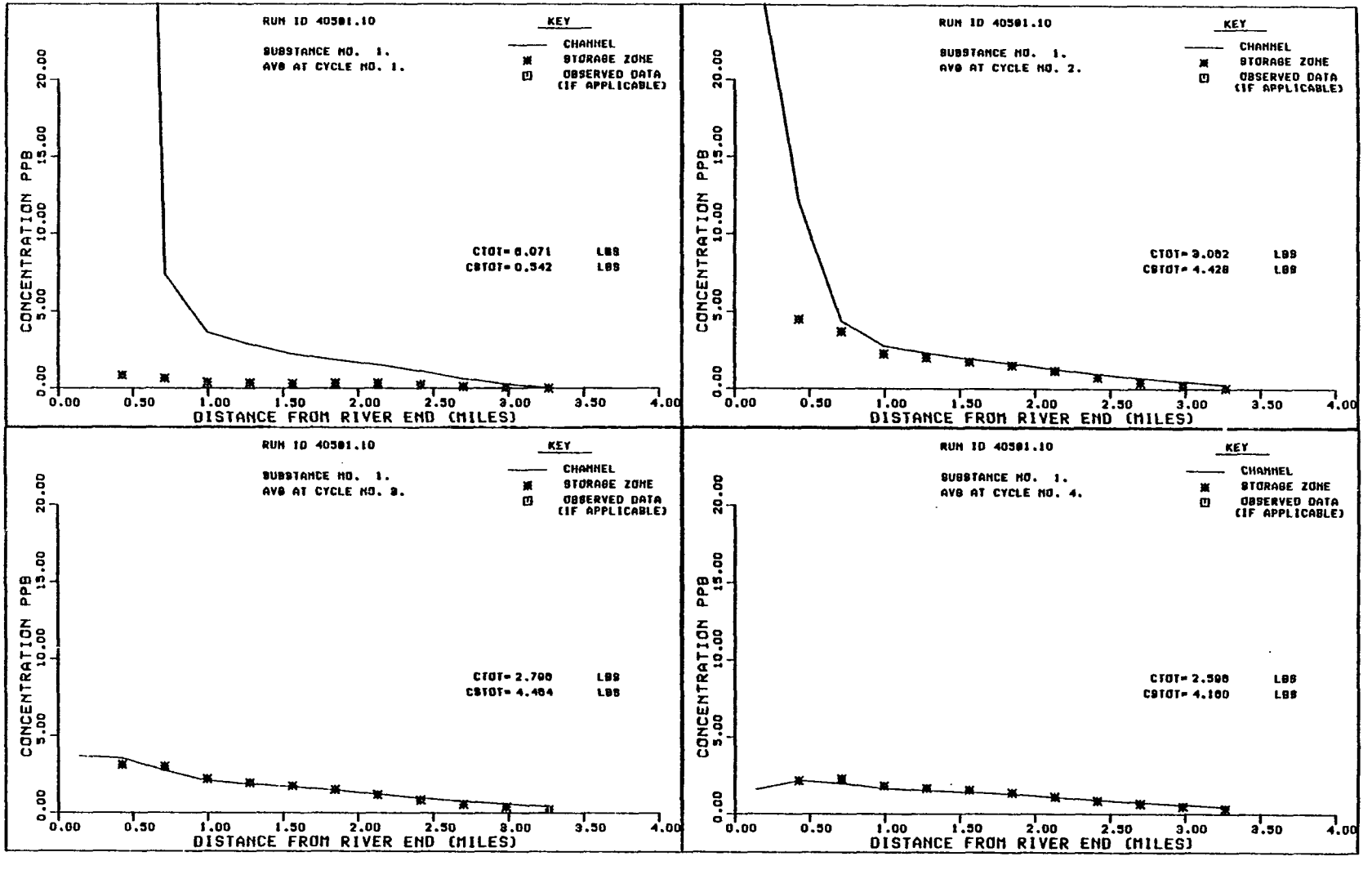

FIGURE B10 LOW FLOW DYE STUDY--AVERAGES

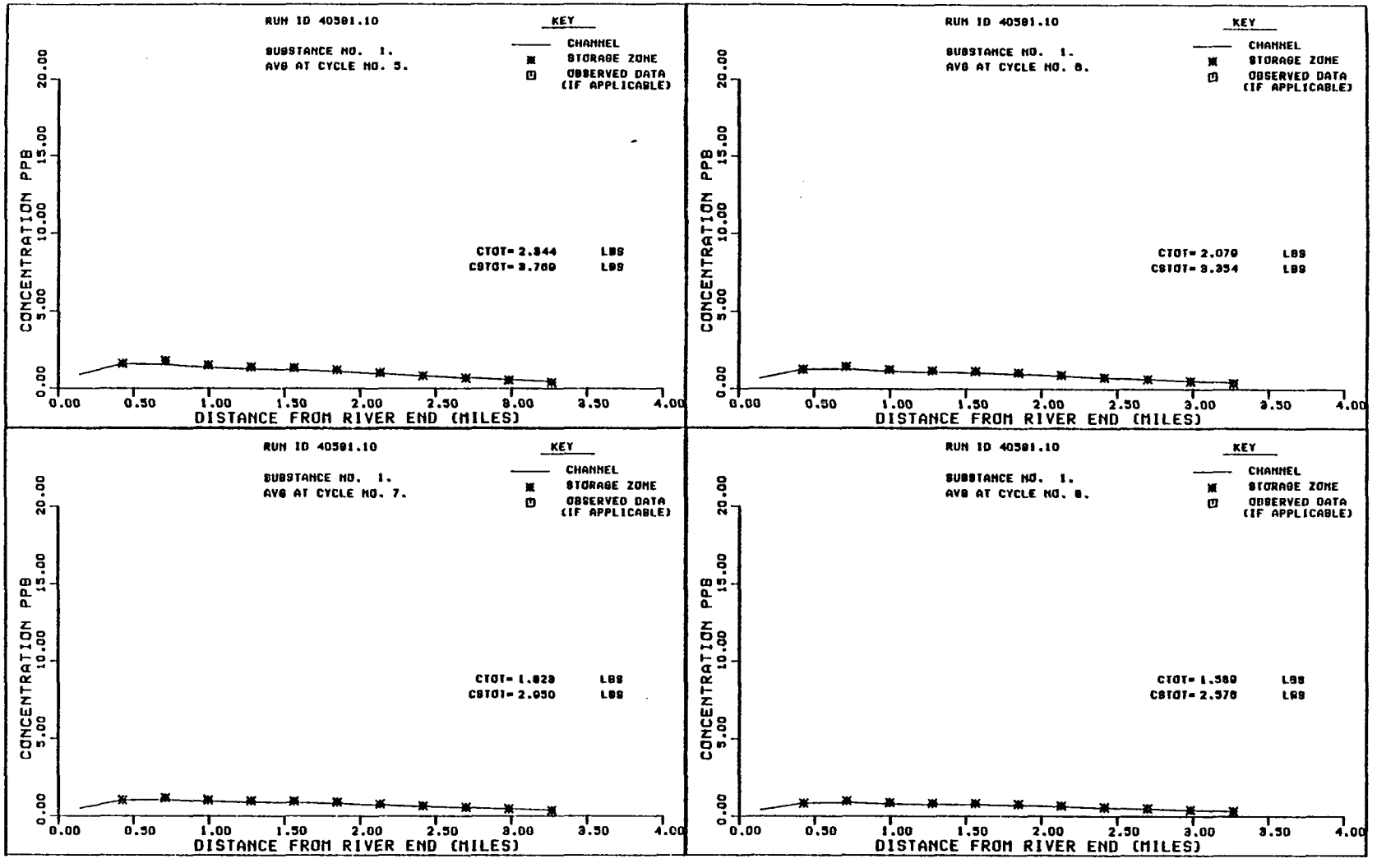

FIGURE B11 LOW FLOW DYE STUDY--AVERAGES

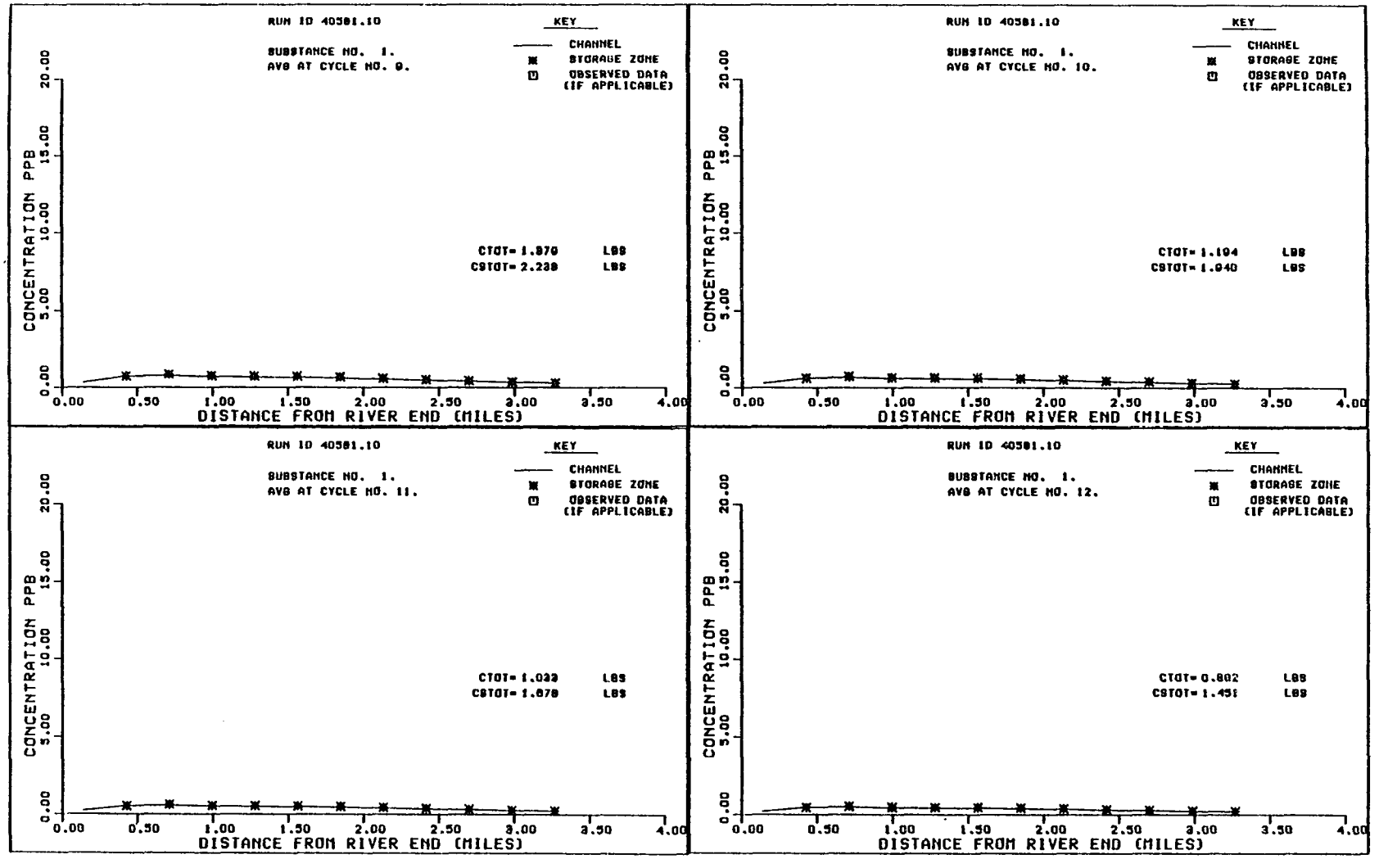

FIGURE B12 LOW FLOW DYE STUDY--AVERAGES

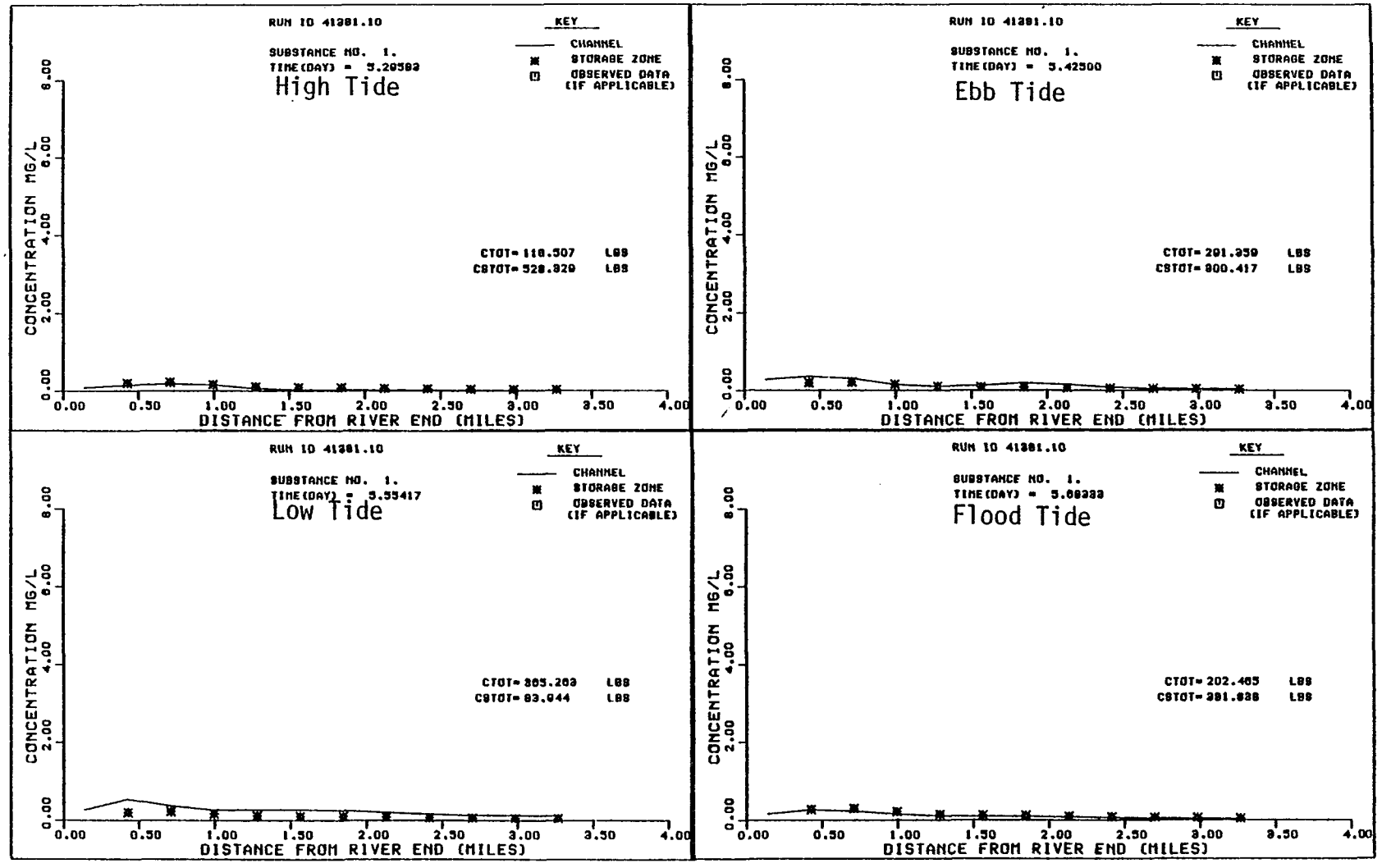

FIGURE B13 STEADY STATE BOD FOR 10 CFS FLOW

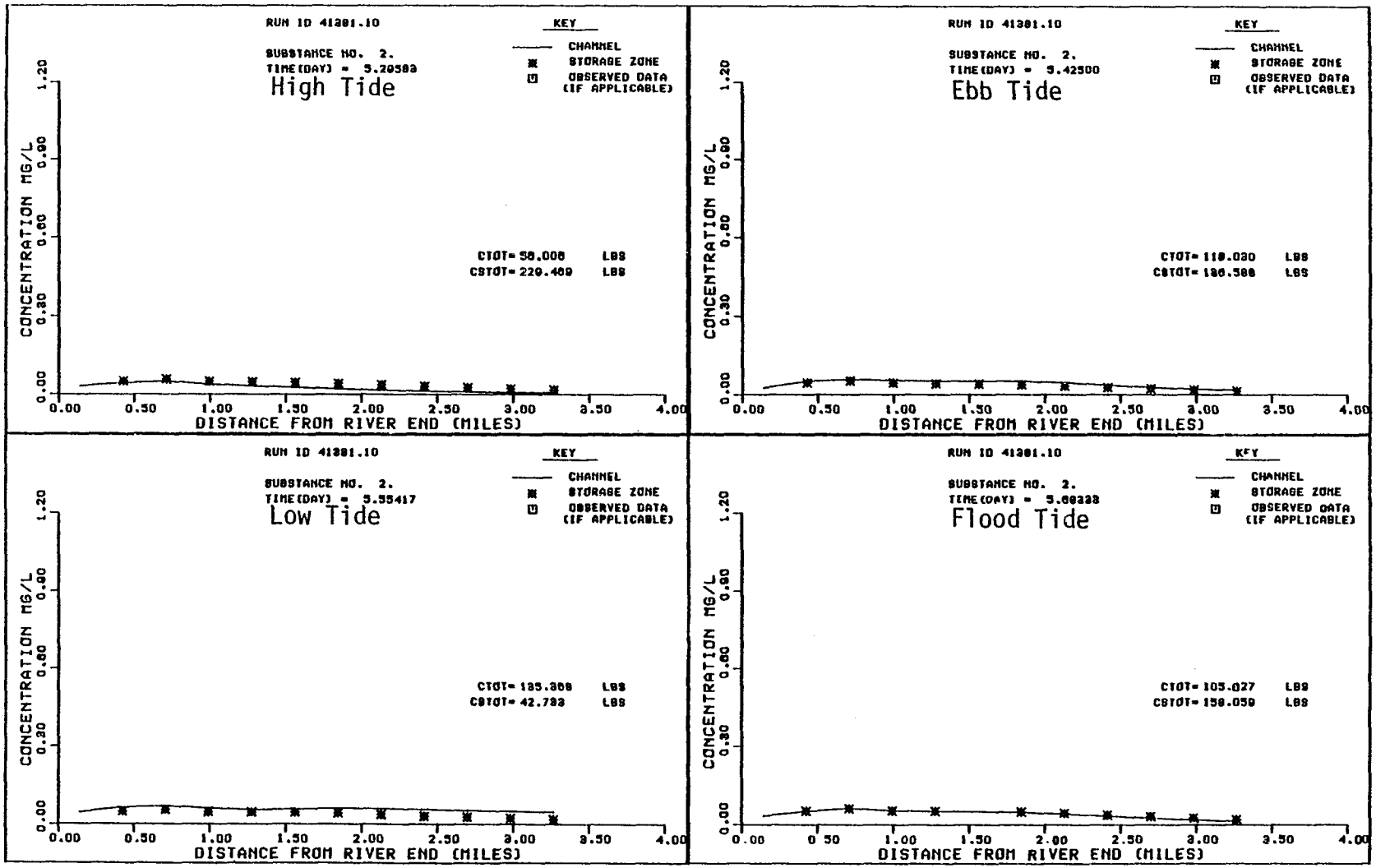

FIGURE B14 STEADY STATE DO DEFICIT FOR 10 CFS FLOW

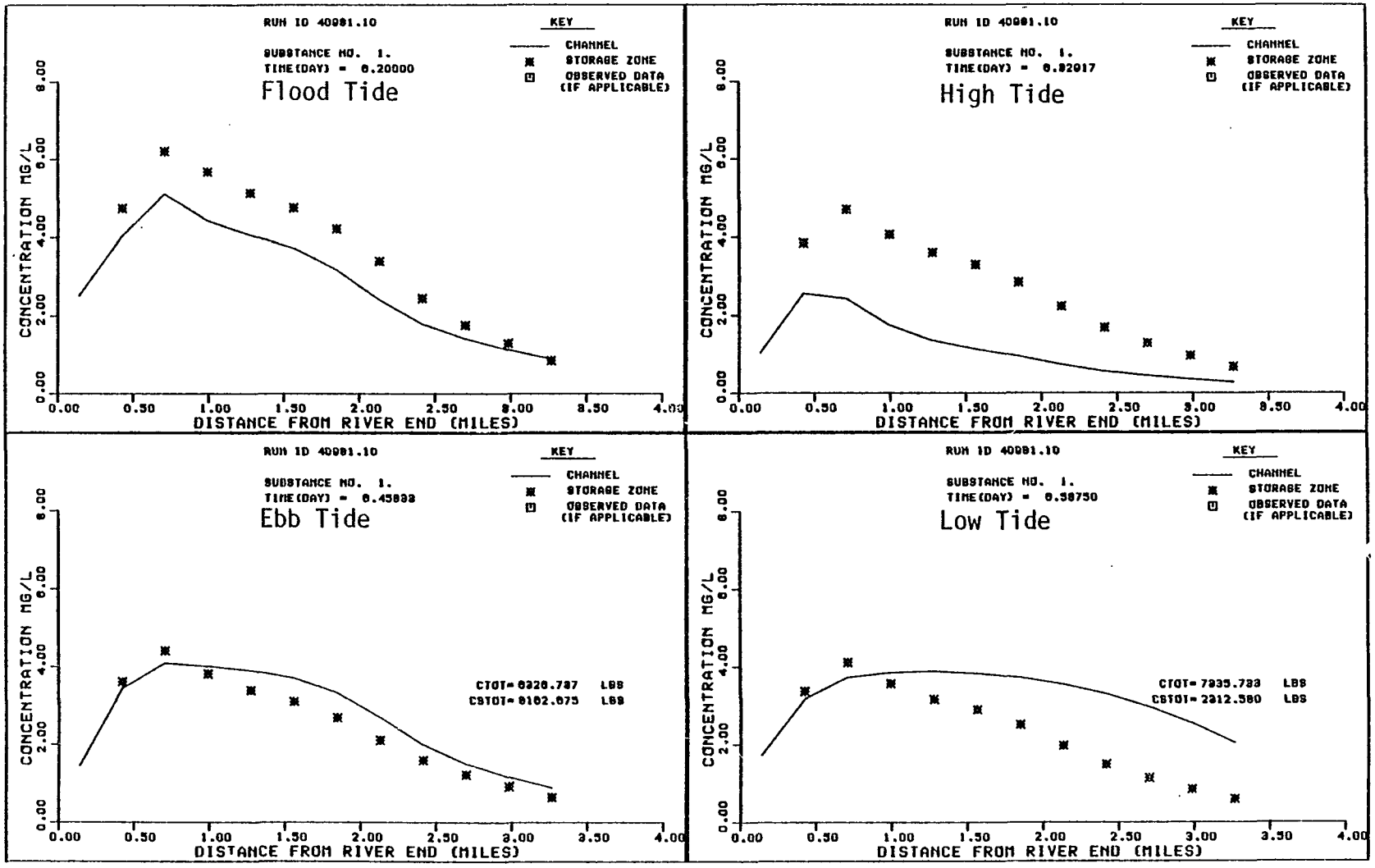

FIGURE B15 BASE LAND USE BOD--TIDAL CYCLE 1

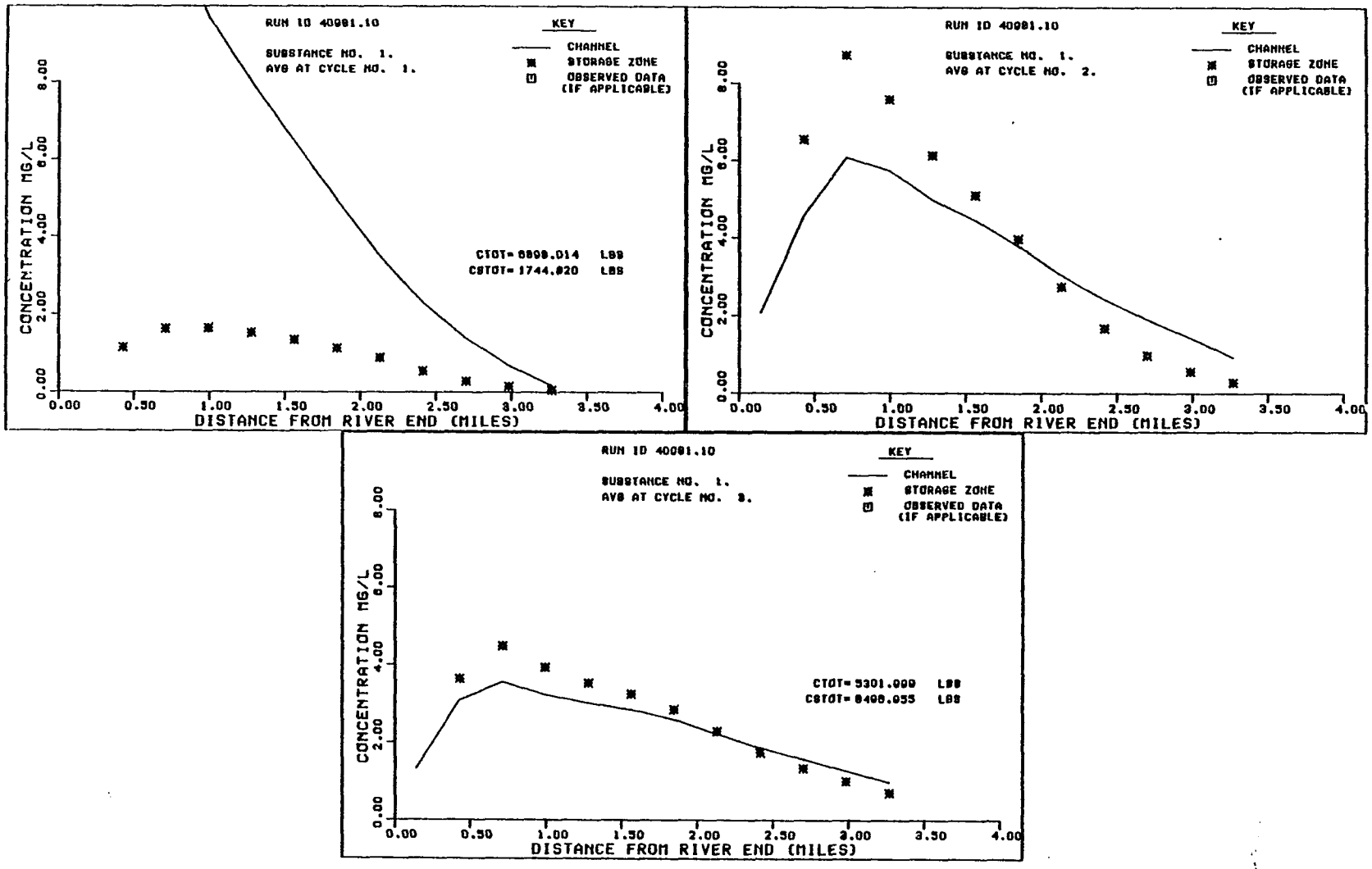

FIGURE B16 BASE LAND USE BOD--AVERAGES

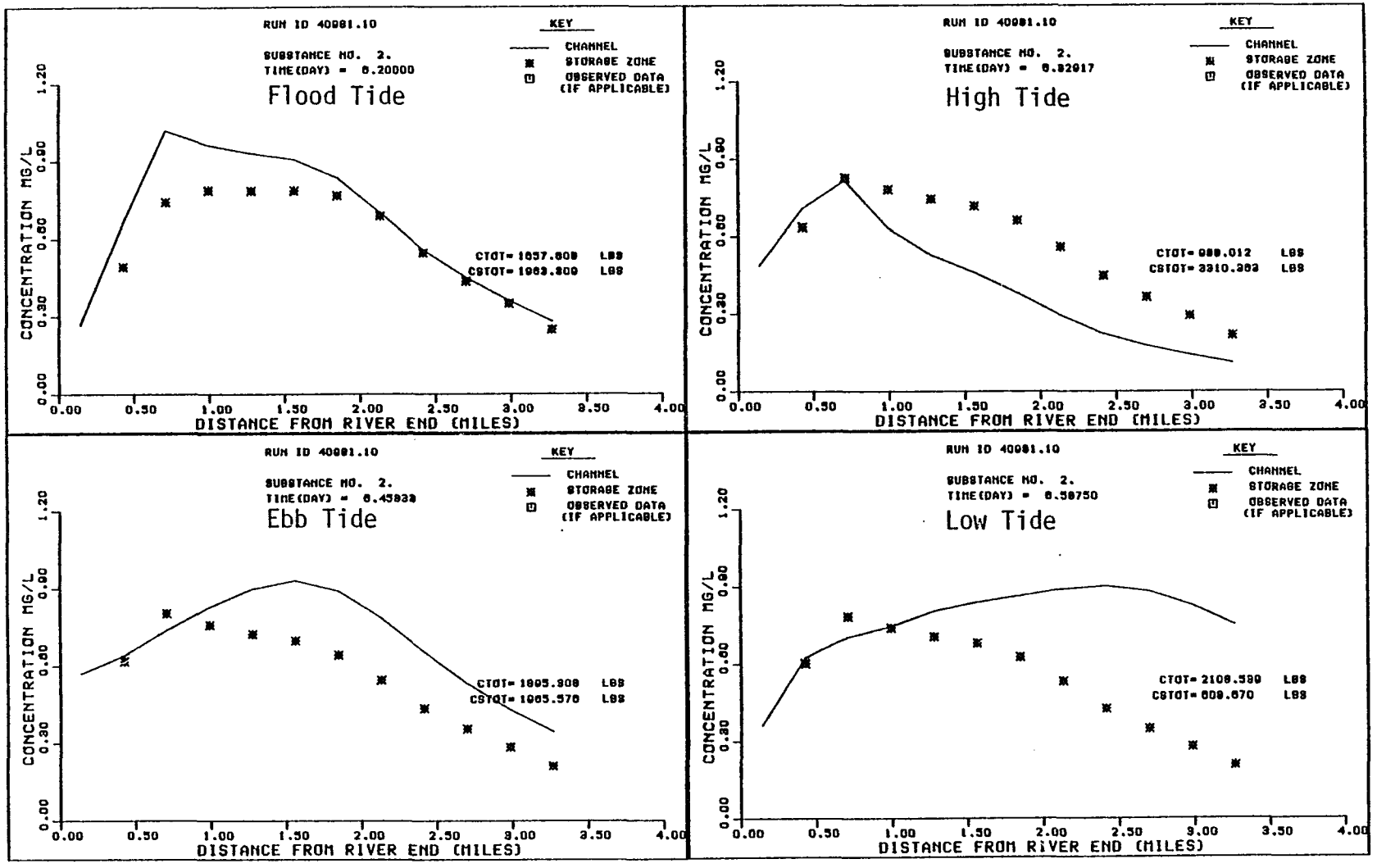

FIGURE B17 BASE LAND USE DO DEFICIT--TIDAL CYCLE 1

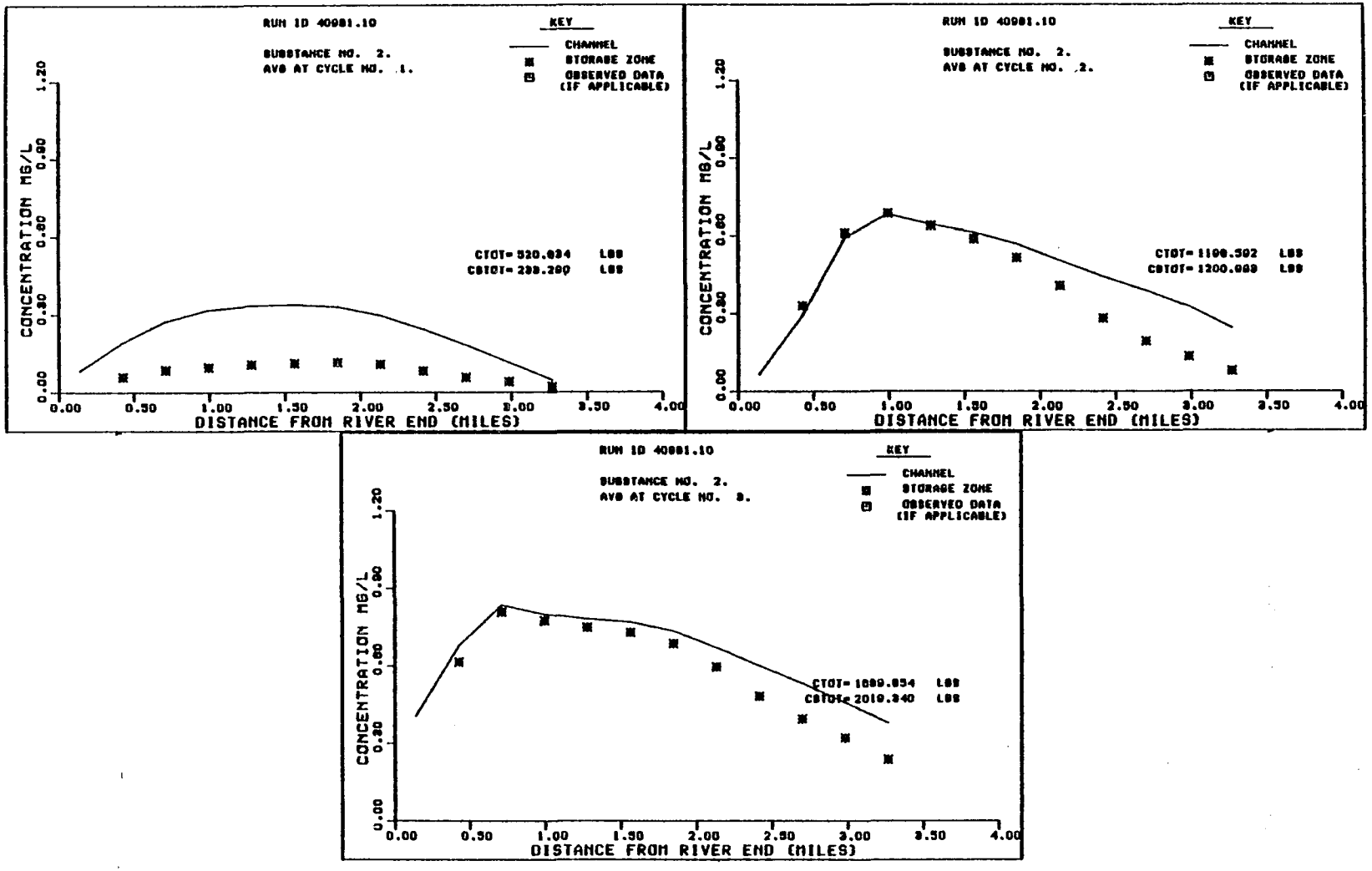

FIGURE B18 BASE LAND USE DO DEFICIT--AVERAGES

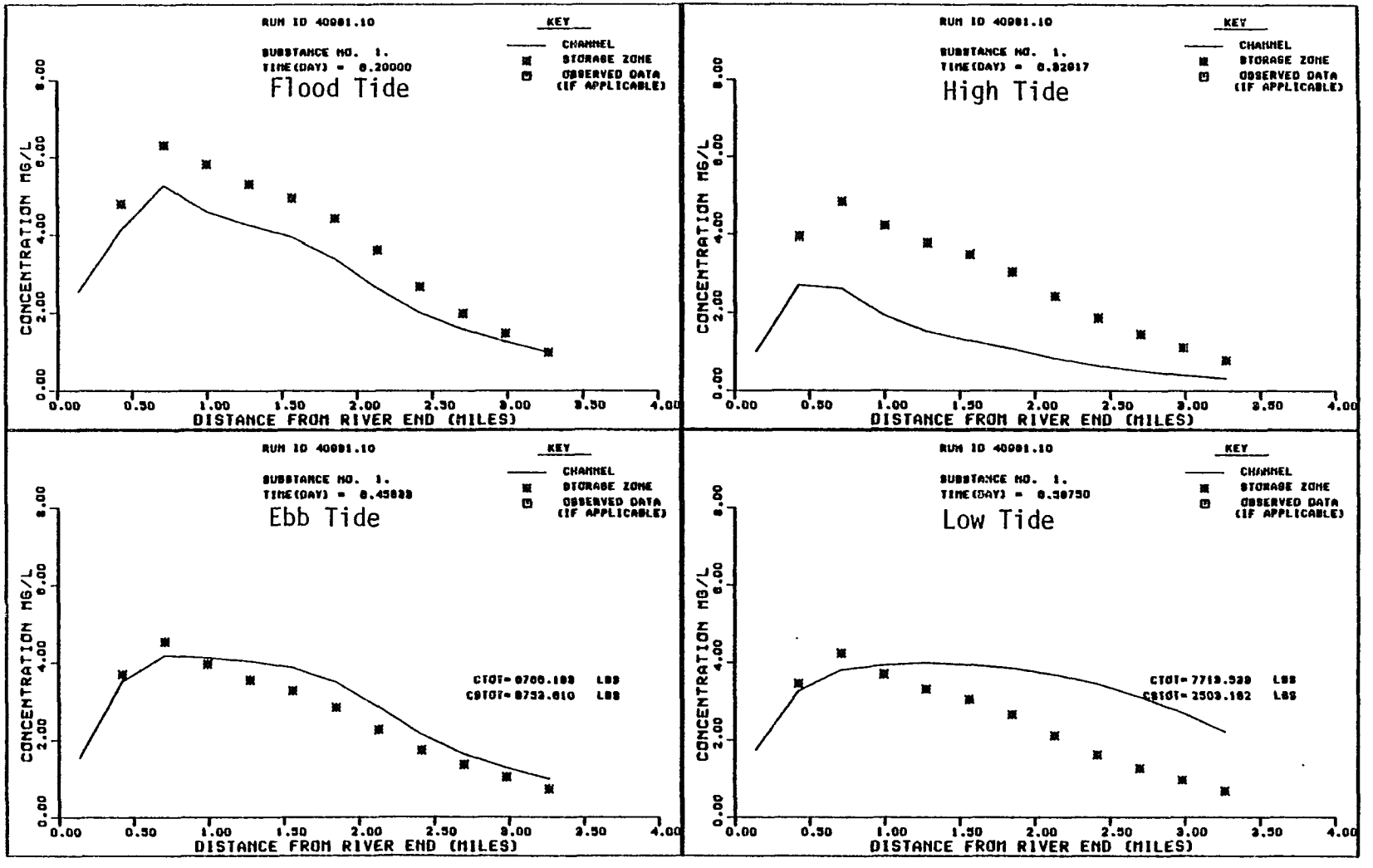

FIGURE B19 CASE 1 LAND USE BOD--TIDAL CYCLE 1

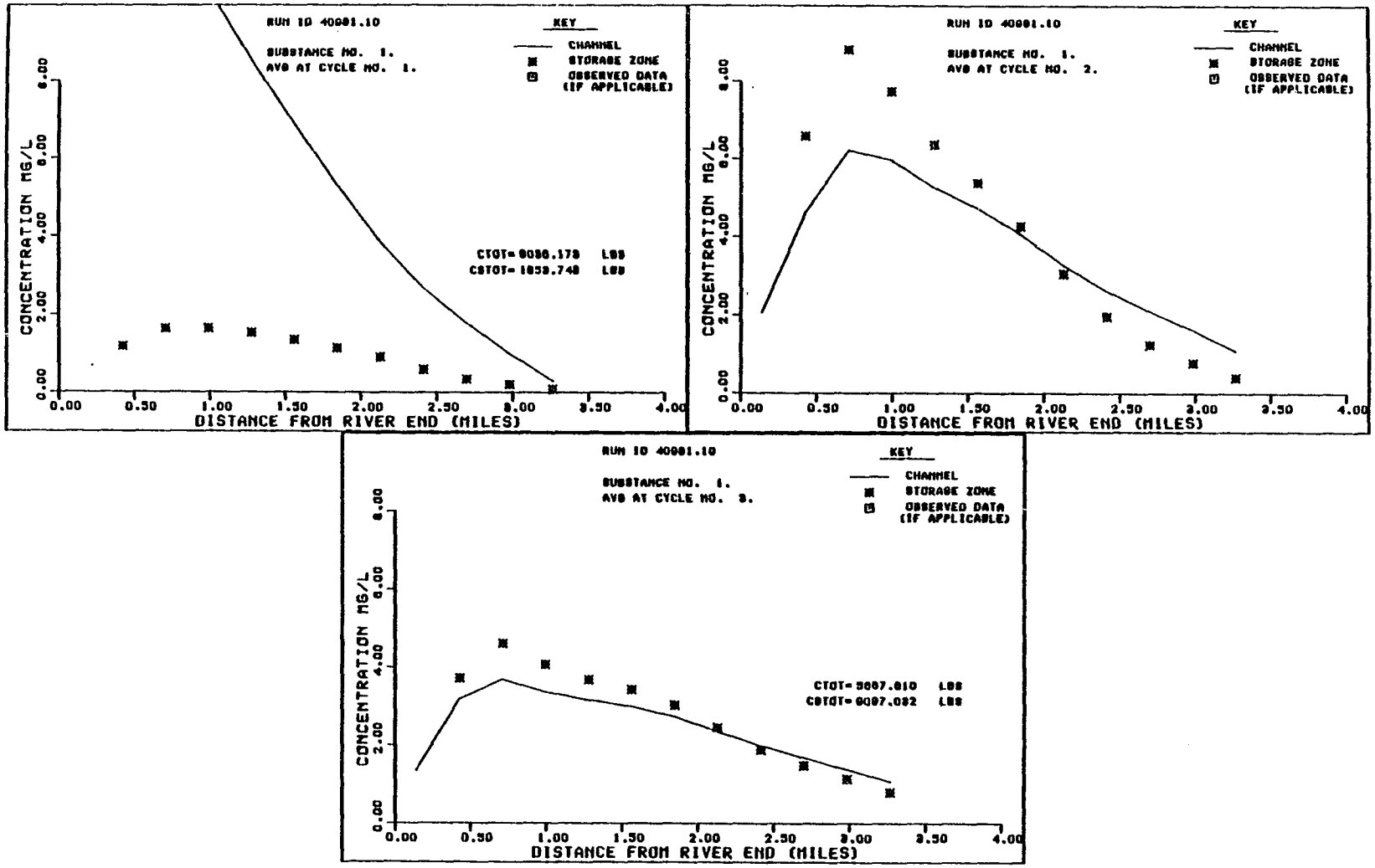

FIGURE B20 CASE 1 LAND USE BOD--AVERAGES

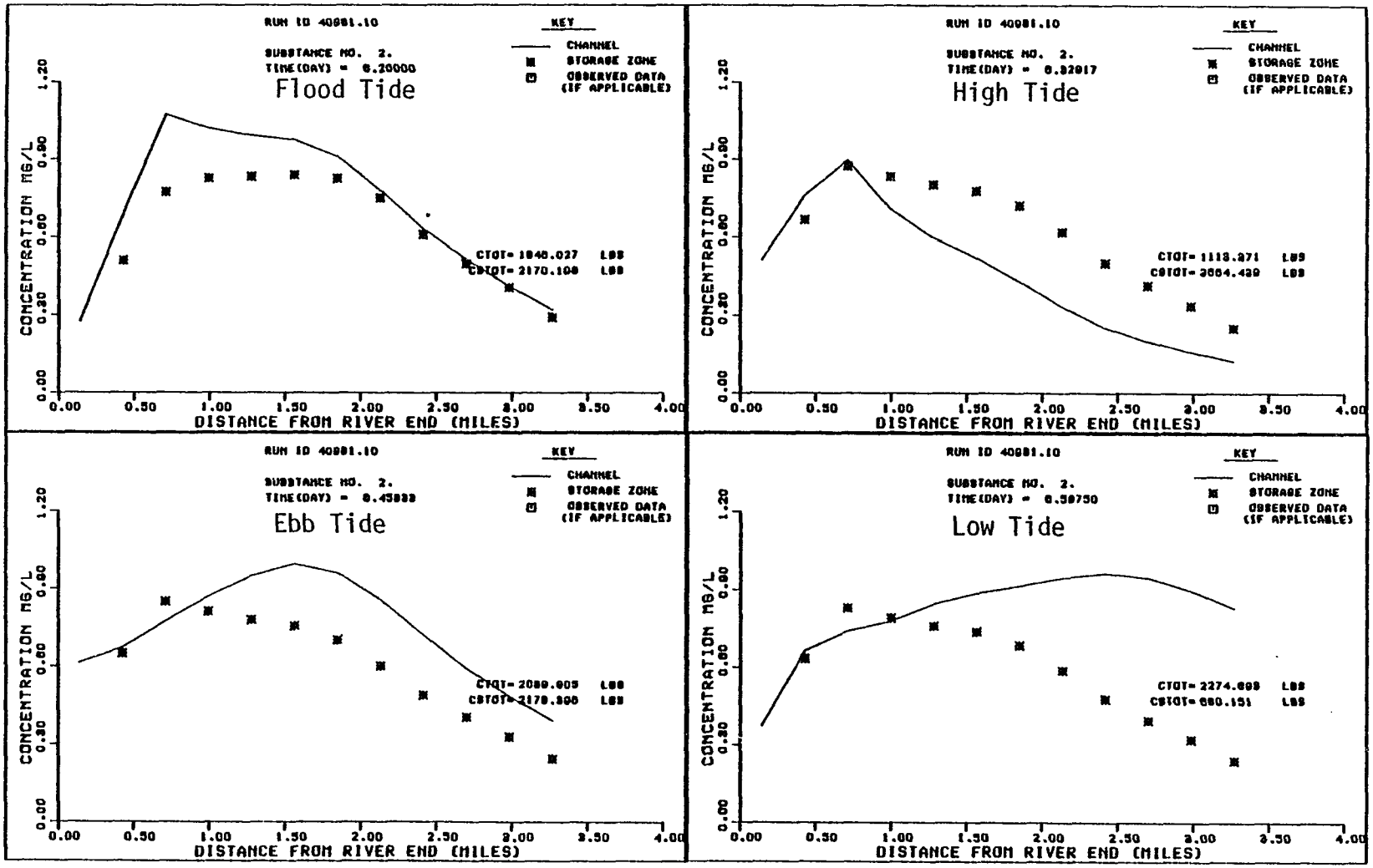

FIGURE B21 CASE 1 LAND USE DO DEFICIT--TIDAL CYCLE 1

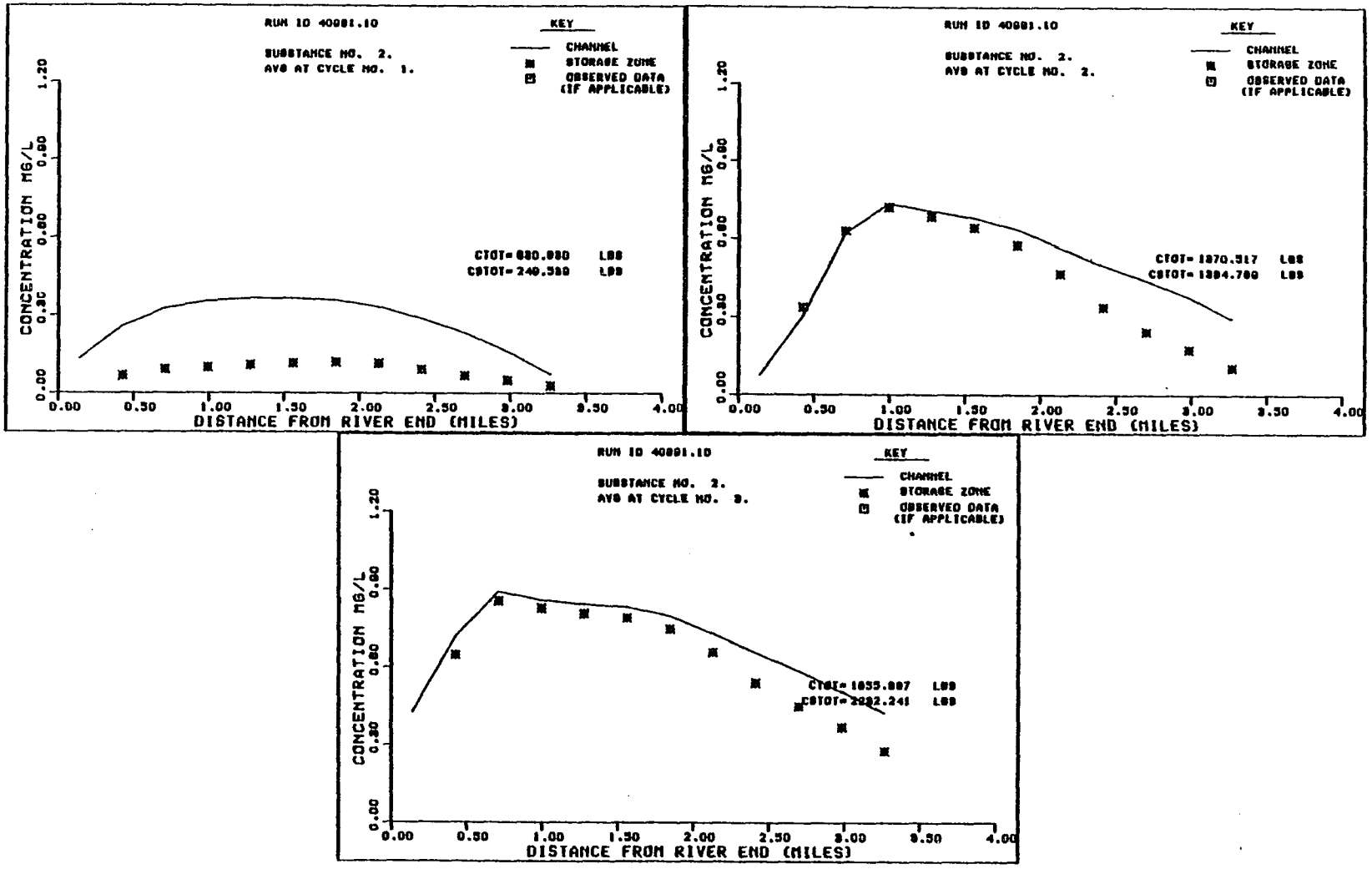

FIGURE B22 CASE 1 LAND USE DO DEFICIT--AVERAGES

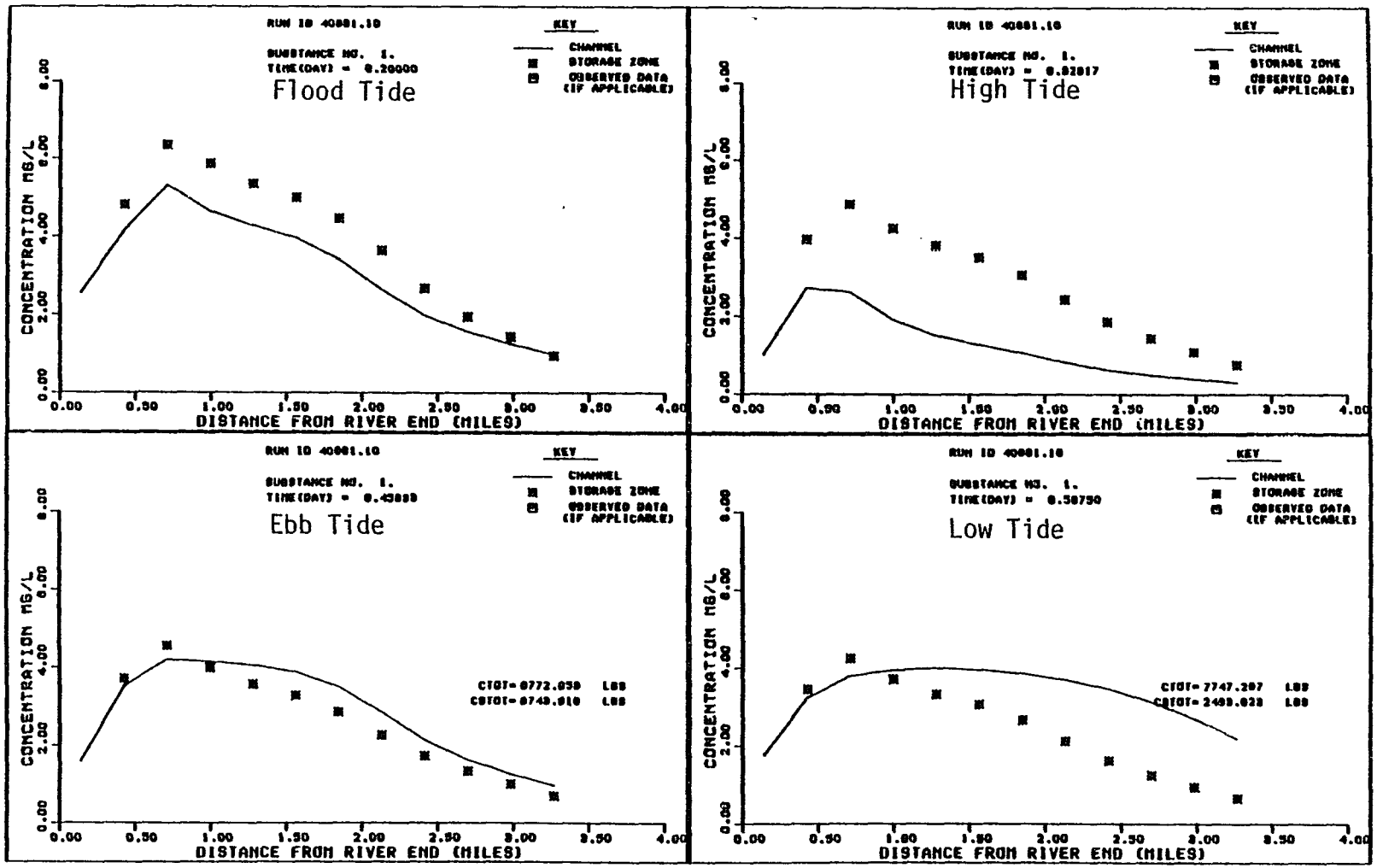

FIGURE B23 CASE 2 LAND USE BOD--TIDAL CYCLE 1

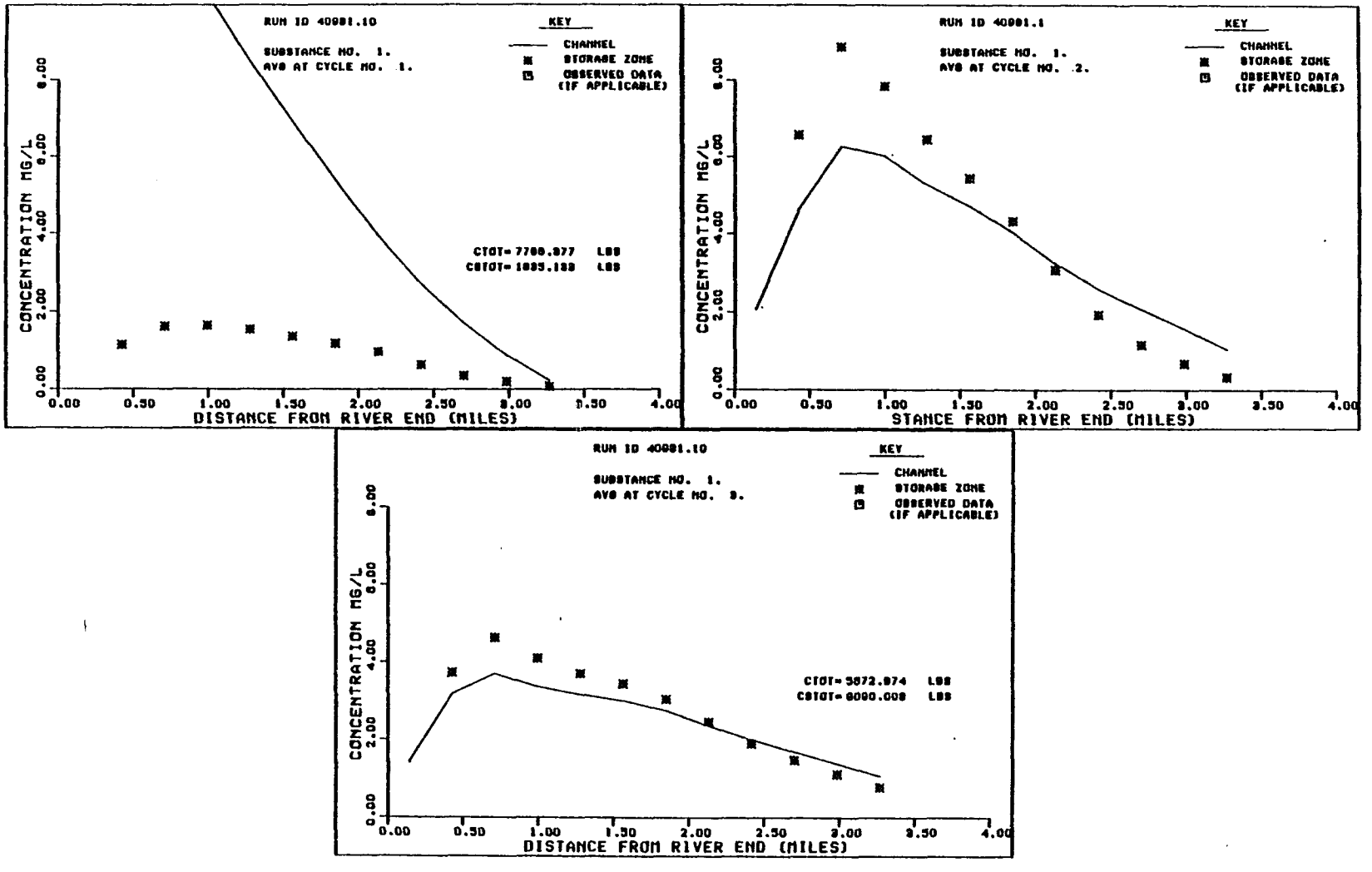

FIGURE B24 CASE 2 LAND USE BOD--AVERAGES

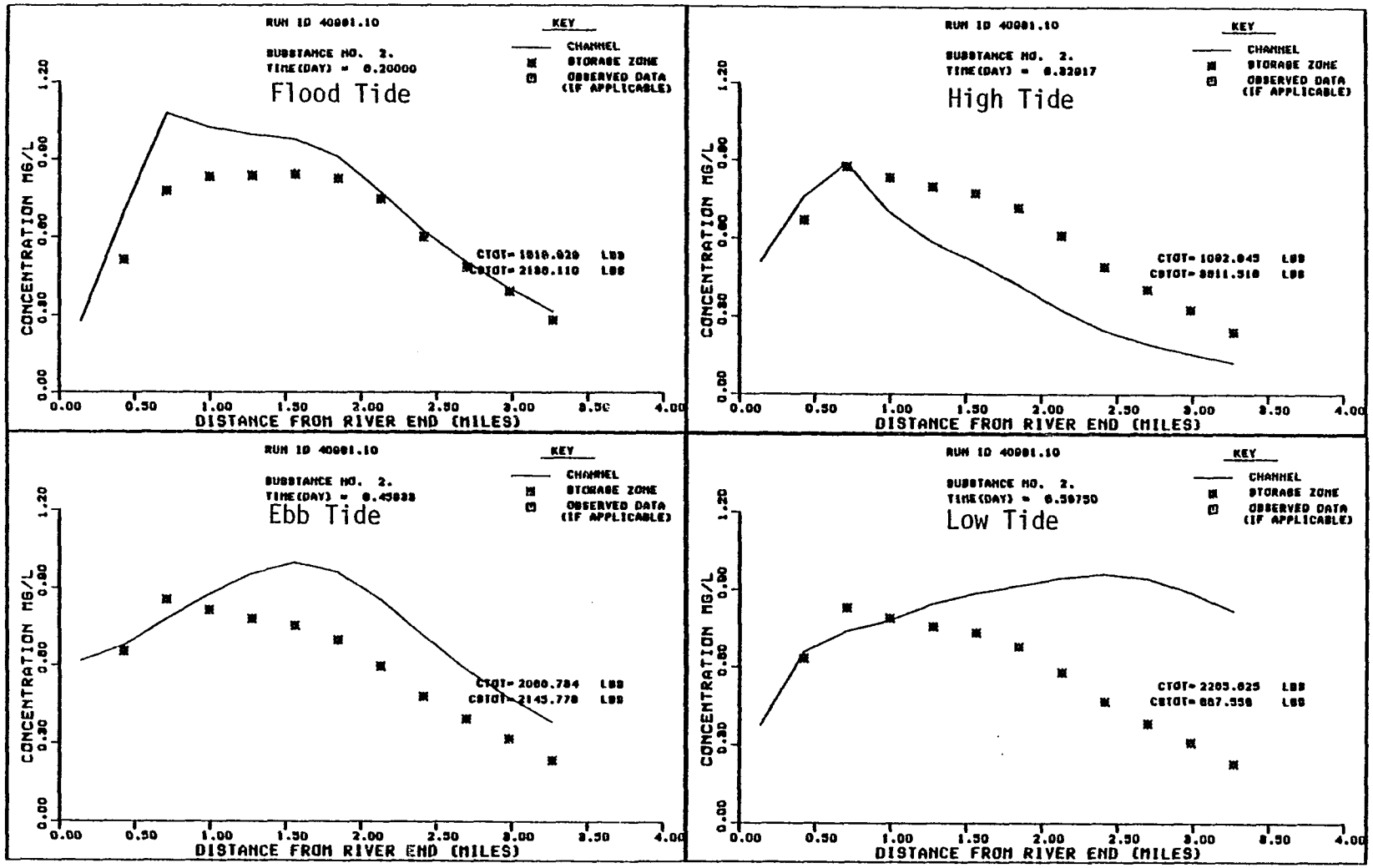

FIGURE B25 CASE 2 LAND USE DO DEFICIT--TIDAL CYCLE 1

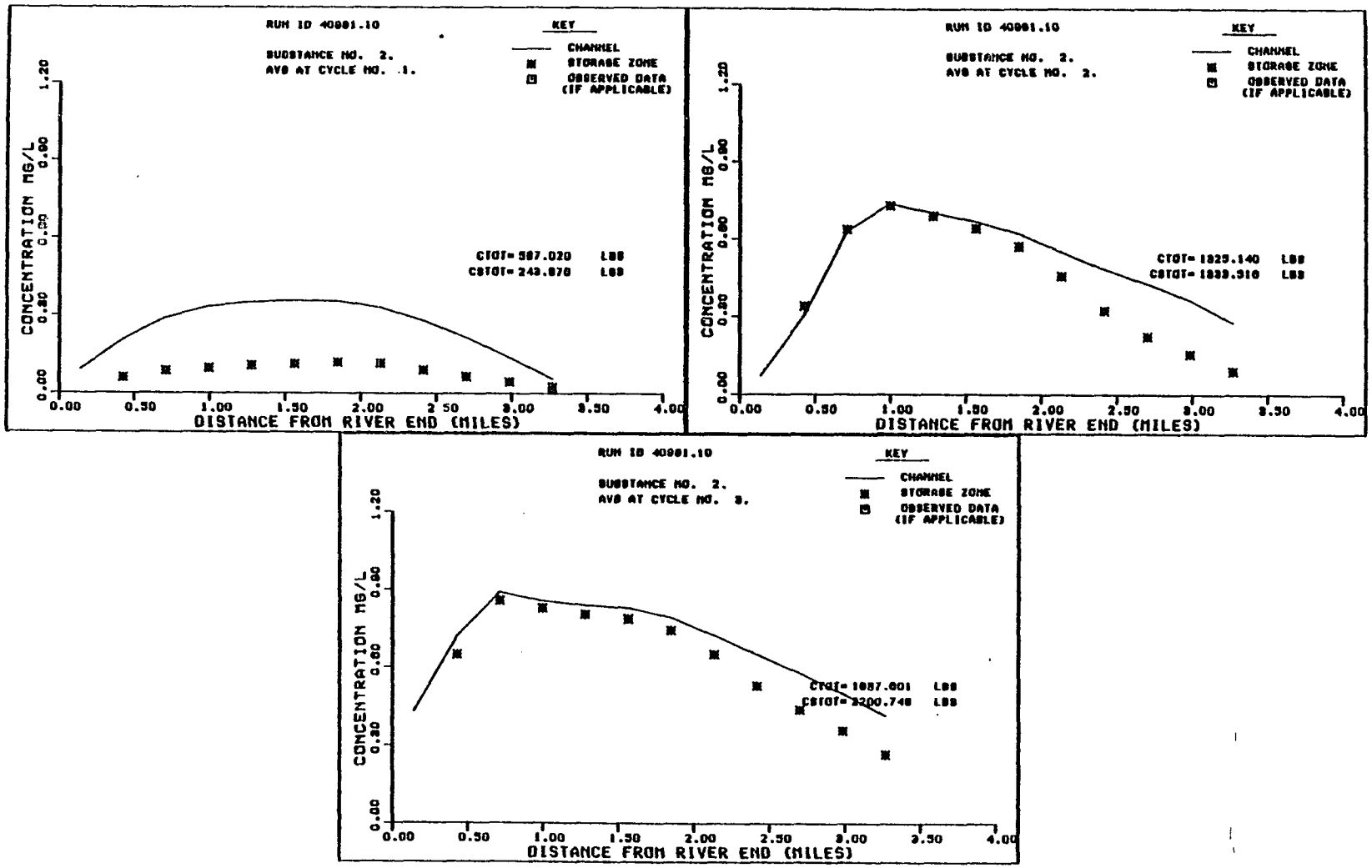

FIGURE B26 CASE 2 LAND USE DO DEFICIT--AVERAGES

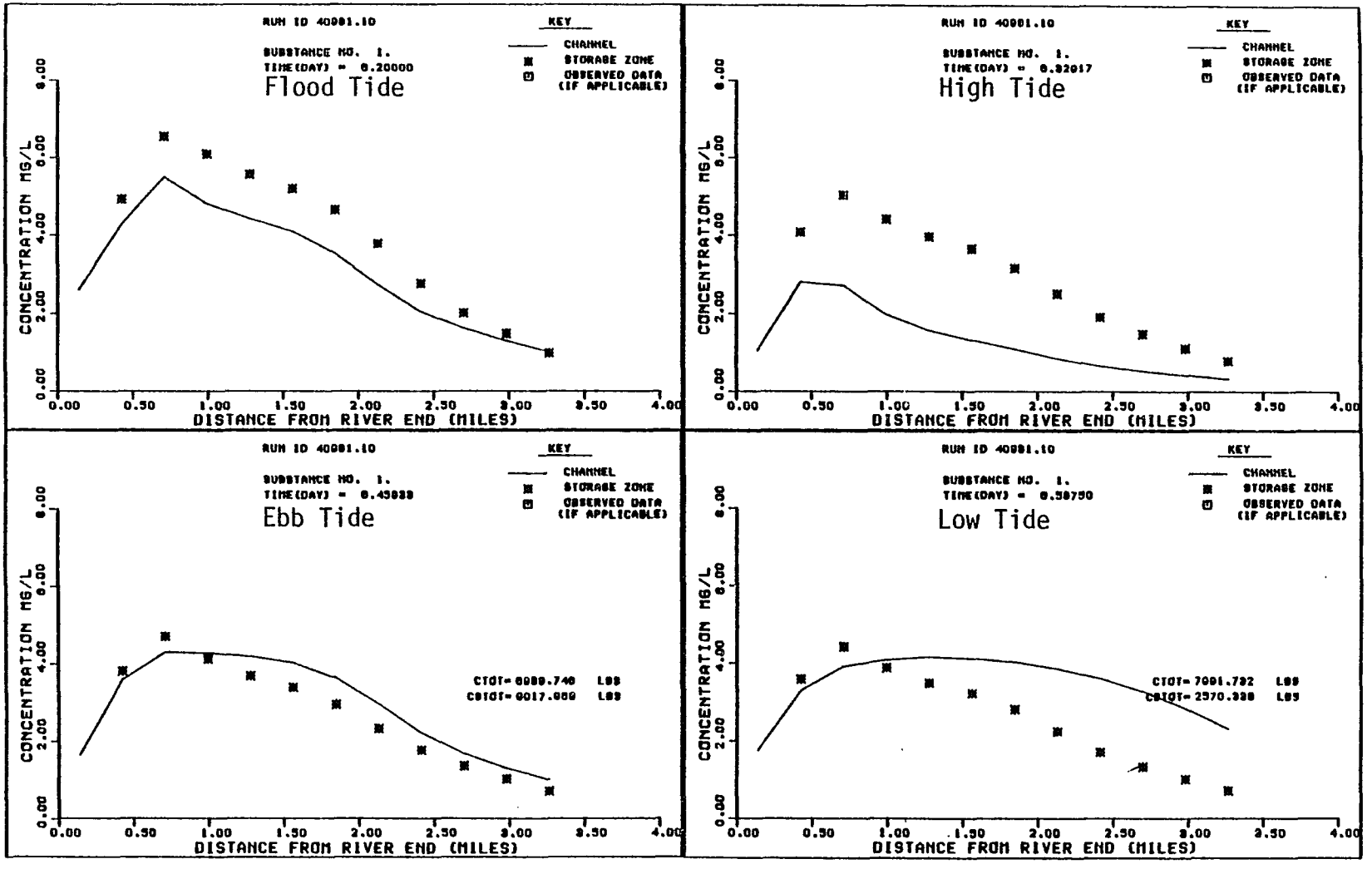

FIGURE B27 CASE 3 LAND USE BOD--TIDAL CYCLE 1

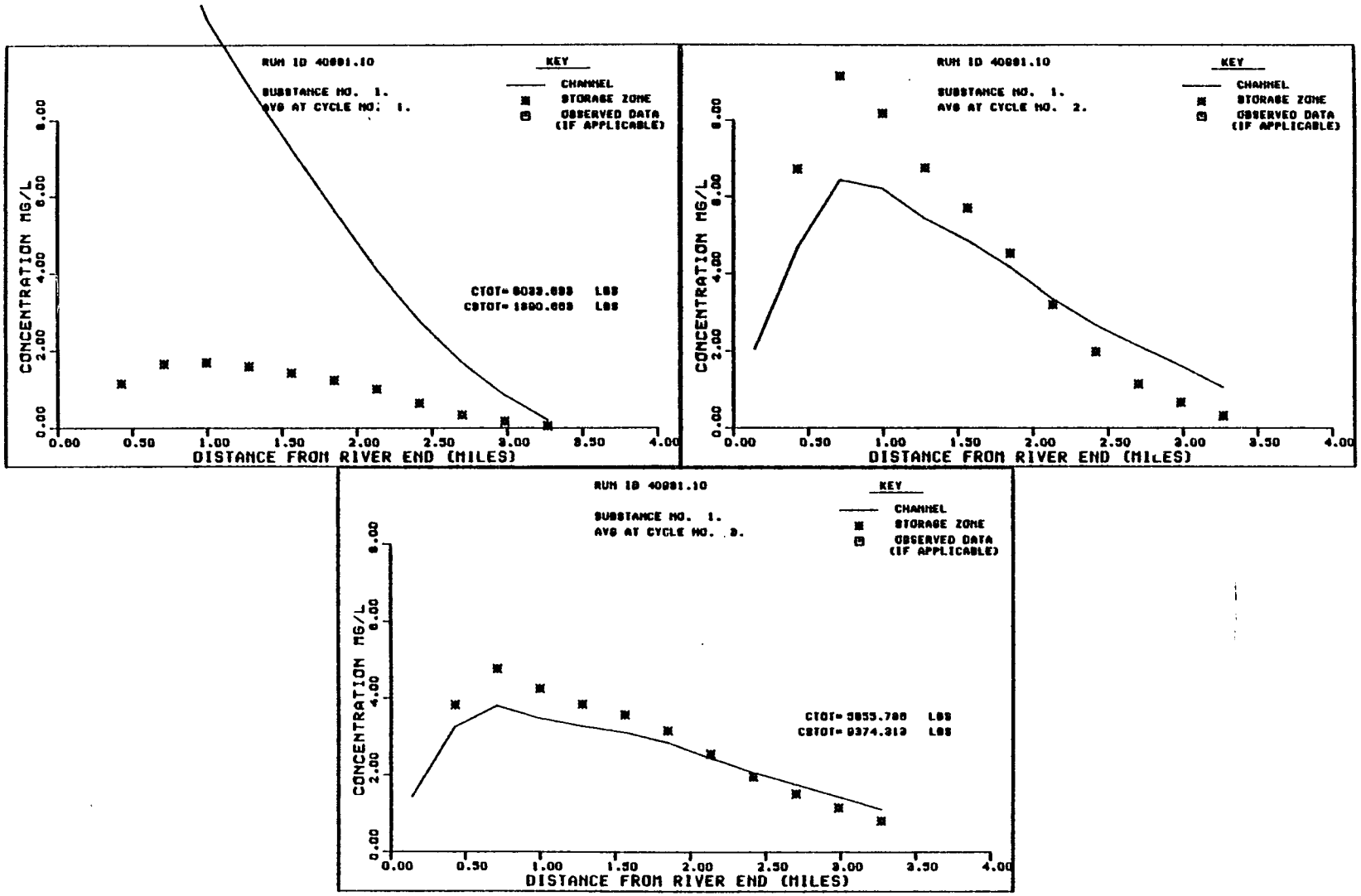

FIGURE B28 CASE 3 LAND USE BOD--AVERAGES

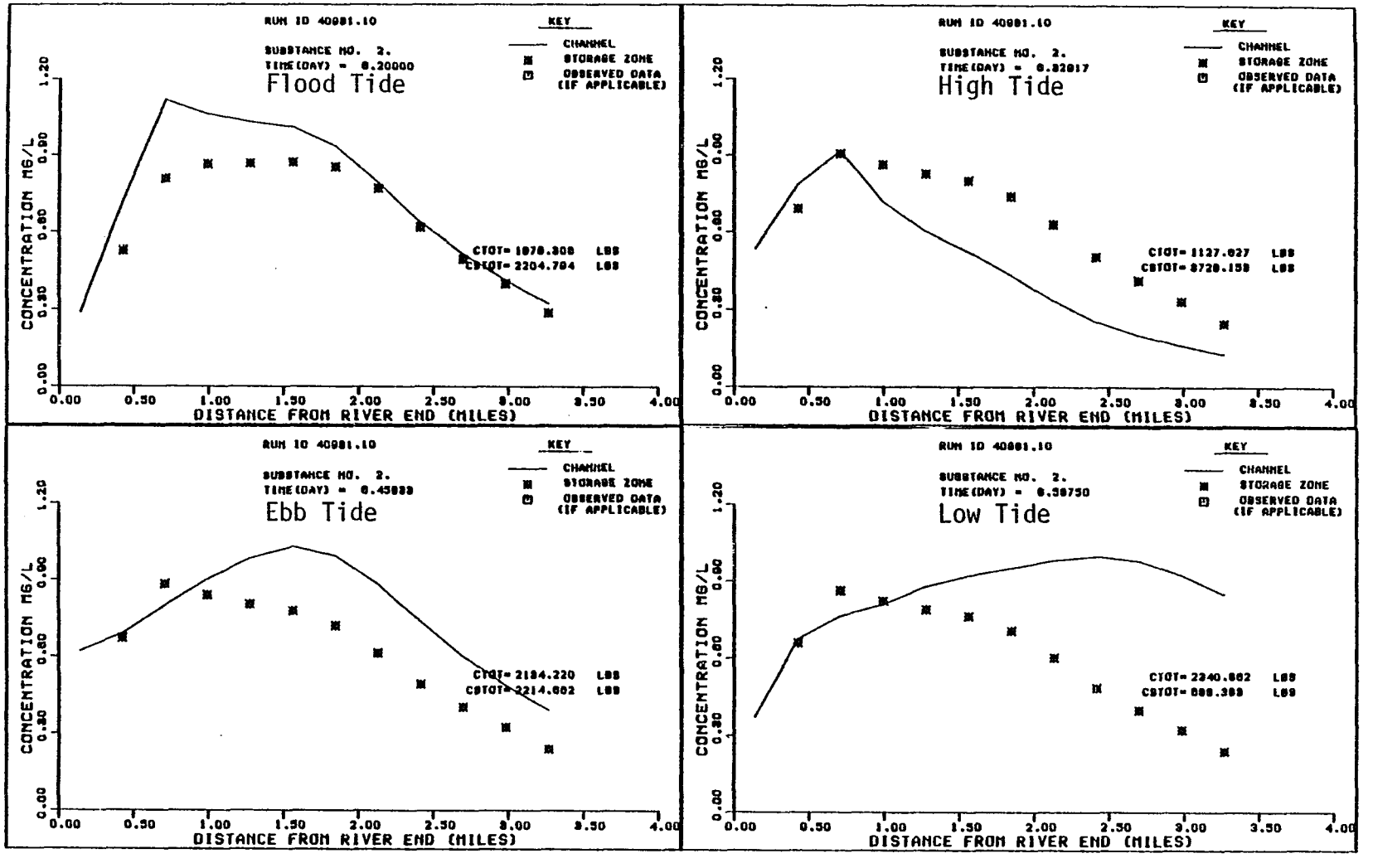

FIGURE B29 CASE 3 LAND USE DO DEFICIT--TIDAL CYCLE 1

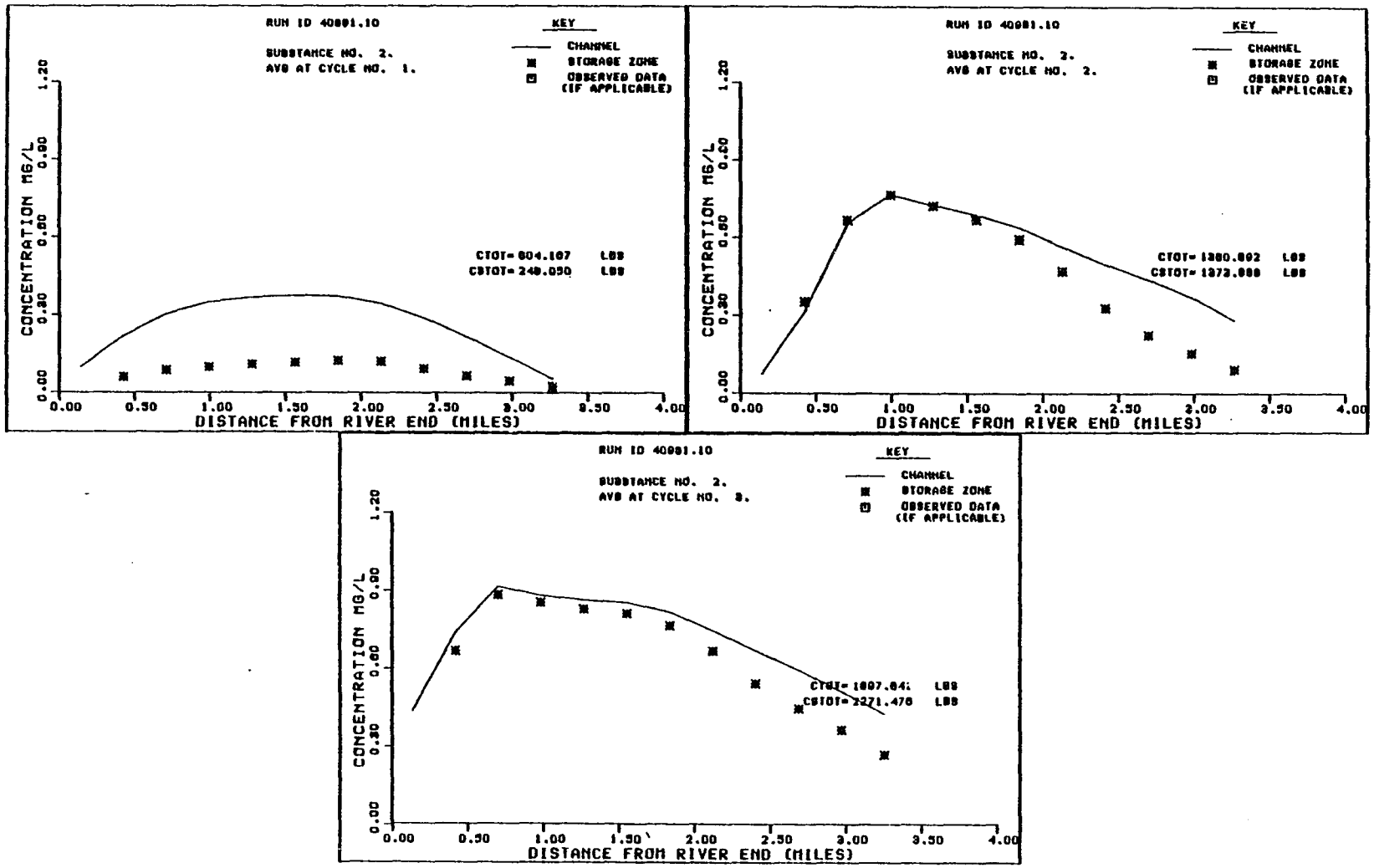

FIGURE B30 CASE 3 LAND USE DO DEFICIT--AVERAGES

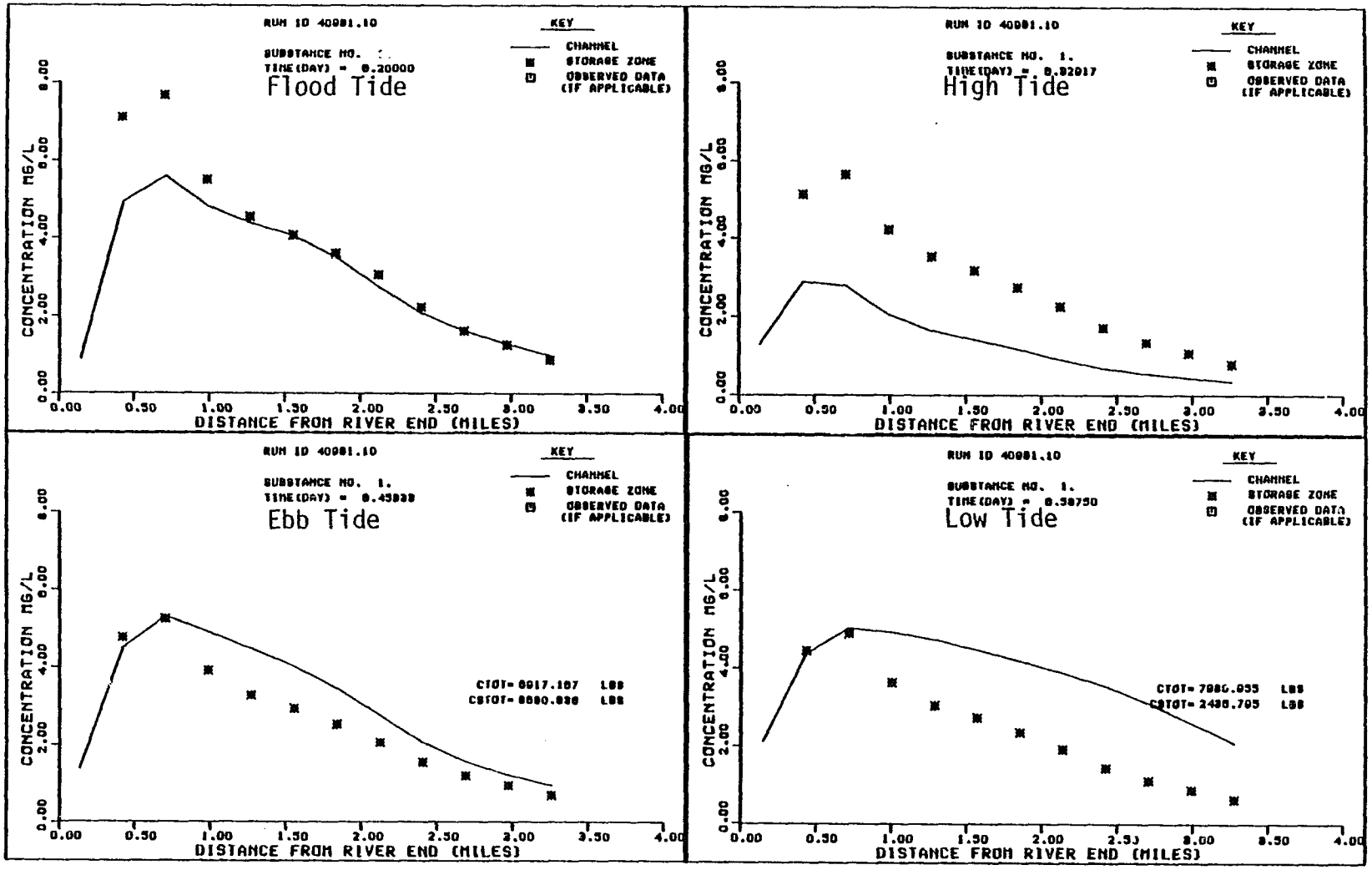

FIGURE B31 EXTENDED STORM BOD--TIDAL CYCLE 1

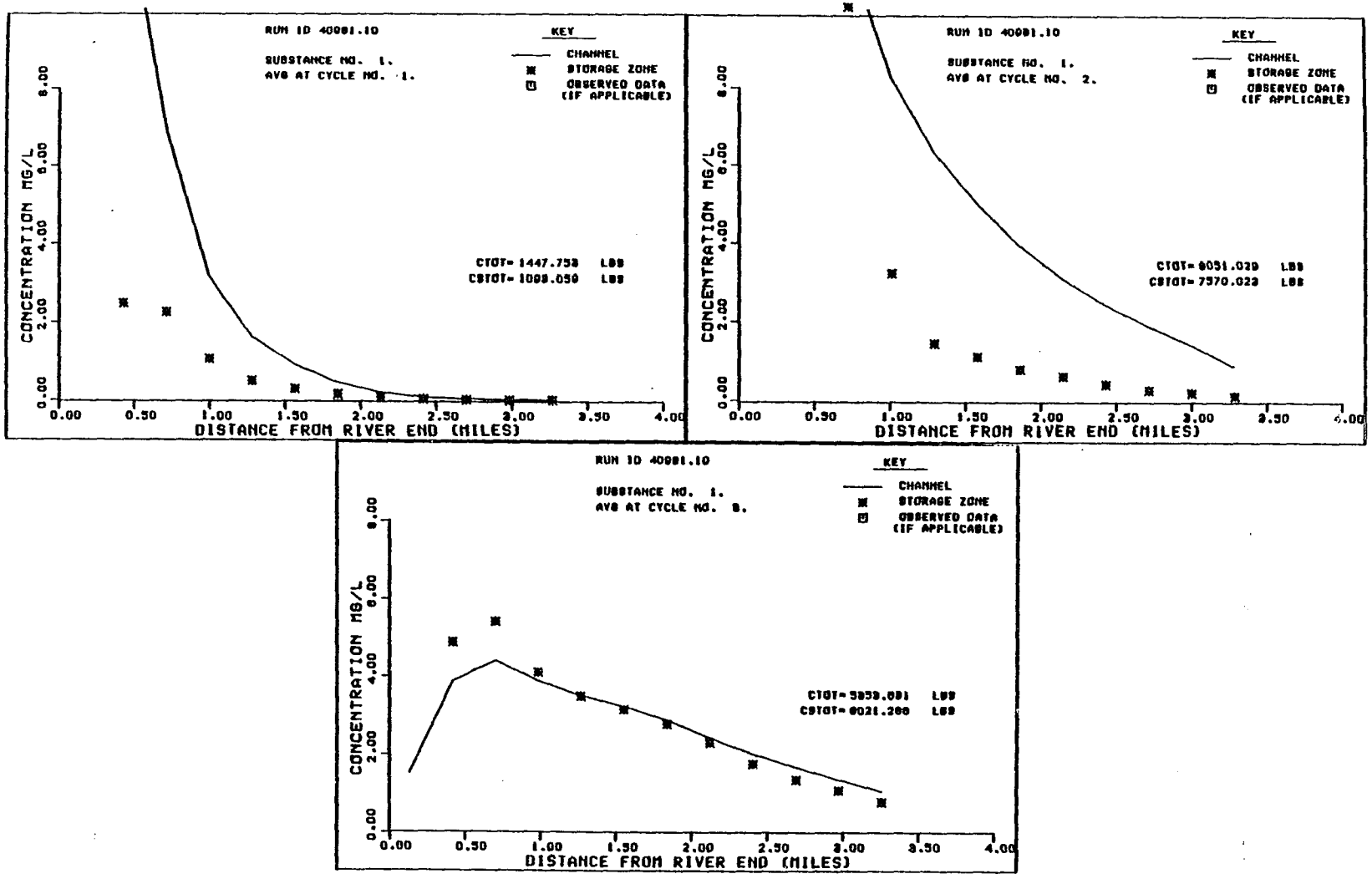

FIGURE B32 EXTENDED STORM BOD--AVERAGES

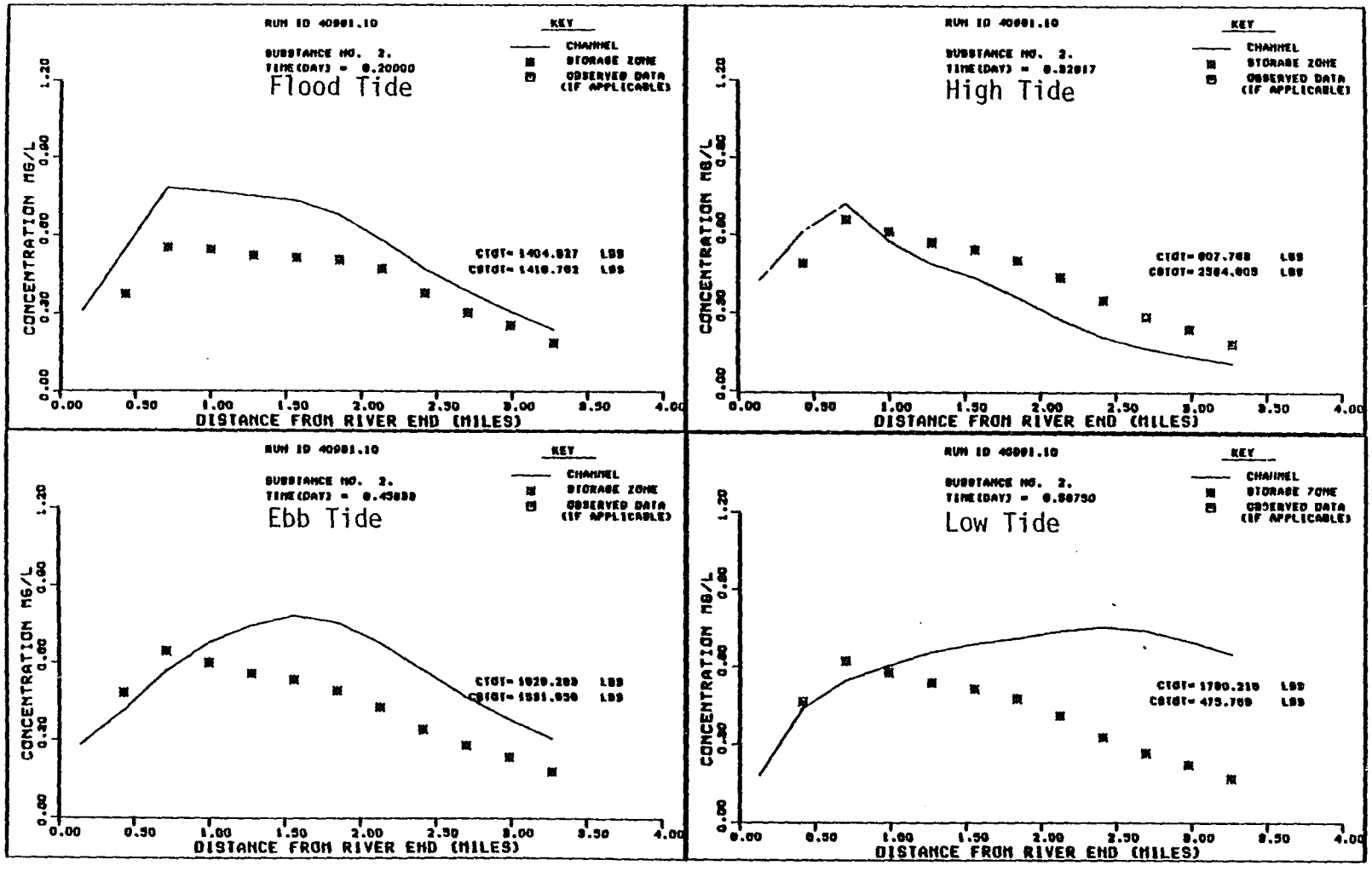

FIGURE B33 EXTENDED STORM DO DEFICIT--TIDAL CYCLE 1

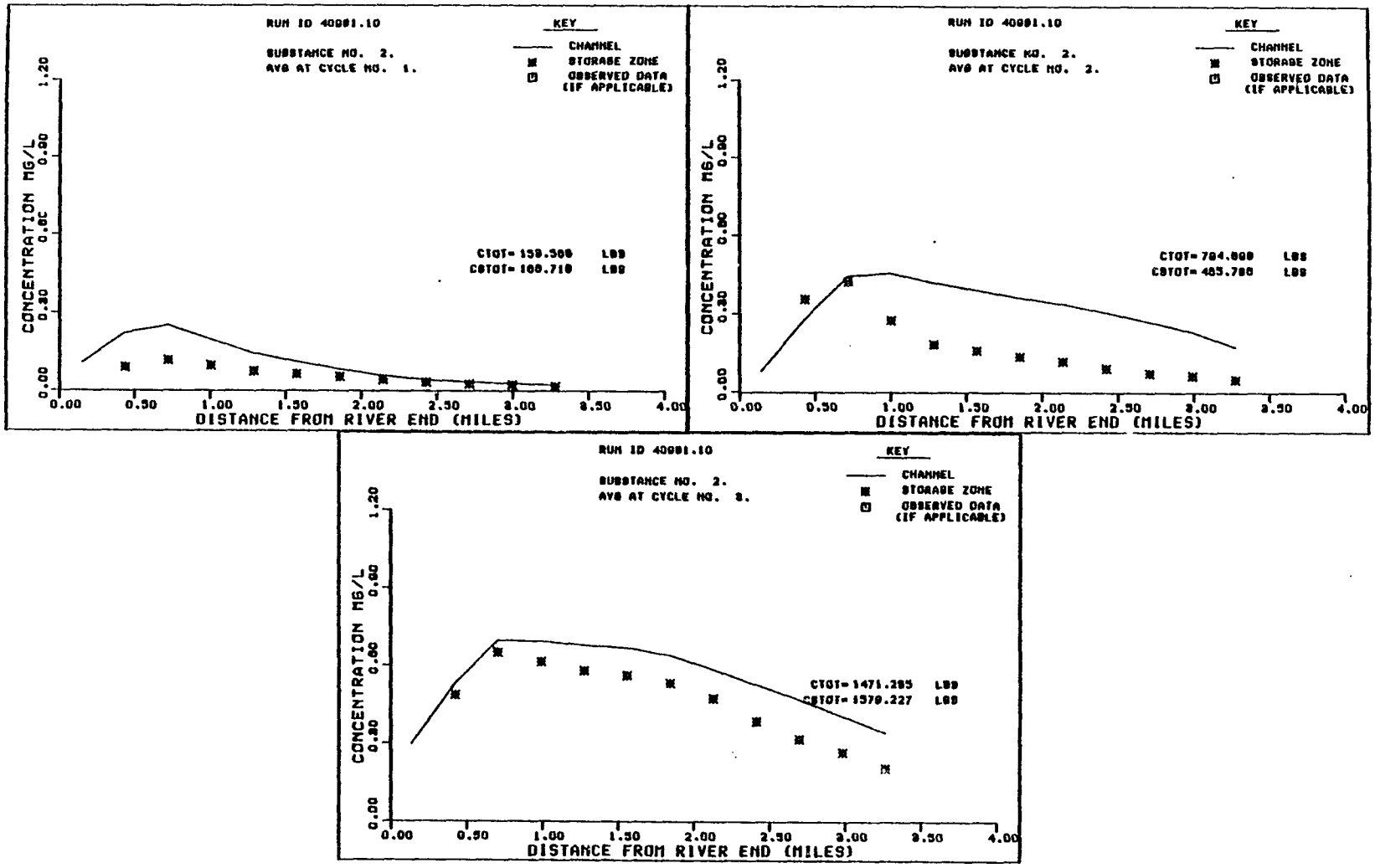

FIGURE B34 EXTENDED STORM DO DEFICIT--AVERAGES